

THESIS

DYNEIN MUTAGENESIS REVEALS THE MOLECULAR BASIS FOR DYNEIN
REGULATION IN BROAD SPECTRUM NEUROLOGICAL DISEASES

Submitted by

Matthew G. Marzo

Department of Biochemistry and Molecular Biology

In partial fulfillment of the requirements

For the Degree of Doctor of Philosophy

Colorado State University

Fort Collins, Colorado

Spring 2020

Doctoral Committee:

Advisor: Steven M Markus

James R Bamburg

Jennifer DeLuca

Ashok Prasad

Copyright by Matthew George Marzo 2020

All Rights Reserved

ABSTRACT

DYNEIN MUTAGENESIS REVEALS THE MOLECULAR BASIS FOR DYNEIN REGULATION IN BROAD SPECTRUM NEUROLOGICAL DISEASES

Eukaryotic cells rely on cytoskeletal networks to organize materials, transport organelles, give cells shape, and provide locomotion. The cytoskeleton is comprised of many diverse proteins, and three classes of polymeric protein structures are the actin, microtubule, and intermediate filament networks. The microtubule network, and its associated motors, dynein and kinesin, is of interest to the field of neurological disease, due to the prevalence of mutations in the microtubule network in human disease. To better understand the molecular basis for the diseases caused by *de novo* dynein mutations, we performed a screen of mutants using budding yeast dynein. The results from our experiments present a platform for the molecular dissection of dynein mutations which can be readily applied to new mutations or precisely explore known mutations. The screen-based approach allowed us to identify a new mechanism of yeast dynein regulation, which is autoinhibition of the dynein motor. We demonstrate that this mechanism regulates dynein activity in cells and functions to limit *in vivo* motor activity in the cytoplasm. Autoinhibition is regulated by Pac1 in yeast, a Lissencephaly-1 homolog, and we demonstrate that Pac1 operates in the dynein autoinhibition pathway by preventing the “closed” autoinhibited state, thereby promoting “open” dynein. This represents an entirely novel function of Pac1/LIS1, and allows us to further refine our model for cortical offloading. These results also directly dispute previous studies

identifying Pac1 as an inhibitor of dynein motility, and represent a paradigm shift in our understanding of dynein regulation across eukaryotes.

ACKNOWLEDGEMENTS

This thesis work represents not only my contributions, but those of many people both within and outside the lab. I would first like to thank the tireless work of one Jacqueline Griswold, a dedicated and talented scientist. I would like to thank my lab mates, Kari Ecklund, Lindsay Lammers, and Tyler Biebighauser, who turned endless days in a dark room into fun and cherished memories. I would also like to thank my PI, Steven Markus, for his support, tolerance, and mentorship. I am grateful for the support and mentorship of my committee members, Jake DeLuca, Jim Bamburg, and Ashok Prasad, who provided insights, and always empowered me to succeed in the lab. Finally, I want to thank my cohort, and the BMB community at CSU, for being my fam for the last five years. It hasn't always been easy, but being a part of this community has made me a better scientist and a better person.

DEDICATION

*“All that is gold does not glitter,
Not all those who wander are lost;
The old that is strong does not wither,
Deep roots are not reached by the frost.*

*From the ashes a fire shall be woken,
A light from the shadows shall spring;
Renewed shall be blade that was broken,
The crownless again shall be king.”*

–J.R.R. Tolkien. *The Fellowship of the Ring*. 1953.¹

This work is dedicated to all the people who helped me along my journey, and to you, the reader.

¹ J.R.R. Tolkien. *The Fellowship of the Ring*. Ballantine Books, New York. 1993;(10).

TABLE OF CONTENTS

ABSTRACT.....	ii
ACKNOWLEDGEMENTS.....	iii
DEDICATION.....	v
LIST OF TABLES.....	viii
LIST OF FIGURES.....	ix
LIST OF TERMS.....	xi
Chapter 1: Introduction and review of literature.....	1
1.1 Structure and function of dynein motor proteins	3
1.2. Dynein associated proteins and regulation of the motor complex.....	8
1.3. Dynein as a driver of neurological disorders.....	14
1.4. Overview of the findings of this thesis work.....	20
Chapter 2: Dynein mutagenesis reveals the molecular basis for dynein dysfunction in motor neuron disease	
2.1. Introduction.....	26
2.2. Materials and Methods.....	31
2.3. Results.....	40
2.4. Discussion.....	79
2.5. Conclusions and Future Directions.....	89
Chapter 3: Yeast dynein autoinhibition and its implications for dynein motor activity and intracellular targeting	
3.1. Introduction.....	92

3.2. Materials and Methods.....	97
3.3. Results.....	110
3.4. Discussion.....	127
3.5. Conclusions	134
Chapter 4: The dynein regulator Pac1/LIS1 is stabilizes an active dynein conformation	
4.1. Introduction.....	135
4.2. Methods.....	137
4.3. Results.....	137
4.4. Discussion.....	149
4.5. Conclusions and Future Directions.....	156
Chapter 5: Pac1/LIS1: opening the door for dynein motility	
5.1. Introduction.....	158
5.2. LIS1 is a required cytoskeletal protein for neurological function.....	160
5.3. Conserved mechanisms of Pac1/LIS1 regulation of dynein.....	170
5.4. Pac1 and LIS1 demonstrate disparate effects <i>in vitro</i>	174
5.5. Pac/LIS1/nudF relieves dynein autoinhibition to assemble dynein-dynactin.....	179
5.6. Conclusions.....	182
Chapter 6: Conclusions.....	188
Works Cited.....	194
Appendix.....	217

LIST OF TABLES

Table 1.....	91
Table 2.....	91
Table 3.....	187
Table 4.....	192

LIST OF FIGURES

Figure 1.....	24
Figure 2.....	25
Figure 3.....	41
Figure 4.....	45
Figure 5.....	47
Figure 6.....	51
Figure 7.....	54
Figure 8.....	57
Figure 9.....	60
Figure 10.....	61
Figure 11.....	62
Figure 12.....	65
Figure 13.....	67
Figure 14.....	71
Figure 15.....	73
Figure 16.....	77
Figure 17.....	80
Figure 18.....	87
Figure 19.....	111
Figure 20.....	115
Figure 21.....	118

Figure 22.....	120
Figure 23.....	123
Figure 24.....	126
Figure 25.....	139
Figure 26.....	143
Figure 27.....	146
Figure 28.....	148
Figure 29.....	150
Figure 30.....	152
Figure 31.....	184
Figure 32.....	185
Figure 33.....	186

LIST OF TERMS

Yeast protein name	Human protein name
Pac1	LIS1
Nip100	p150 ^{glued}
Jnm1	Dynamitin
Num1	NuMA
Ndl1	Ndel1, NudE, NUDEL
Bik1	CLIP170
Bim1	End binding proteins (EB1, EB3)
Dyn2	Dynein Light Chain (LC8)
Dyn3	Dynein Light Intermediate Chain (DLIC)
Pac11	Dynein Intermediate Chain (DIC)

CHAPTER 1: Introduction and review of literature

The inside of a cell is a chaotic symphony of life. Thousands of different proteins, unique nucleic acid components, and diverse and specialized oligosaccharides and fatty acids, all cooperate *en masse* to coordinate the functions of life. The interplay between these disparate organic molecules makes them more than simply the sum of their parts, and the interplay between them provides the emergent properties of life, as cells grow, divide, thrive, and eventually, perish. To ensure the survival of complex eukaryotic cells, and in turn, the survival of large and complex multicellular organisms, the movement of materials within these eukaryotic cells must be regulated. And in order to generate movement, many cells, especially eukaryotes, rely on the cytoskeleton and its associated molecular machines which work in tandem to crawl, swim, sustain force, stretch, and divide^{1,2,3}. From the humble yeast to dynamic animal cells, the cytoskeleton provides the means for unique and specialized movement through the use of many homologous protein elements.

In higher eukaryotes, dynamic networks of proteinacious polymers called microtubules provide the cell structural support and shape it⁴. The microtubule network is of paramount importance in larger and more specialized cells, as many cellular processes which position organelles, orchestrate cellular division, and transport large materials rely primarily on the microtubule cytoskeletal network to accomplish diverse tasks⁵⁻⁷. While the structures formed by microtubule networks can differ greatly across organisms, and indeed, between different cell types of individual multicellular organisms, the foundational elements for these structures is the same. Dimeric tubulin

subunits composed of an alpha and beta tubulin monomers, can rapidly oligomerize into small, polarized assemblies or into long protofilaments⁸. These protofilaments self-associate and create cylindrical tubes, the so-called microtubule. Both tubulin subunits bind GTP, but only beta tubulin is competent for GTP hydrolysis, and hydrolysis of GTP, and its conversion to GDP give rise to different subunit structures. GTP-bound tubulin is added to the growing end (plus end) of microtubules, which stabilizes the growing end⁸. Upon incorporation in the lattice, and maturation of the microtubule structure, tubulin subunits become strained⁹. This strain stores mechanical energy within the microtubule lattice, which can rapidly trigger depolymerization of the structure, so-called “catastrophe” events. Rapid polymerization of tubulin dimers from the plus ends is punctuated by periods of catastrophe, giving rise to a cytoskeletal network founded on dynamic instability¹⁰. The growing and shrinking of tubulin polymers allows cells to dynamically restructure the internal environment to generate forces in accordance with the changing needs of cells. These otherwise simple tubules are arranged into higher order structures which manifest many unique emergent properties, and provide structure and force for different cell types¹¹.

In addition to their role in cellular organization and force generation, microtubule tracks provide thoroughfares for transport by many diverse molecular motors. While many motor proteins exist in higher eukaryotes, few of these protein complexes are as remarkable as the minus end directed motor, dynein¹. The first dyneins were isolated from axonemes from *Tetrahymena pyriformis*, which provide the ciliary forces for beating^{1,12}; however, cytoplasmic dynein-1 (hereafter referred to as dynein) was isolated and identified (originally as MAP 1C) from calf brain white matter some time after¹³.

Dynein is a massive (>1MDa) protein complex, composed of many individual polypeptide components (Figure 1A)¹⁴. In the kingdoms of animals and fungi, dynein motors are the primary motor associated with retrograde transport along microtubules, which, in most cell types, involves trafficking from the cell periphery to the nucleus, where the minus-end of microtubules are anchored to centrosomes¹⁵. Dynein has been extensively studied since its discovery as a minus-end directed protein due to its myriad cellular roles¹⁶. Dynein-mediated microtubule transport is vital for vesicular trafficking, driving the movement of mRNAs¹⁷, lysosomes¹⁸, mitochondria¹⁹, the Golgi²⁰, and other cellular cargos. Dynein also has extensive roles in regulating mitosis—nuclear envelope breakdown at the G2-M phase transition is facilitated by dynein²¹, and in animal cells, progression through mitosis is known to require dynein²² to attenuate intracellular signaling of mitotic checkpoint proteins. Orientation of the mitotic spindle along the plane of division is driven by dynein motor activity²³ and is important for positioning of cells within tissues. This veritable compendium of activities is a microcosm of the dynein motor itself, which boasts considerable complexity for a motor protein, and has many layers of regulation that modulate dynein function.

1.1. Structure and function of dynein motor proteins

1.1.1. Structure of the cytoplasmic dynein holoenzyme complex

The cytoplasmic dynein-1 complex is a large dimeric holoenzyme, comprised of the catalytic heavy chain, and several non-catalytic accessory chains^{24,25}. Dynein is a AAA (ATPase Associated with various cellular Activities) ATPase, which is highly structurally similar to other hexameric helicases²⁶ but is unique in that the entire catalytic domain (containing 6 AAA motifs) is made of a single polypeptide, rather than

being an oligomer of individual ATP binding modules. Dynein's ATPase domain forms the core catalytic component of the structure²⁷, and by utilizing the energy of ATP hydrolysis, this domain powers the remodeling of the AAA core, which in turn remodels the linker, the dynein mechanical element which spans between the motor and tail domains²⁸. From the ATPase core of the motor spans a coiled-coil domain terminating in a globular microtubule-binding domain^{29,30}. The ATP-dependent remodeling of the AAA core drives the sliding of the coiled-coil domain, which in turn coordinates with the buttress to transduce mechanical signals across the complex³¹. The MTBD can adopt several stable registries, which tune its affinity for the microtubule lattice. Intramolecular interactions within 7 alpha helices provide the mechanical basis for transitioning between these states, as demonstrated through a combination of structural and biochemical studies^{30,32,33}.

The tail domain of dynein is the least conserved of all subdomains among eukaryotes. It is comprised of the N-terminal dimerization domain and a flexible unstructured region, which is responsible for binding accessory chains (the intermediate and light-intermediate chains), dynactin, and other effector proteins³⁴⁻³⁶. Despite the tail domain's size and distance from the motor domain, there is strong evidence that the tail domain directly tunes motor activity^{34,35,36}. However, despite the importance of this region for dynein activity and regulation, many molecular details about protein-protein interactions remain obscured by the difficulties in obtaining atomic resolution of this unstructured flexible region.

The dynein tail domain binds to the intermediate chain (DIC, Pac11 in yeast), and interactions between the tail, intermediate chain, and dynactin or adaptor proteins have

been shown to be important modules for regulating motor activity^{37,38}. The intermediate chain itself binds to the light chains, additional accessory proteins in the dynein motor complex. While three light chains exist in the mammalian complex, TcTEX, Roadblock, and LC8, only a single light chain, Dyn2 (a homolog of LC8) is present in the *S. cerevisiae* complex³⁹. A third accessory component, the light-intermediate chain, binds to dynein closer to the motor domain than the intermediate chain, and this protein has been implicated in stabilizing the heavy chain⁴⁰. These different classes of accessory chain have been shown to have important roles as chaperones, and one proposed function of these components is to stabilize dynein during translation and protein folding and studies in yeast have shown that Pac11 and Dyn2 are important for dimerization and maintaining dynein protein levels in the cell³⁹. Additionally, many isoforms of dynein accessory chains exist which are differentially spliced, and are potentially targets for tissue specific PTMs⁴⁰. One of the most well studied examples of this phenomenon is the IC2a, the neuronal specific isoform of the intermediate chain which has been shown to exhibit isoform-specific interactions with dynein effectors⁴¹.

1.1.2. Mechanochemistry of the dynein motor domain

Dynein mechanochemistry is complex and involves a number of important structural changes at key subdomains, and mutation of key amino acids in these subdomains is sufficient to disrupt normal mechanical signaling across the protein complex. The study of dynein in diverse organisms has given the field an appreciation for the similarities between the mechanochemistry of different dynein isoforms. The current model for dynein mechanical remodeling and its ATPase cycle relies on the synthesis of different X-ray crystal structures from yeast, human cytoplasmic dynein-2,

and dynein from the slime mold *Dictyostelium discooidium* to produce a clear picture of dynein's conformational changes between the no nucleotide, ATP, ADP-P_i, and ADP conformation⁴²⁻⁴⁶. In the no nucleotide state, the dynein AAA ring is in an "open" conformation²⁵, with openings between the AAA1 small subdomain and AAA2 large subdomain⁴³, and the MTBD is in a high microtubule-affinity state. This is in contrast to the mechanochemistry of kinesin-1, which is in the high microtubule-affinity conformation when ATP is bound to its motor head⁴⁷. Upon ATP binding to AAA1 Walker A motif, AAA1 module closes around the ATP bringing the AAA1 small subdomain into contact with AAA2 large subdomain, which drives conformational changes in the AAA ring. These changes primarily entail the major AAA folds of the AAA2, AAA3 and AAA4 coming closer together, which causes the overall structure of the ring to be more compact³¹. This remodeling of AAA1-4, in turn, causes changes in the registry of the coiled-coil stalk⁴⁴. There is evidence in yeast dynein that communication between AAA1 and the coiled-coil stalk is itself gated by the nucleotide state of AAA3. Studies using purified yeast dynein have demonstrated that ADP or ADP-P_i bound to AAA3 allow communication across the AAA+ ring, but not when ATP is bound at AAA3⁴⁸. This AAA3 site is present in human cytoplasmic dynein-1, but in cytoplasmic dynein-2 (intraflagellar transport dynein) the motor lacks the Walker B motif needed for ATP hydrolysis⁴⁹, which may indicate this is a conserved mechanism to regulate cytoplasmic dyneins but not intraflagellar transport dyneins. Evidence that dynein's AAA3 nucleotide state differentially regulates allosteric communication across the ring adds a further level of regulation to dynein motor activity, which may be important when switching between high-load and low-load cargo requirements⁴⁸.

The changing of the registry of the coiled-coil stalk in turn changes the conformation of the buttress domain, which in turn changes the MTBD from a high-affinity to low-affinity state, a transition mediated by extensive intramolecular contacts within the seven alpha helices within the MTBD^{25,30}. The MTBD is now able to unbind from the microtubule, and is positioned above an adjacent tubulin dimer. At this stage, the dynein MTBD begins a stochastic search for nearby binding sites between alpha- and beta-tubulin, a binding site which it shares with many conventional kinesins⁵¹. Subsequent hydrolysis of ATP to ADP-Pi initiates a rigid body movement of the AAA5 and AAA6 domains to contact AAA1, giving the ring a final, “closed” conformation, with a substantially smaller hole at the center of the AAA ring than is present in the open conformation^{36,37}. Closure of the ring causes a steric clash between the ring and linker element, which forces the linker to move from its docking site at AAA5 on the ring⁵⁰. The linker has been demonstrated to favor two major conformations: a straight conformation which is present when the linker is docked at AAA5; or a bent conformation, in which this domain is “cocked” at a 90⁰ angle from its resting state and perpendicular to the stalk^{27,28}. After a stochastic search, the weak affinity MTBD contacts a new binding site, and switches from a low- to high-affinity state. The release of inorganic phosphate from AAA1 occurs upon rebinding of the microtubule^{25,52}. This rebinding reverses the allosteric changes in the coiled-coil and subsequently the AAA ring. This allows the linker to swing forward (the “powerstroke”) and return to its docking site on the AAA ring, driving the motion of the motor^{53,54}. After the linker swing, dynein is in a post-powerstroke state with the MTBD in the high affinity state and ADP is bound in AAA1.

Having completed the mechanochemical cycle, dynein can now release ADP and rebind ATP, beginning the cycle anew.

Dynein's mechanochemical cycle shares several key distinctions from the kinesin mechanochemical cycle. Firstly, dynein stepping and processive movement are stochastic, and motor heads are not coordinated while walking^{53,54}. Experiments with yeast dynein have demonstrated that the vector of linker swinging is a major determinant of the directionality of motor movement, and that perturbing this motion changes dynein's directionality⁵². This has also been shown in studies analyzing dynein's movement about the microtubule lattice, as dynein moves helically about the microtubule, stochastically switching between left- and right-handed helical pitch independent of the twisting of the microtubule lattice⁵⁵. This method of dynein locomotion has been coined by many in the field as the "drunken sailor" mode of walking, and this is may be part of why dynein is much more effective at navigating obstacles on the microtubule lattice than kinesins, which walk hand-over-hand along a single microtubule protofilament⁵⁵. This stochastic stepping mechanism also means dynein is able to take backwards steps and change tracks during processive runs^{54,56}, further setting it apart from its kinesin counterpart^{56,57}.

1.2. Dynein associated proteins and regulation of the motor complex

1.2.1. Dynactin and adaptor proteins

The heavy and accessory chains of the dynein complex make up the core catalytic subunit of a motile complex. Still, dynein relies on a wider arsenal of protein complexes as cofactors to effect motility and to sustain productive forces within cells. Many cofactors have also been shown to be essential for dynein recruitment to sites of

activity in cells, including dynactin and adaptor (or effector) proteins¹⁶. Dynactin is the most well-characterized effector of dynein activity in cells, and is itself a large (>1 MDa) protein complex comprised of 23 proteins in mammals^{18,58-60}. This complex is assembled from an actin-like filament comprised of several ARP1 proteins along with a single Beta actin monomer. This minifilament is capped at the “barbed” end by CapZA/B proteins, and at the pointed end by the ARP10 subunit and the p25, p27, and p62 subunits⁶¹. These proteins have roles in both scaffolding dynein and changing its motility during cargo transport^{61,62}. This remarkable combination of actin and microtubule cytoskeletal elements serve many purposes. Dynein tail domains may bind along the helical pitch of this pseudo-actin filament, which has the effect to position and separate the tail domains in the motor by ~2 nm, positioning the motor domains in a configuration conducive to processive motion⁶³. Four copies of p50 (dynamitin, so named for the overexpression phenotype of “blowing up” dynein complexes in cells⁶⁴) and two p24/22 subunits bind the actin minifilament forming the “shoulder” of the complex⁶¹. Binding to this shoulder are two copies of the p150^{glued} protein, a long coiled-coil that terminates in a CAP-GLY microtubule-binding domain^{61,65}. This domain has been shown to be important for targeting of dynein to microtubules to initiate transport⁶⁶, as well as having a number of biologically important splicing isoforms⁶⁷ and moonlighting as a MAP⁶⁸. The p150 microtubule-binding domain has further been shown to be important to initiate transport along axons, and tubulin tryrosination has been shown to be necessary for this domain to initiate transport⁶⁹. Dynactin serves as an important regulator of dynein motility in cells, and is important for recruitment of dynein to sites of activities in all organisms⁷⁰⁻⁷². The conserved mechanism of

recruitment of dynein to the cell cortex requires dynactin, and dynactin is therefore required for dynein-mediated positioning of the mitotic spindle⁷³.

The yeast dynactin complex is highly similar to its mammalian counterpart⁷⁴⁻⁷⁶, in that the main structural component is an actin minifilament composed of the actin related protein ARP1, with the pointed end bound to another actin related protein, ARP11^{77,78}. At the barbed end of the filament, the dynamitin homolog Jnm1 binds to the top of the ARP1 filament⁷⁹, and finally, the p150^{glued} homolog in yeast, NIP100⁸⁰. Just as in higher eukaryotes, Nip100 has a CAP-GLY domain and predicted microtubule binding affinity, which studies suggest may assist dynein in force production during nuclear migration⁸¹. Most of our current understanding of yeast dynactin comes from genetic studies which systematically assigned the interactome of dynactin components. Purification of high purity, intact yeast dynactin complexes has eluded researchers, and no structural data exists for the yeast dynactin complex. While highly similar to mammalian dynactin, it is possible that the yeast dynactin complex has different requirements for assembly. Dynactin in many eukaryotes has been demonstrated to directly interact with dynein and track polymerizing microtubules⁸². However, plus-end dynein-dynactin (in yeast or human) is strangely immobile, and does not initiate minus-end directed motility^{83,84}. To initiate processive movement, dynein-dynactin must bind a coiled-coil adaptor protein⁸⁵. In both yeast or mammals, these complete dynein-dynactin-adaptor complexes are necessary for fully functional dynein activity *in vivo*.

The third component of the dynein machinery is the adaptor (or effector) protein, which confers cargo specificity to the dynein-dynactin complex which allows the single isoform of dynein to perform distinct cellular functions^{16,86-87}. These proteins are

characteristically a single polypeptide, with the most common feature a coiled-coil region that forms a highly stable tripartite complex with dynein-dynactin^{61,88}. However, in yeast, only a single adaptor exists, Num1⁸⁹, which is homologous to the mammalian Nuclear positioning Mitotic Apparatus (NuMA), which links dynein-dynactin to the cell cortex⁹⁰. Num1 in yeast is similar to mammalian NuMA, with differences in their linkages to the cell cortex—Num1 is linked through an PH domain directly to PIP_{4,5} lipids⁹¹, whereas NuMA is linked to the cell cortex by interactions with the proteins Gai and LGN⁹². The coiled-coil region of Num1, which binds dynein-dynactin, is sufficient to activate processive dynein motility along astral microtubules when expressed in cells⁸⁵.

It has been shown recently that adaptor-specific interactions can leverage the dynein-dynactin complex to perform different tasks, and strikingly, some adaptors allow two dynein dimers to bind dynactin simultaneously^{93,94}. Binding two dynein dimers to a single dynactin has been shown to increase the speed and force generation of mammalian dynein complexes^{94,97}, but it was unclear prior to this thesis work if a similar process occurs with yeast dynein-dynactin-Num1 complexes, or indeed, for the mammalian NuMA adaptor which has not been studied *in vitro*. It has been shown that dynactin and adaptor proteins are necessary cofactors to effect processive dynein motility for the mammalian complex *in vitro*^{86,87,94,95}; however, dynactin is dispensable for processive motility of the yeast complex. It is unclear still whether yeast dynactin may also position the motor heads of yeast dynein. However, preliminary data from our laboratory suggests that these activities may be conserved by yeast dynactin and the adaptor Num1/NuMA.

1.2.2. Plus end targeting and microtubule surfing

A number of other microtubule-associated proteins (MAPs) and plus end tracking proteins (+ tips) interact with dynein complexes. One group of MAPs of particular interest in dynein research is the plus end complex, which targets dynein-dynactin to microtubule plus ends and maintains these proteins in an inactive state, prior to offloading to adaptor proteins. The yeast/mammalian microtubule plus-end targeting apparatus consists of: Bim1/EB1, Bik1/CLIP-170, Pac1/Lis1, dynein and dynactin (FIGURE 1). It has been demonstrated in cell biological assays^{84,98,99} and biochemical reconstitution^{95,96} that this complex is responsible for targeting dynein-dynactin to the plus ends of microtubules, where they may be offloaded to adaptor protein receptors. This large plus end targeting complex allows dynein to “surf” along the growing and shrinking microtubule plus end, and prevents dynein from diffusing back into the cytoplasm. Within this cadre of proteins, distinct sub-complexes exist^{95,96}. The microtubule binding function of Bim1 enhances plus-end tracking, but is not strictly required for plus end association of dynein in yeast⁸⁴. Bik1-Pac1-dynein complexes (yeast)^{100,101}, and dynein-CIP170-LIS1¹⁰² complexes as well as dynein-dynein-dynactin complexes (mammals), may track microtubules⁹⁵. The likely function of this complex is to maintain dynein at the plus-end where it is primed for processive movement towards the minus end, upon delivery to cortical sites. However, the mechanisms which prevent dynein from moving away from the plus-end are unclear, but one hypothesis is that dynein is maintained at the plus ends in a conformation where microtubule interaction by the dynein MTBD is limited. It is also possible that the high valence of these protein-protein interactions contributes sufficient force to counteract dynein processive motility

away from the plus end. Bik1/CLIP170 has been shown to track with end-binding proteins such as the end-binding protein family of tip trackers, and this protein may bind microtubules independently of dynein or Pac1¹⁰⁰. Surfing of Bik1/Pac1/dynein along microtubules is important to cortically anchor dynein at Num1/NuMA, and this process has been shown to be mechanistically very similar between yeast and animals^{98,99,103}. The tripartite interaction between Bik1/Pac1/dynein also appears highly conserved; loss of either Pac1 or Bik1 causes a drastic reduction in plus end targeting of dynein to the cell cortex in yeast and *C. elegans*, and the mammalian kinetochore¹⁰²⁻¹⁰⁴. This Bik1-Pac1-dynein complex appears wholly conserved, and serves as a minimal complex for targeting dynein to microtubules and to regulate its activity.

Despite the homology of Pac1 and LIS1 in cell biological experiments, these proteins previously appeared to have conflicting roles experimentally. It was shown that Pac1 decreases the velocity of dynein in single-molecule assays^{101,105-107} and that LIS1 reduces mammalian dynein velocity in a dose-dependent fashion in ensemble microtubule gliding assays^{96,108}. However, Pac1 is also required for dynein activity in yeast cells^{99,109}, and LIS1 increases dynein-dynactin association in animal models¹¹⁰. Furthermore, LIS1 has no effect⁹⁵ or increases velocity^{96,111} of dynein-dynactin-BicD2 in single molecule assays. It was unclear if many distinct mechanisms of LIS1 existed, or if Pac1 was simply a different effector in yeast systems. While it is reasonable to expect a yeast and mammalian homolog may have different functions, these conflicting data represent fundamentally incompatible mechanisms of action of LIS1. Furthermore, the filamentous fungus, *Aspergillus nidulans* homolog, nudF, has demonstrated many similar roles to its mammalian and yeast counterparts¹¹². This protein is necessary to

localize dynein to microtubules^{113,114}, loss of nudF prevents initiation of transport of dynein along microtubules. These activities are much in line with Pac1/LIS1 in other organisms, and perhaps indicate deficiencies in studying these proteins *in vitro*.

1.3. Dynein as a driver of neurological disorders

1.3.1. Dynein motors and neurological development

Due to its immense complexity and its many levels of regulation, dynein activity in a cell must be kept in a delicate balance. In large cells, where microtubule based transport is the primary mode of transport for many long-distance processes, dynein drives most retrograde transport. This process is extremely important in motor neurons, where axons can reach up to 1 meter in length¹²¹, which dynein must amazingly traverse using 16nm steps, in an odyssey that can take as long as days for fast axonal transport, and as slow as a year for some modes of slow axonal transport¹¹⁷. The flux of dynein and kinesin trafficking must be carefully regulated to maintain homeostasis¹¹⁸, and minor perturbations to these proteins' structures introduced by *de novo* mutation can have severe consequences^{119,120}. Local synthesis of dynein and kinesin components along the axonal endoplasmic reticulum has also been shown to be important to maintain the homeostatic balance of antero- and retrograde transport along long axons^{121,122}. At synapses, dynein is responsible for the trafficking of proteins from the cell surface back to the soma and nucleus, including postsynaptic receptors^{123,124}. In this way, dynein is able to transmit biochemical signals from axonal afferents to generate long-term responses to stimuli by downstream remodeling of synaptic receptors. The interaction of these long range microtubule transport phenomena with short range actin transport is unknown, but some evidence suggests cargos may be

handed off from MT motors to the actin cytoskeleton for localization in small compartments found in dendritic boutons.

The establishment of neuronal processes has been demonstrated to be itself a dynein-mediated process. Dynein and kinesin transport pre-assembled microtubule filaments from the soma to developing neurites¹²⁶, and while the mechanisms governing these process are poorly understood, the establishment of unipolar axons and multipolar dendrites requires the interplay of dynein and kinesin transport modules^{84,116,118}. Axonal specification may be a dynein and kinesin driven process as well¹²⁷, and the dynamic interplay between these motors helps newly developing neural cells reach out into surrounding extracellular environment^{121,127}. The maintenance of these structures require the coordination of dynein motors, both for transport of cargos and for organizing microtubules¹²⁹⁻¹³¹. Accordingly, the axon growth cone is highly enriched in dynein, dynactin, and kinesin^{69,116}.

In addition to its roles in trafficking, dynein activity is essential to position the mitotic spindle along the plane of cell division which is vitally important for the development of tissue layers^{131,132}. Dynein, kinesin, and myosin all cooperate in the long-range transport of nuclei, which is an important step in the development of the mammalian brain cortex. During the primary stage of neocortical development of neurons, pluripotent stem cells within the subventricular zone (SVZ) called radial glial precursor cells are responsible for forming layers of the cortex¹³³⁻¹³⁵. The nuclei of these cells are kept in a continuously renewing state by a complex gradient of molecular signals which are asymmetrically localized within the large intracellular space. Activation of kinesin-1 initiates the movement of nuclei from the basal lumen of the SVZ to the

apical surface of the ventricular zone (VZ), where the waxing gradient of pro-mitotic cytokines induces cells to undergo cell division¹³¹⁻¹³³. After cell division, pulling forces from actin-myosin cables and dynein forces on the nuclear-anchored centrosome move the nucleus back to the basal surface, where cytokines maintain the stem cell nucleus in a pluripotent state. One important aspect of this process is that the migration of the nucleus is preceded by the movement of the centrosome, and long microtubules emanating from the centrosome arranged in a parallel configuration provide the tracks for dynein movement¹³². The asymmetric localization of different mitotic factors is carefully maintained in these cell types to allow for rapid cell proliferation, and to maintain the integrity of the stem cell pool. The movement of nuclei in this process has been termed interkinetic nuclear migration (INM)¹³⁵, and is vital for the production of neurons along the VZ¹³⁶. Recruitment of the dynein arm of the microtubule motor assembly has been shown to be mediated by various dynein effectors including LIS1¹³⁷ and BicD2, which has itself been shown to be recruited through small GTPase activity in the RanBP2/RAB6 pathway¹³⁸. Loss of dynein motor activity during this process through mutations to the motor or ectopic disruption of dynein-effector interaction is sufficient to decrease proliferation of cells and migration away from the ventricular zone to the cortex^{139,140}.

It is therefore unsurprising that spontaneous *de novo* mutations in many microtubule-associated proteins, namely kinesin, tubulin, dynein and LIS1 (named for its role in the lissencephaly disorder), have been demonstrated to have profound effects on the proper formation of cortical layers^{119,140-143}. Development of the many distinct cortical layers of the brain is a delicate and highly dynamic process, and minor

deficiencies in protein function would be expected to have dramatic changes for proper development. However, it can be appreciated through the phenotypic consequences of even single dominant-negative dynein mutations that even minor perturbations to established mechanisms of cytoskeletal construction have deleterious effects on the health of complex organs and organisms^{119,143-151}. Interestingly, while mutations affecting dynein-driven processes have been shown to affect the establishment of cortical layers in the developing brain, these same mutations do not present similarly obvious or potent defects in cardiac tissue, or elsewhere in tissues that require polarity. This opens up the possibility that some mutations will cause phenotypes that have specificity to tissue types, or that other genetic factors are able to compensate for dynein functions in other tissues. Control of the kinesin and dynein cytoskeletal components in neural cells is aided by a number of neuronal specific MAPs, which allow different cellular compartments to limit, or enhance motor activities^{152,153}. The selectivity of different motor isoforms and myriad of neuron-specific regulatory proteins may also explain the neuronal specificity of certain *de novo* point mutations, or why the patient symptoms are much more severe in neuronal tissues.

1.3.2. Understanding how dynein mutations cause neurological disorders

(dyneinopathies)

Historically, our understanding for how mutations in dynein drive motor neuron diseases and other neuropathies have come from work done using mouse models of dynein. These models relied on generation of mutants by chemogenic methods and mutations were introduced randomly into the dynein tail domain. The importance of dynein as a driver of disease, outside of severe cases such as lissencephaly, was truly

not appreciated until the advent of whole-exome sequencing as a tool to identify *de novo* point mutations¹⁴³⁻¹⁵¹. Since the 2010s, dozens of mutations in dynein have been identified by whole exome sequencing as primary effectors of a spectrum of motor neuron diseases and developmental disorders, referred to here as dyneinopathies. The mutations span the entire heavy chain (Fig. 2), and there existed no clear correlation (prior to the start of this thesis) between mutant identity and disease state. As work with mouse models have shown, hemizygotes for dynein were viable and presented no obvious phenotypes at early developmental stages¹⁵⁵. However, even single base pair changes in the mutant dynein mouse models (referred to as *loa*, *cra*, and *swa*¹⁵⁴) demonstrated severe phenotypes. Therefore, mutations identified in the host of human patients must be behaving in a dominant-negative fashion, and indeed, individuals are primarily heterozygous for dynein mutations. Furthermore, familial cases of where homozygous mutations accumulate result in very severe phenotypes. However, heterozygous patients may vary dramatically in disease presentation, age of onset, rate of disease progression, and quality of life.

Several major classes of neuropathies derive from dynein mutations, but they are primarily represented by (1) motor neuron disorders and (2) developmental disorders. Motor neuron disorders include Spinal Muscular Atrophy with Lower Extremity Deformity (SMA-LED), Charcot-Marie-Tooth disease, and congenital muscular dystrophy. In many of these cases, the age of onset is childhood, and many developmental abnormalities may persist such as talipes, scoliosis, and cranial-facial malformation. In most of these motor neuron disorders and muscular dystrophies, slow muscular development is typically followed by muscular and neuronal degeneration in the peripheral nervous

system, which persists into adulthood. These symptoms are reminiscent of neurological disorders caused by protein aggregation, which is an anticipated consequence of disrupting homeostatic balance of axonal transport. Outside of gross physiological deficits, affected patients also suffer from impaired coordination, and in some cases slowed cognitive development^{143,145}. Despite many difficulties associated with these disorders, initial formation of much of the nervous system is sufficient for mostly normal development in most tissues of the body, and these disorders are rarely fatal to individuals at young ages. This would imply that dynein function is impaired very subtly by the mutations, as many dynein-dependent processes such as neuronal migration and neurite outgrowth are seemingly unperturbed in initial stages of development. However, as symptoms persist over time and get progressively more severe, this would further imply that these mutations do have negative consequences which compound over long periods of time.

The second major class of dyneinopathies is developmental disorders, in many cases clinically referred to as malformations of cortical development (MCD)¹⁴⁴. While many muscular dystrophy related diseases present symptoms of impaired development of the peripheral nervous system, MCD disorders grossly affect the development of the central nervous system. Microcephaly, polymicrogyration of cortical layers, and loss of cerebellar development have been observed in many instances of dynein mutation. These diseases in most instances lead to severe loss of cognitive function^{144,145,149} and are typically fatal in the long-term. While muscular atrophy is not typically observed in these patients, the initial severity of the disorder and the typically fatal diagnoses may be preventing the identification of further symptoms. As MCD disorders are evident *in*

utero, it is likely that these mutations are interfering with a number of important dynein functions such as interkinetic nuclear migration. Furthermore, it is possible both gain- and loss-of-function of dynein could be equally important for disrupting normal cortical layers, as the timing of neurological development is precisely timed with cellular migration and extracellular signaling^{137-139,161}. Overall loss of dynein activity would be expected to drive phenotypes such as Lissencephaly, in which proliferation and gyration of cortical layers is nearly non-existent^{141,159}.

1.4. Overview of the findings of this thesis work

With so many complex roles to play on the cellular stage, understanding how mutations affect the dynein complex *in vivo* are difficult. To this end, we have established a system for assessing disease-correlated phenotypes using budding yeast dynein, which simplifies both *in vivo* and *in vitro* assessment of dynein activity. Cellular yeast dynein activity relies on many of the same factors as human dynein for activity, including Bik1, Pac1/LIS1, dynactin, and the coiled-coil effector Num1. While this system does not recapitulate the complicated cellular activities of dynein in neurons, it is ideally suited to answer biological questions at the molecular level regarding dynein motility, force production and nuclear movement, plus-end targeting, and mitotic spindle positioning. The advantages of yeast cell biology are further complemented by the advantages of *in vitro* assays using yeast dynein, which is processive in single-molecule experiments without the need for dynactin or adaptors which mammalian dynein requires¹⁶⁰. Yeast dynein is an excellent biochemical model whose properties can be studied through varied microtubule (and other proteins) binding assays, and ATPase assays¹⁶³, more readily than its mammalian counterparts.

This thesis work will first focus on the dynein motor, and how *de novo* mutations affect protein's mechanochemistry and regulation at the molecular level. Prior to the start of this thesis work, dozens of mutations in the dynein heavy chain were identified as dominant negative drivers of a diverse spectrum of muscular dystrophy and neurological diseases^{119,143-151}. However, prior to this work very little was known about how dynein mutations caused such motor neuropathies, outside of work done in classical mouse models generated by random mutagenesis. The *swa*, *cra*, and *loa* models provided much of the initial biological data on phenotypic consequences at the organism level¹⁵⁴, but little biochemical data was available for mutations corresponding to human disease states¹⁴⁶. The initial goal of this research was to use the advantages of yeast dynein to assess how seventeen different mutations from human disease states could drive dysfunction.

However, during the course of this thesis work, another study was published investigating the effects of disease correlated mutations on dynein function using human proteins¹⁶⁴. While initially disheartening, this study provided solid confirmation of our data from yeast, and did not provide any *in vivo* data on the effects of mutations. Importantly, the findings of both studies were highly congruent, and allow us to better understand the possible cellular consequences dynein mutations have for an individual. Finally, using the high-throughput nature of yeast biology we wished to find ways to rescue mutant phenotypes, either through pharmacological action or through engineering in compensatory mutations. This approach is ideal for our yeast system but presents significant difficulties to perform in mammalian systems, which we believe gives our yeast system a key advantage.

As fortune would have it, one of the mutations identified in this study was a key residue regulating dynein motor activity. In 2017, a seminal finding¹⁶⁵ from the field emerged that dynein is maintained in an autoinhibited conformation in the cytoplasm, and that this autoinhibited state is necessary for normal cellular function. This work further identified several key amino acids which stabilize this autoinhibited conformation, and to our surprise, one of these stabilizing residues was identified as driving phenotypes in our yeast screen. This led to our discovery that yeast dynein is autoinhibited using near-identical residues to human dynein, and we now believe that this represents an evolutionarily conserved mechanism unique to nearly all isoforms of cytoplasmic dynein-1.

Finally, this discovery was also integral to our understanding how a key dynein regulator, Pac1, activates dynein for motility. Elucidating the mechanism of Pac1/LIS1 activity has been a major focus of this doctoral research, and doing so required challenging a number of previously published experiments¹⁰⁴⁻¹⁰⁸. These experiments allowed us to determine a novel mechanism for Pac1 regulation of dynein, whereby Pac1 binding to the open, uninhibited dynein stabilizes this open conformation of the motor and coordinates its localization. These results directly contradict past experiments, which have proposed that Pac1 is an inhibitor of yeast dynein. However, our results have dove-tailed beautifully with several other lines of research in the field that demonstrate binding of LIS1/nudF has an identical role in maintaining dynein in the open state¹⁶⁵⁻¹⁶⁹. This mechanism explains why dynein-dynactin complex formation and activity is enhanced by Lis1, and why yeast dynein requires Pac1 to form the dynein-dynactin-Num1 complex. This understanding has allowed us to revise our model for

dynein offloading in yeast, and propose a mechanism for dynein activation which is conserved across Eukaryotes¹⁰³.

The findings of this doctoral research will be presented in three sections. Initially, the methodology and the results of our mutagenesis screen of disease-correlated dynein point mutants will be presented, followed by subsequent experiments that followed as natural avenues of reasoning pursuant to these data. Secondly, the results of the investigation of dynein autoinhibition and the role of Pac1/LIS1 in regulating autoinhibition will be presented, as well as data challenging the current model for how Pac1/LIS1 function to regulate dynein activity. Finally, a review of Pac1/LIS1 in the literature will be presented synthesizing the past work on these proteins toward building a synergistic model for this protein's function in regulating dynein activity.

Figure 1

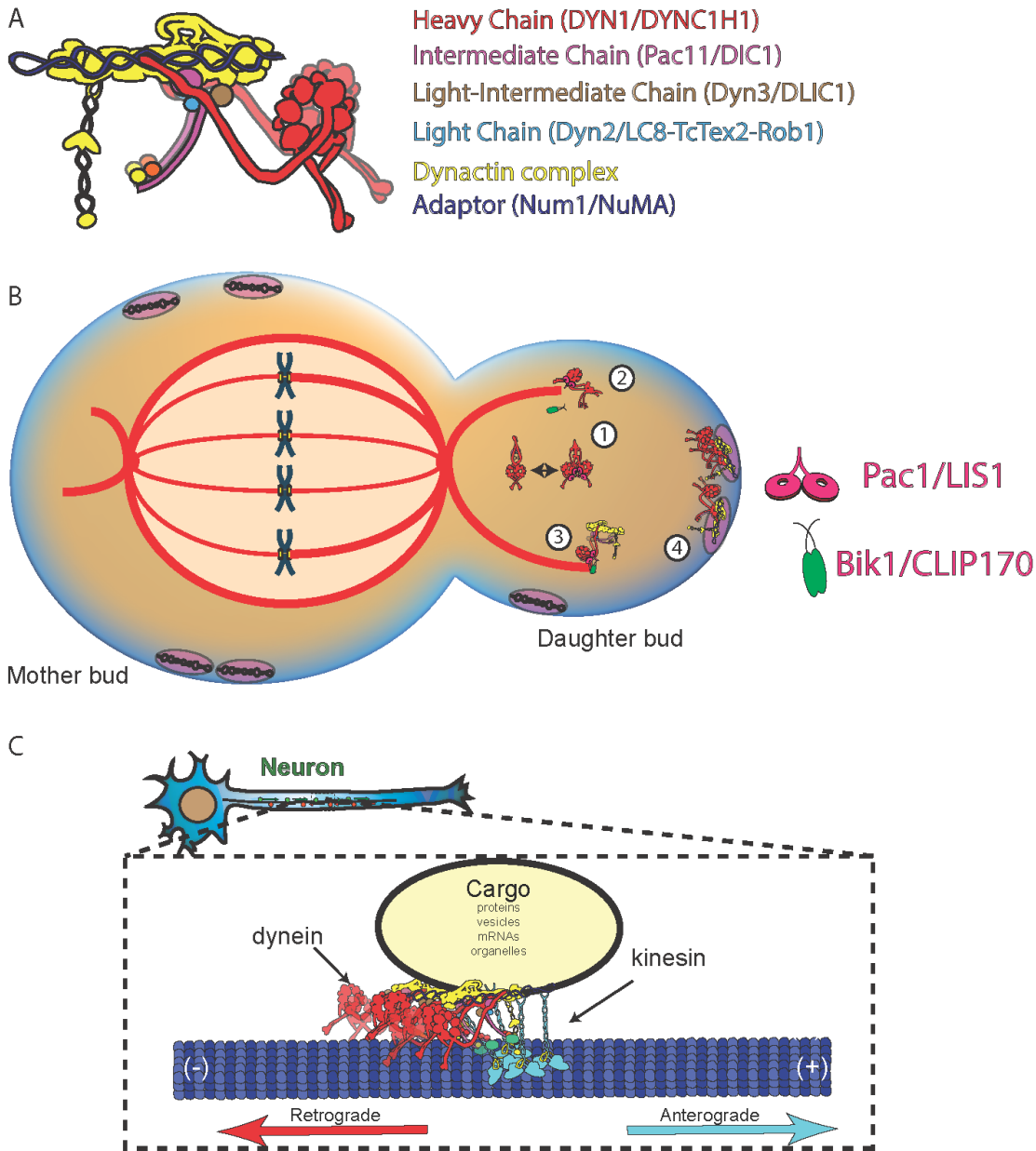


Figure 1. Structure and function of cytoplasmic dynein (A) Schematic of the dynein-dynactin-adaptor complex. The various heavy and accessory chains are indicated with both yeast and human gene names, respectively. The adaptor complex leverages the affinity between the dynactin (yellow) and dynein complexes, which allows them to bind in a way conducive to processive motility. (B) Budding yeast offloads dynein prior to mitosis sequentially. First, dynein samples open and autoinhibited conformations, until the open conformation is stabilized by Pac1. Second, Pac1-dynein binds to Bik1 along astral microtubules. Third, dynein-Pac1-Bik1-Bim1 bind dynactin at the plus end. Fourth and finally, dynein-dynactin bind cortically anchored patches of Num1. (C) Dynein functions in diverse roles in higher eukaryotes, including nuclear transport, various important intracellular trafficking roles (such as in axonal transport) and several important mitotic functions.

Figure 2

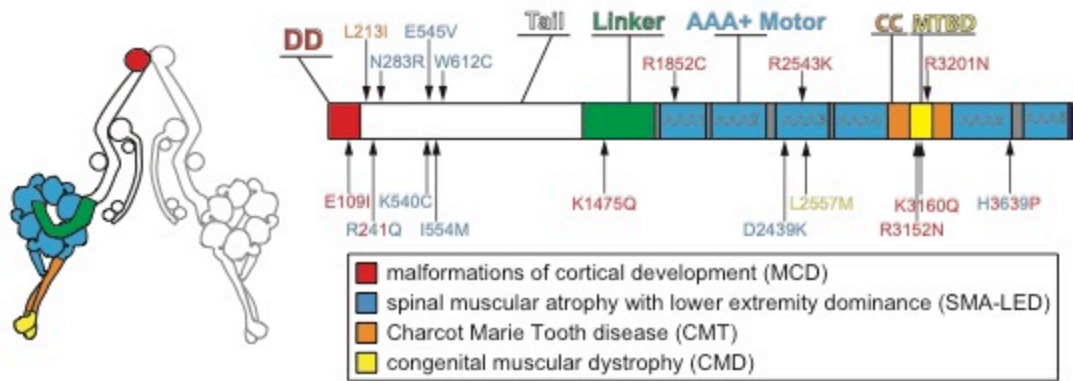


Figure 2. Schematic of dynein heavy chain and mutation assignment (A) Color-coded cartoon representation of the full-length dynein complex (left; with associated accessory chains; Dyn2, dynein light chain; Dyn3, dynein light-intermediate chain; Pac11, dynein intermediate chain; Dyn1, dynein heavy chain), and a linear schematic of Dyn1 with indicated disease-correlated mutations (right; DD, dimerization domain; CC, coiled-coil; MTBD, microtubule-binding domain). The equivalent human residues and disease-correlated substitutions are indicated in parentheses for each residue. ‡Note that we mistakenly substituted an asparagine for residue R3201 instead of a glutamine, the latter of which was identified as correlating with MCD. R3201N was used throughout this study.

CHAPTER 2: Dynein mutagenesis reveals the molecular basis for dynein dysfunction in motor neuron disease

2.1. Introduction

Dynein is the primary motor associated with the majority of retrograde transport along microtubule networks in mammals. In its role as a motor protein dynein is necessary for important vesicular microtubule transport functions in all cell types, and for regulating large-scale microtubule networks^{19,35,126}. These functions are of special importance in axons, where a single unipolar microtubule array is established upon axon specification^{116,118}, which means dynein is responsible for nearly all microtubule transport from the axon tip back to the soma. As axons can reach lengths of microns to hundreds of millimeters¹¹⁷, and dynein moves primarily using 8-16 nm steps^{97,167}, slow axonal transport processes can take weeks to even months¹¹⁶, making high fidelity transport and coordination of motor processes extremely important to establishing and maintaining homeostasis within neurons. Beyond its roles in transport, dynein and kinesins are important for the establishment of microtubule arrays in axons and dendrites¹²⁴⁻¹²⁶. Various studies have demonstrated that ensemble force generation by teams of kinesins, dyneins and myosins are responsible for moving nuclei during interkinetic nuclear migration, a process that establishes cortical layers of the neocortex and is necessary to generate a sufficient number of differentiated cells for brain development¹³³⁻¹³⁵. Finally, dynein and several of its cofactors is necessary for neuronal migration activities^{137,138} during brain development.

Owing to its importance in neuronal health, defects in dynein introduced by mutation can have deleterious effects on cellular and organismal health. It has been determined from sequencing of patients that over 40 distinct point mutations in the dynein heavy chain are major drivers of neurological diseases, especially muscular dystrophy related diseases, and that even greater numbers of mutations exist in associated microtubule associated proteins¹⁴³⁻¹⁵¹. Mutations are almost exclusively missense, dominant-negative, *and de novo* mutations, with a few mutations originating from familial inheritance¹¹⁹. The symptoms of these various muscular dystrophy related dyneinopathies usually vary in symptom presentation and in age of onset from patient to patient. Quizzically, a single mutation may produce distinct symptoms in patients of different genetic backgrounds. A major effort of ongoing research is aimed at the study and treatment of similar diseases, such as Duchenne's muscular dystrophy¹⁷⁰.

Currently, the use of mammalian cell culture techniques is limited in its individually investigate and assess the molecular consequences of a single dynein mutation, let alone the dozens of mutations found in disparate human disease states. Dynein is required for cell viability, so complete loss of function mutations may be lethal to cells in culture, which would preclude study of such a mutation. Dynein performs myriad tasks within mammalian cells, from mitotic functions, to organelle positioning, to interphase cargo transport, which potentially makes assessment of mutation phenotypes confounding. A number of the human mutations can have subtle effects at the level of the individual, and such small (but incremental changes) in a whole organism would likely translate to subtle defects at the cellular level. What is more, dynein isoforms^{40,41} and adaptors^{16,171} can be different between different cell types in

mammals, which could lead to no observable phenotypes in commonly used *in vitro* cell lines, such as HeLa and HEK293 cells. Therefore, it is not clear if all mutations would evoke the same phenotype in *in vitro* mammalian cell culture that they do in the context of highly specialized cortical neurons. Furthermore, expression of dynein in mammalian cells has not been achieved using the simpler and more traditional means of plasmid gene delivery. Successful endogenous expression of tagged or mutant dynein isoforms can only be achieved using bacterial artificial chromosomes¹⁶⁵ (BACs), CRISPR/Cas9 targeting of the endogenous dynein locus, though one HeLa cell line stably expressing the wild type dynein-GFP does exist¹⁷². Since both techniques are difficult and time-consuming, performing an assessment of dynein mutant function in mammalian cells remains challenging.

For these various reasons, achieving a systemic understanding of how the intracellular environments of higher eukaryotes are perturbed by single dynein mutations is a difficult undertaking. To circumvent difficulties that arise from studying the processes of pluripotent proteins, researchers have historically turned to simpler eukaryotic systems, such as *S. cerevisiae*, to understand basic mechanisms of cellular regulation and protein mechanics. Yeast dynein has been studied at great lengths to understand better its mammalian counterpart, and much of what we know of dynein mechanochemistry was learned from humble budding yeast. Studies have demonstrated that dynein has only a single known microtubule transport function in yeast, the positioning of the mitotic spindle prior to anaphase^{22,108}. This function relies on many of the same essential cofactors and therefore presents an ideal system for study basic mechanisms of dynein mitotic spindle positioning and nuclear

migration^{72,84,85}. By studying this simple dynein function, we can assay the degree of dysfunction introduced by *de novo* point mutations. Dynein has a lesser appreciated function in depolymerizing microtubules in both yeast⁸¹ and mammals¹⁷³, though it is unclear what the exact biological purpose regulation of astral microtubule length serves in budding yeast. It is true that a yeast system cannot be expected to recapitulate the complex array of defects which may follow from mutations in higher eukaryotes, but this system greatly simplifies the investigation of structure-function correlates when determining the molecular mechanisms underlying single amino acid changes to a protein. Furthermore, the simplicity of yeast genetic tools allows us to generate mutants rapidly, and introduce additional mutations to explore mutant defects at the single amino acid level. As dynein is only one pathway of mitotic spindle positioning, with actin-myosin providing microtubule spindle positioning through the Bim1-Kar9 pathway¹⁷⁴, mutations which result in total loss of function will not lead to compromised cell viability. This thesis work investigated 17 different mutations in yeast dynein determined to be conserved (or in some cases, homologous) to mutations implicated in human neurological disease.

The long-term goal of this thesis project was to create a pipeline capable of (1) assessing dynein mutant functions, (2) determining, precisely as possible, the molecular defects introduced by this mutation, and (3) attempting to correct the molecular defect. The readout of all *in vivo* assays of yeast dynein is simply the positioning of the mitotic spindle, which presents a robust and high-throughput means to assess functionality of dynin-dynactin-Num1 complexes at the cell cortex. This simplifies our data when attempting to correct this dysfunction through the engineering of compensatory

mutations or through pharmacological action. This *in vivo* approach was complemented with an *in vitro* assessment of motor function, and yeast dynein provides the benefit of being simple, inexpensive, and quick to purify¹⁶⁰. This system gives a method to assess motor-intrinsic properties of mutant protein and provides some advantages over the human dynein-dynactin-adaptor complexes used for analogous *in vitro* single molecule studies. Importantly, the yeast and human dynein complex have a high degree of homology, especially in the AAA catalytic core^{24,25}, which should make structure-function predictions highly translational between systems. During this mutant screen, I established the SF9 cell culture system for the expression and purification of human dynein mutants. This gives our system direct relevance to understanding how mutations affect the human motor, and provides the *in vitro* method of microtubule gliding assays¹⁰⁸ to validate any potential mechanisms of correcting mutant dysfunction *in vitro*.

This chapter will present the findings from our screen of seventeen mutant phenotypes from a battery of different assays. From this large data set, I next investigated the potential mechanisms by which mutations introduce dysfunction, and the successes and failures in attempting to correct mutant phenotypes will be detailed. In two cases, which represented the most severe neurological correlates in patients^{144,149,151}, we were successful in ameliorating the mutant phenotypes. One of these mutations was further validated using recombinant human dynein, demonstrating the translational nature of our dynein system. I will also present our efforts at correlating the phenotypic consequences of mutations to different disease states, in a method that hopefully demonstrates how the results of this study can be both translational and predictive in assessing other mutations in dynein as they are identified. Finally, several

surprising pieces of data which demonstrates further the homology between yeast and humans will be discussed. The findings from this mutant screen truly demonstrate the high degree of homology between yeast and human dynein complexes, in both their structure and regulation.

2.2 Methods

2.2.1. Strain construction and cloning

All strains used in this thesis work are derived from either W303 or YEF473A¹⁷⁷ and are listed in Table 5. We transformed yeast strains using the lithium acetate method¹⁷⁸. Strains carrying mutations were constructed by PCR product-mediated transformation¹⁷⁹ or by mating followed by tetrad dissection. Proper tagging and mutagenesis was confirmed by PCR, and in most cases sequencing (all point mutations were confirmed via sequencing). Fluorescent tubulin-expressing yeast strains were generated using plasmids and strategies described previously^{180,181}. Yeast synthetic defined (SD) media was obtained from Sunrise Science Products (San Diego, CA).

2.2.2. Spindle positioning assay

YEF473 yeast cells were grown to senescence overnight, then diluted in YPD media to reenter log phase. After 1-1.5 hours, cells were arrested by shifting incubation to a low (16° C) temperature, which has been previously demonstrated to enrich cells for anaphase spindles and prevent mitotic exit²⁹. Following this arrest, assessment of spindle positioning is performed by visualizing fluorescent microtubules and determining the fraction of properly positioned versus mispositioned mitotic spindles (Fig. 3). Imaging was performed for a single time-frame in three dimensions (7 Z images at 0.2 μm).

2.2.3. Spindle oscillation (dynamics) assay

To complement the simple approach of spindle positioning with a more refined measurement of dynein activity, I performed time-lapse microscopy to visualize the movement of the mitotic spindle by dynein pulling forces on astral microtubules via GFP-labeling of tubulin which permits labeling of microtubules in cells without noticeably perturbing microtubule dynamics^{108,180}. To focus on dynein dynamics in mitotic cells, we prepared yeast as before—growing yeast cells overnight, then diluting cells in fresh YPD to log-phase. Yeast cells are then arrested for 2.5 hours in a metaphase-like state using the drug hydroxyurea²². To only observe solely dynein-mediated spindle dynamics, all strains are deleted for the *kar9* gene, which directly links the Bim1-microtubule lattice to non-muscle myosin II motors at the cell cortex¹⁷⁴. Deletion of the Kar9 protein was accomplished through the mating of yeast strains, which provides an additional benefit of assessing synthetic interactions between the dynein and *kar9* pathways. Cells that are both *dyn1Δ* and *kar9Δ* are severely compromised for spindle positioning, so mutations which greatly compromise dynein function would present synthetic growth defects during the generation of these strains. These cells have compromised health, but may still divide, and our *dyn1Δ/kar9Δ* cells presented a further opportunity to understand mitotic spindle movements in the absence of microtubule or actin-based motor.

For time lapse movies (10s frames acquired for ~10 min, 23 Zs at 0.2 μm) images were collected on a Nikon Ti-E microscope equipped with a 1.49 NA 100X TIRF objective, a Ti-S-E motorized stage, piezo Z-control (Physik Instrumente), an iXon DU888 cooled EM-CCD camera (Andor), a stage-top incubation system (Okolab), and a

spinning disc confocal scanner unit (CSUX1; Yokogawa) with an emission filter wheel (ET525/50M for GFP, and ET632/60M for mRuby2; Chroma). Lasers (488 nm and 561 nm) housed in a LU-NV laser unit equipped with AOTF control (Nikon) were used to excite GFP and mRuby2, respectively. The microscope was controlled with NIS Elements software (Nikon). These movies were quantified for various parameters of dynein activity: velocity and displacement of each dynein-mediated spindle movement, the frequency and total distance of individual spindle movements, and the total time spent by dynein pulling the mitotic spindle. Using this assay it is also possible to assess force generation by dynein-dynactin complexes by proxy of spindle-pull through successes. *S. cerevisiae* undergo closed mitosis, and the large diameter of the nucleus must be pulled through the relatively narrow mother-bud neck. Previous studies have demonstrated that compromising dynein activity by eliminating important cofactors She1, a *S. cerevisiae*-specific dynein regulator¹⁶³, or by deleting the microtubule-binding CAP-GLY domain Nip100^{B1} (homolog of p150^{glued}), leads to decreased mitotic spindle transit through the mother-bud neck. These six parameters (spindle velocity, spindle displacement, movements per minute, displacement per minute, time of activity, and spindle pull-through success) were assessed for all seventeen mutants. Analysis was performed by automated tracking of the GFP-tubulin signal using a custom-written Matlab code aided by manual threshold setting of the GFP signal and by manual picking of dynein-mediated spindle events. Attempts were made to fully automate this spindle tracking, but these efforts were complicated by instances of microtubule depolymerization, microtubule growth pushing on the mitotic spindle, and dynein-

mediated spindle movements stalling at the bud neck. Therefore, manual curation of spindle movies was required for reliable quantification of dynein-dynactin activity.

2.2.4. *Dynein localization assay*

To assess the effects of mutation on dynein localization, YEF473 yeast cells were grown to log phase as previously described. Cells expressing Dyn1-3GFP and mRUBY-TUB1 (as used in the spindle positioning assay), were analyzed using time-lapse microscopy (10s frame acquired every 90s, using 13 Z stacks of 0.2 μm). Images were acquired on the NikTiE microscope set-up utilized for the spindle dynamics assay. Dynein localization at canonical cellular compartments—the spindle pole body, microtubule plus ends, and the cell cortex—was determined by manually scoring frequency and intensity of dynein molecules using ImageJ software.

2.2.5. *Purification of yeast dynein complexes*

Yeast dynein was purified as previously described⁶⁸. Purification of yeast dynein (ZZ-TEV-Dyn1-HALO, under the native *DYN1* promoter; or, ZZ-TEV-6His-GFP-3HA-GST-dynein₃₃₁-HALO, under the control of the galactose-inducible promoter, *GAL1p*) was performed as previously described^{114,163}. Briefly, yeast cultures were grown in YPA supplemented with either 2% glucose (for full-length dynein) or 2% galactose (for GST-dynein₃₃₁), harvested, washed with cold water, and then resuspended in a small volume of water. The resuspended cell pellet was drop frozen into liquid nitrogen and then lysed in a coffee grinder (Hamilton Beach). After lysis, 0.25 volumes of 4X dynein lysis buffer (1X buffer: 30 mM HEPES, pH 7.2, 50 mM potassium acetate, 2 mM magnesium acetate, 0.2 mM EGTA) supplemented with 1 mM DTT, 0.1 mM Mg-ATP, 0.5 mM Pefabloc SC (concentrations for 1X buffer) was added, and the lysate was clarified at

22,000 x g for 20 min. The supernatant was then bound to IgG sepharose six fast flow resin (GE) for 1–1.5 hr at 4°C, which was subsequently washed three times in 5 ml lysis buffer, and twice in TEV buffer (50 mM Tris, pH 8.0, 150 mM potassium acetate, 2 mM magnesium acetate, 1 mM EGTA, 0.005% Triton X-100, 10% glycerol, 1 mM DTT, 0.1 mM Mg-ATP, 0.5 mM Pefabloc SC). To fluorescently label the motors for single molecule analyses, the bead-bound protein was incubated with either 6.7 μM HaloTag-AlexaFluor660 (Promega) or HaloTag-Tetramethylrhodamine for 10 min at room temperature. The resin was then washed four more times in TEV digest buffer, then incubated in TEV buffer supplemented with TEV protease for 1–1.5 hr at 16°C. Following TEV digest, the beads were pelleted, and the resulting supernatant was aliquoted, flash frozen in liquid nitrogen, and stored at –80°C.

2.2.6. Purification human dynein complexes

The human dynein complex was expressed and purified from insect cells (ExpiSf9 cells; Life Technologies) as previously described with minor modifications^{58,97}. Briefly, 4 ml of ExpiSf9 cells at 2.5×10^6 cells/ml, which were maintained in ExpiSf CD Medium (Life Technologies), were transfected with 1 μg of bacmid DNA (see above) using ExpiFectamine (Life Technologies) according to the manufacturer's instructions. 5 days following transfection, the cells were pelleted, and 1 ml of the resulting supernatant (P1) was used to infect 500 ml of ExpiSf9 cells (5×10^6 cells/ml). 72 hours later, the cells were harvested (2000 x g, 20 min), washed with phosphate buffered saline (pH 7.2), pelleted again (1810 x g, 20 min), and resuspended in an equal volume of human dynein lysis buffer (50 mM HEPES, pH 7.4, 100 mM NaCl, 10% glycerol, 1 mM DTT,

0.1 mM Mg-ATP, 1 mM PMSF). The resulting cell suspension was drop frozen in liquid nitrogen and stored at -80°C .

For protein purification, 30 ml of additional human dynein lysis buffer supplemented with cOmplete protease inhibitor cocktail (Roche) was added to the frozen cell pellet, which was then rapidly thawed in a 37°C water bath prior to incubation on ice. Cells were lysed in a dounce-type tissue grinder (Wheaton) using ≥ 100 strokes (lysis was monitored by microscopy). Subsequent to clarification at $40,000 \times g$, 45 min, the supernatant was applied to 2 ml of IgG sepharose fast flow resin (GE) pre-equilibrated in human dynein lysis buffer, and incubated at 4°C for 2–4 hr. Beads were then washed in batch with 50 ml of human dynein lysis buffer, and 50 ml of human dynein TEV buffer (50 mM Tris pH 7.4, 150 mM potassium acetate, 2 mM magnesium acetate, 1 mM EGTA, 10% glycerol, 1 mM DTT, 0.1 mM Mg-ATP). The bead-bound protein was incubated with $3 \mu\text{M}$ SNAP-Surface Alexa Fluor 647 (NEB) for 40–60 min at 4°C (to fluorescently label the protein), washed five times in human dynein TEV buffer, then incubated with TEV protease overnight at 4°C . The next morning, the recovered supernatant was applied to a Superose six gel filtration column (GE) equilibrated in GF150 buffer (25 mM HEPES pH 7.4, 150 mM KCl, 1 mM MgCl_2 , 5 mM DTT, 0.1 mM Mg-ATP) using an AKTA Pure. Peak fractions (determined by UV 260 nm absorbance and SDS-PAGE) were pooled, concentrated, aliquoted, flash frozen, then stored at -80°C .

2.2.7. Single molecule and ensemble motility assays

The yeast dynein single-molecule motility assay was performed as previously described with minor modifications¹⁶³. Briefly, flow chambers constructed using slides

and plasma cleaned and silanized coverslips attached with double-sided adhesive tape were coated with anti-tubulin antibody (8 µg/ml, YL1/2; Accurate Chemical and Scientific Corporation) then blocked with 1% Pluronic F-127 (Fisher Scientific). Taxol-stabilized microtubules assembled from unlabeled and fluorescently-labeled porcine tubulin (10:1 ratio; Cytoskeleton) were introduced into the chamber. Following a 5–10 min incubation, the chamber was washed with dynein lysis buffer (see above) supplemented with 20 µM taxol, and then purified dynein motors were introduced in the chamber. After a 1 min incubation, motility buffer (30 mM HEPES pH 7.2, 50 mM potassium acetate, 2 mM magnesium acetate, 1 mM EGTA, 1 mM DTT, 1 mM Mg-ATP) supplemented with 0.05% Pluronic F-127, 20 µM taxol, and an oxygen-scavenging system (1.5% glucose, 1 U/ml glucose oxidase, 125 U/ml catalase) was added. TIRFM images were collected using a 1.49 NA 100X TIRF objective on a Nikon Ti-E inverted microscope equipped with a Ti-S-E motorized stage, piezo Z-control (Physik Instrumente), and an iXon X3 DU897 cooled EM-CCD camera (Andor). 488 nm, 561 nm, and 640 nm lasers (Coherent) were used along with a multi-pass quad filter cube set (C-TIRF for 405/488/561/638 nm; Chroma) and emission filters mounted in a filter wheel (525/50 nm, 600/50 nm and 700/75 nm; Chroma). We acquired images at 2 s intervals for 8 min. Velocity and run length values were determined from kymographs generated using the MultipleKymograph plugin for ImageJ (http://www.embl.de/eamnet/html/body_kymograph.html)

Human dynein-mediated microtubule gliding assays were performed as previously described¹⁶⁴ with minor modifications. Briefly, flow chambers were prepared by affixing an ethanol-flamed coverslip to a glass slide using double-stick tape. The

chamber was then incubated on an ice block, washed with 1% Pluronic F-127, following by addition of purified dynein (five chamber volumes of 60 nM dynein complex).

Unbound motors were washed out with GF150 buffer. Subsequently, motility buffer (30 mM HEPES pH 7.0, 50 mM KCl, 5 mM MgSO₄, 1 mM EGTA, 1 mM DTT, 2.5 mM Mg-ATP, 40 μM taxol) supplemented with 1.5% glucose, the oxygen scavenging system (see above), and 150 nM fluorescent microtubules was added to the chamber. Images were acquired every 1 s (for wild-type) or 1-5 s (for mutants), and analysis of microtubule gliding was performed using ImageJ software.

2.2.8. Cell lysis and immunoblotting

Yeast cultures were grown to similar mid-log phase densities (OD₆₀₀ ~ 2) in 4 ml SD media, and harvested. Cell pellets were resuspended in 0.2 ml of 0.1 M NaOH and incubated for 10 min at room temperature as described¹⁸². Following centrifugation, the resulting cell pellet was resuspended in sample buffer. Equal amounts of total cell lysate (as determined from cell density prior to lysis) were loaded into each lane, transferred to PVDF and probed with a monoclonal anti-GFP antibody (at 1:250; Abm) followed by an HRP-conjugated goat anti-mouse antibody (at 1:10,000; Jackson ImmunoResearch Laboratories). Electroblothing to PVDF was performed in 25 mM Tris, 192 mM glycine supplemented with 0.05% SDS and 20% methanol. Chemiluminescence signal was acquired with a Chemidoc MP (BioRad). Immunoblots were exposed (durations ranged from 2 to 5 min) without saturating the camera's pixels.

2.2.9. Statistical analyses

Statistical tests were performed as described in the figure legends. Unpaired Welch's t tests (for Gaussian distributed velocity data) and Mann-Whitney test (for exponentially

distributed displacement data) were performed using Graphpad Prism. Z scores, which are a quantitative measure of difference between two proportions, were calculated using the following formula: $Z = (\hat{p}_1 - \hat{p}_2) / [\hat{p}(1-\hat{p})(1/n_1 + 1/n_2)]$ where: $\hat{p} = (y_1 + y_2) / (n_1 + n_2)$ Z scores were converted to two-tailed P values using an online calculator.

2.2.10. Coefficient of dynein dysfunction (CDD) score calculation

To calculate the CDD scores, we used the following approach to quantitatively measure of difference between mean values obtained for wild type versus those obtained for each mutant. Graphpad Prism was used to calculate q values (i.e., the difference between the two means divided by the standard error of that difference), whereas Z scores were calculated as described above (all values are shown in Table 1). We then converted the q values and Z scores for each mutant (for each assay) into a 'normalized relative variance' score (nrv), which reflects the relative difference between two mean values (e.g., between wild-type and mutant 1; as reflected in the Z scores and q values, or 'v'), where $nrv = |v|/v_{max}$ for each range of scores (for each column shown in Table 1). To convert the nrv values into a final CDD score for each mutant, we used the formula shown in Table 2. Briefly, the nrv values for each assay for a given mutant was added, with the spindle positioning nrv (nrvSP) weighed five times that of the others, as described within the Results. In the two cases where a value wasn't determined (due to insufficient observations, such as in the case for neck transit success for the H3639P mutant), the denominator was reduced from 6 to 5.

2.3. Results

2.3.1. Dynein mutations cause mitotic spindle positioning defects

In our first assay we employed fluorescence-based microscopy to assess mitotic spindle positioning in yeast at anaphase by arresting log phase cells at a low temperature (16°C). Despite our initial expectations, spindle mispositioning was mostly unperturbed in our battery of mutants (Fig. 3). Small amounts of spindle mispositioning and microtubule morphology changes were apparent in linker and motor domain mutants, which was expected due to the high degree of conservation between humans and yeast dynein motor domains. Interestingly, the most extreme phenotype was observed in H3639P, located in the AAA5 domain, which led to a dynein null phenotype. This result was unexpected, as this region of the motor does not bind or hydrolyze ATP, nor does this domain participate in any known inter- or intramolecular interactions. This result was so surprising at the time that this strain was remade and assayed a second time, and then the mutant allele was mutated back to wild type, just to confirm the accuracy of our assay. An explanation for this extreme phenotype was that mutation to proline caused a loss of flexibility within the dynamic mechanochemical module of the motor domain. Alternatively, this domain may be important for facilitating the AAA5 large and small subdomain interaction during normal mechanochemistry, as proposed by the previous study examining disease-correlate dynein mutations¹⁶⁴.

However, as most spindle positioning defects were mild, a more detailed examination of dynein dynamics was needed to more precisely dissect the phenotypes we observed. Furthermore, the majority of mutants assessed in these experiments had no gross spindle mispositioning phenotypes, indicating that this assay was not sensitive

enough to detect minor perturbations as might be implicated in some late-onset degenerative motor neuron diseases. These results initially raised the possibility that the majority of the selected mutations may not cause obvious defects in our yeast system. However, as some of the conserved motor mutations introduced mildly negative phenotypes, and one complete loss-of-function, we continued undeterred.

Figure 3

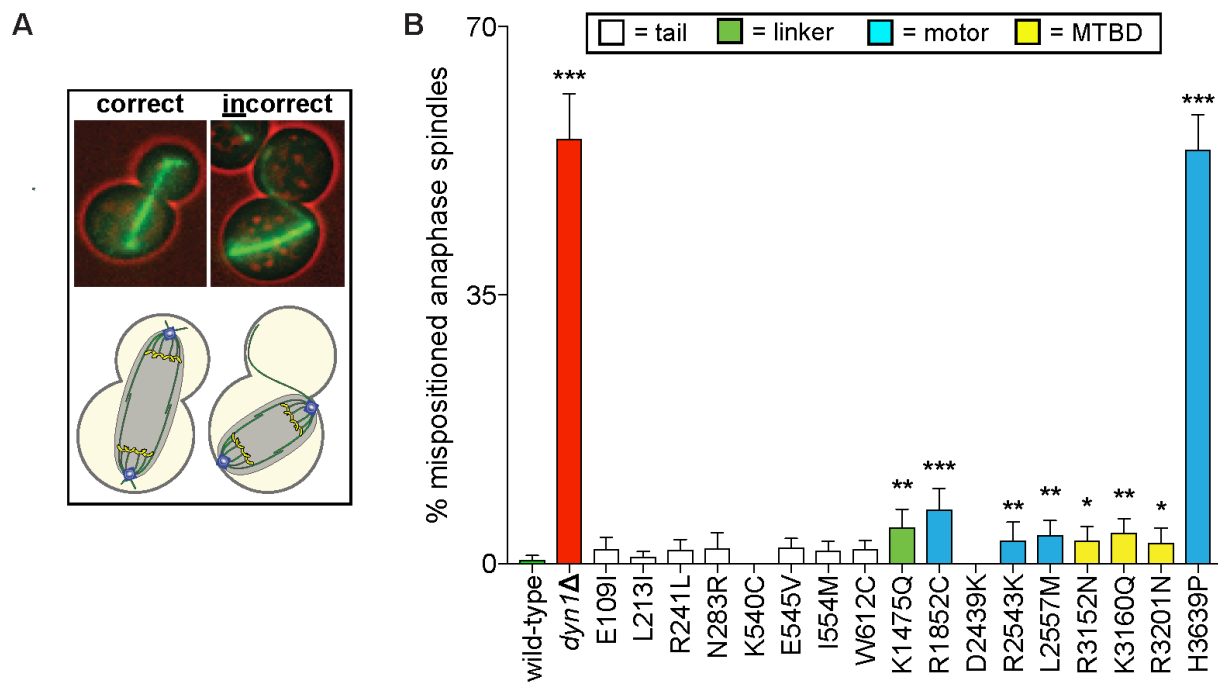


Figure 3. Spindle positioning assay provides coarse assessment of mutant dynein dysfunction. (A) Representative fluorescence image (left; green, GFP-Tub1; red, contrast enhanced brightfield image to illustrate cell cortex) and (B) quantitation of spindle positioning phenotypes in the 17 disease-correlated Dyn1 mutants, along with wild-type and dynein knock-out (*dyn1Δ*) cells. Each data point represents the fraction of mispositioned anaphase spindles along with standard error (weighted mean \pm weighted standard error of proportion; $n \geq 99$ anaphase spindles from three independent experiments for each strain). Statistical significance was determined by calculating Z scores, as described in the Materials and Methods (*, $p \leq 0.1$; **, $p \leq 0.05$; ***, $p \leq 0.001$).

After observing that the majority of mutants demonstrated minimum defects in spindle positioning, I first sought to improve the sensitivity of this readout for understanding dynein dysfunction. Ideally, this assay could be implemented as high-throughput screening techniques using fluorescent spindle positioning as a readout. The

most logical step to increase the sensitivity of this assay was to exacerbate the spindle positioning dysfunction. We elected to reemploy this assay in cells lacking Kar9, the second component of the mitotic spindle positioning pathway. These strains were readily available, as they were created for each mutant in our spindle oscillation assay, and cells lacking both dynein and Kar9 (as would be expected for our H3639P dynein null phenotype) are viable, just slow growing. However, attempting to perform this assay in cells lacking Kar9 was initially problematic, as growing these cells at 16^o C to arrest cells in anaphase (as had been done in the first assay), produced considerable morphological defects and cellular death. To circumvent this issue, we designed a strategy employing a GAL1p:CDC20 plasmid to arrest cells in mitosis. We constructed a plasmid containing the budding yeast CDC20 gene under the control of a galactose-inducible promotor, which was then linearized and transformed into cells, directly upstream of the endogenous CDC20 allele. With this strategy, we could quickly and easily repurpose our spindle oscillation strains for use in this modified spindle positioning assay without need for mating to create strains again. Strains would be grown in culture containing galactose and raffinose, and switching these cells to media containing only yeast media plus dextrose would lead to a mitotic arrest in anaphase by depletion of CDC20, an essential component of the anaphase promoting complex.

We then performed this modified spindle positioning assay for wild-type yeast and several mutants (H3639P, R1852C and L2557M, K540 and E109I), which were representative of severe, mild, and no phenotypes in our previous assay, respectively. To our surprise, the increases in spindle mispositioning were uniform across all strains, regardless of dynein allele (Data not shown). The baseline level of spindle positioning

for wild-type rose from less than 1% to 30%, but our E109I and K540C demonstrated similar degrees of dysfunction. Furthermore, our R1852C/*kar9* Δ mutant only demonstrated slightly higher spindle mispositioning than wild type still, and only displayed the additive mispositioning (for instance, 10% plus 30%, for a total 40%) between the dynein and Kar9 knockouts. While this experiment was unsuccessful in improving the spindle positioning assay, it is informative of some mechanisms of yeast mitotic spindle regulation. The overall increase in spindle mispositioning was additive between the loss of dynein and the loss of Kar9, rather than either pathway exacerbating the other, and compromising these pathways can independently cause defects in mitotic positioning. Both Kar9 and dynein-dependent spindle mechanisms are required for high fidelity spindle positioning, but these data indicate that these two pathways have limited cross talk. In conclusion, our spindle positioning assay could not accommodate for the subtle loss-of-function effects we may expect from a number of our mutants

2.3.2. Spindle dynamics assay provides a sensitive readout of dynein function

To explore the dynamics of spindle positioning with higher precision, we turned next to our spindle oscillation assay, which provides quantitative data about the motility of dynein-dynactin-Num1 (DDN) complexes at the cell cortex. In this assay, log-phase cells are arrested in a metaphase-like state with hydroxyurea, and the Kar9 spindle positioning is deleted to limit observation to dynein-mediated spindle positioning. The mitotic spindle is fluorescently labeled and dynein-mediated spindle positioning is tracked over an extended period. Additionally, movies of *dyn1* Δ and *kar9* Δ can be analyzed to understand movement parameters of the mitotic spindle (via microtubule

pushing forces and diffusive movement) in the absence of motors. Movements are quantified by a custom Matlab tracking routine and instances of dynein-mediated transport are manually assigned.

Using this assay, we observed substantially more phenotypes across mutants. The most commonly observed effect of dynein mutation was to drive partial to severe loss-of-function in most mutants, although partial gain-of-function phenotypes were observed in isolated cases (Figs. 4, 5). Nearly all mutants presented notable phenotypes, with only two mutations, E109I and R2439K, demonstrating essentially wild-type parameters across all assays. Overall, less severe phenotypes were caused by tail mutation, with intermediate phenotypes present in all three MTBD mutants, and the most severe phenotypes clustering in the motor domain (as was observed in the spindle positioning assay). One of the most striking conclusions of the data obtained in these experiments is that the mutations associated with the most severe disease states (i.e., developmental disorders and brain malformation) had the most severe loss-of-function in this assay. This correlation between disease severity and loss-of-function in our assays was expected, as the most severe mutations cluster in the motor domain, which is the most conserved region of the protein as previously noted. Decrease in velocity was the most common outcome of dynein mutation, with 13 of 17 mutants having this phenotype. Mutants L213I and R241L demonstrated a large decrease in overall velocity, but interestingly L213I had increased time of spindle activity, indicating that velocity and activity parameters of the motor may not necessarily be co-dependent. Two closely spaced tail mutations, K540C and E545V were particularly interesting, as both mutations demonstrated no defect in velocity parameters and had nearly opposite

Figure 4

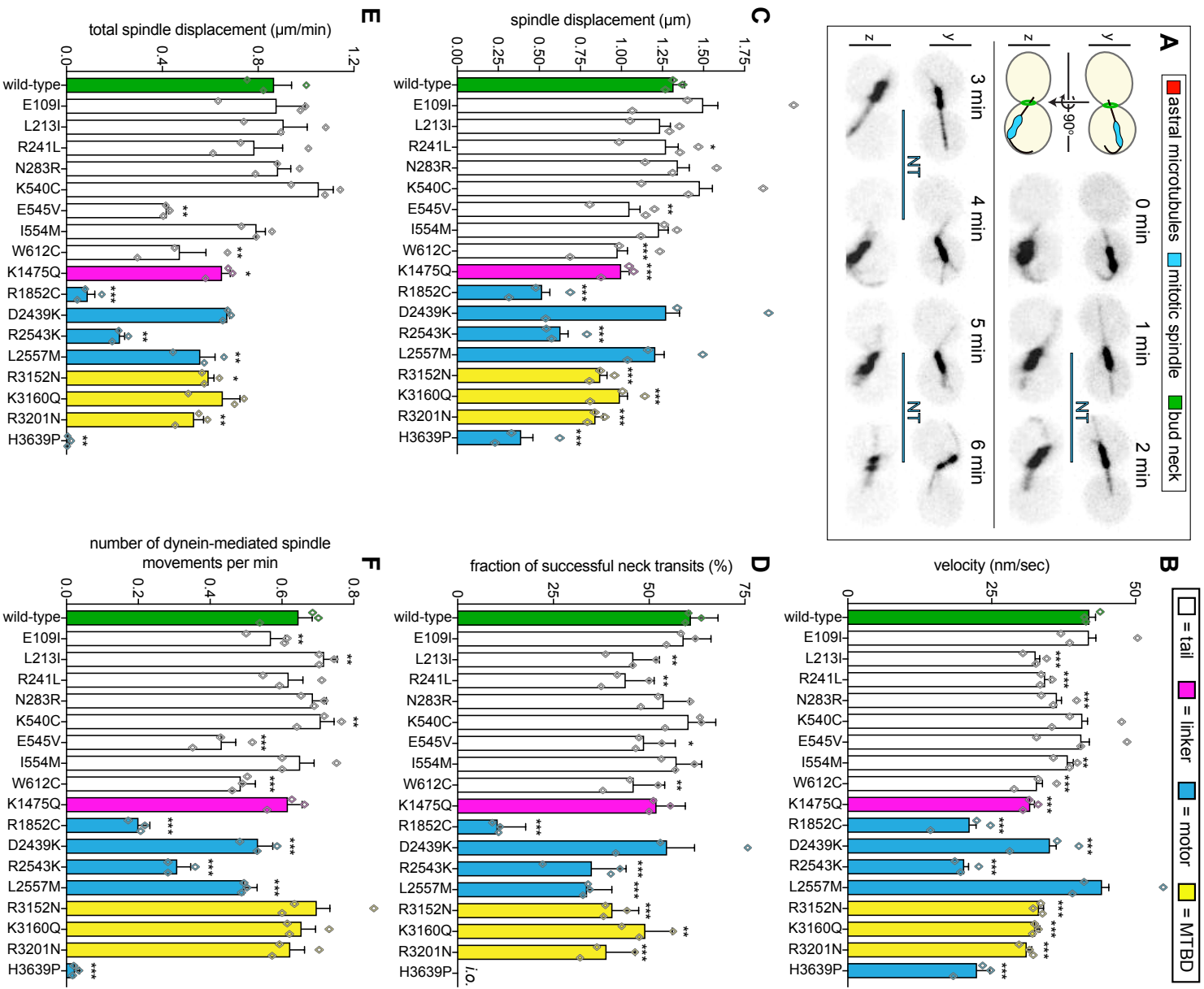


Figure 4. Quantitative assessment of dynein-dynactin-mediated spindle dynamics reveals refined insight into mutant dysfunction. (A) Cartoon and representative time-lapse inverse fluorescence images of a hydroxyurea (HU)-arrested *kar9Δ* cell exhibiting typical dynein-mediated spindle movements, analysis of which is presented in panels (B – F). Maximum intensity (X-Y projection; top) and Y-Z projections (bottom) are shown for each time point (NT, neck transit; note, line spans time frames over which the NT occurs). (B – F) Plots of indicated parameters for spindle dynamics in haploid wild-type and mutant strains. Briefly, the mitotic spindles were tracked in 3-dimensions using a custom written Matlab code. Dynein-mediated spindle movements were manually selected from the tracking data, from which velocity (B), displacement (C, per event; or, E, per minute), and the number of dynein-mediated spindle movements per minute (F) were obtained. The fraction of successful neck transits (successful attempts divided by total attempts) were manually scored (i.o., insufficient observations; for H3639P, only one unsuccessful neck transit attempt was observed). Each bar represents the weighted mean \pm weighted standard error (or standard error of proportion for D; n = 42 to 60 HU-arrested cells from three independent experiments were analyzed for each strain; diamonds represent mean values obtained from each independent replicate experiment). Statistical significance was determined using an unpaired Welch's t test (B and E), a Mann-Whitney test (C), or by calculating Z scores (D and F; *, $p \leq 0.1$; **, $p \leq 0.05$; ***, $p \leq 0.005$).

activity in some parameters (total time of movement) of this assay. In K540C spindles had increases in overall displacement compared to wild type but E545V spindles having a large decrease in overall displacement and greatly compromised spindle pull-through activity, which may further indicate a loss of force generation. The E545V mutant was used in further experiments (Fig. 6) to determine if loss-of-function mutations would behave dominant negatively in diploid yeast cells. Examining the location of the homologous amino acids within the human structure indicated that both were located on the dynein surface that interfaces with the intermediate chain of a *neighboring* adjacent heavy chain of the newly characterized 2 dynein: 1 dynactin complex^{103,104}. This stretch of amino acids was recently identified as being important to stabilize the binding of a second dynein complex to dynactin⁹³⁻⁹⁴, and may help position the two dimers relative to each other in the 2 dynein dimer: 1 dynactin complex. This data suggests that the ability to recruit two dynein complexes to dynactin is conserved in yeast, and that disrupting this complex can compromise force generation (Fig. 6D) or activity (Figs. 6E and F, also see Figs. 7 and 32), as demonstrated in mammalian complexes. One other mutation near this site, W612C, demonstrated similar defects in spindle pull-through and activity

parameters; however this residue was sufficiently distal to the 540-545 interface region. Further, this mutant also demonstrated severe reductions in overall motility, which may indicate an intermediate loss of motor function not detectable by our spindle positioning assay.

Figure 5

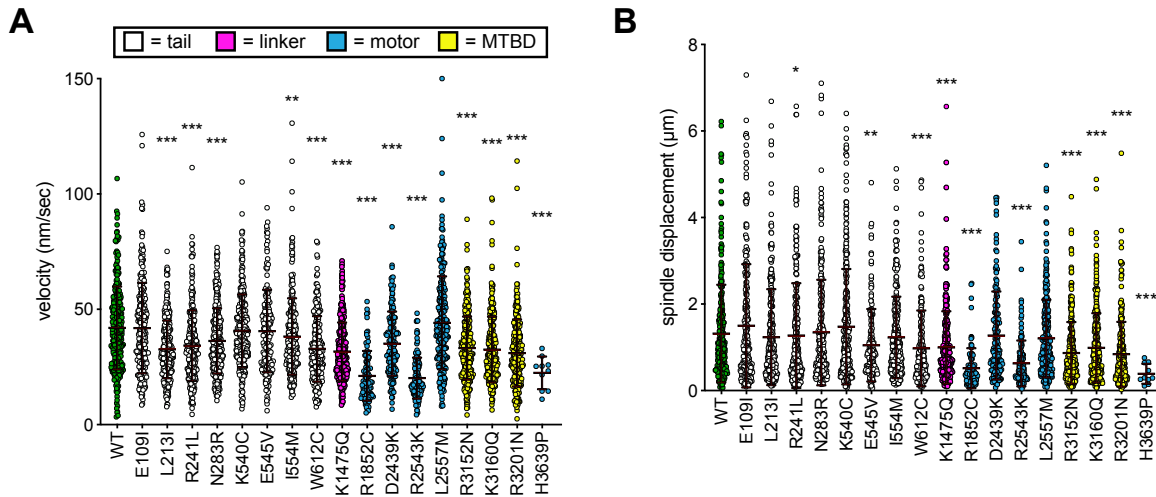


Figure 5. Distribution of spindle motility data from haploid cells. Scatter plots depicting (A) individual velocity values per spindle displacement event, and (B) individual displacement values per spindle displacement event (from Figure 4). Mean values and standard deviations are also depicted with red lines. Mean velocity values for all mutants were fit to a normal distribution and all displacement values were fit to a single exponential decay.

The motor domain mutants presented the most striking loss-of-function phenotypes in this assay. The three most severe mutations, as observed in our spindle positioning assay, were R1852C, R2543K, and H3639P. Notably, the R1852C and R2543K mutants, which demonstrated minor defects in spindle positioning, demonstrated striking loss-of-function phenotypes in this assay. These mutants had drastic reductions in velocity and displacement of the spindle (Fig. 6B, C), an expected consequence given these mutations are present in the AAA1 and AAA3 catalytic domains. Both also had reductions in time of activity, less initiation of dynein transport,

and fewer neck-cross successes (Fig. 6D-F). The R1852C mutant demonstrated substantially less activity than either wild type or R2543K alleles, and the total spindle displacement over time was nearly the same as the H3639P mutant, which again evidenced a dynein-null phenotype, in line with the results from our spindle positioning assay. Importantly, this mutant presented with synthetic lethality in conjunction with *kar9* Δ alleles (Fig. 11E), a phenotype not evident in other mutants, further suggesting that this mutant is a complete loss-of-function mutant. However, repeated careful observation identified that a *very* small fraction of cells demonstrated spindle movement, including a solitary instance (In 60 cells) of movement into the bud-neck. It is important to note that positioning into the bud-neck and processive, directed spindle movements are never observed in *dyn1* Δ /*kar9* Δ mutants. This indicates some proportion of motors were likely active despite overall major loss of motor function. This result was unexpected given spindle positioning and genetic data, and led to two possibilities; (1) near total loss of protein levels through degradation or misfolding or that (2) a small proportion of translated motors were active.

Two final noteworthy mutations that demonstrated some spindle positioning defects were K1475Q and L2557M, located near the linker domain and AAA3 domain, respectively. The former mutation behaved normally in both frequency of activity and initiation, but had substantially reduced velocity and displacement for individual events. It seemed likely at the time that this mutant had a defect in the powerstroke or some other mechanochemical activity of the linker domain. While this hypothesis seemed reasonable the time, subsequent investigation of this mutation revealed it to be incorrect. During this thesis work the K1475 residue (K1567 in humans) was identified

as an important amino acid in stabilizing dynein's autoinhibited conformation¹⁶⁵. Therefore, this mutant's altered motility is potentially a consequence of altered dynein autoinhibition. The L2557M mutant had normal velocity and displacement; however, spindle movements frequently stalled at the bud neck, which decreased both neck-transit frequency and time of activity (due to frequent stalls). This indicated the potential of this mutant to have compromised force production. This was an interesting prospect, as this mutant is located in AAA3, and could be conceivable for this mutant to compromise AAA3 ATPase activity, which tunes the MTBD affinity and has functions in allosteric communication across the AAA ring. Due to having comprised spindle positioning and spindle pull through phenotypes, it is conceivable that this mutant could affect force production without overtly changing other motility parameters. Finally, D2439K, evidenced minimal loss of dynein function. While an uninteresting result, it was useful to have a mutant in the motor domain with minimal dysfunction, as it gave us more confidence in the robustness of this assay. Mutation of the motor domain may not always lead to compromised motor activity in a non-specific manner, and that the phenotypes we had observed with other mutants in conserved residues have translational biological significance in higher eukaryotes.

Microtubule-binding domain mutants presented phenotypes of intermediate severity between motor and tail mutants. All three MTBD mutants exhibited fairly similar degrees and types of defects in effecting spindle movements, including reductions in velocity, displacement, and neck transit success. Structural analysis revealed that all three mutations mapped to the surface of the MTBD that makes contacts with the microtubule. Given all three substitutions constitute the replacement of a positive charge

with a neutral amino acid, it is likely that the phenotypic outcome of each mutations lead to a reduction in the affinity of the MTBD for the negatively charged surface of the microtubule lattice. The reduced activity metrics for R3152N and R3201N in particular could thus be a reflection of a reduction in association kinetics of the mutants for the microtubule. This is supported by a study that found reduced microtubule binding for the analogous amino acid substitutions using a fibroblast-derived MTBD fragment construct¹¹⁹. It is also possible that these mutations interfere with structural changes within side-chains inside the MTBD important for changing MTBD registry. Overall, nearly all mutations analyzed changed dynein motility parameters, and the most severe loss-of-function mutations were correlated with the most severe states. This assay is likely the most suitable for assaying loss dynein function in future mutant studies.

2.3.3. *Mutations exert dominant-negative effects on spindle dynamics*

One of the key advantages to the budding yeast dynein system is the haploid genome we typically manipulate in our cell biological studies. This further simplifies the interpretation of dynein mutants and eliminates confounding factors, such as heterogeneous dynein complex composition, or unequal expression due to changes in mRNA expression or protein expression levels. In the context of human disease, by contrast, *de novo* mutations are almost exclusively heterozygous by their very nature, and must therefore have dominant negative effects on dynein function. In this study, we sought to determine whether dynein mutations in yeast act in a dominant negative fashion, as they do in mammalian systems. If our yeast dynein-based system is to be a suitably tractable system for assaying dynein mutations, they *should* lead to dominant-negative effects when observed in diploids. Further, if mutations in a dimeric motor

Figure 6

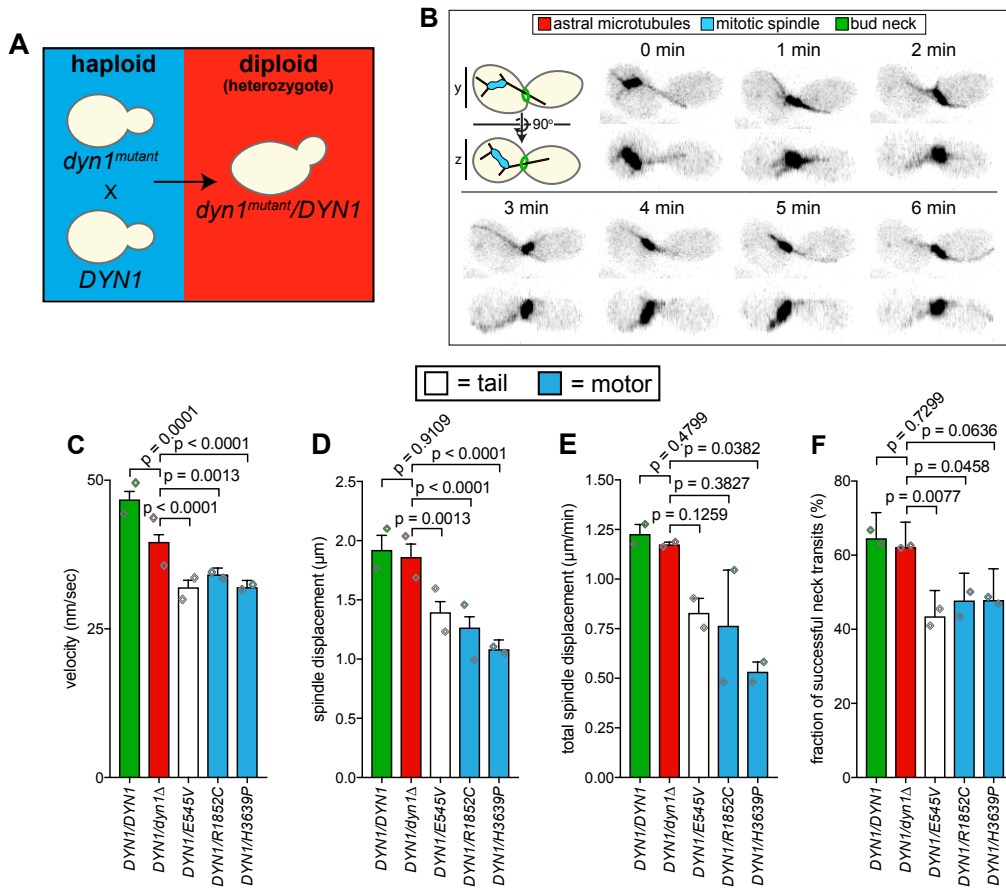


Figure 6. Quantitative assessment of spindle dynamics in heterozygous diploid cells reveals dominant nature of mutations. (A – B) Schematic depicting experimental approach to assess dynein-dynactin activity in heterozygous diploid cells (B), and representative inverse fluorescence images of a diploid hydroxyurea (HU)-arrested $kar9\Delta/kar9\Delta$ cell exhibiting typical dynein-mediated spindle movements. Maximum intensity (X-Y projection; top) and Y-Z projections (bottom) are shown for each time point. (C-F) Plots of indicated parameters for spindle dynamics in indicated diploid yeast strains. Each bar represents the weighted mean \pm weighted standard error (or standard error of proportion for F; $n \geq 29$ HU-arrested cells from two independent experiments were analyzed for each strain; diamonds represent mean values obtained from each independent replicate experiment). Statistical significance was determined using an unpaired Welch's t test (C and E), a Mann-Whitney test (D), or by calculating Z scores (F).

protein exert dominant negative effects, two possibilities then arise. First, there may be ensembles of homodimeric mutant and wild-type dyneins, which would be the case of dynein complexes were cotranslationally dimerized, as has been demonstrated for $p53^{183}$. A second possibility is that dominant negative effects are due to formation heterodimeric complexes wild type/mutant complexes, as has been demonstrated for $kip2$ in yeast¹⁸⁴. While it is unclear what might be the mechanistic or phenotypic

differences between an ensemble of (1) homodimeric wild-type and mutant complexes or (2) heterodimeric wild-type/mutant complexes, we turned to the plethora of yeast cell biological tools to answer this question.

To understand if mutations are acting in a dominant-negative manner, we first generated a wild-type dynein strain with a background amenable to mating with our spindle oscillation strain (*kar9* Δ , GFP-TUB1; Fig. 6A-B). During this thesis work we also generated *dyn1* Δ /*kar9* Δ /GFP-TUB1 strains to construct a diploid strain as a *dyn1*^{+/-} hemizygotes, to see if a single copy of dynein would be sufficient to mediate mitotic spindle movements. Mating of our spindle oscillation strains, both wild-type and mutant alleles, with the wild-type background (DYN1-GFP/GFP-TUB1/*kar9* Δ) generated our diploid heterozygous dyneins.

Using our new and improved spindle oscillation assay with diploid yeast demonstrated that while loss of one dynein allele was sufficient to reduce maximal motor velocity, the overall activity parameters of dynein (frequency of activity and fraction of time active) were mostly unchanged (Fig. 6C-F). This data encourages further analysis, and indicates that a single dynein gene is sufficient for cellular activity within yeast cells. Whatever transcriptional feedback controls are in place to synthesize and recruit dynein, they are maintained even in the case of hemizygous expression to ensure normal spindle positioning. The observed decrease in maximal velocity for hemizygotes, despite maintaining normal activity parameters (time of movement, initiation rate), indicates that single or small groups of dynein may be competent to move the mitotic spindle. However, it may be the case that a critical number of dyneins may be necessary for maximal velocity, or that a critical concentration of the motor is

necessary for complex assembly, which would indicate both alleles of dynein are needed for completely normal cellular activity.

In stark contrast to the hemizygous mutant, all three mutant heterozygotes analyzed in this study demonstrated notable loss-of-function phenotypes. Even E545V, which itself had no effect on dynein velocity or processivity in a haploid background, led to loss of velocity and processivity in the context of diploid cells. This result satisfactorily recapitulates the dominant-negative nature of these mutations in the context of human disease states. Interestingly, the H3639P mutant, identified as being almost a dynein-null phenotype in other assays, had substantially worse motility parameters than the *dyn1*^{+/-} hemizygotes, indicating presence of a mutant dynein causes more severe phenotypes than complete loss of a single gene within a diploid genome. In the dynein hemizygotes, the entire gene was replaced for a gene encoding a selectable marker, which may prevent unproductive transcription from the gene. However, in the case of H3639P, the protein is likely expressed in some level comparable to wild-type, such that the presence of the poorly functional mutant protein inhibits healthy dynein function. The motility data suggest that the mutant motor is incorporated into dynein ensembles at the cell cortex, as velocities ranged from very slow (as observed for H3639P haploids), to near wild-type (near 40 nm/s).

To better understand how these mutations exert dominant-negative effects, we next sought to determine if dynein dimer complexes in diploid cells was comprised of a cotranslationally assembled dynein dimer from a single gene, or if heterodimeric complexes were formed between mutant and wild-type alleles. To this end, we designed a strategy for to assess the composition of dynein complexes from diploid yeast strains

using our *in vitro* motility assay. These cells contained one copy of a GFP-tagged dynein heavy chain allele (*DYN1-GFP*), and a second dynein allele containing N-terminal affinity tag for purification and a C-terminal HALO tag (*ZZ-DYN1-HALO*) which could be used to fluorescently label the motor (Fig. 7A). Lysate from these cells was subjected to IgG affinity chromatography and subsequent incubation with a red (tetramethylrhodamine) HALO ligand (HALO-TMR). Bound *ZZ-DYN1-HALO* protein was eluted and used in a single molecule imaging experiment (See Methods). If

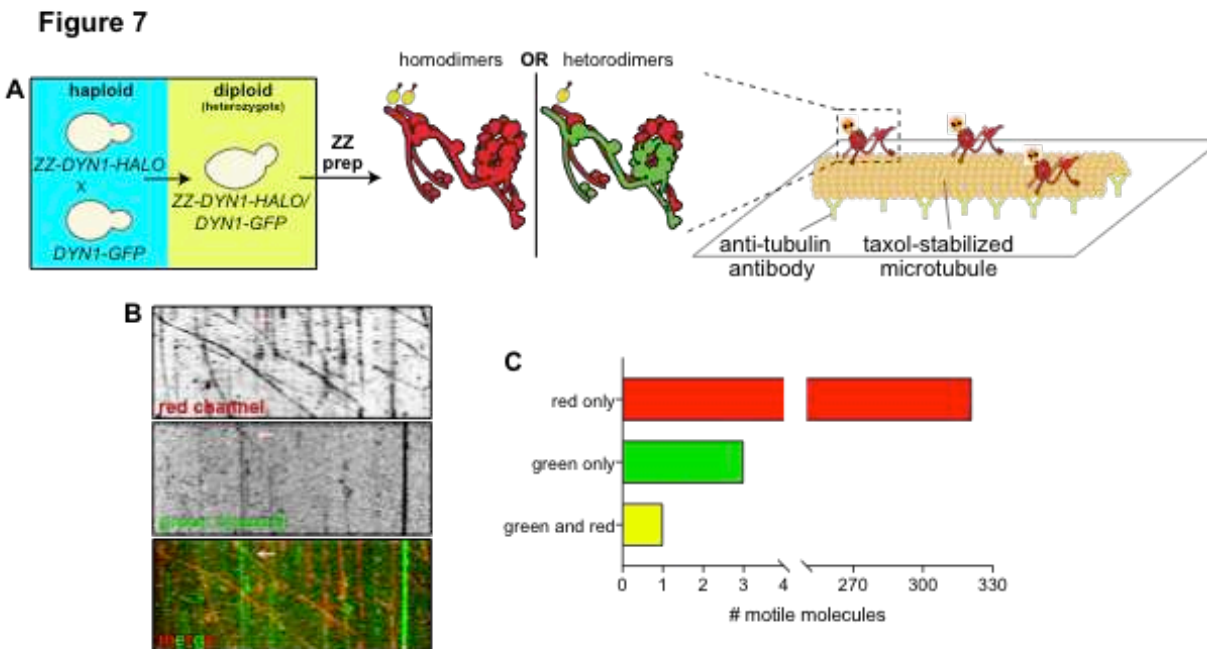


Figure 7. Dynein dimers are likely comprised of two polypeptides from a single allelic locus. (A) Schematic depicting experimental approach to determine whether distinct proteins from two different dynein alleles homo- or heterodimerize. (B and C) Representative kymograph (B) depicting large proportion of red (HA-LO-tagged) dynein molecules walking along microtubules (only one of which colocalized with a GFP-tagged dynein; arrow), along with associated quantitation (C).

heterodimers assemble within cells, we expected to observe some proportion of dual-color labeled molecules comigrating in this experiment (green and red); however, if only homodimers form, then we expected to observe only red molecules (Fig. 7A). In over 300 dynein molecule runs, only a single dual labeled molecule (0.3% of the total; Fig.

7B arrow) was observed, and the vast majority of motile molecules (98.8%) were exclusively red, indicating that dynein very rarely, if ever, forms heterodimers (Fig. 7C). We observed a small number of motile green molecules (~1% of the total; likely due to contaminating Dyn1-GFP molecules in the protein preparation), and observed substantially more green molecules in protein preparations that were not completely washed after the bead binding step. This suggests a co-translational dimerization model for dynein complex assembly, similar to what has been observed for p53¹⁸³. This result was an important experiment in understanding dominant negative mutations in dimeric proteins expressed in diploid cells, and provide us with a means in future experiments to analyze the assembly of dynein-dynactin-Num1 complexes in in future experiments.

2.3.4. Dynein localization is perturbed by tail and motor domain mutants

The final *in vivo* assay used in these experiments was analysis of dynein localization during mitosis. Log phase cells were imaged in 13 Z-stacks using time-lapsed fluorescent microscopy of labeled dynein and microtubules. As discussed previously, dynein localizes to three cellular locations (Fig. 8A). Plus end dynein localization is known to require Bik1 and Pac1^{84,98} and cortically anchored dynein requires both dynactin⁷² and Num1^{85,91}. Dynein also localizes infrequently to spindle pole bodies in yeast, but the functional relevance of this population is unclear. Spindle pole body localization may indicate active dynein motors⁸⁵ or it may be important for the interaction of dynein and kinesin complexes^{101,184}. Finally, localization of dynein can be impaired by loss of accessory chain binding³⁹. This simple but robust system should inform us if the highly conserved cortical offloading pathway of dynein was perturbed by any of our mutants. We omitted several motor domain and MTBD mutants from this

experiment, both due to the results from the spindle oscillation assay, and because these mutants would likely have minimal changes in localization.

Several tail mutants demonstrated altered dynein targeting frequency, namely L213I, N283R, E545V, I554M, and W612C (Fig. 8B-D). The W612C mutant demonstrated decreased frequency of dynein at microtubule plus ends (along with a decrease in fluorescence intensity) and the cell cortex. This data, and the overall loss of motility for W612C in our spindle dynamics assay, these data may indicate that this mutation induces protein misfolding leading to loss of active motors, or that this mutation may be ablating binding interactions with dynein effectors necessary for normal recruitment. Both E545V and I554M altered dynein localization frequency, which are located in a (putative) region that may stabilize dynein-dynein binding interface present in the mammalian 2 dynein:1 dynactin complexes. The I554M mutant had a decrease in plus-end targeting, but the E545V mutant had an increased localization of dynein to the cortex. This could further indicate the potential for mutant to interrupt dynein-dynein interactions necessary to form higher order dynein assemblies, as suggested previously for K540C and E545V. Two other tail domain mutation (L213I and N283R) demonstrated an increase in dynein intensity at microtubule plus ends, despite not changing frequency of localization, and it is interesting to note these mutants had increased transport frequency in our spindle dynamics assay, which could indicate these mutants cause overactive dynein.

Several motor domain mutants—K1475Q, R1852C, R2543K, and H3639P—demonstrated altered localization phenotypes which provided insight into their associated altered spindle dynamics (Fig. 8B-D). The R1852C, R2543K, and H3639P

Figure 8

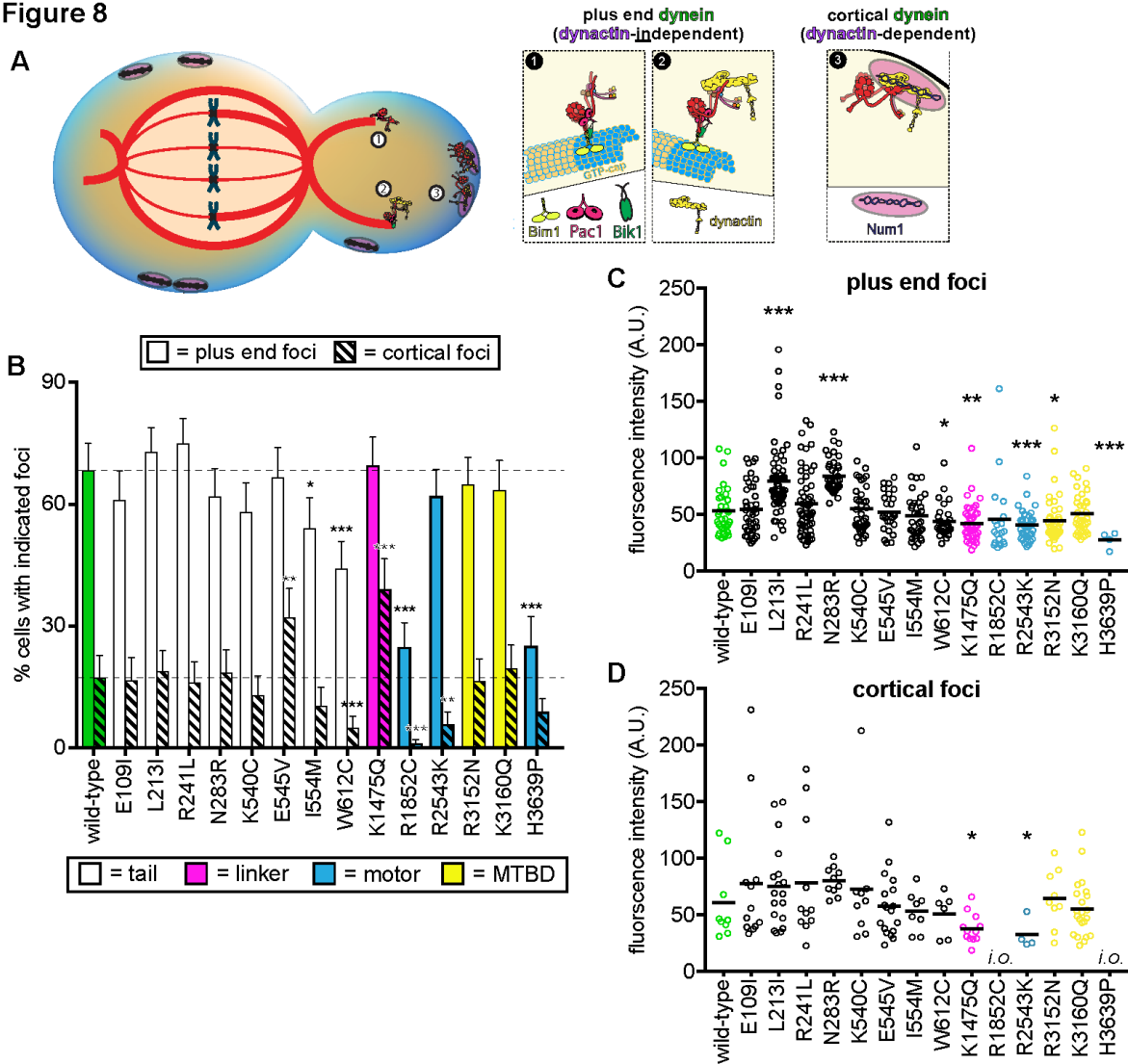


Figure 8. Quantitative assessment of dynein localization reveals potential basis for mutant dysfunction. (A) Cartoon representation depicting the two main sites of dynein localization, and the molecular basis for each. Dynein plus end localization (1) requires Bik1, Pac1, and possibly Bim1, but does not require dynactin. Rather, dynactin plus end localization (2) relies on dynein. Association of dynein with the cortex requires (3) dynactin and the cortical receptor, Num1. (B) The frequency of dynein localization to either microtubule plus ends or the cell cortex is plotted for indicated strains. To enrich for mitotic cells, overnight cultures were diluted into fresh media for 1.5 hours prior to imaging. To further reduce variability due to cell cycle-dependent changes⁸⁹, localization frequency was scored for mitotic cells only. Each data point represents the weighted mean \pm weighted standard error (68 to 111 mitotic cells from at least two independent experiments were analyzed for each strain). (C and D) Fluorescence intensity values for either plus end (C) or cortical (D) dynein foci observed in mitotic cells described in B (4 to 59 plus end foci, and 4 to 22 cortical foci from two independent experiments were analyzed; i.o., insufficient observations; only 1 cortical focus was observed for both R1852C and H3639P). Statistical significance was determined by calculating Z scores (B), or by applying an unpaired Welch's t test (C and D; *, $p \leq 0.1$; **, $p \leq 0.05$; ***, $p \leq 0.005$).

had large reductions in cellular activity, with the latter appearing highly similar to *dyn1Δ* yeast strains. This dynein-null like phenotype persisted in the localization assay, in which R2543K had reduced cortical dynein and substantial decreases in fluorescence intensity at the cell cortex. Strikingly, both R1852C and H3639P were greatly reduced in both the frequency of dynein targeting and fluorescence intensity metrics. This indicates that the loss of spindle dynamics is could be a result of depletion of dynein from astral microtubules and from the cell cortex. Loss of localization in these mutants may be a result of misfolding disrupting binding interactions, or misfolding causing proteasomal digestion thereby decreasing protein levels within the cells. While misfolding could explain loss of interaction with dynein binding partners, our phenotypes are unlikely to be related to simple protein aggregation, as mutant dyneins demonstrated no aggregates in cells. The overt loss of localization in our motor domain mutants mutant further explains why the H3639P mutant behaves so similar to *dyn1Δ* cells in our assays, and also why R1852C has such low activity levels in cells.

Since many of our mutants demonstrated loss of dynein targeting or decreases in fluorescence intensity, the logical question was to ask if these mutations were decreasing protein expression, either by reducing mRNA expression¹⁷⁶ or by causing protein misfolding and subsequent proteasomal degradation. All strains for purification had been constructed to have a *myc* tag on both Pac11 and Dyn3 for western blot analysis. However, as blotting against these accessories could only inform of dynein complex expression by proxy, western blot analysis was performed by blotting for the C-terminal GFP tag present in all live-cell strains used for our localization assay (See Methods). This experiment produced the unexpected result that all dynein mutants were

indeed expressed similarly to wild-type (Fig. 9); therefore, disruptions to normal protein-protein interactions, rather than decrease in protein expression, was responsible for driving the phenotypes observed in our localization assay. This result was expected given that the previous study which biochemically analyzed eight of the same mutants used in this thesis work did not see a loss of protein expression when purifying mutant recombinant human dynein from SF9 cells¹⁶⁴. It is likely that most dynein mutations behave in a dominant negative manner due to altered cellular localization and loss of motor function, rather than factors upstream of expression.

The K1475Q mutant phenotype was of great interest to us, as this mutant demonstrated a dramatic increase in cortical dynein foci, but an overall decrease in fluorescence intensity of plus end and cortical dynein foci. This result was not expected given the decrease in activity for this mutant in our spindle dynamics assay. While the results of the spindle dynamics assay led us to initially hypothesize that this linker mutation affects dynein mechanochemistry, this hypothesis could not explain such a robust increase in dynein localization. However, during this course of this thesis work, another study identified this residue as important for stabilizing dynein in an autoinhibited conformation in mammals¹⁶⁵. It was not obvious at the time of these experiments that yeast dynein was autoinhibited, as the motor is processive without the need for dynactin or adaptors¹⁶¹. Previous studies from our lab have proposed a mechanism of dynein “masking”, whereby intramolecular interactions between tail and motor domains limits association with dynein regulators including Pac1, dynactin, and Num1⁸⁴, in a mechanism reminiscent of kinesin autoinhibition^{185,186}. If the K1475Q

mutation were disrupting putative dynein autoinhibition, it would be expected to increase the association of dynein with dynactin¹⁶⁵, leading to increased cortical offloading.

Figure 9

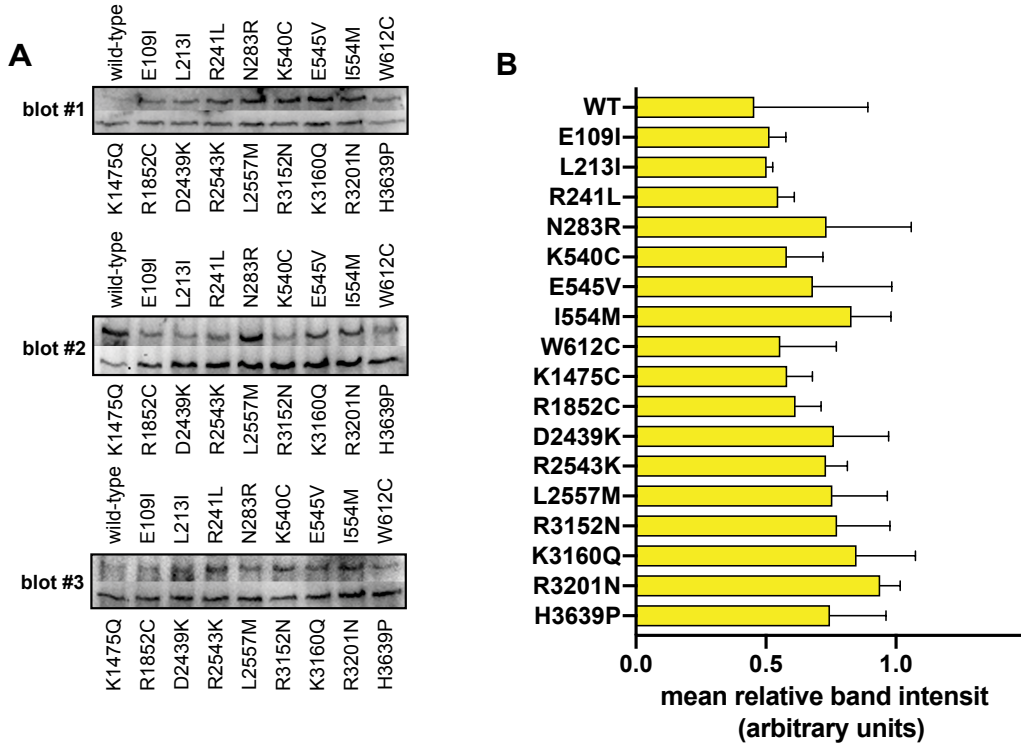


Figure 9. Change of protein levels is likely not responsible for any mutant phenotypes. (A) Immunoblots from three independent experiments (i.e., blot #1, #2 and #3) along with (B) plot depicting mean relative band intensity \pm standard deviation for each. Equal amounts of total cell lysate were loaded into each lane, transferred to PVDF and probed with a monoclonal anti-GFP antibody (also see Materials and methods). Note the high degree of variability between each independent immunoblot is likely a consequence of variations in transfer efficiency for the enormous dynein heavy chain protein to the PVDF membrane.

To determine if the K1475Q mutation increased dynactin interaction, I performed ratiometric fluorescence imaging of Dyn1-GFP and Jnm1-3mCherry (Fig. 10). This analysis was done in cells lacking Num1 to avoid complications of cortical offloading and to limit our analysis to plus end dynein-dynactin complexes. This experiment indicated that K1475Q did indeed increase dynein-dynactin interaction, as indicated by

a 50% increase in the Jnm1/Dyn1 signal at microtubule plus ends. These data further indicated the potential for this mutation to disrupt dynein autoinhibition.

Figure 10

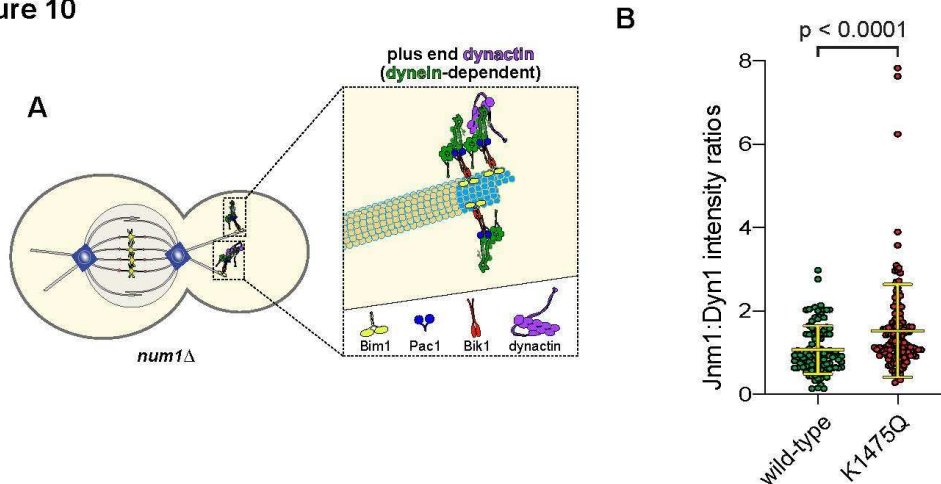


Figure 10. K1475Q recruitment of dynactin is enhanced. (A) Cartoon representation depicting the dynein-dependent localization of dynactin to plus ends. Limiting amounts of dynactin at plus ends with respect to dynein (~3 dynein:1 dynactin), is depicted based on previous quantitative ratiometric imaging (Markus et al., 2011). (B) Scatter plot (shown with bars depicting mean and standard deviation values) of the ratios of fluorescence intensity values for Jnm1-3mCherry:Dyn1-3GFP at microtubule plus ends and SPBs (n = 97–131 foci from two independent experiments). Background corrected intensity values of colocalizing Jnm1-3mCherry and Dyn1-3GFP foci were divided to obtain individual ratio values. Statistical significance was determined by applying an unpaired Welch's t test.

2.3.4. Single molecule *in vitro* motility of purified dynein mutants

The results of our *in vivo* assays provided valuable data about the effect of dynein mutation on cellular dynein-dynactin-adaptor activity, and how mutations impacted cortical offloading. In order to isolate the effects of mutation on intrinsic dynein motor activity we turned to our *in vitro* single molecule assay. In this experiment, natively-expressed dynein is isolated from yeast through affinity chromatography, and added to a coverslip containing taxol-stabilized microtubules for single molecule analysis using TIRF microscopy (Fig. 11A). The benefit of this system over using human

Figure 11

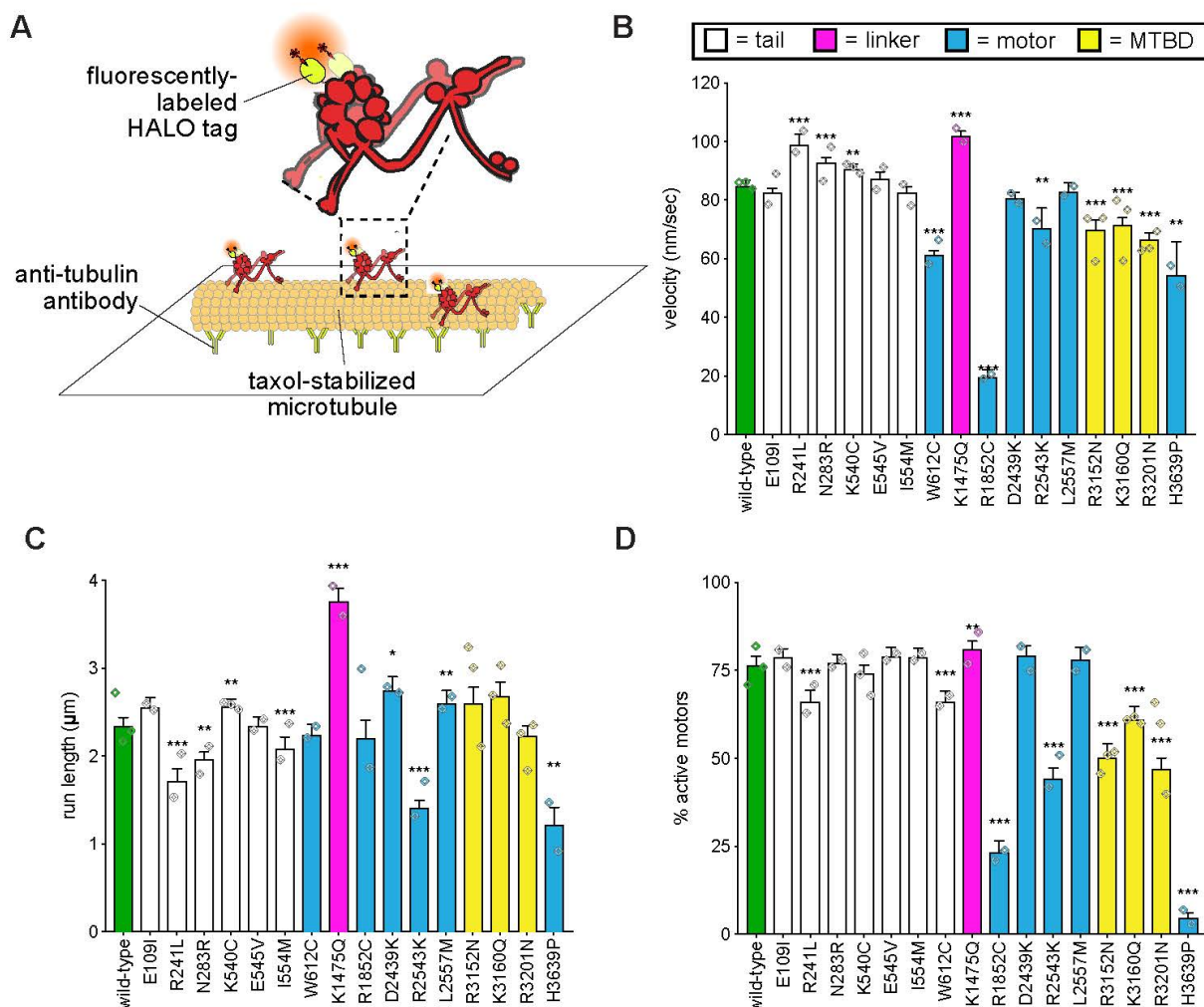


Figure 11. Single molecule analysis reveals insight into dynein-intrinsic dysfunction. (A) Cartoon representation of experimental approach. (B – D) Quantitation of indicated parameters of single molecule motility. Each bar represents the weighted mean \pm weighted standard error (or standard error of proportion for D; $n \geq 284$ single molecules from at least two experiments from independent protein preparations; diamonds represent mean values obtained from each independent protein preparation). Technical difficulties precluded us from generating the L213I mutant in the yeast strain used for protein purification. Statistical significance was determined using an unpaired Welch’s t test (B), a Mann-Whitney test (C) or by calculating Z scores (D; *, $p \leq 0.1$; **, $p \leq 0.05$; ***, $p \leq 0.005$).

proteins is that only dynein complexes are present in this system, which gives details about dynein-intrinsic motor property without the confounding effects of dynactin or different adaptors present. Taken together with our *in vivo* results, we can form a comprehensive picture of how dynein mutations impact motor function.

Using this assay, we found that the many of our mutants demonstrated both loss-of-function and gain-of-function parameters. Tail domain mutations produced the most minor *in vitro* motility deficits, and these phenotypes did not exclusively align with the deficits identified in our *in vivo* assays. Mutants R241L and N283R surprisingly had an increase in motor velocity, despite decreases in velocity *in vivo*, along with a decrease in motor processivity. Nearby residue K540C demonstrated a marginal increase in motor velocity and run-length; interestingly, this mutant was one of few gain-of-function mutations in our spindle dynamics experiment. Given that no dynactin is present in this experiment, it is there unlikely that this mutation is causing a disruption with dynactin or other dyneins within cells. Finally, W612C had marked decreases in velocity and activity, which matched the *in vivo* loss of cortical targeting and dampened spindle dynamics.

MTBD mutants had surprisingly similar phenotypes among all three tested. All motors had decreased velocity, and decreased number of processive motors, to similar degrees. There was no decrease in processivity, which was the expected outcome of loss-of-charge mutations at the microtubule-motor interface which itself is an interaction dominated by charged amino acids. However, the loss of velocity and increase in bound but non-processive motors, could indicate a problem in the microtubule binding domain's communication within the globular subdomain. It may be that this recognition of the MTBD for the microtubule lattice is impaired, or that transitioning between different MTBD conformations is stalled.

All three motor domain mutations had phenotypes highly similar to those evidenced in the spindle dynamics assay. While R2543K was only somewhat slower

than wild-type, motor run-length and activity were severely impaired. R1852C demonstrated severe reductions in all parameters measured, reinforcing all motility data from our *in vivo* experiments. As in our *in vivo* experiments, H3639 at first did not appear at all mobile. After analyzing hundreds of motors, it appeared that a very small fraction of these motors were indeed active; these results were only possible at first using our GST-DYN1 motor construct, which could be overexpressed at high enough levels to observe multiple moving motors at once. Consistent with our *in vivo* assays, a small population of motors had some level of near-normal motility. Interestingly, the motility of active motors was within the expected distribution for the wild type motors (Fig. 12A). This further indicates that the vast majority of H3639P dynein motors are non-functional, yet a small population of individual heavy chains may have normal function, leading to dimers with one functional and one non-functional heavy chain.

Surprisingly, K1475Q had faster motors, more processive motors, and more active motors. This result was unexpected due to the loss-of-function seen in the *in vivo* motility assay, and these results could not immediately explain why increased localization of dynein would lead to such dramatic increases in motors processivity and activity. It seemed unclear how these results could be related to dynein autoinhibition in some way. However, if these mutations affected the linker domain structure, it was feasible this could have an impact on motor speed or initiation of motility. It was also possible that this mutation caused aggregation of motors, which would explain the increased run length. Performing intensity analysis of single molecules in this study demonstrated no increase in motor aggregation (Fig. 12D), demonstrating that the increase in run length was a motor-intrinsic property. It is interesting to note that *in vitro*

gain-of-function mutants (R241L, K1475Q) had decreased motility in cells, indicating that gain-of-function for a single motor can have negative consequences in ensembles.

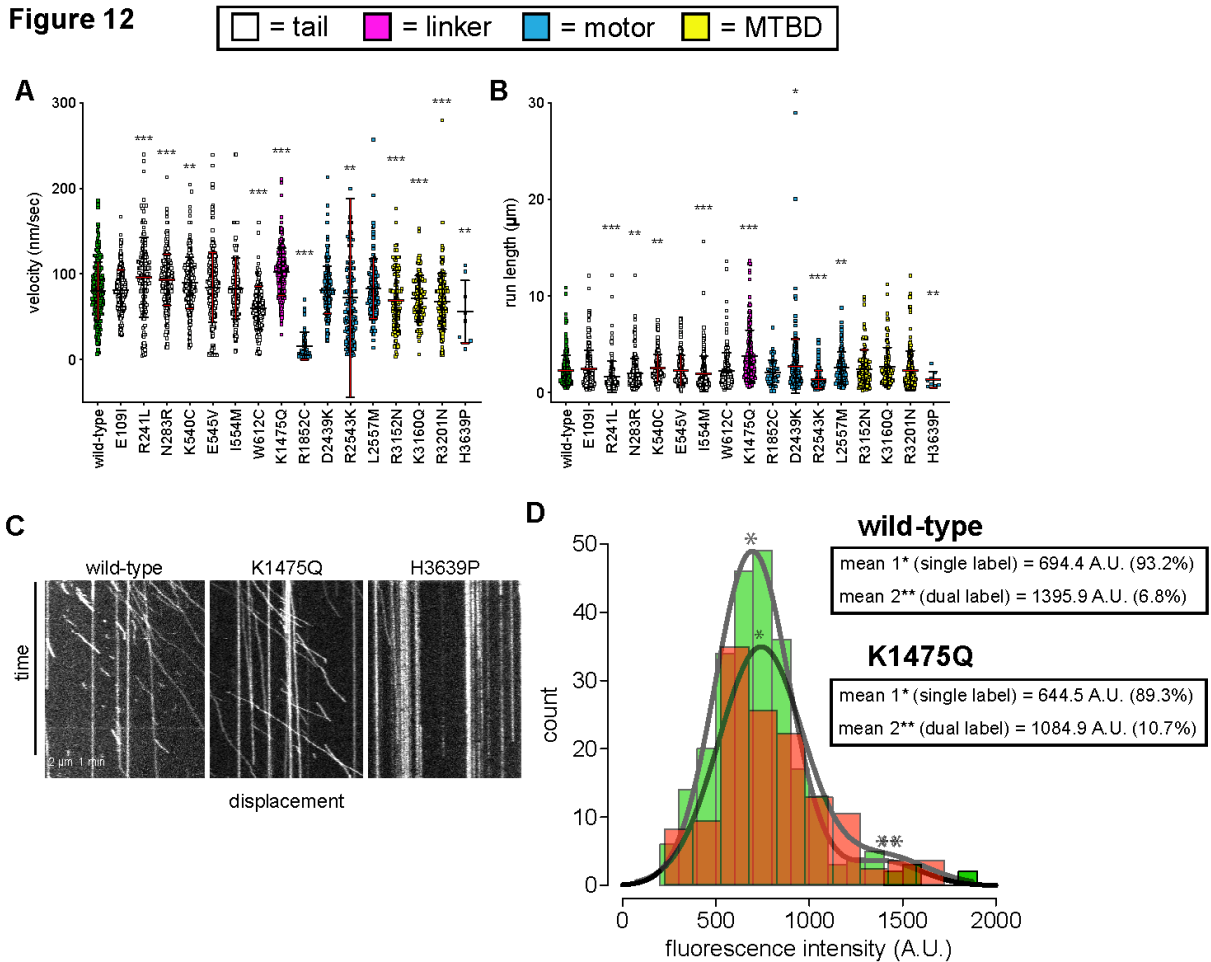


Figure 12. Extended single molecule data (A and B) Scatter plots depicting (A) velocity, and (B) displacement values for single molecule motility assays (from Figure 8). Mean values and standard deviations are depicted with red lines. (C) Representative kymographs depicting single molecules of full-length dynein (wild-type or mutants, as indicated) walking along microtubules in vitro. Green arrow within H3639P panel depicts the only moving complex within the kymograph. (D) Histogram of fluorescence intensity values for single molecules of motile wild-type (top; $n = 254$ molecules) and K1475Q (bottom; $n = 115$ molecules) dynein, along with accompanying Gaussian fits and modeled parameters (determined using the model-based clustering algorithm Mclust; Fraley and Raftery, 2007). The percentages reflect the relative proportion of molecules that fall within each component (i.e., for mean 1, and mean 2). The two mean values for each (indicated with asterisks) likely represent single-labeled (mean 1, *) and dual-labeled (mean 2, **) dynein dimers, respectively. Importantly, the values for K1475Q are not higher than wild-type, indicating the increased processivity for this mutant is not a consequence of increased motor

2.3.5. The H3639P mutation disrupts dynein activity due to loss of flexibility in AAA5 domain

The severity of H3639P mutation phenotype was initially an unexpected result, given that it is located in a flexible domain of dynein that does not bind or hydrolyze ATP, nor does it participate in any previously demonstrated intra- or intermolecular interactions (Fig. 13A). Despite this, this mutant led to an almost dynein-null phenotype in all of our assays, and has been shown to severely compromise the functionality of human dynein-dynactin-effector complexes¹⁶⁴ *in vitro*. To better understand why mutation of a histidine to a proline could cause a dynein null phenotype, I employed a mutagenesis-based approach using the spindle-positioning assay. Selective mutagenesis of the H3639 residue of interest revealed that only the proline substitution at this site caused loss-of-function phenotypes; neither serine, nor asparagine, nor valine caused the same phenotype (Fig. 13B). Molecular modeling revealed that the registry of the phi-psi angles along this loop region rotated substantially between the ADP-bound and ATP-bound crystal structures of dynein. Proline's ability to rotate about its phi-psi axis is limited to adopting either a *cis*- or *trans*- registry, and this rigidity might be causing the extreme phenotypes we observed

To determine if a loss of flexibility due to proline incorporation was causing the phenotype, I performed scanning mutagenesis within the loop region (Fig. 13B). Introducing single proline mutations from amino acid residues 3638-3645 indicated that this region could not tolerate incorporation of proline at either the H3639 or Y3641 position, indicating that presence of proline was driving this phenotype. The limitation of

Figure 13

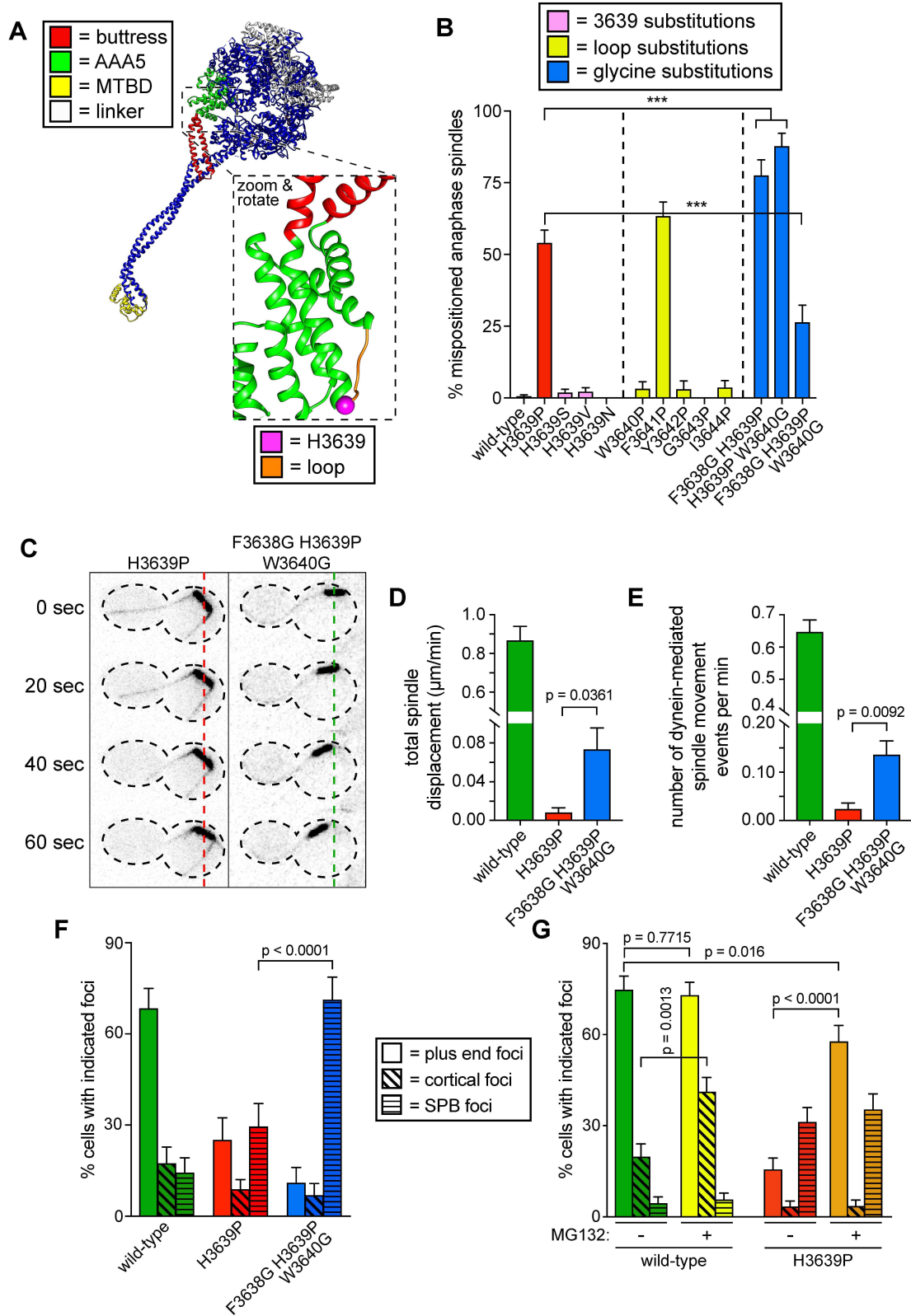


Figure 13. Detailed dissection of the molecular basis for dysfunction in H3639P. (A) Color-coded structural model of the dynein motor domain (from PDB 4RH765) with zoomed in region depicting H3639 residing within an inter-helical loop within AAA5. (B) Fraction of cells with mispositioned spindles are plotted for yeast strains with indicated dynein mutations. Each data point represents the fraction of mispositioned anaphase spindles along with standard error (weighted mean \pm weighted standard error of proportion; $n \geq 67$ anaphase spindles from at least two independent experiments for each strain; ***, $p \leq 0.0001$). (C) Representative time-lapse inverse fluorescence images of two indicated hydroxyurea (HU)-arrested *kar9 Δ* cells. Note the lack of spindle translocation in H3639P, but the clear dynein-mediated movement in the F3638G H3639P W3640G (dashed lines provide a point of reference). Maximum intensity projections are shown for each time point. (D - E) Plots of two activity parameters for spindle dynamics in indicated haploid strains (total displacement, D; and number of events per minute, E). Each data point represents the weighted mean \pm weighted standard error (D) or standard error of proportion (E; $n \geq 29$ HU-arrested cells from at least two independent experiments were analyzed for each strain). (F and G) The frequency of dynein localization to either microtubule plus ends, the cell cortex, or spindle pole bodies (SPBs) is plotted for indicated strains and drug treatment (for mitotic cells only). In addition to the indicated alleles and drug treatment, the plot in panel G depicts cells that possess the *prd1-DBD-CYC8* allele, which represses transcription of pleiotropic drug resistance genes⁹², thus promoting intracellular retention of MG132. These cells were treated with 75 μ M MG132 for 1.5 hours prior to imaging (control cells were treated with an equal volume of DMSO). Each data point represents the weighted mean \pm weighted standard error (73 to 107 mitotic cells from two independent experiments were analyzed for each strain). Statistical significance was determined by calculating Z scores (B, E, F and G), or by applying an unpaired t-test with Welch's correction (D).

proline to *cis*- or *trans*- isomers could further explain why the majority of proteins are inactive, with one isomer being less tolerated for normal mechanochemistry than the other. It is unclear if the proline rigidly limits this structure, or if isomerization could happen within individual motors to activate or inactivate them.

Before performing the western blotting experiment due to technical challenges, I first determined if proteasomal degradation of H3639P mutants was causing loss of the dynein foci present in the localization assay. To do this, I repeated the localization assay using MG132 to inhibit degradation of misfolded motors (Fig.13G). To overcome yeast response to actively exporting drugs from the cytoplasm, these experiments were done using *pdr Δ* strains, which eliminate the main transcription factor responsible for transcription of the 3 distinct dynein export pumps. Treatment with MG132 caused an arrest of cells in mitosis by inhibition of the APC/C complex, preventing metaphase exit². In wild-type cells, this led to no increase in plus-end dynein foci but a robust increase in cortical foci. This supports previous data that cortical offloading, rather than

plus end targeting, is a rate limiting step for dynein targeting to Num1^{81,98}. Imaging H3639P mutants revealed an increase in plus-end foci to near wild-type levels; however, this did not in turn lead to concomitant increase in cortical foci. Furthermore, after western blotting analysis (Fig. 9) of dynein expression revealed no change in protein levels between wild-type and H3639P cells. These two experiments reveal that while proteasomal degradation does not explain the H3639P phenotype, arresting cells in mitosis does allow the mutant motor to accumulate at microtubule plus ends, but not at the cell cortex. This could potentially occur through a subset of motors properly folding and eventually accumulating at the plus end following mitotic arrest, but may indicate mutants still have a more difficult time binding to the cortical receptor.

To further test the hypothesis that loss of flexibility in this region was causing loss of dynein function, I next incorporated single glycine residues to flank the proline residue. We hypothesized that by adding flexibility to this loop region in the form of glycines, we could overcome the rigidity of proline driving mutation. For reasons that are unclear, addition of a single glycine flanking the H3639P mutation at the 3638 or 3640 position did not rescue the dynein null phenotype (Fig. 13B). However, combining both flanking two glycines and creating a F3638G/H3639P/W3640P mutant led to a stark rescue in spindle positioning which was markedly less severe than a dynein-delete phenotype. I next tested the effects of this “GPG” mutant in compensating for the H3639P mutant in the localization and single molecule assays (Fig.13F, Fig.14F-J). Strikingly, expression of this mutant led to a marked increase in dynein foci; however, this mutant did not properly accumulate at the plus-ends of microtubules (Fig. 13F). This mutant localized at the spindle pole body, though the consequences of this new

localization pattern are unclear. Even though this mutant did not have a wild-type localization phenotype, this increase in dynein foci was accompanied by an increase in overall activity parameters in the spindle oscillation assay compared to the H3639P alone (Fig. 13C-E). This increase in frequency of movement is consistent with the 50% decrease in spindle positioning for GPG over the H3639P mutant (Fig. 13B). However, the overall poor quality of spindle movements was maintained in the GPG mutant (Fig. 14A-D). Finally, comparing the H3639P and GPG mutants in single-molecule experiments (Fig. 14F-J) revealed no change in either fraction of active motors or motility parameters, which indicates that the increase in flexibility does not compensate for the intrinsic loss of motor function caused by the proline mutation.

The addition of flexible glycines flanking the proline mutants led to a partial rescue in activity in cellular assays, but did not improve motility parameters in *in vitro* experiments. The increased flexibility provided by the GPG mutant may allow dynein to isomerize between *cis*- and *trans*- proline registries, or simply shift the equilibrium towards more active motors. This mutant phenotype in the spindle oscillation and positioning assay indicates that even a small increase in cortical dynein activity greatly rescues spindle-positioning outcomes, potentially by allowing dynein to better interact with the plus-end targeting machinery and cortical targeting receptor Num1. However, as this mutant did not rescue for single-molecule activity, it is possible the replaced residues F3638 and W3640 are important for motility, or that even with improved flexibility there is still substantial loss of normal mechanical remodeling of AAA5. These results demonstrate that *de novo* proline mutations can disrupt important flexible regions in protein structures.

Figure 14

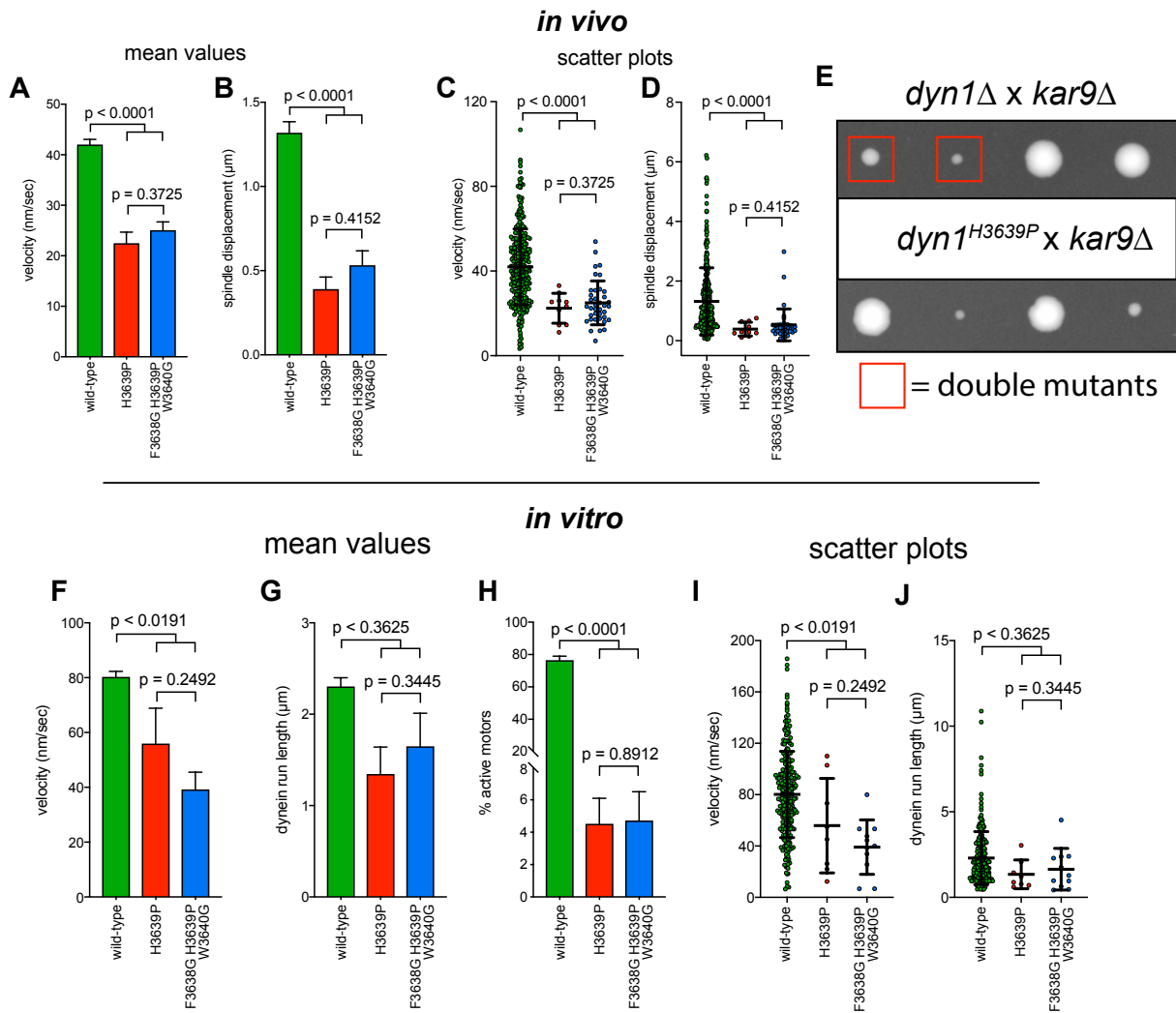


Figure 14. Extended data for H3639P mutagenesis in *in vivo* and *in vitro* assays. (A - D) Plots depicting the velocity (A and C) and displacement (B and D; per event) values obtained from the spindle dynamics assay for the indicated haploid strains. For panels A and B, each data point represents the weighted mean \pm weighted standard error (at least 29 HU-arrested cells from at least two independent experiments were analyzed for each strain). For panels C and D, mean values and standard deviations are depicted with black lines. (E) Cells expressing *dyn1*[H3639P] exhibit synthetic growth defects with *kar9Δ* that are as severe as *dyn1Δ kar9Δ*. Tetrads were dissected on YPAD media, and subsequently genotyped by growth on selective media. One representative tetrad each from a mating of a *kar9Δ* strain with either *dyn1*H3639P or *dyn1Δ* is shown. Double mutants are indicated with red boxes. (F-J) Quantitation of indicated parameters of single molecule motility. For panels F– J, each data point represents the weighted mean \pm weighted standard error (F and G), or \pm standard error of proportion (for H; at least 234 single molecules from at least two independent experiments were analyzed for each motor variant). For panels (I and J), mean values and standard deviations are depicted with black lines. Statistical significance was determined using an unpaired Welch’s t test (A, C, F and I), a Mann-Whitney test (B, D, G and J), or by calculating Z scores (H).

2.3.6. The R1852C mutation introduces an ectopic disulfide bond

The second most severe mutations characterized in this study was the R1852C mutant, which severely compromised both *in vivo* and *in vitro* motor activity, and led to a depletion of dynein foci from cellular compartments. This mutation also led to complete loss-of-function for the dynein motor using human dynein in microtubule gliding assays and single molecule assays²⁷. Analysis of the yeast crystal structure revealed that this mutation was in AAA1 domain, the primary site of ATP hydrolysis necessary to effect motor activity. However this substitution of arginine to cysteine does not occupy a position within the Walker A or Walker B site of AAA1, and is not positioned to effect ATP binding or hydrolysis. However, after examination of the crystal structure of this domain, it became evident that this mutation positions the new 1852 cysteine residue approximately 3.5 Å away from a neighboring cysteine residue, C1822 (Fig. 15A). Both the sequence at the C1822 site and residues at the R1852C site were highly conserved across eukaryotes (Fig. 15B). We reasoned then that the severe phenotype from this mutation could be due to formation of a disulfide bond between the C1822 native residue and the R1852C ectopic residue. While disulfides are normally not present in dyneins, this was our best hypothesis, given the high degree of conservation, the highly suitable bond angle and positioning between the two cysteines, and the severity of phenotype expected to follow from crosslinking two different subdomains in AAA1.

Figure 15

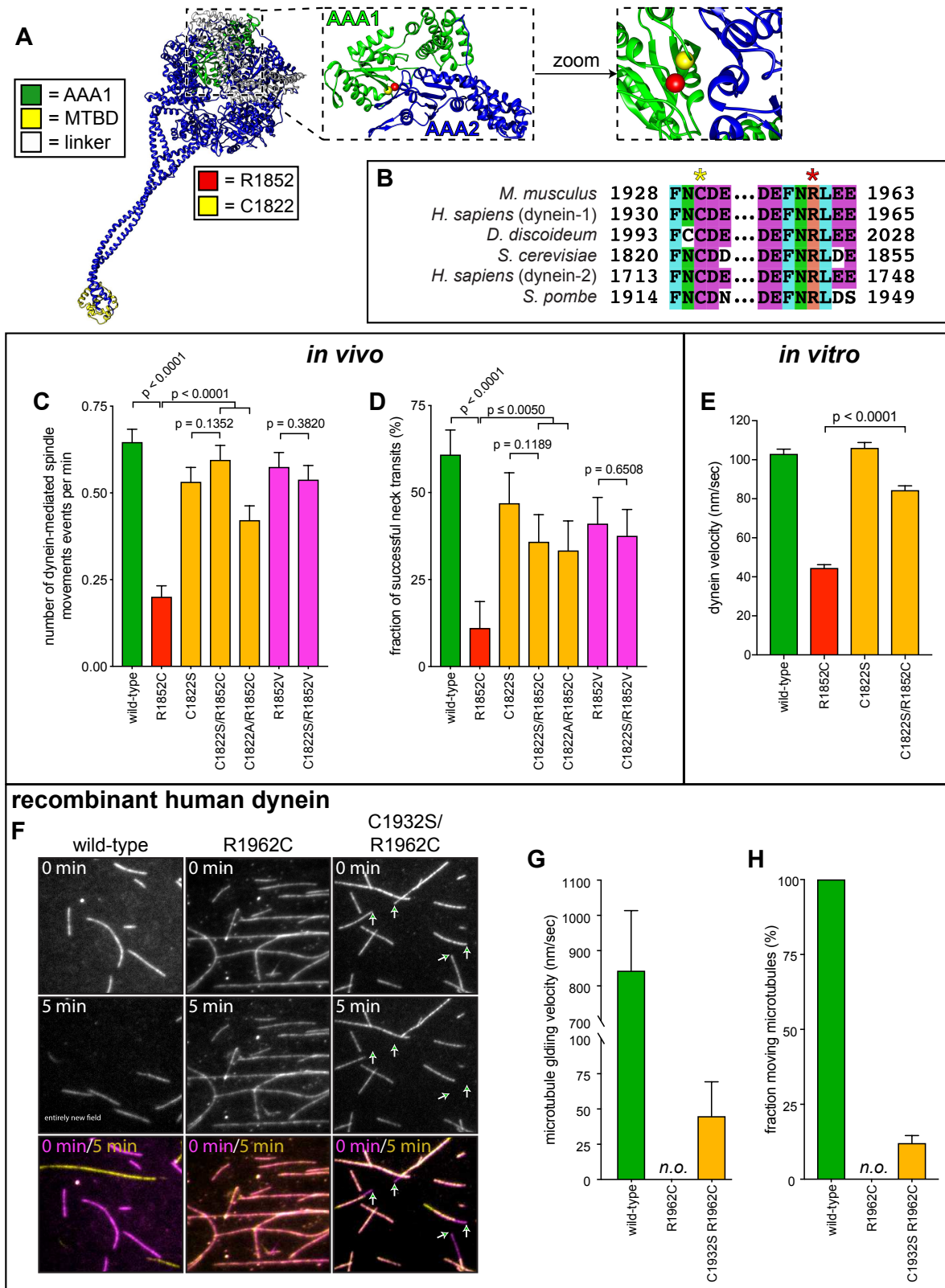


Figure 15. Detailed dissection of dysfunction in R1852C reveals an ecopic disulfide bond formation is likely driving mutant phenotypes. (A) Color-coded structural model of the dynein motor domain (from PDB 4RH7; Schmidt et al., 2015) with zoomed in region depicting R1852 residing within AAA1 near its interface with AAA2. (B) Sequence alignment illustrating the high degree of conservation for C1822 (yellow star) and R1852 (red star) among various dynein heavy chains. (C and D) Plots of two activity parameters for spindle dynamics in indicated haploid strains (total displacement, C; and, fraction of successful neck transits, D). Each data point represents the weighted mean \pm weighted standard error (C) or standard error of proportion (D; $n \geq 28$ HU-arrested cells from two independent experiments were analyzed for each strain). (E) Plot of velocity values for single molecules of indicated GST-dynein331 variants ($n \geq 158$ single molecules from at least two independent experiments were analyzed for each motor variant). (F) Representative fields of microtubules being translocated by surface-adsorbed recombinant human dynein complexes. (G and H) Plots depicting velocity (G) and fraction (H) of microtubules (at least 50 microtubules from two independent experiments were analyzed for each variant; 'n.o.', none observed). Statistical significance was determined by calculating Z scores (B and E), or by applying an unpaired Welch's t test (D).

To first test this hypothesis, I generated a series of mutations at the C1822 and R1852 site for analysis in our localization and spindle oscillation assay. In our localization assay, we first asked if substituting a serine for the cysteine at position 1822 could compensate for the loss of foci introduced by the R1852C mutation. We were surprised to find that this substitution (C1822S/R1852C) did indeed rescue dynein foci to near wild-type levels for both plus-end and cortical foci. The control strain C1822S had wild-type foci levels as well, indicating that this rescue was not due to excess accumulation of dynein due to the C1822S residue (Fig. 16D). However, it was still not clear that this effect was due to a disulfide bond. It was feasible that the R1852C mutant phenotypes could be due to the incorporation of a hydrophobic cysteine at the site of an electrostatic residue, which could “blow up” the otherwise hydrophilic pocket. Therefore we tested if a R1852V mutation would have the same effect as the R1852C phenotype. Indeed, the R1852V mutants had comparably low levels of dynein foci as the R1852C mutant. However, in agreement with our disulfide bond hypothesis, the C1822S/R1852V mutant did not rescue the cellular dynein foci level at all, and instead maintained the R1852V phenotype. Therefore, we concluded that as the C1822S/R1852C phenotype

produced the only rescue, it could indeed be due to the introduction of an ectopic disulfide bond.

To further test if an ectopic disulfide bond was responsible for the R1852C phenotype, cells were treated with two different reducing agents, dithiothreitol (DTT) and N-acetylcysteine. While we expected these treatments to restore dynein foci, treatment of cells with these compounds led to no increase in dynein foci at concentration ranges from 1 to 10 μ M. While these data do not support our hypothesis (data not shown), there are two possibilities for why we observed no rescue. Firstly, these experiments were done in yeast with active export pumps, which may have prevented saturation of intracellular dynein with reducing agents. Secondly, analysis of the structure indicates that these residues are buried within the AAA1 domain and are likely not solvent exposed, especially if this domain is folded cotranslationally. If this were the case, ectopic treatment with chemical reducing agents would not have an effect on disulfides present internal to the motor.

As the C1822S/R1852C mutant was capable of rescuing the localization phenotype, we next asked if this increase in cortical dynein would lead to a concomitant increase in dynein activity in our spindle oscillation assay. While the C1822S mutant alone was sufficient to compromise all metrics of *in vivo* motility: velocity, processivity, and activity, the C1822S/R1852C mutant had comparable motility metrics (Fig. 15C,D). This rescue mutant performed substantially better in the activity metric than the R1852C mutant alone, further indicating that this rescue was due to disulfide bond formation. As expected from the localization assays, the R1852V mutants demonstrated reduced activity. However, the C1822S/R1852V mutants behaved identically to the single

R1852V mutants, indicating that while the valine mutant leads to compromised motor activity, it is most likely affecting the motor domain differently than the R1852C mutant. Further, these results disfavor a model where the incorporation of a cysteine is driving hydrophobic expansion of the AAA1 site. As a final test, a C1822A/R1852C mutant was sufficient to rescue the loss-of-function of the R1852C mutant; however, this mutant had less activity than the C1822S/R1852C mutant, indicating maintaining the polar nature of residues in this region is important for dynein mechanochemistry.

Given this cellular data, we turned to our *in vitro* motility assay to determine if the C1822S/R1852C rescue improved the motility of single dyneins. In contrast to the limited rescue we obtained from the H3639P mutants, the incorporation of the C1822S/R1852C mutation did in fact lead to increased motor velocity and processivity (Fig. 15E), indicating the *in vivo* rescue was indeed indicative of improved individual motor function. As in the live cell assays, treatment of purified motors with additional DTT (beyond what is normally present in these buffers) did not lead to improved motor function, and instead decreased the activity of even wild-type dynein. This result is consistent with the R1852C residue residing internal to the motor structure and unable to interact with solvent. Unexpectedly, expressing the R1852C mutant in our GST-dynein motor truncation (lacking most of the tail region) led to a large increase in percent of motor activity, while still leaving velocity and processivity compromised. In this background, the C1822S/R1852C mutant did not increase the fraction of active motors, but did improve velocity and processivity metrics (Fig. 16E-G). While it is unclear why expressing the R1852C mutant in the GST-dynein motor domain fragment is more active than the full-length, we propose that the disulfide bond introduced by the R1852C

Figure 16

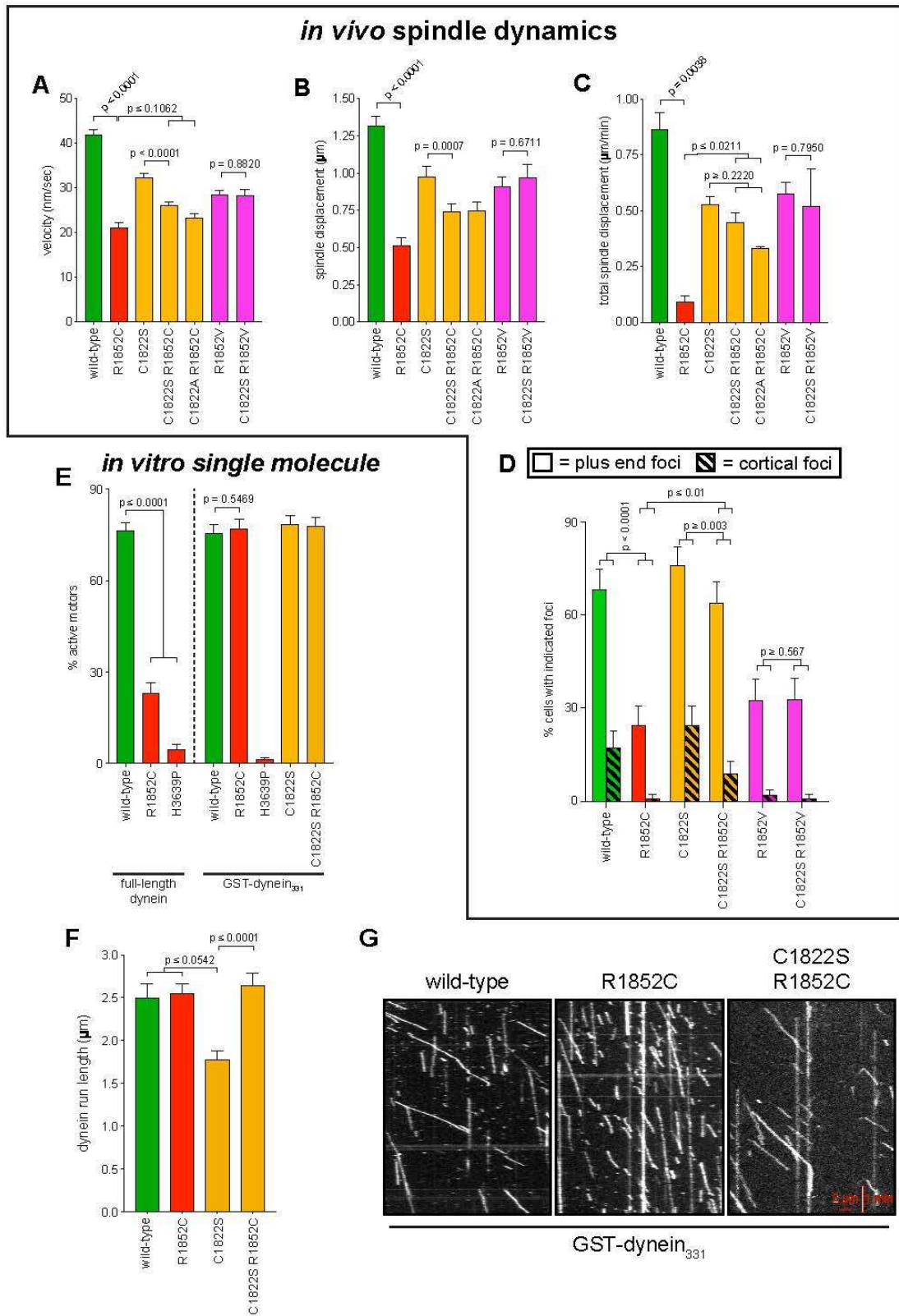


Figure 16 Extended data for characterization of R1852C mutant. (A – C) Plots depicting the indicated motility parameter values obtained from the spindle dynamics assay for the indicated haploid strains. Each data point represents the weighted mean \pm weighted standard error (at least 28 HU-arrested cells from at least two independent experiments were analyzed for each strain). (D) The frequency of dynein localization to either microtubule plus ends or the cell cortex is plotted for indicated strains (scored as described in Figure 5 legend). Each data point represents the weighted mean \pm weighted standard error (94 to 105 mitotic cells from at least two independent experiments were analyzed for each strain). (E) Plot depicting the fraction of active motors for the indicated full-length complexes (left), or the minimal motile fragment (GST-DYNEIN; see text; right). Note the minimal fragment rescues the reduced fraction of active motors in the R1852C mutant. (F) Plot depicting single molecule run length values for indicated GST-DYNEIN variants. (G) Representative kymographs depicting single molecules of GST-DYNEIN (wild-type or mutants, as indicated) walking along microtubules in vitro. Statistical significance was determined using an unpaired Welch's t test (A and C), a Mann-Whitney test (B and F), or by calculating Z scores (D and E).

mutation is incorporated co-translationally, and that expressing the motor fragment may prevent the formation of the ectopic disulfide. It is worth noting that expression of the H3639P mutant in the GST-dynein background did not lead to a similar increase in activity (Fig. 16E), which further confounds explanation of why the GST-dynein rescues R1852C motility.

Finally, to further validate the efficacy of this rescue mutation, we turned to the SF9 expression system to produce recombinant dynein mutant complexes. A previous study¹⁶⁴ demonstrated that in human dynein, the R1962C (R1852C in yeast) mutant led to a complete loss-of-function of the motor in ensemble microtubule gliding assays. In this type of assay, dynein motors are adsorbed to a coverslip and taxol stabilized microtubules are added to the chamber. Adsorbed dynein motors then translocate the microtubule, which informs about the intrinsic motility of human dynein in the absence of dynactin or effector proteins required for single molecule motility. To test the efficacy of our rescue mutant, I purified wild-type, R1962C, and C1932S/R1962C dynein constructs. Firstly, I was able to reproduce previous results of the R1962C mutant having no activity¹⁶⁴. Satisfactorily, the 932S/R1962C rescue mutant was able to partially restore functionality to this mutant, which validates our yeast dynein results.

While this rescue was less pronounced than in our yeast system, and still led to poor motor activity, the C1932S mutant led to marked reductions in motor velocity (100-200 nm/s, versus 800 nm/s for wild type, data not shown). These data indicate that the rescue mutation identified in yeast was translational in human proteins. This experiment demonstrates the experimental power of our yeast system complemented by the SF9 system, and its suitability for translational studies of human dynein. Further these data confirms the high degree of similarity between mutant behaviors in yeast and human dynein and provides a platform in which yeast mutations can be analyzed and introduced into the human motor for validation of rescue mutation efficacy.

2.4. Discussion

2.4.1. How human mutations drive dynein dysfunction in our yeast model system

The summarized results of all of our assays are summarized as a heat map (Fig. 17), color-coded on the basis of degree of deviation of mutant phenotype from that of the wild type. A surprising result of this study was that nearly all mutants demonstrated phenotypes, which demonstrates the suitability of our yeast platform to understand dynein point mutations. Many mutants demonstrated both loss- and gain-of-function mutations, with the former typically associated with motor domain mutants and the latter with tail domain mutants. Most, but not all, of the severe mutations, clustered in the motor domain, which was an expected result, given this is the most evolutionarily conserved region of dynein. Mutations in AAA1 and AAA3, the primary catalytic sites of ATPase activity, dramatically impacted motor function and localization. However, the most severe mutation was in AAA5, which is not associated with catalytic activity, indicating that dysfunction in mechanochemistry can be caused by mutations outside of

sites of ATP hydrolysis. Mutants in the MTBD produced moderately severe phenotypes in our assays, which is an expected outcome due to the similarity of the MTBD between

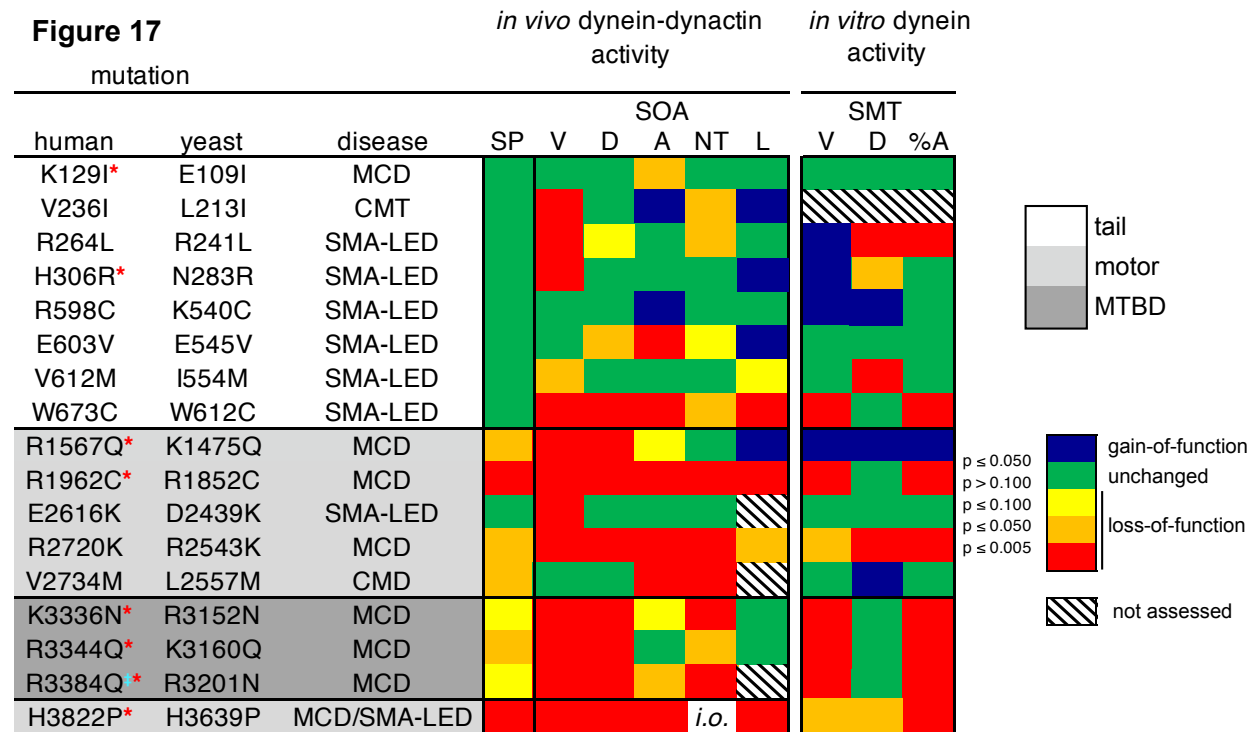


Figure 17. Summary of phenotypic analysis of our mutant library. Heat map depicting degree of statistical significance for difference between each mutant and wild-type cells for the indicated assays (SP, spindle positioning (Figure 3); SOA, spindle oscillation assay parameters; (Figure 4 and 5) V, velocity; D, displacement per event; A, activity; NT, neck transit; L, localization. SMT, single molecule tracking parameters; (Figure 11 and 12) V, velocity; D, displacement, %A, percent active motors. Disease column: MCD, malformations in cortical development; CMT, Charcot-Marie-Tooth disease; SMA-LED, spinal muscular atrophy with lower extremity dominance; CMD, congenital muscular dystrophy). Red asterisks depict mutants that were assessed in a previous study using recombinant human dynein (Hoang et al., 2017). Deviation from wild-type cells in either the ‘total spindle displacement’ (see Figure 4E), or the ‘number of dynein-mediated spindle movements per minute’ (see Figure 4F) metric was used for the activity column (‘A’). Mutants are listed from N- to C-terminus of Dyn1 (shading indicates in which domain of Dyn1 each mutation resides). Significance was calculated as indicated in previous figure legends corresponding to each assay.

yeast and humans. As each of these mutations led to the loss of positively charged residues at the MTBD-microtubule surface, or proximal to these regions, these phenotypes may simply be explained by the loss of ionic strength in the dynein-microtubule interaction. However, this simplified model is not necessarily true, as these residues may participate in intramolecular interactions that aid in switching the MTBD

from high to low affinity states, and vice-versa. Finally, mutations to the more divergent tail domain produced phenotypes in *in vivo* dynamics assays, and expectedly, led to less severe phenotypes than those present in the motor domain. A possible explanation for these milder phenotypes is that tail contacts with dynactin and effector proteins are more poorly conserved, especially in tail regions, which may differentially bind unique effectors and cargo present in neuronal systems but not present in yeast.

One promising result of this project was that the most severe mutant phenotypes correlated with the most severe disease states in humans. While this correlation does not hold true for every mutation, the three most severe loss-of-function phenotypes—R1852C, R2543K, and H3639P—are correlated with MCD and developmental disorders. R2543K is of particular interest, as the mutation was identified in germ line cells of one patient and caused all offspring to be non-viable after several weeks of gestation¹⁴⁶, presumably due to a loss of dynein activity from zygote derived dynein after the pool of maternally loaded dynein proteins and mRNAs had been depleted. In the two most severe mutation phenotypes, we were able to ameliorate mutant loss-of-function through compensatory mutagenesis. While we were able to narrow down potential molecular defects of the R1852C and H3639P mutants, and correct them through mutagenesis, it is unclear how in the R2543K mutant such a small change—an arginine to a lysine—would elicit such a profound loss-of-function. However, what we may surmise from these data is that the greater the loss-of-function in our assays, the more pronounced the disease state present in human neurological disorders. This does not account for the gain-of-function phenotypes evidenced by mutations in the linker or tail domain, however.

Finally, the results of our experiments line up closely with those results generated using recombinant human dynein complexes¹⁶⁴, which also identified the R1852C and H3639P mutations as the most severe phenotypes. Important to note is that this study was limited by the time it takes to generate mutants of recombinant human dynein and to purify mammalian dynactin from whole brains, and our own study presented many benefits over the former. Namely, that a large number of mutations could be introduced to compensate for the disease-correlated mutation, making our yeast system is ideal for exploring and dissecting the defects introduced by single amino acid substitution. Our validation of our rescue mutation with human proteins (Fig. 15F-G) indicates that yeast dynein does in fact have the potential to correctly determine molecular mechanisms governing motor dysfunction. Furthermore, it indicates yeast would make a rugged platform for high throughput system for drug discovery before testing on higher eukaryotes.

While the interactions between dynein, dynactin, and effectors may be divergent due to the need for higher eukaryotes to distinguish cargos, one piece of data that warrants further experimentation was mutants in the 540-554 region, and the implications for the assembly of dynein-dynactin-Num1 complexes at the cortex. Previous studies has shown that up to two dynein dimers may bind to a single dynactin in mammals^{93,94}, and that this multivalent interaction is differentially bridged by different effector proteins. To date, no data has indicated that two dyneins may bind dynactin in complex with human NuMA, or indeed that two yeast dynein dimers may bind a single yeast dynactin. However, three mutants with disparate phenotypes clustered in the tail region that has been shown to be important for mediating this interaction between one

dynein dimer heavy chains with the intermediate chain of the second dimer.⁹⁴. While atomic resolution of this region has not been obtained, this region appears to encompass K540C, E545V, and I554M. In these assays, K540C, E545V, and I554M all led to phenotypes, and the latter two led to a decrease in *in vivo* motility parameters and changed the localization patterns of dynein. As E545V had no change in velocity but instead had a decrease in force generation (as determined by neck transit frequency) and an increase in cortical foci, it seems highly probable that this mutant is a result of disrupting dynein-dynein-dynactin interaction. Additionally, the E545V mutant demonstrated severe loss in function in our spindle oscillation assays using diploid cells, which was an unexpected result at the time. If this mutant does disrupt high order assemblies of dynein-dynactin, it would explain the severity of the dominant negative phenotype. Further experiments will be needed to be completed to determine if yeast dynein shares the ability to form a dynein-dynein-dynactin-effector complex.

One of the key advantages to the budding yeast dynein system is the haploid nature of yeast in our cell biological studies. However, in the context of human disease, *de novo* mutations are almost exclusively heterozygous in nature by definition, and must therefore have dominant negative effects on dynein function. We addressed these questions with complementary *in vivo* and *in vitro* motility approaches to understand how mutations affected dynein function. Surprisingly, all three mutants (E545V, R1852C, H3639P) tested in this assay had severe loss-of-function phenotypes, despite the E545V mutant having much subtler loss-of-function in our assays using the haploid complex. As discussed above, this may be due to loss of maximally activated dynein-dynein-dynactin-effector complexes; however, the phenotype was similar to the

WT/R1852C heterozygote. This suggests dynein heterodimers may be a more biologically relevant way to assess the effects of dominant negative phenotypes. Finally, analyzing the distributions of motor activity in this assay revealed that in all mutants, even the WT/H3639P heterozygote, had instances of motility comparable to wild-type, and some much closer to mutant-only dynein, which indicated some dynein cortical pools were comprised entirely of the wild-type or the mutant complex. It was still unclear from just this data if dynein could exist as a heterodimer within cells or if it only existed as a homodimeric complex; however, the results of our single molecule experiments using diploid strains revealed that within yeast, dynein exists almost exclusively as homodimeric complexes. These could be formed by cotranslational folding of dynein monomers from a single mRNA, as has been observed for p53¹⁸³.

While this result was unexpected, it is likely important for consideration in all disease states which present as dominant negative mutations, especially given the potential for mechanistic differences between homo- and heterodimeric motor protein assembly^{163,184}. Mutations with dominant-negative effects are an abundant finding since the advent of whole exome sequencing, and targeted therapeutics are more likely to be employed against broader classes of mutation varieties than with the pin-point accuracy needed to treat any given individual with a point mutation. In the case of dynein, or any motor that is cotranslationally assembled, hemizyosity may present with subtler effects than dominant-negative mutations¹⁵⁶, evident in the case of heterozygous dynein mutants. Given this, it is more likely that treatment aimed at silencing the mutant genetic locus, or by knocking down select mRNA transcripts, would be substantially more feasible than targeted gene repair. Development of such treatment are already studied

for applications in treating congenital muscular dystrophies, many of which are due to mutation of the dystrophin gene. Kinase inhibitors which modulate protein splicing, and which can preferentially prevent splicing of a commonly mutated exons, have demonstrated successes in rendering the disease state more manageable^{170,187}. If similar compounds could be found which target the upstream effectors of dynein assembly, they represent the best currently available treatment to diseases caused by single point mutations.

Finally, our data acquired from analyzing the K1475Q mutation provided us the first evidence that yeast dynein undergoes autoinhibition comparable to human dynein. This result was unexpected, as yeast dynein was not expected to form an autoinhibited state due to its *in vitro* activity¹⁶¹ and previous structural studies using the GST-dynein motor⁴⁹. This mutant increased cortical offloading and interaction with dynactin, which has the expected consequences of disrupting autoinhibition. Despite the increased cortical offloading, these cells had dampened spindle dynamics, indicating loss of autoinhibition may affect normal mitotic spindle positioning, as has been observed in human cells *in vitro*¹⁶⁵. Quizzically, this mutation also increases dynein motility *in vitro*, a result not readily reconciled at the time of the mutant screen. However, we later determines why disrupting autoinhibition changes *in vitro* motility. These data were limited at the time, but provided our first look at the function of dynein autoinhibition in yeast. Finally, as many different disease causing mutations are located in regions expected to maintain dynein autoinhibition, such mutations represent a promising path to develop therapeutics, such as inhibitors that counteract dynein overactivity.

2.4.2. A correlative approach to linking dynein mutation with disease severity

As noted previously, our three most severe loss-of-function mutants were correlated with the most severe human disease states. However, this correlation is superficial and does not account for more subtle loss-of-function and the gain-of-function phenotypes we observed for the library of mutants. To correlate phenotypic outcome with disease state in a more precise way, we developed the metric of cumulative dynein dysfunction (CDD) score (Fig. 18). The tabulation of CDD scores presented a statistics-driven analysis of phenotype-genotype correlation (Tables 1 and 2), and we found that there is indeed a correlation between deviation from wild-type dynein function and severity of disease state. In tabulating these scores, we chose to focus specifically on *in vivo* dynein activity, due to dynein's reliance on dynactin for function in all these assays.

Furthermore, it was necessary to consider both loss-of-function and gain-of-function, which accounts for present models of dynein regulation in neurons. That is, that a dynamic equilibrium is established between anterograde and retrograde transport, and minor perturbations to transport in either direction may have severe consequences for cell health, especially in long microtubule processes as those found in the axons motor neurons. Therefore, it is not only loss-of-function mutants that negatively impact neuronal health but also overactive dynein mutants, an important finding that needs be considered when assessing dominant-negative phenotypes in many classes of motor proteins. It was noteworthy that the most severe drivers of disease are both complete loss-of-function, as may be expected for a protein, but also robust gain-of-function. Both disease states may exert dominant negative effects when

considering the delicate homeostatic balance that is maintained within neurons, and too much dynein activity may demonstrate the same *in vivo* phenotypes as no dynein activity. While this paradigm is confounding when dissecting the phenotypic outcome of disease states, it further demonstrates the efficacy of our yeast dynein system. By measuring the overall discrepancy from wild-type we can obtain informative data of potential for disease severity of a given mutation.

Figure 18

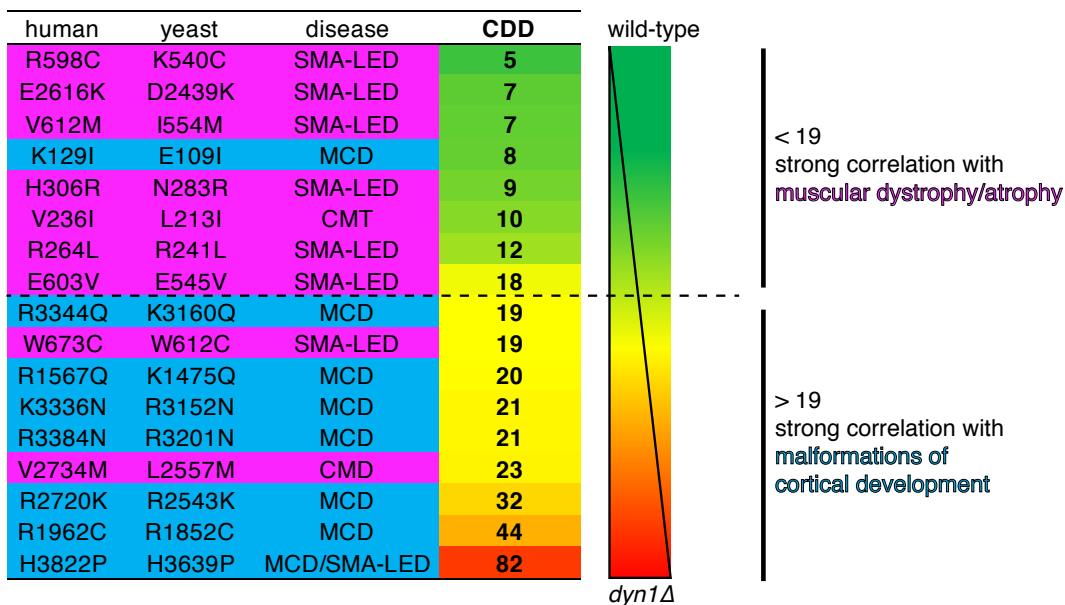


Figure 18. Correlation of composite deviation from wild type informs on severity of disease. Each coefficient of dynein dysfunction score (CDD; see text, Table 1 and 2, and Figure 17) was assigned by creating a composite nominal score of how each mutant deviated from wild type dynein in our *in vivo* assays. At a threshold CDD of ~18, mutations transition from strongly correlated with muscular dystrophy/atrophy to increasing correlation with developmental neurological disorders, suggesting a critical threshold requirement for dynein activity during development

The results of our CDD tabulation indicated that there is, broadly, a “tipping point” for dynein dysfunction between the two broad classes of diseases, motor neuron diseases and developmental disorders. At low levels of dysfunction, dynein mutations

primarily drive motor neuropathy related diseases. In these disease states, a subtle loss of dynein functions may introduce minor defects that do not overtly or dramatically impact dynein during development. However, when these defects accumulate over an individual's life they become more progressively more severe, as is the case for many spinal muscular atrophy. This hypothesis is supported by our correlation of phenotype to disease state, as very minor loss-of-function phenotypes in our *in vivo* assays correlate with diseases with late onset and muscular degeneration. Mutations that are drivers of more severe disease states, such as malformations of cortical development, may share this mechanism of disease progression as defects in retrograde trafficking accumulate. Unfortunately, the more severe defects and early age of onset presented by these developmental diseases may mask symptoms shared with motor neuron disease. Our tabulation of CDD scores also suggests that at some critical threshold, dynein mutations transition from primarily causing muscular atrophy to primarily driving the more severe developmental disorders, including malformations of cortical development. This demonstrates that severe loss-of-function of dyneins may cause gross morphological changes to tissues, and their potential lethality early in life¹⁴⁶. While omitted from our consideration, the genetic background of an individual with a disease-causing point mutation may have profound effects on the severity of the mutation disease-correlates. Defects in other microtubule-associated processes may exacerbate dynein mutation phenotypes in a way that may not be predicted by our yeast system. Further, changes in expression of mutant alleles, or compensatory mutant backgrounds, may mask such phenotypes. However, we must first reach a basic understanding the basal mechanisms

for dysfunction, before decoding the layers of regulation of the microtubule cytoskeleton, to understand the effects a single protein mutation can have at the organism level.

5. Conclusions

The results of our analysis of disease-correlated mutations in yeast yielded many insights into the function and regulation of dynein and revealed insights into potential mechanisms of disease. These experiments provide the experimental basis to create a pipeline capable of assessing dynein mutants. Using this system, we were successful in precisely determining the molecular defects introduced by the two most severe mutations and, pursuant to these findings, correct the defect through engineering of additional mutations.

Several mutations that affect highly conserved regions of dynein, particularly in the motor domain, have highly similar effects on dynein motility between yeast and humans. Secondly, the most severe reductions in motor function, or mutations which caused motor gain-of-function, are associated with developmental disorders; whereas, mutations driving subtler phenotypes are associated with motor neuron disorders. Importantly, the identification that an AAA5 mutant (located in an otherwise innocuous region) leads to the most severe loss-of-function phenotype is a teachable moment. Not all structure function problems may be obvious at the outset, and the least obvious candidates at causing dysfunction may be impacting genes in the most profound ways. We were successful in pinpointing the molecular defect introduced by the two most severe mutations, and had some success in ameliorating mutant phenotypes through rationally targeted mutagenesis. For one mutation, we were successful in mitigating the loss-of-function phenotypes in both the yeast and human protein by rational

mutagenesis of neighboring residues. This demonstrates our ability to pinpoint the basis for molecular dysfunction, as well as the suitability of our system for translational studies in mammalian systems. Mutation phenotypes were correlatively linked to disease state, which demonstrated that the more severe deviations from wild type parameters were associated with the most severe disease states. Finally, yeast dynein is an excellent system to assay for mutant phenotypes that are caused by mutations in human diseases, and has a striking similarity to the human protein. This work revealed that dynein mutations drive dominant negative phenotypes in yeast, which is most likely caused by loss of ensemble activity by pools of homodimeric motors. Finally, regulation of yeast dynein, especially as it pertains to motor autoinhibition and complex assembly, may be more similar to the mammalian system than previously supposed.

These mutations that increase dynein activity by disrupting normal motor autoinhibition may be attractive targets for pharmaceuticals in the future. A large number of these mutants have been identified at residues that overlap with residues identified to be important for stabilizing dynein in an autoinhibited state²⁸. As this dynein motif becomes better characterized in human diseases, it may be necessary to identify novel inhibitors of dynein that negatively regulate motor activity and complex assembly. This avenue of therapeutic identification may indeed present more promising avenues of research than treatment of loss-of-function mutations, as the use of pharmaceuticals to increase dynein activity in cells seems a more unlikely prospect. Ideally our yeast system could be utilized, especially the diploid spindle dynamics assay, to test the efficacies of such treatments in the future.

Table 1. Calculations of Z scores for in vivo assays.

mutation			<i>in vivo</i> dynein-dynactin activity						
human	yeast	disease	Z score	q value	q value	q value	Z score	Z score	
			SP	V	D	ΣD	# events/min	NT	
K129I	E109I	MCD	1.180	0.062	2.128	0.122	-2.416	-0.319	
V236I	L213I	CMT	0.451	7.591	1.007	0.445	2.299	-2.577	
R264L	R241L	SMA-LED	1.081	6.016	0.542	0.912	-0.860	-2.789	
H306R	N283R	SMA-LED	1.158	4.566	0.322	0.189	1.280	-1.238	
R598C	K540C	SMA-LED	-1.012	0.990	1.965	2.079	1.995	-0.100	
E603V	E545V	SMA-LED	1.288	0.947	2.793	4.981	-6.627	-1.928	
V612M	I554M	SMA-LED	1.011	2.993	1.068	0.812	0.143	-0.659	
W673C	W612C	SMA-LED	1.219	6.759	3.831	4.370	-4.895	-2.349	
R1567Q	K1475Q	MCD	2.588	8.202	3.861	2.413	-0.934	-1.482	
R1962C	R1852C	MCD	3.339	11.700	6.835	8.650	-13.798	-0.627	
E2616K	D2439K	SMA-LED	-0.991	4.607	0.456	2.168	-3.453	-1.036	
R2720K	R2543K	MCD	1.703	13.810	6.628	7.149	-10.184	-3.683	
V2734M	L2557M	CMD	2.180	1.728	1.334	3.424	-4.922	-4.659	
K3336N	R3152N	MCD	1.870	7.043	5.453	3.035	1.618	-3.477	
R3344Q	K3160Q	MCD	2.286	7.567	3.996	2.379	0.267	-2.019	
R3384N	R3201N	MCD	1.652	8.541	5.656	3.714	-0.721	-3.537	
H3822P	H3639P	MCD/SMA-LED	12.276	4.085	2.949	9.540	-19.195	<i>i.o.</i>	
<i>dyn1Δ</i>			11.900	33.960	16.180	9.629	-20.584	-	

Table 2. Normalized variance (nrv) from wild type. Relative difference between mean values (Z scores and q values, ‘v’) for mutant and wild-type cells are expressed as normalized relative variance (nrv), where $nrv = |v|/v_{max}$ for each column. Colors indicate relative degree of difference between mutant and wild-type for each value. (C) Coefficient of dynein dysfunction (CDD) was calculated from the values shown in panel B. In the two cases where a value wasn’t determined (due to insufficient observations), the denominator was reduced from 6 to 5. Note that in two instances, the Z score for

normalized relative variance (nrv) from wild-type

mutation			<i>in vivo</i> dynein-dynactin activity						
human	yeast	disease	SP	V	D	ΣD	# events/min	NT	
K129I	E109I	MCD	0.481	0.002	0.132	0.013	0.117	0.053	
V236I	L213I	CMT	0.184	0.224	0.062	0.046	0.112	0.428	
R264L	R241L	SMA-LED	0.440	0.177	0.033	0.095	0.042	0.463	
H306R	N283R	SMA-LED	0.471	0.134	0.020	0.020	0.062	0.205	
R598C	K540C	SMA-LED	0.000	0.029	0.121	0.216	0.097	0.017	
E603V	E545V	SMA-LED	0.524	0.028	0.173	0.517	0.322	0.320	
V612M	I554M	SMA-LED	0.412	0.088	0.066	0.084	0.007	0.109	
W673C	W612C	SMA-LED	0.496	0.199	0.237	0.454	0.238	0.390	
R1567Q	K1475Q	MCD	1.054	0.242	0.239	0.251	0.045	0.246	
R1962C	R1852C	MCD	1.360	0.345	0.422	0.898	0.670	1.000	
E2616K	D2439K	SMA-LED	0.000	0.136	0.028	0.225	0.168	0.172	
R2720K	R2543K	MCD	0.694	0.407	0.410	0.742	0.495	0.611	
V2734M	L2557M	CMD	0.888	0.051	0.082	0.356	0.239	0.773	
K3336N	R3152N	MCD	0.762	0.207	0.337	0.315	0.079	0.577	
R3344Q	K3160Q	MCD	0.931	0.223	0.247	0.247	0.013	0.335	
R3384N	R3201N	MCD	0.673	0.252	0.350	0.386	0.035	0.587	
H3822P	H3639P	MCD/SMA-LED	5.000	0.120	0.182	0.991	0.933	-	
<i>dyn1Δ</i>			4.847	1.000	1.000	1.000	1.000	-	
wild-type			0.000	0.000	0.000	0.000	0.000	0.000	

CDD calculation

$$nrv = \frac{|v|}{v_{max}}$$

$$CDD = \frac{(5 \cdot nrv_{SP}) + nrv_V + nrv_D + nrv_{\Sigma D} + nrv}{6}$$

Chapter 3: Yeast dynein autoinhibition and its implications for dynein motor regulation and cortical targeting.

3.1. Introduction

Throughout nature, there are many examples of proteins using self-association to regulate their specific *in vivo* activities. There are many instances of cytoskeletal proteins undergoing self-association leading to autoinhibition, from kinesin-1, to dynein cargo adaptor BicD2, to myosin^{186,188-189}. It has been shown that in various kinesins, autoinhibition can be relieved by the binding of cargo to the tail domain^{185,186}. Similarly, binding of cargo (such as mRNA) to BicD2 has been shown to relieve autoinhibition of this adaptor¹⁷ which activates dynein transport of BicD2 bound vesicles. Autoinhibition of different kinesins has been further shown to decrease ATPase rates of the motor, and association with the microtubule lattice is important for stimulating kinesin-1 ATPase activity. These forms of autoinhibition presumably limit motor activity *in vivo* to sites of required activity, and prevent motor activity in the absence of a productive cellular task. For many years, it was unclear if dynein was similarly regulated. However, the discovery of the mammalian dynein autoinhibited state, both for cytoplasmic dynein-1¹⁶⁵ and cytoplasmic dynein-2⁴⁹, and the importance of these mechanisms of autoinhibition for dynein regulation *in vivo* and *in vitro*, has prompted a flurry of new research into understanding how this autoinhibited modality regulates dynein activity and interaction with binding partners.

In this and the following chapter, we will discuss two of the most important findings of this thesis work: our characterization of yeast dynein autoinhibition; and its implication for the functions of the Pac1/LIS1 regulator of dynein. The determination that

yeast dynein undergoes autoinhibition was done using a combinatorial approach of negative-stain EM, cellular biology, single-molecule assays, and biochemical characterization. The results of these experiments revealed that *in vitro* processivity of yeast dynein is principally limited by the stochastic termination of motor motility through formation of the autoinhibited state. Both motor-motor and tail-tail intra-dimer contacts are important for stabilizing the autoinhibited conformation, and these experiments explore the possibility that the tail domain initiates or stabilizes autoinhibition of the motor domains. Furthermore, this research demonstrates the *in vivo* relevance of the autoinhibited conformation, which coordinates dynein's activity and localization within cells. Importantly, these data determine that autoinhibition of dynein is a stochastic and dynamic process that can be stabilized by other proteins, namely, Pac1/Lis1. By tuning the proportion of dyneins which are active in the cell, either through post-translational modification or localization of Pac1/LIS1 or other regulatory proteins, dynein is targeted to microtubules and then to the cell cortex. The results of these experiments are corroborated by three other papers with similar biochemical findings using recombinant human dynein and cell biology experiments using *aspergillus nidulans*¹⁶⁶⁻¹⁶⁹. These studies demonstrate that dynein autoinhibition is an evolutionarily conserved mechanism, which governs dynein behavior from the humble yeast¹⁶⁹, to filamentous fungus¹⁶⁶, to the mammalian dynein system¹⁶⁷⁻¹⁶⁸.

3.1.1 History of understanding dynein autoinhibition

Despite the ubiquitous nature of autoinhibition across many families of motor proteins and cytoskeletal regulators, it was unclear for many years what relevance such motifs of autoregulation state held for cytoplasmic dynein motors. Yeast dynein has

been extensively characterized for its properties as a processive motor when purified *in vitro*¹⁶¹, suggesting that the yeast protein does not undergo autoinhibition. However, it has been demonstrated that mammalian dynein, which is not a processive motor on its own, requires both dynactin and a cargo adaptor for processive motility *in vitro*^{86,87}. Furthermore, human dynein is not processive even when artificially dimerized through the use of a GST-motor chimeric construct^{86,190}, unlike its yeast counterpart¹⁶¹. However, experiments have demonstrated that separating the motor domains through engineering of a helical linker between the two motor domains was sufficient to convert the human protein into a processive motor¹⁹¹, at the cost of decreasing diffusional parameters *in vitro*. This data together proposed dynein autoinhibition was important for understanding the limited mobility of mammalian dynein *in vitro*, and pointed to mammalian dynein autoinhibition occurring between physical interaction of the two heavy chains of a dimer.

A major breakthrough in understanding dynein came from new cryo-electron microscopy experiments¹⁶⁵ that were published during this thesis work, which revealed that mammalian dynein is maintained in an inactive conformation through a series of stabilizing intramolecular interactions on the surface of the motor. Previous negative stain electron microscopy¹⁹² had identified this conformation, terming it the “Phi-particle” for the resemblance of the particles to the Greek letter Phi. In this inactive conformation, the tail domains of each monomer are twisted about each other, and while atomic resolution could not be obtained for the tail regions, it is evident that substantial tail-tail interactions (and likely accessory chain interactions) are needed to stabilize the autoinhibited state. Several motor-motor domain contacts were identified in the linker-

AAA4 interface and the AAA5-AAA5 interface which stabilized the Phi particle state. Furthermore, the stalk domains of each monomer were crossed with respect to each other, which would preclude processive motility, and two hydrophobic interactions within the stalk were important for stabilizing these contacts. A number of the stabilizing residues within the motor domain have been previously identified in neurological disorders¹¹⁹ which were not included in our initial survey¹⁹³, and ablation of electrostatic interactions between dimers through protein mutagenesis was sufficient to completely disrupt the autoinhibited conformation¹⁶⁵ as determined by electron microscopy. The autoinhibited dynein complex demonstrated limited ATPase rate, microtubule landing, and association with cargo binding proteins, namely dynactin and adaptor proteins, compared to the fully open counterpart. Interestingly, these limitations are in many ways reminiscent of dyneins' anterograde transport counterparts, kinesins¹⁸⁵⁻¹⁸⁶, many of which employ autoinhibition to limit motor activity.

Interestingly, significant variation between conformational states was identified through the many class averages generated from individual particles. Human dynein was identified in a "fully closed" Phi-particle state, with motor domains stacked and tails twisted with respect to each other, as well as "fully open", with motor domains separated completely and tail domains separated and extended. However, a number of averages depicted a range of intermediate states between these fully open or closed conformations; some showed motor-motor separation in the absence of tail separation, and many different intermediates of tail-tail topography were identified¹⁶⁵. This potentially indicated that dynein may stochastically switch between open and closed states in solution, but the *in vivo* relevance of this data was unclear at the time.

Similar results have been reported for mammalian cytoplasmic dynein-2, which is responsible for intraflagellar transport. Cryo-EM studies⁴⁹ have demonstrated that the motor domain of this protein is sufficient to form the so-called “Phi-particle” state when artificially dimerized using a GST-dynein chimeric protein, which has not been observed from cryo-EM structures of the yeast GST-dynein fusion protein. The identities of the intramolecular contacts between motor domains were assigned, and strikingly, the residues important for stabilization of cytoplasmic dynein-2 were not shared with cytoplasmic dynein-1. This indicates that while mechanisms of autoinhibition are shared amongst different dynein isoforms, it is resultant from convergent evolution from these divergent motors. This may potentially indicate that the regulation of the autoinhibition of these two highly similar proteins is accomplished by different cellular factors, reflecting their distinct compartmentalization. Autoinhibition is therefore similarly important for cytoplasmic dynein as it is for other cytoskeletal proteins.

These data comprehensively examined how mammalian dynein autoinhibition affected *in vitro* activity of the protein; however, yeast dynein was not expected to undergo autoinhibition. Previous work from our lab has demonstrated that separating the tail and motor domains leads to plus end independent targeting of dynein to the cell cortex^{84,194}, prompting a model that the tail and motor domains were somehow interacting to limit association with Pac1, Bik1, dynactin and/or Num1. However, outside of this cellular localization data, no further evidence existed which indicated that yeast dynein undergoes autoinhibition. However, our mutagenesis screen identified residue K1475Q as being potentially important for autoinhibition due to increasing interaction with the cell cortex, increased dynein-dynactin interaction at microtubule plus ends, and

increases in *in vitro* activity and processivity¹⁹³. Though these data were unexpected and difficult to explain at the time, all the *in vivo* evidence pointed to yeast dynein undergoing some form of autoinhibition akin to its mammalian counterpart.

We then explored the possibility that yeast dynein was autoinhibited, using our previous results from studies on yeast dynein regulation. Using negative-stain EM, we identified the structure of the full-length intact dynein complex in an inactive autoinhibited state which was highly similar to that of human dynein. Using *in vitro* single molecule assays, we next determined that Phi-particle formation is run length-limiting for the yeast complex, and that this is a result of stochastic switching between “open” and “closed” states of the protein, a phenomena which was noted for the human dynein complex in solution. Finally, yeast dynein autoinhibition limits association with binding partners in the cytoplasm, namely Pac1 and dynactin. Taken together, these data demonstrate that yeast dynein is maintained in an inactive in the same manner as mammalian dynein, and this autoinhibitory mechanism is likely conserved across all metazoan isoforms of cytoplasmic dynein-1.

3.2. Methods

3.2.1 Strain construction and cloning

All strains used in this thesis work are derived from either W303 or YEF473A¹⁷⁷ and are listed in Table 5. We transformed yeast strains using the lithium acetate method¹⁷⁸. Strains carrying mutations were constructed by PCR product-mediated transformation¹⁷⁹ or by mating followed by tetrad dissection. Proper tagging and mutagenesis was confirmed by PCR, and in most cases sequencing (all point mutations were confirmed via sequencing). Fluorescent tubulin-expressing yeast strains were

generated using plasmids and strategies described previously^{180,181}. Yeast synthetic defined (SD) media was obtained from Sunrise Science Products (San Diego, CA). Strains overexpressing the yeast dynein complex (or the GST-dynein fragment) were generated by transforming p8His-ZZ-SNAPf-Dynein, p8His-ZZ-HALO-Dynein, or pZZ-dyneinMOTOR-HALO (wild-type or mutants; see below) linearized by digestion with Apal (cuts within the URA3 gene; see Fig. 19A). Integration was confirmed by PCR. Yeast synthetic defined (SD) media was obtained from Sunrise Science Products (San Diego, CA).

3.2.2 Plasmid generation

For overexpression and purification of the yeast dynein complex (wild-type or mutants), we generated a polycistronic plasmid expressing all four dynein complex subunits using strategies analogous to the biGBAC assembly^{164,195}. We first made a yeast expression "library" vector – pLIBy – which enables generation of a gene expression cassettes (GEC) with a strong, inducible GAL1 promoter (GAL1p) on the 5' end, and a synthetic terminator sequence (Tsynth3¹⁹⁶) on the 3' end. A PCR product encompassing GAL1p, and an oligonucleotide containing Tsynth3¹⁹⁶ and a multicloning site (XbaI-NotI-SpeI-BamHI) were assembled into pRS305 digested with BamHI and NotI using Gibson assembly¹⁹⁷, yielding pLIBy. We also generated a yeast genomic-integration vector with optimized linker sequences for Gibson assembly¹⁹⁷ flanked by PmeI restriction sites (equivalent to pbiG1a and pbiG1b). These plasmids – pbiG1ay and pbiG1by– were generated by using Gibson assembly to insert a PCR product encompassing these elements from pbiG1a and pbiG1b into pRS306. PCR products encompassing the DYN2 (without the native intron), DYN3 or PAC11 open reading

frames were assembled into pLIBy digested with BamHI and NotI. Subsequently, these GECs were amplified from each respective pLIBy vector using oligonucleotides that include regions for priming preceded on the 5' end by predefined "Cas" sequences¹⁹³: the DYN2 GEC was amplified with Cas α -forward and Cas β -reverse; the DYN3 GEC was amplified with Cas β -forward and Cas γ -reverse; and, the PAC11 GEC was amplified with Cas γ -forward and Cas ω -reverse. These three PCR products were assembled into pbiG1by digested with SwaI to generate pbiG1by:GAL1p:Dyn2::GAL1p:DYN3::GAL1p:PAC11.

We generated pLIBy:6His-StrepII-SNAPf-DYN1 using Gibson assembly. However, due to complications generating a PCR product from this vector, we chose to clone everything into this vector. We first substituted the LEU2 expression cassette in the pLIBy backbone with a URA3 marker by assembling a PCR product encompassing the URA3 cassette from pRS306 into pLIBy:6His-StrepII-SNAPf-DYN1 digested with KasI and AatII, yielding pLIBy:6His-StrepII-SNAPf-DYN1::URA3. To enable assembly of the DYN2/DYN3/PAC11 polygene cassette into pLIBy:6His-StrepII-SNAPf-DYN1::URA3, we inserted the optimized "B" and "C" linker sequences for Gibson assembly into this plasmid by assembling a PCR product encompassing "B"-PmeI site-"C" into pLIBy:6His-StrepII-SNAPf-DYN1::URA3 digested with KpnI and Sall. Subsequent to digestion with PmeI, this plasmid was assembled with the PmeI restriction digest product from pbiG1by:GAL1p:Dyn2::GAL1p:DYN3::GAL1p:PAC11 (encompassing GAL1p:Dyn2::GAL1p:DYN3::GAL1p:PAC11), yielding pLIBy:GAL1p:Dyn2::GAL1p:DYN3::GAL1p:PAC11::GAL1p:6His-StrepII-SNAPf-Dyn1::URA3, hereafter referred to as p6His-StrepII-SNAPf-Dynein. Prior to using this plasmid for pilot

tests, we decided to swap the 6His-StrepII affinity tag for an 8His-ZZ tag (followed by a tandem TEV protease recognition site). We did this by assembling a PCR product encompassing 8His-ZZ into p6His-StrepII-SNAPf-Dynein digested with AatII and XhoI, yielding p8His-ZZ-SNAPf-Dynein. We replaced the SNAPf tag with a HALO tag using a similar strategy, yielding p8His-ZZ-HALO-Dynein. All mutations were engineered into these plasmids using common strategies.

Due to difficulties in engineering the D2868K mutation into the GST-dynein expressing yeast strain (SMY1008), we generated a plasmid that overexpresses this fragment in yeast. Like the full-length dynein complex expression plasmids described above, this plasmid can also be integrated into the *ura3-1* locus. PCR products encompassing the entire GAL1p:ZZ-2TEV-6His-GFP-GST-dyn1331-HALO cassette (comprised of 4 individual pieces, each with 23 nt of overlapping sequences; amplified from SMY1008) were assembled into pRS305 digested with KpnI and BamHI using Gibson assembly²²⁹, yielding pZZ-dyneinMOTOR-HALO. The D2868K mutation was engineered into this plasmid using common strategies.

3.2.3 Protein purification

Purification of yeast dynein (ZZ-TEV-Dyn1-HALO, under the native DYN1 promoter; or, ZZ-TEV-HALO-(or SNAPf)-Dynein, with all genes under control of the GAL1p promoter; or, ZZ-TEV-6His-GFP-3HA-GST-dyneinMOTOR-HALO, under the control of the GAL1p promoter) was performed as previously described with minor modifications used for the overexpressed complex^{161,193}. Briefly, yeast cultures were grown in YPA supplemented with either 2% glucose (for non-overexpressed full-length dynein) or 2% galactose (for the GAL1p-inducible strains; overexpression of the full-

length dynein complex was induced for no more than 3 hours), harvested, washed with cold water, and then resuspended in a small volume of water. The resuspended cell pellet was drop frozen into liquid nitrogen and then lysed in a coffee grinder (Hamilton Beach). For most purifications (with exception of those used for negative stain/EM imaging) we used the following procedure: after lysis, 0.25 volume of 4X dynein lysis buffer (1X buffer: 30 mM HEPES, pH 7.2, 50 mM potassium acetate, 2 mM magnesium acetate, 0.2 mM EGTA) supplemented with 1 mM DTT, 0.1 mM Mg-ATP, 0.5 mM Pefabloc SC (concentrations for 1X buffer) was added, and the lysate was clarified at 22,000 x g for 20 min. The supernatant was then bound to IgG sepharose 6 fast flow resin (GE) for 1-1.5 hours at 4°C, which was subsequently washed three times in 5 ml lysis buffer, and twice in 5 ml TEV buffer (50 mM Tris, pH 8.0, 150 mM potassium acetate, 2 mM magnesium acetate, 1 mM EGTA, 10% glycerol) supplemented with 0.005% Triton X-100, 1 mM DTT, 0.1 mM Mg-ATP, and 0.5 mM Pefabloc SC. To fluorescently label the motors for single molecule analyses, the bead-bound protein was incubated with either 6.7 μM HaloTag-AlexaFluor660, HaloTag-AlexaFluor488, or HaloTag-TMR (Promega), or SNAP-Surface Alex Fluor 647 (NEB), as appropriate, for 10-20 minutes at room temperature. The resin was then washed four more times in TEV buffer supplemented with 1 mM DTT, 0.005% Triton X-100, and 0.1 mM Mg-ATP, and then incubated with TEV protease for 1-1.5 hours at 16°C. Following TEV digest, the beads were pelleted, and the resulting supernatant was collected, aliquoted, flash frozen in liquid nitrogen, and stored at -80°C. Protein preparations used for negative stain/EM imaging were subject to tandem affinity purification. To do so, subsequent to lysis, 0.25 volume of 4X NiNTA dynein lysis buffer (1X buffer: 30 mM HEPES, pH 7.2,

200 mM potassium acetate, 2 mM magnesium acetate, 10% glycerol) supplemented with 1 mM beta-mercaptoethanol, 0.1 mM Mg-ATP, 0.5 mM Pefabloc SC (concentrations for 1X buffer) was added, and the lysate was clarified as above. The supernatant was then bound to NiNTA agarose for 1 hour at 4°C, which was subsequently washed three times in 5 ml NiNTA lysis buffer. The protein was eluted in NiNTA lysis buffer supplemented with 250 mM imidazole by incubation for 10 minutes on ice. The eluate was then diluted with an equal volume of dynein lysis buffer, which was then incubated with IgG sepharose 6 fast flow resin for 1 hour at 4°C. The beads were washed and the protein was eluted as described above. Eluted protein was either applied to a size exclusion resin (Superose 6; GE), or snap frozen. The gel filtration resin was equilibrated in GF150 buffer (25 mM HEPES pH 7.4, 150 mM KCl, 1 mM MgCl₂, 5 mM DTT, 0.1 mM Mg-ATP) using an AKTA Pure. Peak fractions (determined by UV 260 nm absorbance and SDS-PAGE) were pooled, concentrated, aliquoted, flash frozen, then stored at -80°C. We noted that prolonged periods of storage in the -80°C (≥ 3-5 days) led to an increase in the prevalence of dynein aggregates (as apparent from fluorescence intensity analysis), which exhibited longer run lengths and slower motility in single molecule assays. We also noted that aggregation was much more prevalent when the motor was labeled with the HALO-AlexaFluor660 than it was with the HALO-AlexaFluor488.

Purification of Pac1-FLAG-SNAP was performed as previously described¹⁰¹, with the addition of a gel filtration step to remove any residual, unbound fluorescent dye. Specifically, TEV protease eluted protein was applied to a size exclusion resin (Superose 6; GE), that was equilibrated in TEV buffer supplemented with 1 mM DTT

using an AKTA Pure. Peak fractions (determined by UV 260 nm absorbance and SDS-PAGE) were pooled, concentrated, aliquoted, flash frozen, then stored at -80°C. For comparison of elution profiles between yeast and human dynein complexes, the human dynein complex was expressed and purified from insect cells (ExpiSf9 cells; Life Technologies) as previously described with minor modifications^{164,165}. Briefly, 4 ml of ExpiSf9 cells at 2.5×10^6 cells/ml, which were maintained in ExpiSf CD Medium (Life Technologies), were transfected with 1 µg of bacmid DNA (see above) using ExpiFectamine (Life Technologies) according to the manufacturer's instructions. 5 days following transfection, the cells were pelleted, and 1 ml of the resulting supernatant (P1) was used to infect 300 ml of ExpiSf9 cells (5×10^6 cells/ml). 72 hours later, the cells were harvested (2000 x g, 20 min), washed with phosphate buffered saline (pH 7.2), pelleted again (1810 x g, 20 min), and resuspended in an equal volume of human dynein lysis buffer (50 mM HEPES, pH 7.4, 100 mM NaCl, 10% glycerol, 1 mM DTT, 0.1 mM Mg-ATP, 1 mM PMSF). The resulting cell suspension was drop frozen in liquid nitrogen and stored at -80°C. For protein purification, 30 ml of additional human dynein lysis buffer supplemented with cOmplete protease inhibitor cocktail (Roche) was added to the frozen cell pellet, which was then rapidly thawed in a 37°C water bath prior to incubation on ice. Cells were lysed in a dounce-type tissue grinder (Wheaton) using ≥ 100 strokes (lysis was monitored by microscopy). Subsequent to clarification at 22,000 x g, 45 min, the supernatant was applied to 2 ml of IgG sepharose fast flow resin pre-equilibrated in human dynein lysis buffer, and incubated at 4°C for 2-4 hours. Beads were then washed with 50 ml of human dynein lysis buffer, and 50 ml of human dynein TEV buffer (50 mM Tris pH 7.4, 150 mM potassium acetate, 2 mM magnesium acetate,

1 mM EGTA, 10% glycerol, 1 mM DTT, 0.1 mM Mg-ATP). The bead-bound protein was eluted with by incubation with TEV protease overnight at 4°C. The next morning, the recovered supernatant was applied to a Superose 6 gel filtration column as above.

3.2.4 Single molecule motility assays

The yeast dynein single-molecule motility assay was performed as previously described with minor modifications^{163,193}. Briefly, flow chambers constructed using slides and plasma cleaned and silanized coverslips attached with double-sided adhesive tape were coated with anti-tubulin antibody (8 µg/ml, YL1/2; Accurate Chemical & Scientific Corporation) then blocked with 1% Pluronic F-127 (Fisher Scientific). Taxol-stabilized microtubules assembled from unlabeled and fluorescently-labeled porcine tubulin (10:1 ratio; Cytoskeleton) were introduced into the chamber, and, within one minute, an additional 1 µl assay buffer was flowed in to align microtubules. Following a 5-10 minute incubation, the chamber was washed with dynein lysis buffer (see above) supplemented with 20 µM taxol. Subsequently, purified dynein motors diluted in motility buffer (30 mM HEPES pH 7.2, 2 mM magnesium acetate, 1 mM EGTA, 1 mM DTT, 1 mM Mg-ATP, 0.05% Pluronic F-127, 20 µM taxol, and an oxygen-scavenging system consisting of 1.5% glucose, 1 U/ml glucose oxidase, 125 U/ml catalase) supplemented with either 50 mM potassium acetate, or as indicated in figure legend, were introduced in the chamber, and imaged.

To image comigrating Pac1-dynein complexes, 500 nM Pac1-SNAP647 (dimer concentration) and 10-50 nM HALOTMR-Dynein were preincubated on ice for 10-15 minutes prior to a 10- to 20-fold dilution into modified motility buffer (30 mM HEPES pH 7.2, 2 mM magnesium acetate, 1 mM EGTA, 1 mM DTT, 1 mM Mg-ATP) supplemented

with potassium acetate or potassium chloride as indicated in figure legends, 0.05% Pluronic F-127, 20 μ M taxol, and an oxygen-scavenging system (as above). The higher yield overexpressed dynein complex was needed for these assays given the low landing rate of dynein in the higher ionic strength buffers. We ensured that comigrating Pac1-SNAP647 spots were not due to bleed-through from the HALOTMR-dynein channel by performing two-color imaging with HALOTMR-dynein alone (no spots were apparent in the far-red channel in these cases). To measure Pac1 fluorescence intensity on microtubules, 50 nM of Pac1-SNAP647 (dimer concentration) diluted in motility buffer was added to chambers containing taxol-stabilized microtubules.

To remove the unstructured E-hooks from microtubules, taxol-stabilized microtubules were digested with a 1 mg/ml subtilisin (Sigma) for 90 min at 37°C prior to preparation of flow chambers. For experiments in which cellular extracts were included in the imaging chamber (Fig. S6D and E), log phase cultures of SMY2532 (cells not expressing dynein; see Table 1) were pelleted, resuspended in a small volume of motility buffer (with 50 mM potassium acetate), drop frozen in liquid nitrogen, lysed by mortar and pestle, and then clarified at 21,000 x g for 15 minutes. To assess Pac1-microtubule binding in the presence of cell extracts, 50 nM Pac1-SNAP647 (dimer concentration) was diluted in motility buffer supplemented with clarified extract (0.96 mg/ml final) and introduced into an imaging chamber. Similar conditions were used to assess the effect of Pac1 on dynein motility in the presence of cell extract, except 25nM Pac1 and ~50-150 pM GST-dynein were also included in the imaging chamber, along with protease inhibitor tablet and an additional 10 mM ATP supplemented in the motility buffer.

Total internal reflection fluorescence microscopy (TIRFM) images were collected using a 1.49 NA 100X TIRF objective on a Nikon Ti-E inverted microscope equipped with a Ti-S-E motorized stage, piezo Z-control (Physik Instrumente), and an iXon X3 DU897 cooled EM-CCD camera (Andor). 488 nm, 561 nm, and 640 nm lasers (Coherent) were used along with a multi-pass quad filter cube set (C-TIRF for 405/488/561/638 nm; Chroma) and emission filters mounted in a filter wheel (525/50 nm, 600/50 nm and 700/75 nm; Chroma). To image non-labeled microtubules (e.g., Fig. 28D), we employed interference reflection microscopy, as recently described¹⁹⁸. For time-lapse movies, we acquired images at 1, 2, or 3 second intervals for 8-10 min. Velocity and run length values were determined from kymographs generated using the MultipleKymograph plugin for ImageJ (http://www.embl.de/eamnet/html/body_kymograph.html). Those motors that moved for ≥ 3 time points were measured. Reported run lengths were determined from fitting raw values to a one-phase decay.

2.5. Negative stain electron microscopy and image analysis

EM grids were prepared with a standard negative stain protocol by applying fresh dynein samples to glow discharged carbon coated 200 mesh copper grids. After ~1 minute incubation, 2% uranyl acetate was added. 1600 micrographs were collected on a FEI Tecnai F20 200kV TEM equipped with a Gatan US4000 CCD (model 984), at a nominal magnification of 90,000X with the digital pixel size 6.19 angstroms. All image analysis was performed in Relion 3.0 on the University of Colorado Boulder High Performance Computer Cluster, Summit. Particles were manually picked from ~20 micrographs (~200 particles), which were used to generate a low-resolution 2D class

average. Using these 2D averages as a starting point, we then used an iterative process to autopick particles that were used to generate our final 2D averages, and for 3D model building (in total, 42,611 particles were used for final averages shown in Fig. 19E).

3.2.6. Calculation of ionic strength

We calculated the ionic strength of our buffers as previously described¹⁹⁹. In brief, we empirically determined the amount of KOH required to pH a 30 mM HEPES buffer to 7.2. We estimated the proportion of protonated to unprotonated HEPES at pH 7.2 to be 2:1 (using the Henderson-Hasselbalch equation). Using the formulation for ionic strength ($I = 1/2 \sum c_i z_i^2$), we determined the ionic strength of the 50 mM K-acetate motility buffer to be 61.5 mM, the 100 mM K-acetate and KCl buffers to be 111.5 mM, and the 150 mM K-acetate and KCl buffers to be 161.5 mM. Note we did not include the proportion of zwitterionic HEPES species (20 mM) in the calculation of ionic strength as it has been demonstrated previously to have no effect on the ionic strength of a solution, despite contributing to electrostatic interactions²⁰⁰.

3.2.7. Dynein-Pac1 binding experiments

Purified, gel filtered Pac1-FLAG-SNAP (0.5 - 0.75 μ g per binding experiment) was bound to FLAG M2 magnetic beads (Sigma Aldrich) by incubation in TEV supplemented with 0.005% Triton X-100, 1 mM DTT, and 0.1 mM Mg-ATP at 4°C. After 1 hour, unbound Pac1-FLAG-SNAP was removed by washing the beads four times with the same buffer. Subsequently, roughly equal amounts of purified dynein proteins (wild-type, mutant, or truncation) were incubated with Pac1-FLAG-SNAP-decorated beads (diluted in same buffer; reaction volume ranged from 50 - 120 μ l among

replicates). After 1 hour, the unbound fraction was removed by pipetting, while the bound fraction was eluted with 0.25 mg/ml 3XFLAG peptide (Sigma Aldrich) by incubation for 20 minutes on ice. Bound and unbound fractions were resolved by SDS-PAGE, and the normalized, relative bound and unbound fractions were determined by measuring background corrected band intensities. Note that we observed no binding of dynein to FLAG M2 magnetic beads in the absence of Pac1-FLAG-SNAP (not shown).

3.2.8. Microtubule co-pelleting experiments

To perform the microtubule co-pelleting assay, 1 μ M microtubules were incubated for 10 minutes at room temperature with 2 nM of either wild-type or mutant dynein in motility buffer supplemented with 0.1 mg/ml bovine serum albumin (Bio-Rad, cat. # 5000206) with or without 1 mM Mg-ATP. Reactions were subsequently pelleted at 21,130 x g for 20 minutes. The supernatant and pellet were separated, resuspended in sample buffer, and run on a 4-15% gradient acrylamide gel. Gels were stained with Sypro Ruby, and then imaged on a Typhoon gel imaging system (FLA 9500).

3.2.9. Live cell imaging experiments

For the spindle dynamics assay, cells were arrested with hydroxyurea (HU) for 2.5 hours, and then mounted on agarose pads containing hydroxyurea for fluorescence microscopy^{163,193}. Full Z-stacks (15 planes with 0.2 μ m spacing) of GFP-labeled microtubules (GFP-Tub1) were acquired every 10 seconds for 9.66 minutes (58 time points) on a stage prewarmed to 30°C. To eliminate any dynein-independent contributions to spindle movements, these assays were performed in cells lacking Kar9, a protein that is required for an actin/myosin-mediated spindle orientation pathway¹⁷⁴. To image dynein localization in live cells, cells were grown to mid-log phase in SD

media supplemented with 2% glucose, and mounted on agarose pads. Images were collected on a Nikon Ti-E microscope equipped with a 1.49 NA 100X TIRF objective, a Ti-S-E motorized stage, piezo Z-control (Physik Instrumente), an iXon DU888 cooled EM-CCD camera (Andor), a stage-top incubation system (Okolab), and a spinning disc confocal scanner unit (CSUX1; Yokogawa) with an emission filter wheel (ET480/40m for mTurquoise2, ET525/50M for GFP, and ET632/60M for mRuby2; Chroma). Lasers (445 nm, 488 nm and 561 nm) housed in a LU-NV laser unit equipped with AOTF control (Nikon) were used to excite mTurquoise2, GFP and mRuby2, respectively. The microscope was controlled with NIS Elements software (Nikon).

3.2.10. Statistics and Reproducibility

All data were collected from at least two independent replicates (independent protein preparations, or cell cultures, for *in vitro* and *in vivo* experiments, respectively). The values from each independent replicate – which are indicated on each plot (see diamonds on relevant plots) – showed similar results. T-tests were performed using Graphpad Prism. Statistical significance was determined using a two-tailed Mann-Whitney test (for single molecule run length values), or with an unpaired two-tailed Welch's t test (for single molecule velocity values). Z scores were calculated using the following formula:

$$Z = \frac{(p_1 - p_2)}{\sqrt{p(1-p)(1/n_1 + 1/n_2)}}$$

where:

$$p \approx (y_1 + y_2) / (n_1 + n_2)$$

Z scores were converted to two-tailed P values using an online calculator.

3.2.11. Data availability

Movies for this study may be found on the SMNAS/_MicroscopeData/Matt Marzo/SMT for NCB Reviews. Data and analysis is also available on the SMNAS . Strains used for this study are available in the Table 4.

3.3. Results

3.3.1. Structure of autoinhibited yeast dynein

The first step to determining if yeast dynein has an autoinhibited conformation was to purify sufficient quantities of purified dynein for negative stain electron microscopy analysis. To this end, a plasmid was constructed using cues from the insect cell expression system to express each of the four subunits of the dynein complex off the same plasmid¹⁹⁵. This plasmid was integrated into the URA locus and each dynein subunit was under the transcriptional control of a galactose-based promoter and synthetic T3 terminator sequence (Fig. 19A)^{195,196}. This allowed us to express the intact full-length dynein complex (Fig. 19A-C) at concentrations much higher than could previously be obtained. This complex demonstrated near identical *in vitro* motility to the natively expressed protein (Fig. 19B), and had a near-identical profile in size-exclusion chromatography as its mammalian counterpart (Fig. 19C). With this high purity complex in hand, we collaborated with Gary Morgan at the UC Boulder EM imaging facility to obtain the first ever negative-stain EM image of the full-length yeast dynein complex (Fig. 19D). Amazingly, yeast dynein formed the phi-particle in proportions similar to those previously reported for the human complex¹⁶⁵. Averaging several thousand particles allowed for the visualization of many different conformational states of dynein. Interestingly, the degree of intra-dimer contacts in these conformational states varied

Figure 19

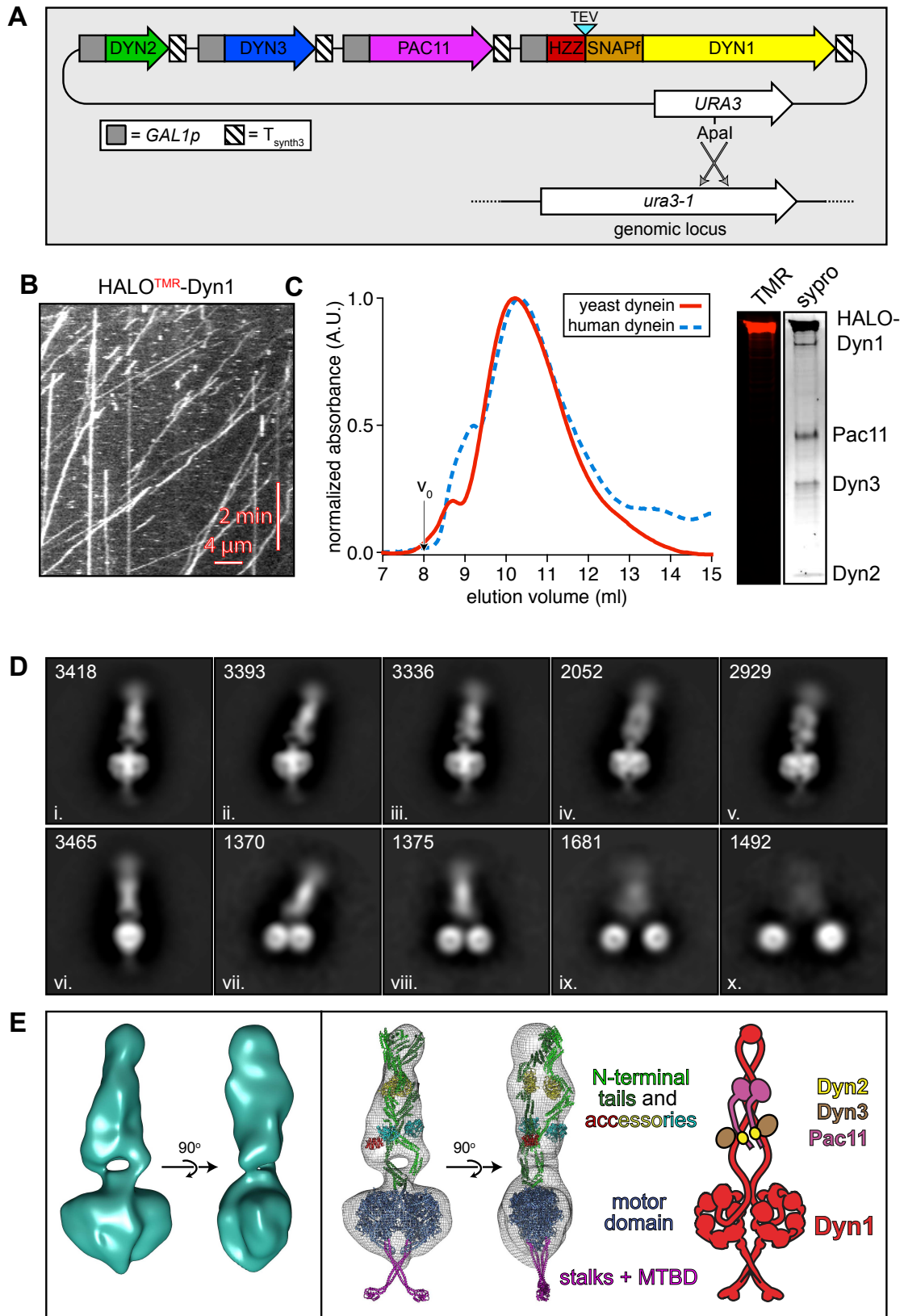


Figure 19. The yeast dynein complex adopts an autoinhibited phi particle conformation. (A) Schematic of the polycistronic plasmid used to produce the intact yeast dynein complex (GAL1p, galactose-inducible promoter; Tsynth3, terminator sequence). Restriction digest with Apal (cuts within URA3 gene) targets the plasmid for homologous recombination into the *ura3-1* locus as depicted. (B) Representative kymograph depicting single molecule motility of the purified overexpressed yeast dynein complex. (C) Representative elution profiles of yeast and human dynein complexes from Superose 6 resin (left), and scans of the same polyacrylamide gel depicting fluorescently labeled Dyn1 (via HaloTag-TMR) and the entire complex (via Sypro Ruby staining; right; 3 independent preparations yielded very similar results). (D) Representative negative stain EM class averages of the intact yeast dynein complex (2D classes were generated from one preparation; however, independent preparations provided very similar raw images). Number of particles used to generate each class indicated in each panel. Classes i – vi depict dynein in the autoinhibited, phi particle conformation, whereas vii – x depict dynein in various open, uninhibited states. (E) 3D models of dynein in the autoinhibited state generated from 2D class averages with (right) and without (left) a high resolution 3D structure of human dynein-1 in the phi particle conformation (pdb 5NVU1) manually docked into it. Note that the structures of the two tail domains have been slightly rotated with respect to the motor domains to better fit the 3D model, and that the structures of both TcTEX and Rob1 have been eliminated due to their absence from the yeast dynein complex.

substantially, just as was apparent in the human dynein structures. Yeast dynein demonstrated both “fully closed” and “fully open” states, but also a number of intermediate states where motor heads and tail domains were separated to varying degrees.

Performing 3D reconstruction of our several averages of dynein in the Phi-particle state allowed us to manually dock the human dynein Phi-particle structure [PDB: 5NVU], and we found these two structures overlapped near-identically [Fig. 19E], with the exception of the presence of two additional light chains (Rob1, TcTex2) in the human dynein complex¹⁶⁵. Important to note is the hole of electron density at the tail region proximal to the motor domain, which overlaps identically with the human high-resolution structure. One of the most interesting findings of both cryo-EM studies is the presence of the varying intermediate states between open and closed dynein conformations, which likely indicates dynein intrinsically possesses the ability to switch stochastically between autoinhibited and active conformations, a process that could potentially be a target for mitotic PTMs²⁰² or the expression of mitosis specific

proteins²⁰², given the importance of dynein in mitotic regulation and spindle positioning²³⁻²⁴.

3.3.2. *Yeast dynein autoinhibition limits in vitro motor activity*

Due to the high degree of similarity between human and yeast autoinhibited structures, we reasoned that our previous data pertaining to the K1475 residue (K1567 in humans) were phenotypes caused by the loss of stabilizing interactions maintaining the autoinhibited conformation. To further test this hypothesis, I performed the single-molecule motility assay for mutants at three of the interfaces that have been shown to stabilize autoinhibited mammalian dynein (Fig. 20A). These data revealed that weakening the interactions at key residues, via charge reversal or alanine mutations, greatly increased the processivity of individual dynein motors. These increases in run-length were independent of velocity effects, which was surprising, indicating the uncoupling of speed and processivity. Further, these data indicates switching of yeast dynein between active and autoinhibited states is possible during a processive run, and this does not require any cofactors outside of the core dynein complex.

Single point-mutations K1475E and K1517E at site 2 between AAA4 and the linker domain led to a near doubling of dynein run-length ($\sim 3.8\mu\text{m}$, Fig. 20B) relative to wild type without substantially effecting motor velocity when fit to a single-exponential decay. Combining mutations to make a K147E/ K1517E mutant doubled the run-length (Fig. 20B ~ 6.8 respectively) of the individual mutations. The analogous human mutations (K1567E/K1607E) were demonstrated to completely abolish Phi-particle formation in the human dynein complex analyzed by cryo-EM. The same run-length phenotype ($\sim 7.1\mu\text{m}$) could be recapitulated by mutating the opposite D2868 residue to

a lysine; therefore, removing both electrostatic interactions by *either* amino acid substitution is sufficient to produce the same phenotype, indicating these residues likely form a tripartite interaction as is indicated in the human dynein structure.

We further confirmed that these residues were interacting to regulate the run length by reintroducing electrostatic pairing to this linker-AAA4 site. Sequential decreases in run-length were achieved by introducing opposite, but near equal, electrostatic pairing combinations. A K1475E/K1517A/D2868K mutant led to a near wild type run-length ($\sim 2.7 \mu\text{m}$ Fig. 20B) for the motor, without affecting velocity. It is possible that this was the electrostatic composition most resembling the native conformation, as presence of a 1 net positive charge (D2868K) with 1 net negative charge (K1475E/K1517A) most closely resembles the 2 net positive charges (K1475/K1517) and 1 net negative charges (D2868K) present in the native structure. This data further implicates electrostatic repulsion from interacting residues as important in stabilization or disruption of the autoinhibited state, and demonstrates that contacts necessary for maintaining the human Phi particle are highly equivalent to those present in yeast. Amazingly, run-length increases ($\sim 7.2 \mu\text{m}$) near identical to our K1475E/K1517E or D2868K mutants were achieved by mutation of stalk-stalk contacts Y3268A or I3272A, even though the latter of these mutations only caused the loss of a single tertbutyl side chain. Both of these mutations led to decreases in motor velocity to similar degrees, which indicates that disruption of normal coiled-coil sliding kinetics^{29,32}, and communication between the motor domain and the MTBD, is likely introduced by these mutations to similar degrees. Finally, charge reversal mutations at the AAA5/AAA5 R3476D and D3847K lead to near-identical increases in run-length for the motor, with

Figure 20

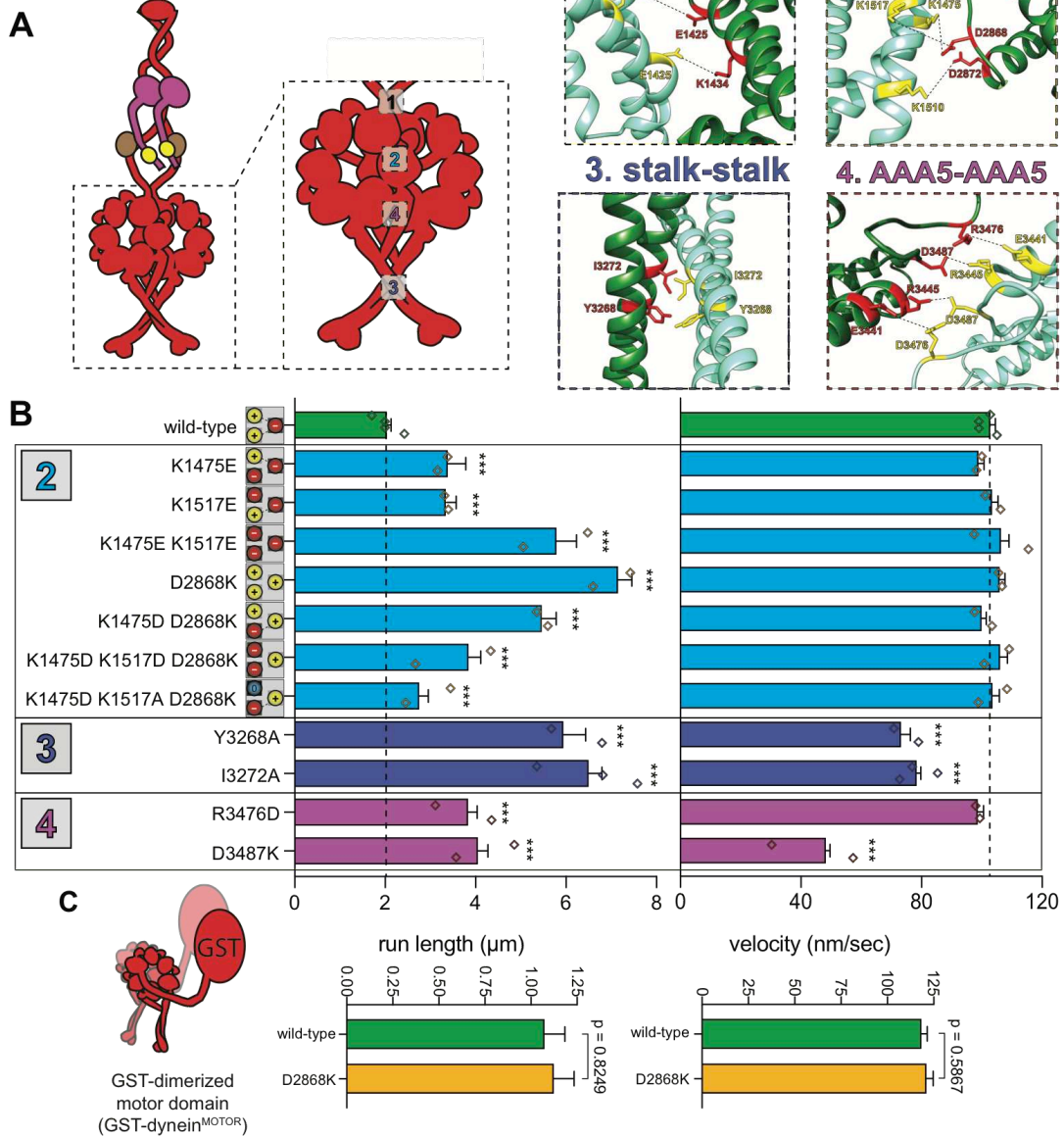


Figure 20. Disrupting phi particle contact points extends single molecule run lengths.

(A) Cartoon depicting four predicted intermolecular contact surfaces within the motor domains that stabilize the phi particle conformation. Four insets show respective regions of yeast dynein modeled into human dynein phi particle structure. Structural models were generated using one-to-one threading of the yeast DYN1 sequence into 5NVU1 on the Phyre2 server. (B) Single molecule run length and velocity values for wild-type and mutant dyneins with phi particle disrupting mutations (at surfaces 2, 3 and 4, as indicated). Cartoons along vertical axis depict electrostatic pairing between residues 1517, 1475 (left circles) and 2868 (right circle) at linker-AAA4 surface. Note that the degree of processivity enhancement is directly proportional to the valence of charge-charge interactions at this surface. Diamonds represent mean values obtained from each independent replicate experiment, error bars indicate standard error). Also note that we generated and tested the motility of two other point mutants at interface 4, E3441K and R3445D, both of which were inactive in single molecule assays (not shown). (C) Schematic of the GST-dynein minimal motor domain, which has been shown not to form the Phi conformation by cryo-EM. The D2868K mutation has no effect when made on this construct lacking the tail domain.

the former leading to a substantial loss in velocity, possibly due to this mutation interrupting dynein mechanochemistry. These two single charge substitutions gave a nearly identical run length increase as the single charge mutants identified at the AAA4-linker site, further supporting our hypothesis. Two further mutations at this site were tested, R3441D and E3445K, but both mutations produced proteins that had little microtubule binding and no activity *in vitro* when purified.

While these data strongly indicated that dynein processivity was being directly affected by its ability to form the autoinhibited conformation, it was important to rule out changes in dynein mechanochemistry as being driving factors for these phenotypes. To this end we made a D2868K mutant, the most prominent run-length increasing mutant in our assays, in the GST-dynein minimal motor construct. As this construct has been extensively characterized *in vitro* and has not been shown to adopt the Phi-particle conformation by cryo-EM¹⁰⁶⁻¹⁰⁷, we reasoned disrupting phi-particle contacts would not affect the motility of this motor. Despite this motor fragment not adopting the Phi-particle conformation, it demonstrates faster velocity (~120nm/s) and significantly shorter run-lengths (~1.2 μm) than the full-length yeast dynein or any of our Phi-particle mutants^{48,106-108}. Confirming our hypothesis, GST-dynein^{D2868K} demonstrated no increase in run-length, and produced identical motor properties to the Dyn1-GST motor. This experiment further confirms the ability to adopt the phi-particle limits dynein processivity. It also indicates that the yeast dynein tail domain is more conducive to processive motility than the GST dimerization domain. It has been previously shown that full-length dynein has increased force production capabilities compared to the GST-

dynein counterpart, consistent with the native tail domain being a better dimerization domain than the GST domain²²⁹.

It has been demonstrated that disrupting the human Phi-particle with the K1567/K1617 mutant increases association of dynein with the microtubule lattice. To determine if the open, uninhibited yeast dynein also had enhanced microtubule binding affinity, we performed calculations of motor landing rate in our *in vitro* motility assays. To our surprise, we observed a small but statistically insignificant increase in landing rate in the D2868K mutant (Fig. 21A). This indicates that the formation of the Phi particle does not limit microtubule landing and the initiation of processive movement in the yeast motor. To further test this hypothesis with a complementary approach, I performed bulk solution microtubule binding assays with both wild type and the D2868K mutant motors in the presence and absence of ATP. Again in this assay, we observed no difference in microtubule binding affinity between the different motors (Fig. 21B). It is not clear why there is such a discrepancy between yeast and human autoinhibited states in these assays, but these results indicate that yeast dynein autoinhibition likely does not prevent the motor from associating with the microtubule lattice. This result may add to the puzzle of why yeast dynein is processive while human dynein is not, as yeast dynein can associate with microtubules even when autoinhibited.

3.3.3 Dynein autoinhibition limits association with plus-end machinery and cortical targeting receptor.

One *in vivo* phenotype that we previously identified in our fluorescence localization assay for K1475Q was an increase in the frequency of dynein cortical foci and improved interaction with dynactin at microtubule plus ends. This could be due to

Figure 21

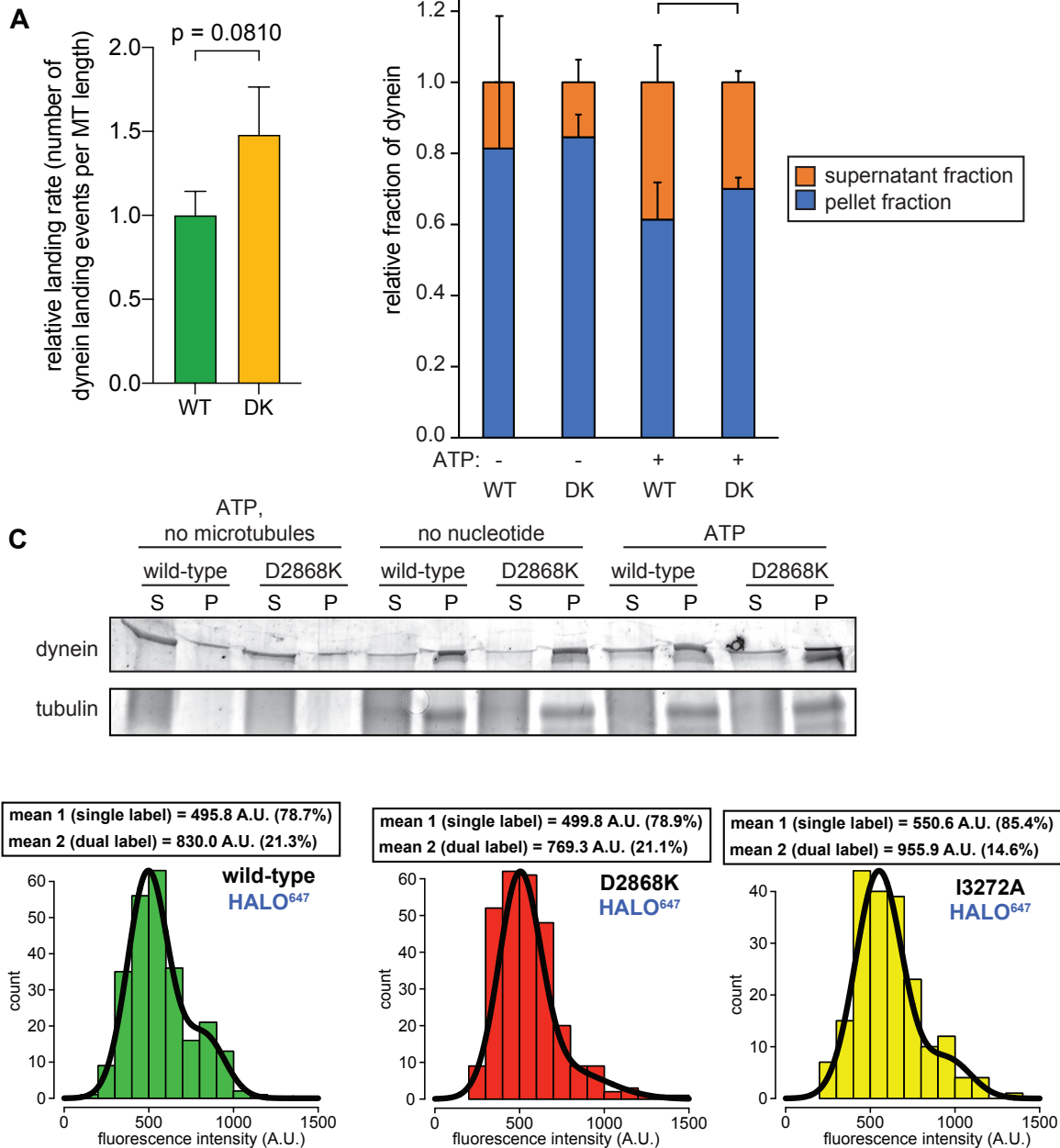


Figure 21. Autoinhibition does not affect the microtubule affinity of yeast dynein *in vitro* (A) Quantification of landing rate of wild type or D2868K mutant complexes in single molecule motility assay from Figure 20. We detected a small but not statistically significant increase in landing rate. (B) Quantification of bulk solution microtubule pelleting assay for wild type or D2868K mutants and (C) representative Sypro gel from this assay. We detected no increase in microtubule binding affinity for the mutant complexes compared to wild type. (D) Fluorescence intensity profiles of the wild type motor and two of the mutants with the longest run lengths. The similarity in profiles indicates increases in run length are due to motor intrinsic properties rather than aggregation.

the native autoinhibited state restricting dynein interaction with cellular binding partners, such as dynactin⁸³ or Num1^{84,85}. We therefore reasoned this phenotype would be recapitulated for our other mutants, and should scale in these same parameters proportional to the loss of electrostatic pairing identified in our single molecule experiments. Indeed, the K1475E mutant led to an even more dramatic increase in both plus-end and cortical foci than the K1475Q mutant (Fig. 8B and 22B), likely due to electrostatic repulsion provided by this mutant relative to the neutral charge substitution. Even more strikingly, the D2868K mutant—which had the most dramatic increase in run length in our single molecule assays—robustly accumulated at microtubule plus ends, the spindle pole body, and the cortex. While many different mechanisms could lead to accumulation at spindle-pole bodies, previous work from our lab demonstrated that activation of dynein-dynactin by the overexpression of the coil-coil adaptor Num1 drove dynein motility from plus ends to minus ends of microtubules⁸⁵. Therefore, it is likely that the spindle-pole body population of dynein was mostly a consequence of active dynein motility along astral microtubules. Attempts were made to categorize movement of dynein along microtubules, but only few instances of dynein activity were observed in most cells. Interestingly, D2868K mutants also had extremely short microtubules; previous work has demonstrated dynein has roles as a microtubule catastrophe factor in both yeast and humans^{83,173}, and that this activity requires active dynein ATPase activity. It is possible that the loss of dynein autoinhibition converts normally inactive pools of cytoplasmic dynein to active processive motors *in vivo*, driving the observed loss of microtubule stability. Cells with the D2868K mutation but also overexpressing the

yeast kinesin Kip2, which promotes dynein transport away from spindle pole bodies and

Figure 22

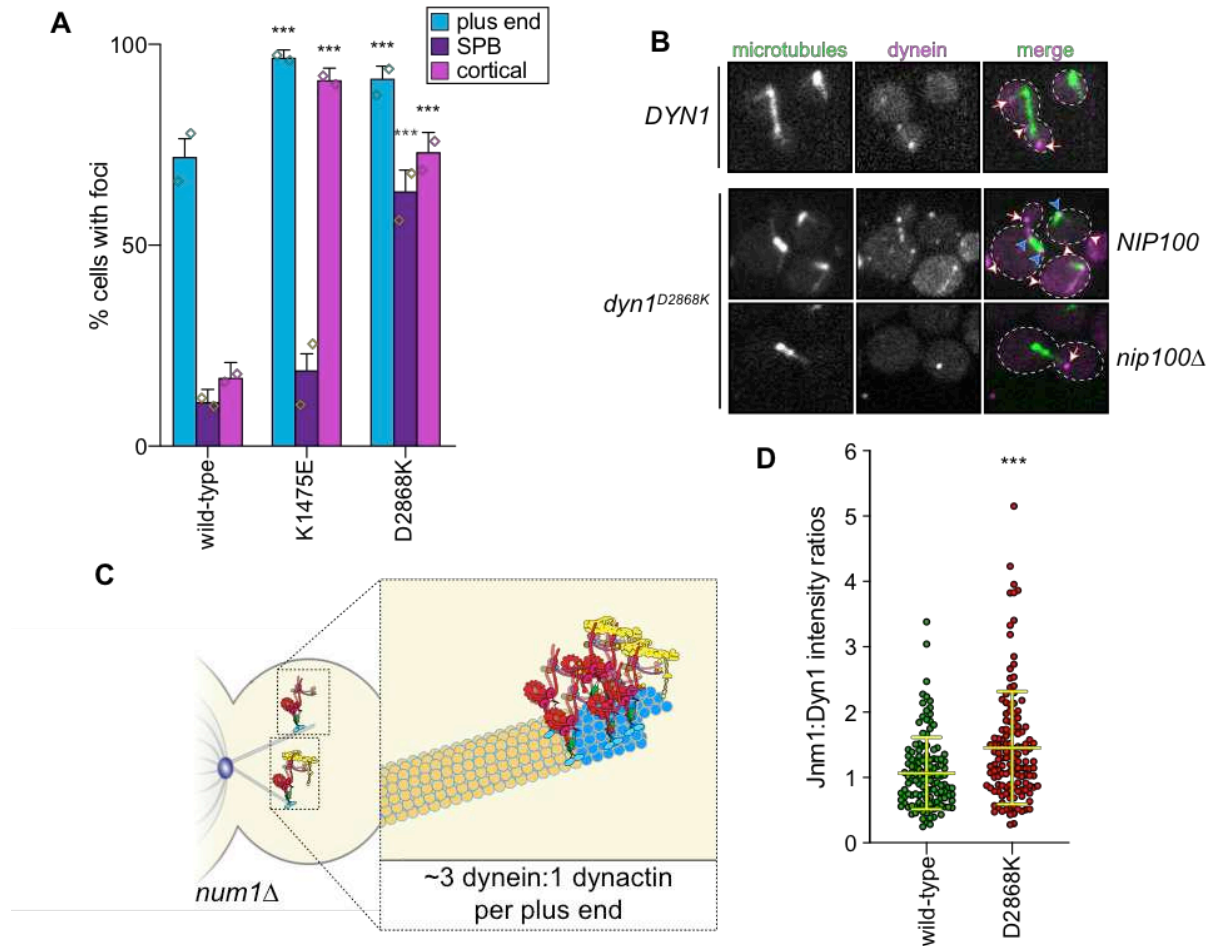


Figure 22. Dynein inhibition limits microtubule and cortical targeting by limiting dynein interaction with cofactors. (A) Plot depicting the fraction of cells (weighted mean) with indicated mutant or wild-type Dyn1-3GFP foci cells ($n = 100, 90, 82$ mitotic cells from two independent experiments; error bars indicate weighted standard error of proportion; diamonds represent mean values obtained from each independent replicate experiment). (B) Representative images of wild-type or mutant dynein (D2868K) localizing in otherwise wild-type or *nip100Δ* (dynactin component) cells. Note the lack of cortical localization of dynein(D2868K) in *nip100Δ* cells (white arrowheads, cortical foci; white arrows, plus end foci; blue arrowheads, SPB foci; similar results were obtained from 2 independent replicates). (C) Cartoon depicting the relative ratio of dynein to dynactin at microtubule plus ends (~3 dynein:1 dynactin), based on previous quantitative ratiometric imaging⁸³. (D) Scatter plot (shown with bars depicting mean and standard deviation values) of the ratios of fluorescence intensity values for Jnm1-3mCherry (dynactin component p50/dynamitin):Dyn1-3GFP at individual microtubule plus ends and SPBs ($n = 132$ and 145 plus ends or SPBs, left to right, from two independent experiments). Background corrected intensity values of colocalizing Jnm1-3mCherry and Dyn1-3GFP foci were each divided to obtain individual ratio values. Measurements were taken from *num1Δ* cells to prevent offloading of assembled dynein-dynactin complexes from plus ends.

increases microtubule length^{107,110,184}, successfully outcompeted the dynein catastrophe effect, and decreased D2868K localization to spindle pole bodies (data not shown).

As the human dynein mutant which disrupted autoinhibition (K1567E/K1607E) used in the previous study was shown to robustly increase dynein-dynactin interaction measured by size-exclusion chromatography, we wondered if the increase in offloading was due, in part, to increased association of mutant dynein with dynactin complexes. The equivalent (K1475E/K1517E) mutation in our motility assay demonstrated nearly identical properties to our D2868K mutant, which should have similar electrostatic pairing at stabilizing residues. The D2868K mutants demonstrated an increased interaction with dynein at the plus ends of microtubules, measured by ratiometric fluorescence intensity imaging of dynein-3GFP/Jnm1-3mCherry at the microtubule plus end. This ratiometric imaging was performed in a *num1*Δ background to eliminate complications introduced by possible differences in rates of cortical offloading from the cytoplasm of microtubules. Finally, all observed cortical targeting phenotypes were dependent on dynactin, as deletion of the dynactin subunit nip100 led to a loss of all cortical dynein foci, but not plus end or spindle-pole dynein pools. These data indicate dynein is maintained in an autoinhibited state in cells, which limits binding to microtubule plus ends, and limits the tail domain binding to dynactin, which has been demonstrated to be one rate-limiting step of cortical targeting^{28,117} and required for interaction with Num1 at the cortex .

3.3.4. Physical separation dynein motor and tail domains disrupts dynein autoinhibition

The robust accumulation of dynein mutants at microtubule ends and the cell cortex was reminiscent of a former dynein mutant construct designed by our lab to test

the hypothesis that the tail and motor domains directly communicated to regulate dynein binding to canonical binding partners Bik1, Pac1, dynactin, and Num1. The “HL3” mutant had a long, rigid alpha-helical linker incorporated between the linker and motor domains. This mutant robustly had similar robust recruitment to microtubules and the cell cortex. More surprisingly, this was one of few mutants which demonstrated cortical targeting in the absence of Pac1 or Bik1, and led to the hypothesis that the motor domain could “mask” the tail domain, preventing cortical targeting in the absence of dynactin or plus end machinery (Fig. 23A, original model)²⁹. While reminiscent of other mechanisms of autoinhibition present in cytoskeletal motors, such as kinesin-1¹⁸⁵⁻¹⁸⁶, no structural or biochemical data could support this hypothesis. In light of our new data on yeast dynein autoinhibition, we then asked if these phenotypes are demonstrated by the HL3 mutant. Separation of the motor and tail domains may prevent intra-motor domain contacts from associating, and may affect the ability of the tail domains to associate. We therefore investigated this HL3 mutant by expression in our yeast dynein system. Unlike previous experiments with this construct⁸⁴, the heavy chain and accessory chains were both overexpressed, as was done for our wild type and other mutant dyneins (Fig. 19A). Analysis of the HL3 mutant with our single molecule motility assay demonstrated even more processive motility than the D2868K mutant (Fig. 23B). This strengthened the case that the previously demonstrated HL3 mutant phenotypes were likely a consequence of loss of dynein autoinhibition. We confirmed by intensity analysis that these phenotypes were not due to aggregation of the motor (Fig. 24C). Interestingly, this motor also demonstrated a higher velocity than the mutant (~120 nm/s), with motility similar to the GST- dynein construct, both of which have been repeatedly shown to be

Figure 23

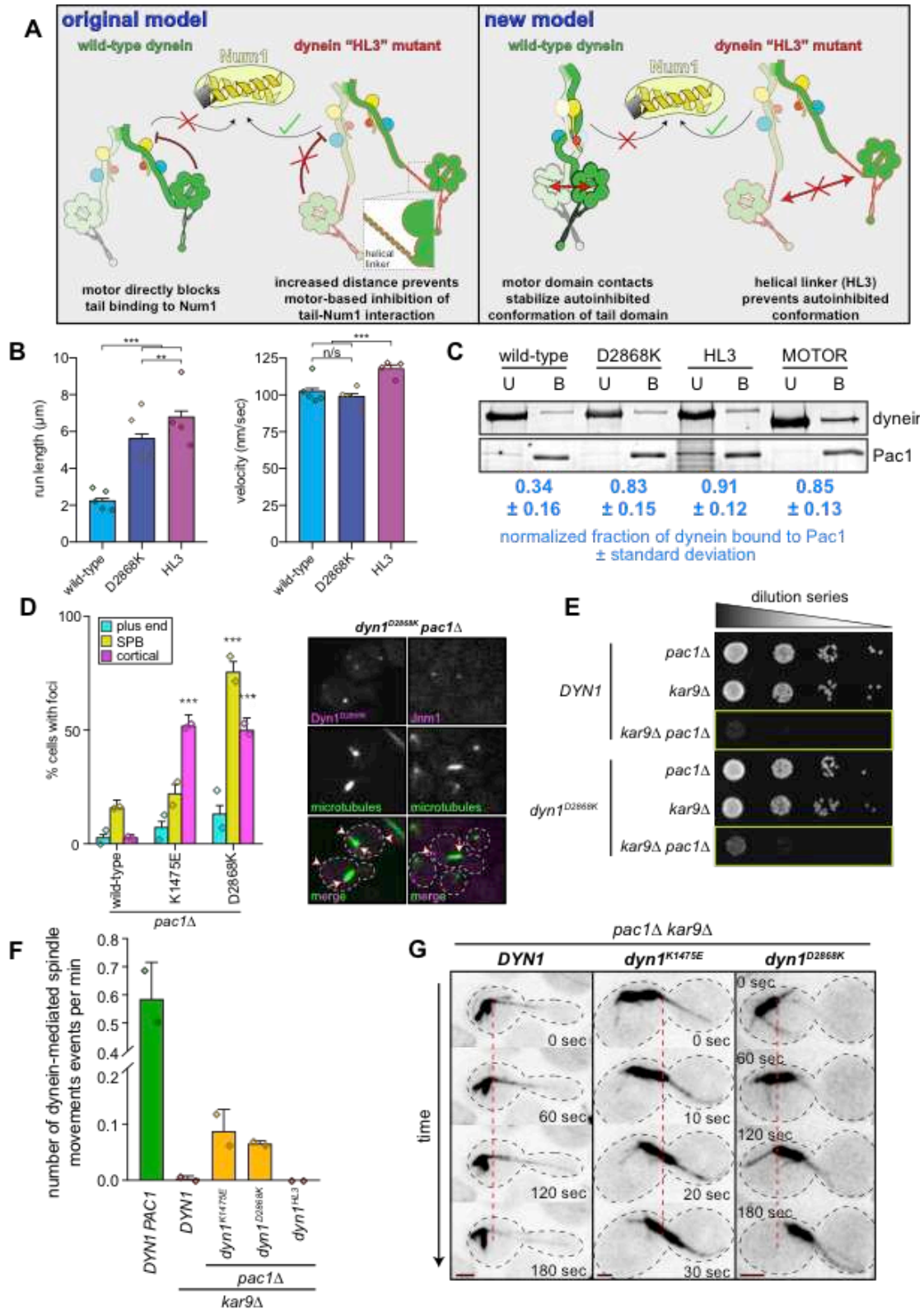


Figure 23. Release of dynein autoinhibition permits Pac1/LIS1-independent localization and function. (A) Cartoons depicting models of possible dynein^{HL3} phenotypes⁸⁴. Dynein tail domain cannot associate with Num1 in the absence of plus end-targeting; however, addition of HL3 between tail and motor domains permits plus end-targeting-independent dynein-Num1 interaction. Our original model posited that this was due to the motor precluding the tail-Num1 interaction. Our new model posits that motor domain contacts stabilize the autoinhibited conformation, in which the tail domains adopt a twisted state that is unable to interact with Num1. We propose that HL3 insertion prevents adoption of the autoinhibited conformation. (B) Motility assay parameters, measured from single molecules of motors purified using the strategy described in Figure 1A (n = 840 [5], 586 [4], 642 [4] motors [independent replicates], left to right; error bars indicate standard error; n/s, p = 0.1563; **, p = 0.0092; ***, p < 0.0001; diamonds, mean values obtained from independent replicates). (C) Bead binding assay illustrating increased affinity of Pac1 for uninhibited dyneins. Values represent the mean corrected band intensities (n = 3, 3, 2, 3) independent experiments, left to right). (D; left) Fraction of cells (weighted mean) with mutant or wild-type Dyn1-3GFP foci in *pac1Δ* cells (n = 113, 108, 90 mitotic cells from two independent experiments, left to right; error bars indicate weighted standard error of proportion; diamonds represent mean values obtained from independent replicates). (right) Representative images depicting the presence of cortical dynein and dynactin (Jnm1) in *dyn1*[D2868K] cells (arrowheads, cortical foci; arrows, SPB foci). (E) Serial dilutions of cells with indicated genotype (note differences in cell growth in yellow boxes; representative assay shown; similar results were obtained from 2 independent replicates). (F and G) Relative in vivo dynein activity with representative time-lapse images (see Methods; n = 35, 30, 30, 30 and 32 cells from two independent experiments; diamonds, mean values obtained from independent replicates; scale bars in panel G, 2 μm; dashed line provides point of reference).

faster than full-length dynein in single molecule assays^{160,163,195}. This indicates that allosteric communication between the tail and the motor domain may be important for normal dynein mechanochemistry, and that loss of tail domain allosteric communication via artificial dimerization in the GST-dynein and HL3 mutants led to increased speeds (Fig. 20C, Fig. 23B). However, the tail domain of yeast dynein, unlike its mammalian counterpart^{86,87}, is sufficient to orient the heads to effect processive motility, even when both tail domains are separated by a nanometer length linker to the motor. Further, the tension of the tail domain, communicated allosterically through the tail and linker domains, may be important for affecting yeast dynein velocity¹²⁰.

The first experiments with the HL3 motor demonstrated that the tail domain and the HL3 mutant were sufficient for recruitment to the cell cortex in the absence of plus-end targeting factors Bim1, Bik1 and Pac1⁸⁴. To test if these previously described offloading phenotypes were a result of a loss of autoinhibition in the HL3 mutant, we

performed our localization assay in cells lacking Pac1 (Fig. 23D). Amazingly, both K1475E and D2868K were recruited to the cortex in the absence of Pac1, with D2868K mutant sharing a very similar localization frequency as was found with the HL3 mutant⁸⁴ (Fig. 23D). Furthermore, *pac1Δ/dyn1^{D2868K}* mutants demonstrated higher frequency of cortical foci than even wild type dynein with normal expression Pac1, indicating that Phi particle formation is indeed limiting dynein association with plus end targeting factors, namely Pac1, dynactin, and Num1.

However, even more striking results were obtained by repeating our spindle oscillation assay for the “open” mutants when Pac1 was deleted (Fig. 23E-G). Whereas wild-type and the HL3 mutant demonstrated no ability to pull the mitotic spindle in the absence of Pac1 (despite the latter’s astounding single molecule activity), both the K1475E and D2868K mutants demonstrated active spindle movement at the cortex. As a natural consequence of making these mutants, we produced *kar9Δ/pac1Δ* mutant alleles corresponding to each Phi-particle disrupting mutation. When analyzing the growth of wild type dynein in the *kar9Δ/pac1Δ* background compared to uninhibited mutants, we found that expression of either Phi-particle mutant was sufficient to rescue synthetic growth defects (Fig. 23E, Fig. 24A, B). These parallel investigations of mechanisms of spindle orientation suggested to us that the active, uninhibited dynein mutants can partly compensate for loss of Pac1. We did not observe a similar growth rescue for cells expressing dynein^{HL3} (Fig. 24C), further suggesting that although the HL3 mutant bypasses Pac1 for cortical localization⁸⁴, and is highly processive *in vitro*, it is inactive at the cell cortex.

Figure 24

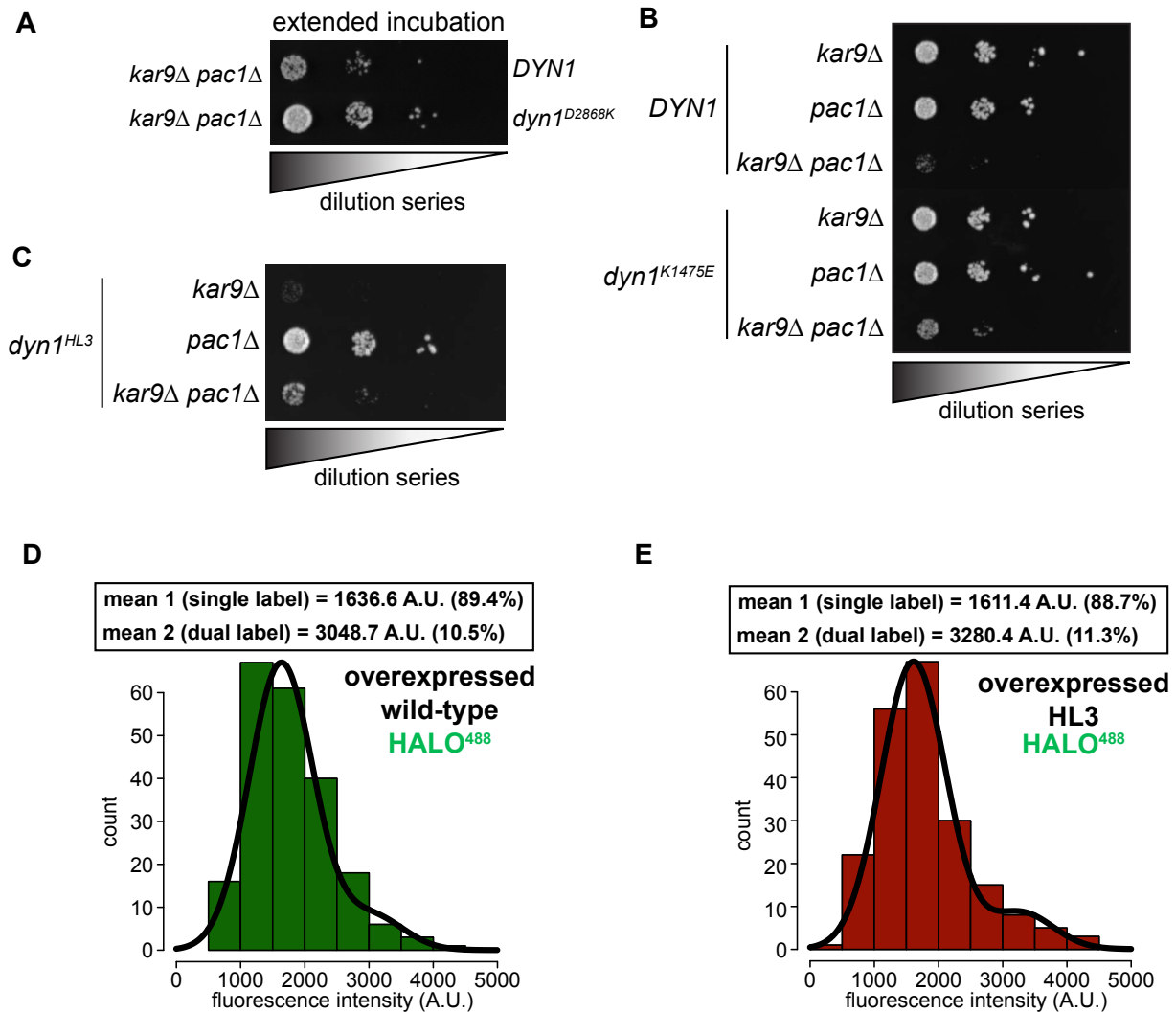


Figure 24. Point mutations which disrupt autoinhibition, but not HL3, compensate for Pac1 deletion. (A) Four day growth of wild type or D2868K mutant in growth assay depicted in Fig 23E. (B) K1475E mutants give similar rescue to D2868K compared to the wild type. (C) The HL3 mutant has appreciably worse growth in this assay than wild-type or the mutants, indicating that this mutant is not functional in cells despite activity in *in vitro* assays. (D and E) Fluorescence intensity profiles of the wild type (D) and HL3 mutant (E) motors analyzed in our motility assays in Fig. 23B. Increase in run lengths was due to motor intrinsic properties, rather than aggregation.

These results inform us of two important aspects of dynein regulation in yeast.

Firstly, dynein in the cytoplasm may directly interact with dynactin and

Num1, and that Pac1 is not necessary to activate dynein motility. Secondly, dynein

autoinhibition limits dynein at the plus end of microtubules and the cortex, and Pac1

promotes dynein activity in parallel with this autoinhibition pathway. It has been previously shown that Pac1-Bik1-dynein form a complex with other components of the plus end machinery^{84,99}. Therefore it may be the case that the plus end machinery is important to accumulate open dynein to form a stable dynein-dynactin, and prevent dynein motor activation and the motor moving to the minus-end of microtubules. Furthermore, limiting offloading of dynein-dynactin complexes until a sufficient number of complexes form may be necessary for optimal spindle positioning activity and force generation of dynein-dynactin-Num1. These experiments led us to investigate if Pac1 had a role in promoting dynein autoinhibition, via direct interaction. These results form the basis for Chapter 4 of this thesis work. Taken together, this work will delineate more clearly the mechanisms that regulation dynein autoinhibition.

3.4. Discussion

3.4.1. Stochastic switching of dynein regulates motor activity and association with cofactors

Our experiments in this chapter demonstrate that yeast dynein is regulated through autoinhibition, which stabilizes the protein in a poorly active state through a series of intramolecular interactions identical to its mammalian counterpart¹⁶⁵. The negative stain and single molecule experiments (Fig. 19 and 20) demonstrate that dynein stochastically switches between active and autoinhibited states, and we propose that these states can tune the kinetics of dynein's interactions with other regulators (Fig. 22, 23). Further, autoinhibition affects dynein's processivity in *in vitro* experiments using unloaded single motors. As negative stain and single molecule experiments were performed in the absence of any other dynein regulatory factors, the degree of open

dynein and observed run-length changes may only be attributed to intrinsic motor properties. The sole hypothesis from these observations is that the switching between a processive motor and autoinhibited motor occurs both in the cytoplasm and *during* processive dynein runs, since these effects are not due to motor aggregation (Fig. 21). This stochastic switching mechanism has been proposed to explain the different intermediate states between open and autoinhibited dynein observed both by our negative stain data and previous cryo-EM experiments of the human dynein complex¹⁶⁵.

These changes in processivity can be tuned at the AA4-Linker contact interface, increasing or decreasing processivity of the motor (Fig. 20) by changing the valence of electrostatic interactions. The absolute number of intact electrostatic interactions at the AAA4-linker interface were the sole determinants of motor processivity and independent of motor velocity effects. Increases in run-length were maximally achieved by removing all interactions between the AAA4-linker site, as well as by ablating hydrophobic interactions in the stalk, despite the latter two mutants (Y3268A and I3272A) likely affecting dynein mechanochemistry. The HL3 mutant—whose phenotypes we propose derive principally from disruption of dynein autoinhibition through separation of the motor and tail domain communication (Fig 23)—shows similar run lengths to these aforementioned point mutants. We believe these various mutants with high processivity may all represent similarly uninhibited dynein complexes.

While it is unclear the exact sequence of events which induces this autoinhibition and eviction from the microtubule lattice, yeast dynein is sufficiently uninhibited in the absence of single point mutations D2868K or Y3268A/I3272A, which indicate that the autoinhibited state of dynein is quite labile. It is likely that the autoinhibited state is

regulated in cells, giving rise to the polarized nature of dynein-mediated spindle movement^{83,194}. Since the HL3 mutant maintains all native residues, but has disrupted tail-motor interactions, it represents an interesting phenomena of dynein regulation which warrants further study. This motor has all native residues, but the tail domain cannot (likely) communicate structural changes to the motor domain to affect its function. Therefore, it is likely that tension in the tail domain, produced by tail-tail interactions, drives the assembly of the motor-motor interactions that regulate the speed of the motor terminate processive motility. It is interesting to note that the HL3 mutant does demonstrate slightly longer run-lengths than any of the point mutants, and this mutant would not be able to communicate allosteric effects between the tail and motor domain due to the presence of the rigid linker domain. Furthermore, several class averages depicted in (Fig. 19D) clearly show the motor domain separation even in the presence of tail domains interaction. The reason this mutant demonstrates faster motility, and more processive motility, could therefore be due to disrupted communication between the tail and motor domain. These data demonstrate that yeast dynein run-length is limited by stochastic switching between open and closed states, which limits processivity of the motor in a dynactin-independent and unloaded experimental set-up.

An interesting outcome of these studies is that when dynein autoinhibition is lost, yeast dynein demonstrates *in vitro* run-lengths similar to its human counterpart when bound to dynactin and an adaptor protein ($\sim 7\mu\text{m}$ vs $5\text{-}9\mu\text{m}$ ^{84,85}). Furthermore, it has been shown by cryo-EM that dynactin binding serves not only to scaffold up to 2 dynein dimers in the mammalian system, but also to orient and separate the motor heads⁹².

This separation may serve to limit tail-tail interactions which drive Phi-particle formation, which potentially indicates that both yeast and mammalian dynactin have a role in stabilizing open conformations of open, uninhibited dynein. However, it is unclear if this mechanism affects dynein at the cortex in yeast cells and if the native dynein-dynactin-Num1 complex can enter autoinhibition while moving processively under load. It is currently unknown what terminates dynein-mediated spindle positioning events, or how dynein is offloaded from cortical patches after assembly into dynein-dynactin-Num1 complexes, if the protein is indeed ever unloaded. The persistence of dynein cortical foci^{193 may} indicate that dynein is not unloaded and repurposed, but instead recycled by the proteolytic machinery. Future experiments will need to address the potential relevance of dynein intrinsic motor termination on *in vivo* dynein activity.

3.4.2. Implications of dynein autoinhibition for regulation and function across eukaryotes.

Despite the apparent simplicity of the yeast dynein pathway, it shares many compositional and functional similarities with the dynein pathway in filamentous fungus⁸² and animals¹⁰³. The similarities are even more apparent with our discovery that yeast dynein is autoinhibited by the exact same residues as its higher eukaryotic counterparts. Our negative stain analysis suggests that the majority of dynein in the cytoplasm is maintained in a mostly autoinhibited state, which tunes dynein-dynactin interaction in the cytoplasm. The stochastic switching of dynein between open and autoinhibited states limits the association of dynein in the cytoplasm with components of the plus end targeting pathway, as demonstrated by our *in vivo* fluorescence experiments. Loss of autoinhibition, which can be accomplished through single point mutations, increases

dynein's interaction with dynactin and the plus end machinery along microtubules, and increases the frequency of dynein cortical targeting (Fig. 22). This demonstrates the labile nature of this autoinhibited conformation in the cytoplasm. Furthermore, these phenotypes scaled in severity in the same manner that our *in vitro* phenotypes scaled for the K1475Q, K1475E, and D2868K mutants, indicating that the kinetics of autoinhibition can be controlled through single electrostatic interactions. These data illustrate how cellular dynein activity may be directly tuned through the kinetics of autoinhibition, and also presents an attractive target to understanding dynein post-translational modifications, as phosphorylation/dephosphorylation would provide new interacting residues to stabilize intermolecular contacts.

Dynein recruitment to microtubule plus end limits dynactin interaction; however, despite dynein and dynactin associating at plus ends, they do not form a processive complex in the absence of a coil-coil adaptor¹⁰⁷, the third integral component known to activate mammalian dynein *in vitro*. This indicates that yeast dynein-dynactin may form a similar inactive microtubule-bound complex as human dynein-dynactin^{95,96}. Experiments using human components have demonstrated that purified human dynein-dynactin-EB3 are sufficient to form plus end tracking complexes, and that these complexes are distinct from CLIP170- Lis1-dynein complexes previously identified^{95,96}. Despite the apparent interaction of these complexes, the architecture of this complex presumably is not sufficient to activate motility. The differences in mutant and wild type dynein activity at plus end provide further evidence that dynein may adopt several different intermediate states between fully active and fully inhibited dynein. Future studies (and new methods for identifying intact yeast dynein-dynactin-Num1 (DDN)

complexes) will be necessary to determine if yeast dynein-dynactin can form similar complexes as the human counterpart.

Furthermore, it is interesting to consider the importance of tension on facilitating dynein activity, and how tension may play a role in activating dynein complexes in cells. Our HL3 mutant demonstrated incredible *in vitro* motility compared to wild type complexes, but despite this, was incapable of moving the mitotic spindle at all. If the tail of dynein is indeed important for communicating and coordinating the activities of the motor heads as has been suggested for both yeast and human dynein^{25,43,53,106} this communication is most likely to be through allosteric changes induced by tension, rather than direct interaction between motor and tail domains.

One of the most surprising findings of our localization studies is that the K1475E and D2868K mutants with compromised autoinhibition bypass the need for Pac1 to reach the cell cortex. These phenotypes are shared by the HL3 mutant²⁹, which similarly bypasses the need for Pac1 to reach the cell cortex (Fig. 23). Despite both the point mutants and HL3 mutant sharing this phenotype, only the point mutants retained DDN activity at the cell cortex. These single point mutants could also rescue for the synthetic lethality of *kar9Δ/pac1Δ* genotypes (Fig. 23 and 24), further indicating these mutants retained dynein activity. However, this activity was severely reduced compared to wild type (Fig. 23 F, G). This indicates that plus end loading of dynein by Pac1 and Bik1 is important to effect nuclear migration during mitosis. This could be due to the need to load a sufficient number of dynein-dynactins on a single microtubule prior to offloading. It may also be the case that multiple dyneins must assemble on a single dynactin or group of dynactins, which would require Pac1 to facilitate the assembly of these higher

valence structures as demonstrated previously for the human proteins^{93,94}. Finally, the fact that mutants had increased cortical foci compared to the wild type (compare Fig. 22A wild type to Fig. 23C) but lower spindle activity overall (Fig. 23D) indicates that microtubule accumulation by Pac1/Bik1 and offloading to Num1 may be coupled to effect normal nuclear migration. Dynein at the plus end of microtubules is ideally suited to move its cargo, and conversion of dynein-dynactin from an inactive complex to an active complex with Num1 may happen upon contact with the cortex. This model would help account for the problems presented by a “search and capture” model of astral microtubule interaction at the cortex. A diffusive search by only two astral microtubules over the surface area of an entire cell would likely be slower and less efficient at finding dynein ensembles at the cortex, than a mechanism by which plus end accumulation and cortical offloading are coupled, especially given the rapid progression of yeast through mitosis. Future work modeling these two possibilities may help understand the need for plus end recruitment.

Since Pac1 was dispensable for cortical dynein activity in mutants, we reasoned that Pac1 is not needed to effect dynein mechanochemistry. Furthermore, the results of our pulldown experiments identified that all candidate mutants with disrupted autoinhibition (GST-dynein, D2868K, and HL3) had higher affinities for Pac1 than wild type dynein. These data, along with the genetic and localization experiments previously discussed, suggested to us that Pac1 participated in the pathway of dynein autoinhibition. We hypothesized that one role of Pac1 was to prevent dynein autoinhibition, which would explain why loss of autoinhibition bypasses the need for Pac1. This is the subject of the next chapter and several lines of evidence from our

laboratory and from human experiments implicate Pac1 as a protein which stabilize open, active dynein.

3.5. Conclusion

In summary, dynein autoinhibition is an evolutionarily conserved mechanism which is responsible for regulating yeast dynein processivity *in vitro* and for *in vivo* targeting of the dynein complex to microtubule plus ends and the cell cortex. While the extent to which the stochastic autoinhibition may be relevant for dynein-dynactin complexes in cells is unclear, it is apparent that the apparent processivity of yeast dynein previously demonstrated did not represent a maximally activated complex¹⁶¹—this requires us to rethink what “maximally activated” motility may mean when comparing *in vitro* motility to *in vivo* trafficking. For instances, despite the relatively fast speeds (~ 0.8-1.2 microns/second) of recombinant human dynein-dynactin-adaptor complexes^{84,85}, vesicular transport can occur at substantially higher speeds *in vivo*—for instance, in neurons—despite the crowded environment of the cell. Our understanding of dynein regulation can be further refined—switching between autoinhibited and open dynein occurs stochastically in the cytoplasm, and limits dynein association with components of the plus end targeting complex and dynactin. Finally, relieving dynein autoinhibition is sufficient to bypass plus end targeting, and for formation active dynein-dynactin-Num1 complexes at the cell cortex in budding yeast, indicating that dynein may associate with dynactin in the cytoplasm and directly bind to the cortical receptor Num1. These mechanisms represent an evolutionarily conserved aspect of dynein regulation and have implications for previous studies of other dynein regulators, importantly Pac1/LIS1, which will be discussed in the next chapter.

Chapter 4: The dynein regulator Pac1/LIS1 stabilizes the active dynein conformation

1. Introduction

Despite millions of years of divergent evolution, the yeast and human dynein complexes share many similarities in cellular function and composition. These proteins demonstrate high degrees of homology²⁴ between motor domains and accessory chains. The yeast dynein-dynactin is structurally and compositionally similar to its mammalian counterpart, and is similarly required for all transport functions *in vivo*⁷⁴. The coiled-coil adaptor Num1 is highly homologous to the human protein NuMA⁸⁹, and this protein is proposed to activate dynein-dynactin motility through direct binding of its coiled-coil domain in a mechanism similar to other dynein adaptor proteins^{85,95}. Besides the core dynein complex, many MAPs serve as effectors of dynein activity in mitosis, including Bik1, Bim1, Kip2, and She1^{83,84,163}. However, experiments exploring the functions of the homologous Pac1 and LIS1 proteins have been confounding. In both humans and yeast *in vivo*, Pac1/LIS1 functions to target dynein to microtubules, but *in vitro* LIS1 has been shown to enhance the motility of dynein-dynactin-adaptor complexes^{96,111}, whereas Pac1 inhibited dynein motility¹⁰⁵⁻¹⁰⁷. Furthermore, LIS1 has been demonstrated to effect the conformation of the dynein AAA ring at AAA3/4 through direct binding¹⁰⁷, and also to increase the force production of dynein alone²⁰⁴, an expected consequence of affecting AAA3⁴⁸.

A detailed discussion of the research concerning both Pac1 and LIS1 in the dynein pathway in published literature will principally be saved for Chapter 5. This

chapter will focus on our experiments re-examining the effects of the yeast regulator Pac1, and how these experiments can reconcile the previous discrepancies observed between Pac1 and LIS1 *in vitro*. In the previous chapter, we demonstrated that dynein autoinhibition regulates *in vitro* motility and the localization of the protein during mitosis. By relieving dynein autoinhibition, we were able to surpass the need for microtubule localization prior to cortical targeting. Further, we showed that cortical targeting could now occur in the total absence of Pac1. Mutants lacking autoinhibition demonstrated cortical localization in the absence of Pac1, and were still competent to position the mitotic nucleus, which demonstrates Pac1 is not required for dynein motor activity at the cortex.

The most likely explanation for our experimental observations was that Pac1 binding to dynein stabilizes the open, uninhibited conformation of dynein by directly binding the motor domain. Rather than activating dynein directly, Pac1 binding sterically prevents the dimer from forming intramolecular bonds which stabilize the autoinhibited conformation. This binding is likely both stochastic and opportunistic, as Pac1 binds dynein in the cytoplasm as it switches between closed and open conformations. That in turn targets dynein-Pac1 to microtubules by binding Bik1, but the exact mechanism that prevents dynein motility after Pac1-dynein localization to microtubules is unclear. By preventing dynein autoinhibition, Pac1 drives assembly of dynein-dynactin at the microtubule plus-end, and these complexes are then offloaded to cortically anchored Num1 patches. This chapter will discuss the biological implications for this targeting mechanism, and reconciles previous Pac1 *in vitro* data with a new model where Pac1 activates, rather than inhibits, dynein motility.

This thesis work also reexamined previously published Pac1 effects, and challenge the findings that this molecule is an inhibitor of dynein function. Our data will demonstrate that relieving dynein autoinhibition, and not affecting mechanochemistry, is the primary biological activity of Pac1. We explore how Pac1 binding microtubules at nanomolar affinities in commonly used assay buffer conditions for TIRF motility assays affects dynein motors non-specifically. Accordingly, previous experiments using micromolar quantities of Pac1 without imaging this protein were likely slowing dynein motility due to simultaneous interactions between dynein, Pac1, and the microtubule lattice. A similar mechanism of inhibition of dynein has been extensively characterized for a second budding yeast dynein regulator, She1¹⁶³. The reason LIS1 does not produce similar effects to Pac1 *in vitro* is because LIS1 has been shown to have much lower affinity for microtubules *in vitro* than the yeast homologue^{95-96,204}, so experiments using this protein have not been subject to similar artifacts.

4.2. Methods

The protocols for experiments in this chapter are discussed in Chapter 3.

4.3. Results

4.3.1. Pac1/LIS1 stabilizes active, uninhibited dynein

One of the important aspects of our localization experiments (Fig. 23) was that both the Phi-particle mutants and the HL3 mutant bypassed the need for Pac1 (but not dynactin) to reach the cell cortex. We reasoned it was possible that this Pac1-independent cortical targeting was due to cytoplasmic binding of mutant “open” dynein and dynactin (Fig. 23D), and direct offloading to Num1. If this were the case, we reasoned that the function of Pac1 in the cytoplasm would be to maintain the open

dynein, to increase interaction with dynactin and the plus end targeting complex. This would maintain dynein in an open conformation and targeting the complex to microtubule plus ends, where dynein and dynactin are known to primarily interact in wild type cells in yeast⁸⁴. It is unlikely that Pac1 would have a direct role in “opening” dynein through some allosteric interaction, as open mutants demonstrated cortical activity in the absence of Pac1 (Fig. 23 E-G) and Pac1 is not observed at the cell cortex^{99,109}.

What mechanism might Pac1 employ to promote the open conformation? We examined two EM structures of dynein to further investigate possible mechanisms of dynein-Pac1 interaction. Superimposing the cryo-EM structure of mammalian dynein in the autoinhibited conformation (PDB 5NVU and PDB 5VH928) with the structure of yeast dynein bound to Pac1^{105,164} revealed the obvious potential for a steric clash between Pac1 bound at AAA3/AAA4 site of one dimer and the second dynein monomer of the autoinhibited structure (Fig. 25A). In the Pac1-bound dynein, interaction between adjacent linker and motor domain surfaces would be precluded due to Pac1 at AAA3/AAA4 site occupying these surfaces. We therefore reasoned that dynein-bound Pac1 would be unable to reenter the autoinhibited conformation, due to loss of stabilizing contacts between the two motor heads.

This structural analysis implicated Pac1-dynein binding as a regulatory step in the kinetics of dynein autoinhibition. If Pac1 bound dynein during stochastic switching between the Phi and open conformations, it could act as a molecular wedge, holding the motor domains apart (analogous to what has been demonstrated for dynactin⁶¹). This structurally distinct complex could then bind to microtubules through Bim1/Bik1 and

subsequently interact with dynactin. However, since *pac1* Δ has a milder mitotic defect

Figure 25

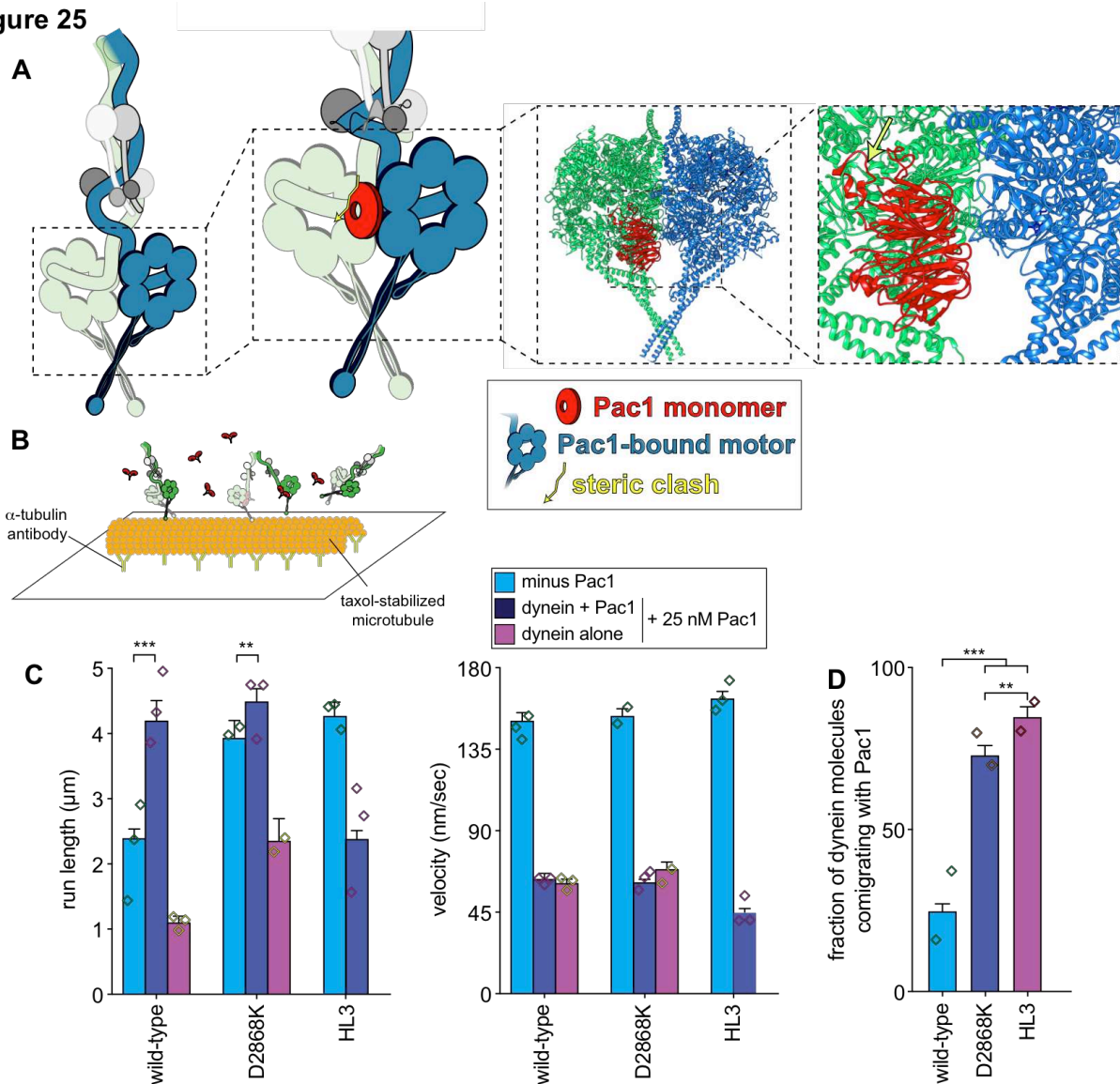


Figure 25. Pac1 promotes release of the autoinhibited conformation of dynein. (A) Cartoon and structural model depicting steric clash between phi particle dynein and Pac1. Structural model was generated by aligning the Pac1-bound dynein monomer structure (pdb 5VH928) into one of the heavy chains in the phi particle structure (pdb 5NVU1). Note the steric clash (depicted with jagged yellow arrow) between the Pac1-bound dynein heavy chain (in blue) with the second heavy chain (in green). (B) Cartoon depicting experimental setup for dynein-Pac1 single molecule assay. (C) Plots depicting motility parameters (left, mean run length values, from fitting of raw data to one-phase decay; right, velocity; error bars indicate standard error) of indicated dyneins moving in the absence (i.e., those not pre-incubated with Pac1, green) or presence of 25 nM Pac1 (dimer concentration). For those experiments in which Pac1 and dynein were pre-incubated, we separately scored those dyneins comigrating with Pac1 (magenta), or migrating without Pac1 (yellow; n values: wild-type, 437, 353, 553 dyneins \pm Pac1 from 3 independent replicates; D2868K, 329, 664, 134 dyneins \pm Pac1 from 2, 3, and 2 independent replicates, respectively; HL3, 595 and 416 dyneins \pm Pac1 from 2 independent replicates; all from left to right; diamonds represent mean values obtained from each independent replicate experiment). Statistical significance was determined using a two-tailed Mann-Whitney test. (D) The fraction of dynein molecules migrating with Pac1 is plotted for the indicated dynein. Error bars depict standard error of proportion (n = 665, 398, and 376 dynein molecules from two independent experiments, left to right; diamonds represent mean values obtained from each independent replicate experiment).

that *dyn1Δ*¹⁰⁹, and since both K1475E and D2868K bypass the need of Pac1 to reach the cortex, it is likely that dynein may still diffusively bind dynactin in the cytoplasm in a wild type cell.

If Pac1 did indeed bind to dynein in an uninhibited state in solution, it would have a higher affinity for mutant complexes lacking autoinhibition. Consistent with this hypothesis, mutants with compromised autoinhibition (GST, D2868K, and HL3) demonstrated much higher affinity for purified Pac1 in pull down assays than the wild-type motor (Fig. 23C). Our other biochemical readout of loss of autoinhibition was an increase in run-length in single molecule assays; if Pac1-bound dynein really was unable to switch to an autoinhibited state, wild-type dynein would experience dramatic run-length increases in our single-molecule assays. However, mutants like D2868K would have minimal increases in run-length, but would demonstrate a higher frequency of comigration with Pac1 than wild-type complexes, consistent with being a more “open” complex. Finally, HL3 mutants would demonstrate even smaller, or no increases in run-length, and GST-dynein would have no change in run-length, as this truncated motor does not form the autoinhibited conformation and is unaffected by Phi-particle mutations (Fig. 20C). We sought to address these questions by performing two-color imaging of fluorescently labeled Pac1 and dynein, which have been characterized extensively *in vitro*. However, performing this experiment under our normal assay conditions was not possible, as Pac1 bound to microtubules robustly even at nanomolar concentrations. This was also strange as Pac1 is not a MAP *in vivo*, and LIS1 has not been described as a MAP *in vitro* at similarly low ionic strength buffers^{94,95,204}. As it was not possible to perform two-color imaging using previously published protocols for analyzing Pac1-

Figure 25

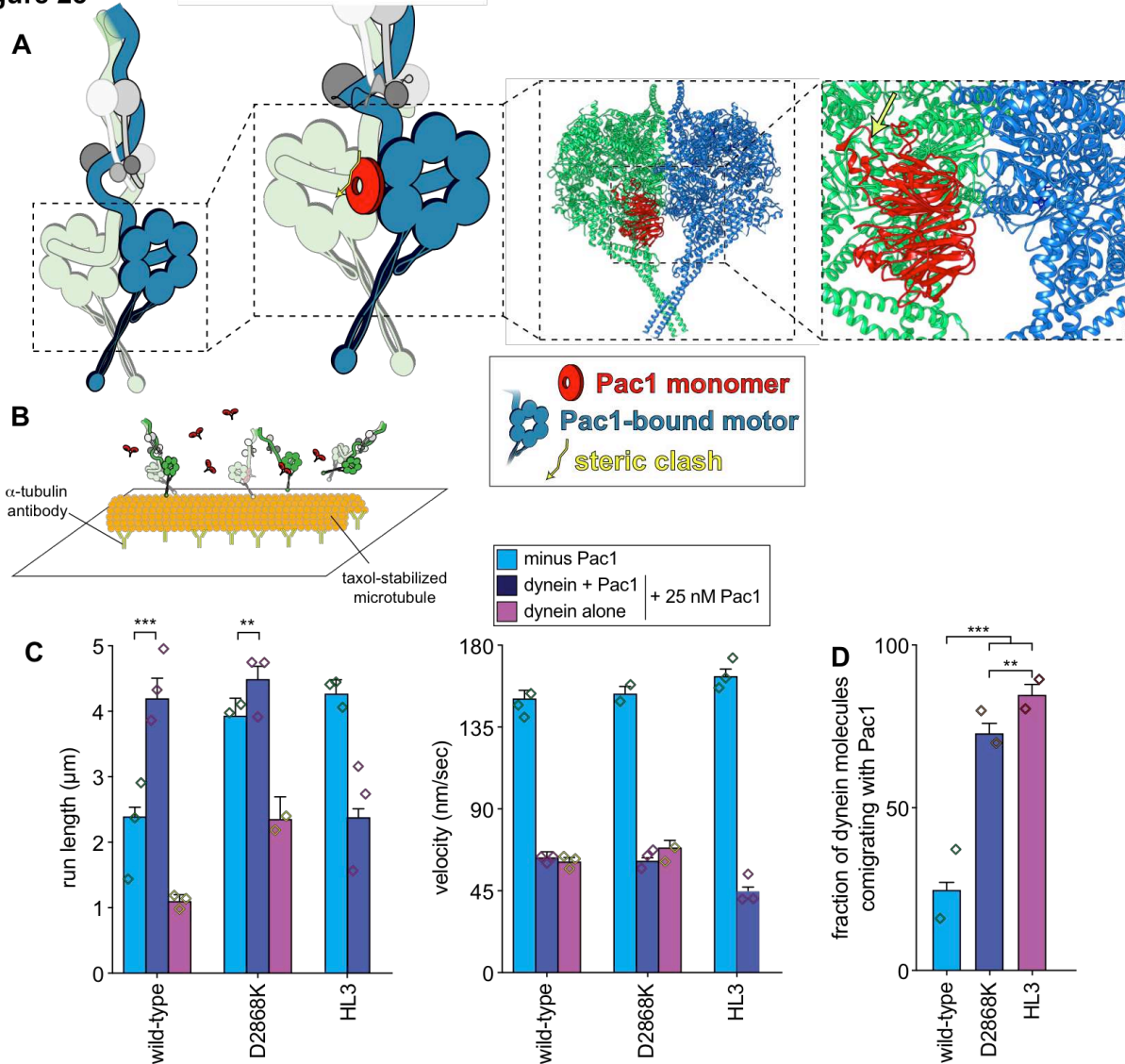


Figure 25. Pac1 promotes release of the autoinhibited conformation of dynein. (A) Cartoon and structural model depicting steric clash between phi particle dynein and Pac1. Structural model was generated by aligning the Pac1-bound dynein monomer structure (pdb 5VH928) into one of the heavy chains in the phi particle structure (pdb 5NVU1). Note the steric clash (depicted with jagged yellow arrow) between the Pac1-bound dynein heavy chain (in blue) with the second heavy chain (in green). (B) Cartoon depicting experimental setup for dynein-Pac1 single molecule assay. (C) Plots depicting motility parameters (left, mean run length values, from fitting of raw data to one-phase decay; right, velocity; error bars indicate standard error) of indicated dyneins moving in the absence (i.e., those not pre-incubated with Pac1, green) or presence of 25 nM Pac1 (dimer concentration). For those experiments in which Pac1 and dynein were pre-incubated, we separately scored those dyneins comigrating with Pac1 (magenta), or migrating without Pac1 (yellow; n values: wild-type, 437, 353, 553 dyneins \pm Pac1 from 3 independent replicates; D2868K, 329, 664, 134 dyneins \pm Pac1 from 2, 3, and 2 independent replicates, respectively; HL3, 595 and 416 dyneins \pm Pac1 from 2 independent replicates; all from left to right; diamonds represent mean values obtained from each independent replicate experiment). Statistical significance was determined using a two-tailed Mann-Whitney test. (D) The fraction of dynein molecules migrating with Pac1 is plotted for the indicated dynein. Error bars depict standard error of proportion (n = 665, 398, and 376 dynein molecules from two independent experiments, left to right; diamonds represent mean values obtained from each independent replicate experiment).

dynein *in vitro*, we increased the ionic strength of our buffer from 50mM to 150mM

K⁺acetate, which we reasoned should mitigate any non-specific interactions of Pac1

with the microtubule. These buffer conditions have been previously been used previously to maintain Pac1-dynein interaction during gel filtration and subsequent negative stain TEM imaging¹¹³, so they should reliably maintain the dynein-Pac1 interaction. This treatment was successful in removing the majority of Pac1 from microtubules.

Performing our TIRF assay with our new conditions revealed that Pac1 robustly increased the run-length of wild-type dynein, and led to a small but significant increase for the D2868K mutant and no increase for the HL3 mutant, consistent with our model that Pac1 prevents dynein from switching to the autoinhibited state (Fig. 26C). The run length of wild type bound Pac1, Pac1 bound D2868K, and the HL3 mutant were all approximately the same length, suggesting that these complexes represent a similarly open, uninhibited dynein. These increases in run length were not due to Pac1 increasing aggregation or crosslinking dynein dimers (Fig. 26C), which similarly does not occur for dynein-LIS²⁰⁴. Furthermore, Pac1 and GST-dynein did not demonstrate a run length increase over the GST-dynein alone, consistent with our previous data (Fig. 20C, Fig. 29C). One of the most important outcomes of these experiments was that dynein velocity was reduced in the presence of Pac1 in the experiment, but this reduction in velocity was nonspecific to stably bound Pac1-dynein molecules (Fig. 26C). That is, adding Pac1 to our assay, even with low levels of microtubule binding, decreases the speed of dynein independent of whether they are stably interacting. Therefore, the Pac1 velocity reduction effect is not specific to stably interacting Pac1-dynein, despite previous reports observing this effect without visualizing Pac1. Finally, the frequency of comigrating dynein-Pac1 complexes increased as the loss of

autoinhibition increased, with all the D2868K and HL3 (Fig. 25D) mutants and GST-dynein (data not shown) demonstrating a higher frequency of comigration than wild type. Just as in the Pac1 pulldown (Fig. 23C), the HL3 mutant demonstrated the highest affinity for Pac1.

Figure 26

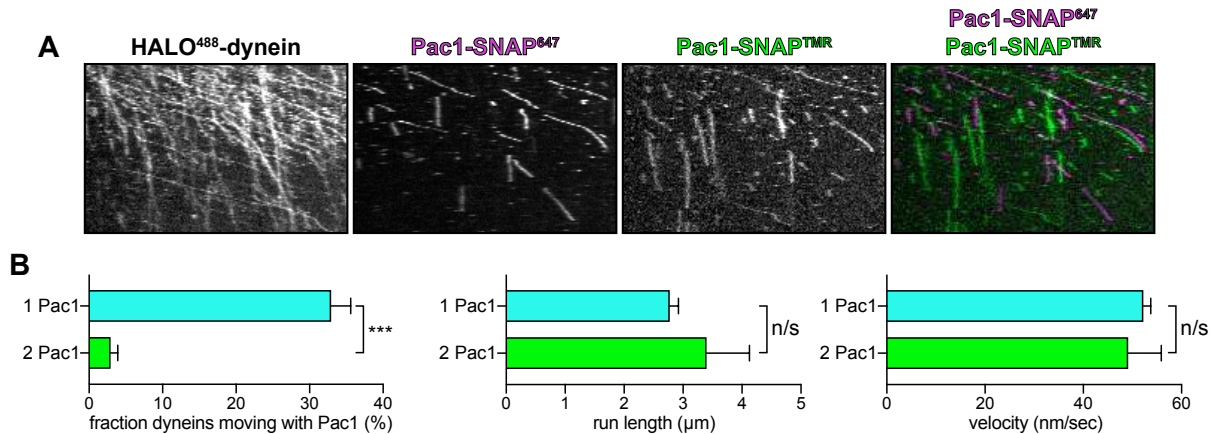


Figure 26. Dynein predominantly binds a single Pac1 stably during processive motility. (A) An example overcrowded kymograph (not used for quantification) to demonstrate that a single Pac1-dynein complex is the predominant species and quantitation (B) of single molecule assay of dynein-Pac1/2xPac1 complex motility (in motility buffer supplemented with 120 mM potassium acetate; $n = 870$ dynein molecules from 3 independent experiments; mean values with standard error are shown, along all datapoints for middle and right plots; similar results were obtained from each replicate). Statistical significance was determined by calculating Z scores (left; ***, $p < 0.0001$), using a two-tailed Mann-Whitney test (middle; $p = 0.6068$), or with a two-tailed Welch's t test (right; $p = 0.6581$). Note the estimated fraction of dynein-2xPac1 complexes (5.7%; see main text) is less than what would be expected if there was no cooperativity for Pac1-dynein binding (i.e., the product of the probabilities of two single, independent binding events, 10.8%).

We next asked if one or two Pac1 molecules might bind dynein during a processive run, since both motor heads of the dimer presumably have the same ability to bind to Pac1. We repeated our single molecule assay this time by incubating Alexafluor488-dynein with Pac1-TMR and Pac1-Alexafluor646 (Fig. 26A, B). Three-color imaging revealed that the majority populations of moving molecules (>95%) were single molecules of Pac1 bound to dynein, which is in agreement with previous studies using human dynein and LIS1¹⁰⁵. Approximating the proportion of dyneins with two

Pac1 bound revealed that the frequency of binding of two dynein was lower than would be expected if binding affinity were sequential and linear. Therefore, we determined that binding of Pac1 to dynein is not cooperative, and may indeed be anti-cooperative, with the first Pac1 molecule preventing the binding of a second by steric constraint. The results of our single molecule experiments confirm the hypothesis from our live cell imaging. Together, these data confirm our hypothesis that Pac1 stabilizes the open conformation, and prevents the formation of autoinhibited state. They also provide further support for the hypothesis that the switch to an autoinhibited dynein complex leads to dissociation from microtubules in single molecule motility experiments, as the wild type-Pac1, D2868K mutant and HL3 mutant all demonstrated greater run lengths in high ionic strength buffer than wild type alone.

4.3.2. Pac1/LIS1 reduces dynein speed non-specifically by simultaneous interactions with dynein and the microtubule lattice.

The binding of Pac1 to microtubules in TIRF motility assays was first identified by Lindsay Lammers in the Markus lab, and this finding was very surprising. Pac1 is not a MAP *in vivo*, and performing *in vitro* single molecule experiments on motor proteins in the presence of MAPs is known to affect the behaviors of these motor proteins^{57,163}. Many previous studies have concluded that Pac1 is an inhibitor of yeast dynein, whose supposed mechanism of action was uncoupling the normal mechanochemical cycle of the dynein linker power stroke and concomitant coiled-coil stalk and MTBD remodeling¹⁰⁵⁻¹⁰⁷. However, the data from these studies never reported that Pac1 binds to microtubules in the assay buffers used for these previous experiments. The velocity reduction of dynein by Pac1 in our *in vitro* assays was independent of stable dynein-

Pac1 interaction (Fig. 25), and most likely appears to be an effect of nonspecific tripartite interactions between dynein, Pac1, and the microtubule lattice. Previous work from our laboratory with yeast dynein effector She1 demonstrated this protein is able to slow dynein movement and increase backwards stepping through simultaneous interactions between the MTBD of dynein and the microtubule lattice. Pac1 binds dynein near AAA3/AAA4 and its coiled-coil stalk, and previous studies have shown there is a great deal of flexibility about the stalk¹⁰³. We hypothesized that this would allow dynein-Pac1 to interact with the C-terminal tails of tubulin during movement; alternatively, Pac1 decorated microtubules would then be able to transiently bind dynein, exerting drag on the motor through electrostatic interactions (Fig. 27A-B).

We therefore wished to determine the nature of the Pac1-microtubule interaction. The budding yeast dynein regulator She1 binds to microtubules through their unstructured C-terminal domains¹⁶³ and effects dynein motility. Similarly, we found that Pac1 binding to microtubules was lost after subtilisin digestion of the tubulin C-terminal tail (Fig. 28C). As most MAP interactions are sensitive to ionic strength of buffers, and since the ionic strength of a cell is likely higher than the ~50 mM effective ionic strength of our assay buffer, we performed these experiments in high-salt buffer conditions (Fig. 28A, 150mM potassium acetate HEPES buffer, 161.5mM ionic strength equivalent, see Methods). While Pac1 has been previously shown to slow dynein motility, presumably by decoupling the mechanochemical cycle from microtubule binding affinity¹⁰⁵⁻¹⁰⁷, analysis of comigrating dynein-Pac1 complexes in these conditions substantially reduced the degree of velocity reduction by Pac1, suggesting that the effects of Pac1 reduction of dynein velocity and Pac1-microtubule binding were related.

Figure 27

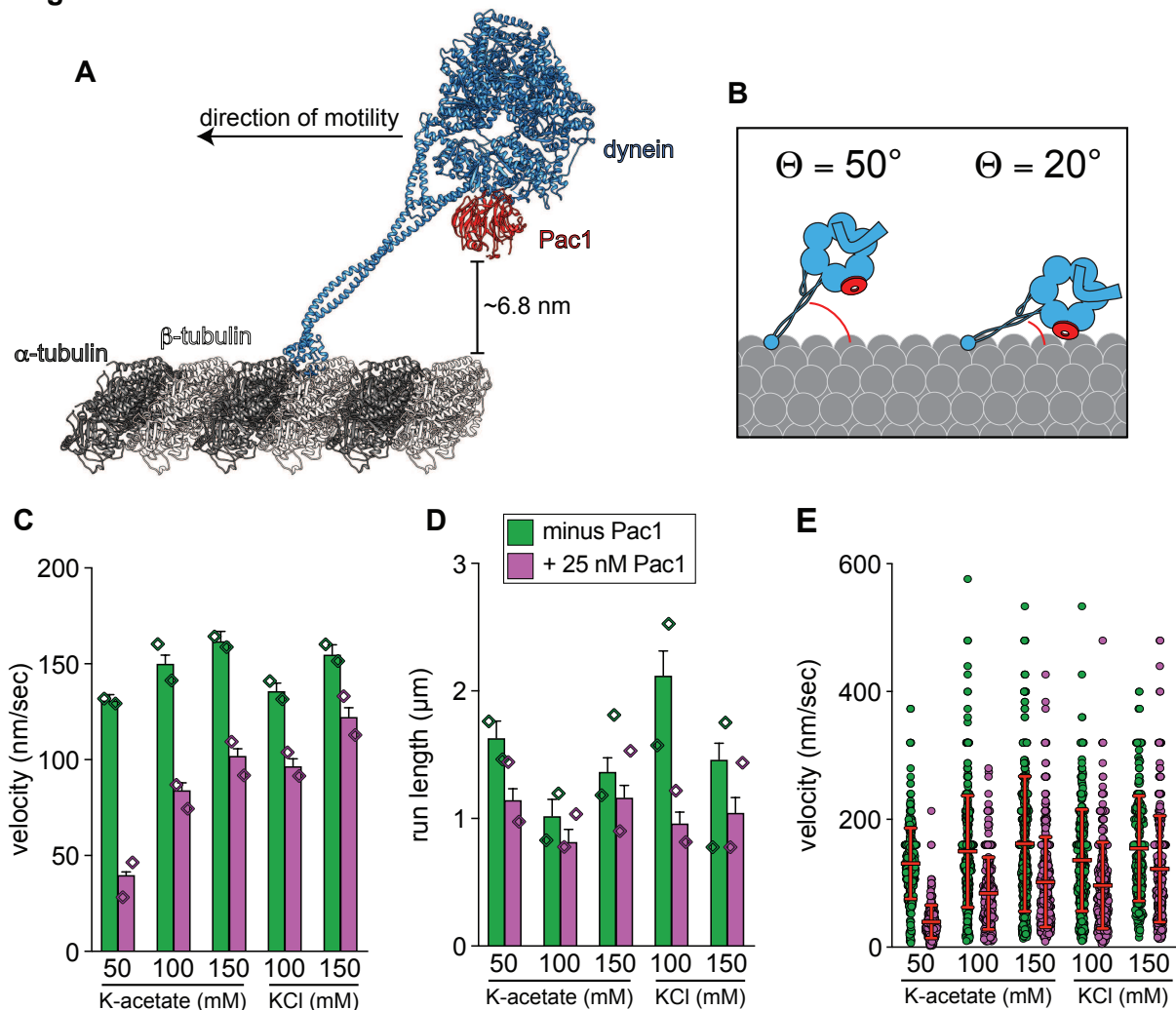


Figure 27. Model for Pac1-dynein interactions with microtubules. (A and B) Structural and cartoon model of a microtubule and Pac1-bound dynein monomer (generated with pdb IDs 4RH737, 3J1T87, 5VH928, and 3J6G88). Note the close proximity of Pac1 to the microtubule surface, the latter of which is lacking the unstructured E-hooks. (D) Cryo-EM data reveals the dynein-microtubule angle varies due to a hinge point within the MTBD, and can be much steeper than that shown in panel A (REF 54), ($Q \geq 15\text{-}20^\circ$, with average = 55°). Cartoons depict range of angles sampled by dynein on microtubules, and thus the distances between Pac1 and the microtubule. (E - G) Non-normalized plots of mean values (E and F) and all data points (G; see Figure 28C) showing the relationship between Pac1-mediated dynein velocity reduction and Pac1-microtubule binding (for panels B left, E, and F, diamonds represent mean values obtained from each independent replicate experiment; for panel G, mean values and standard deviations are depicted with red lines). In all conditions a normal distribution persists, suggesting velocity reduction occurs uniformly across populations of motors.

To determine if microtubule binding activity of Pac1 was the reason for nonspecific reduction of dynein velocity in the presence of Pac1, I performed single molecule assay salt titration experiments using the motile GST-dynein fragment, which has been extensively used to characterize dynein-Pac1 interaction in the past. Increasing salt content in our assay buffers, either using potassium acetate or potassium chloride, led to a proportional decrease in Pac1 binding to microtubules (Figs. 28A-B,H, and 29A-B). This decreased binding to microtubules led to decreased magnitude of velocity reduction in each assay condition, with 150mM KCl buffers (ionic strength slightly higher than cytoplasmic estimate) having a minimal effect on velocity reduction (Figs. 27C, 29C). Plotting the relationship between microtubule binding and relative velocity reduction reveals a linear correlation between the two (Fig. 27D), indicating that nonspecific interactions between Pac1 and tubulin were indeed the cause of dynein velocity reduction. As the degree of velocity reduction is related entirely to the degree of Pac1-microtubule binding, we reasoned that the previous studies using Pac1 were likely identifying this contaminating artifact rather than a biologically relevant activity of dynein. Treatment of microtubules with subtilisin to remove tubulin C-terminal domains also prevented dynein binding to microtubules, and repeating the motility experiment in 100mM KCl with subtilisin microtubules led to a combinatorial increase in motility between the two conditions (data not shown). Finally, we repeated the single molecule assays in normal salt conditions (50mM potassium acetate) with the addition of dilute (<0.1 mg/ml) cytosolic extracts (Fig. 28D-G). This condition was the most effective at removing Pac1 from the tubulin lattice and led to the smallest decrease in dynein velocity reduction, indicating that in the context of the cell, Pac1-microtubule

Figure 28

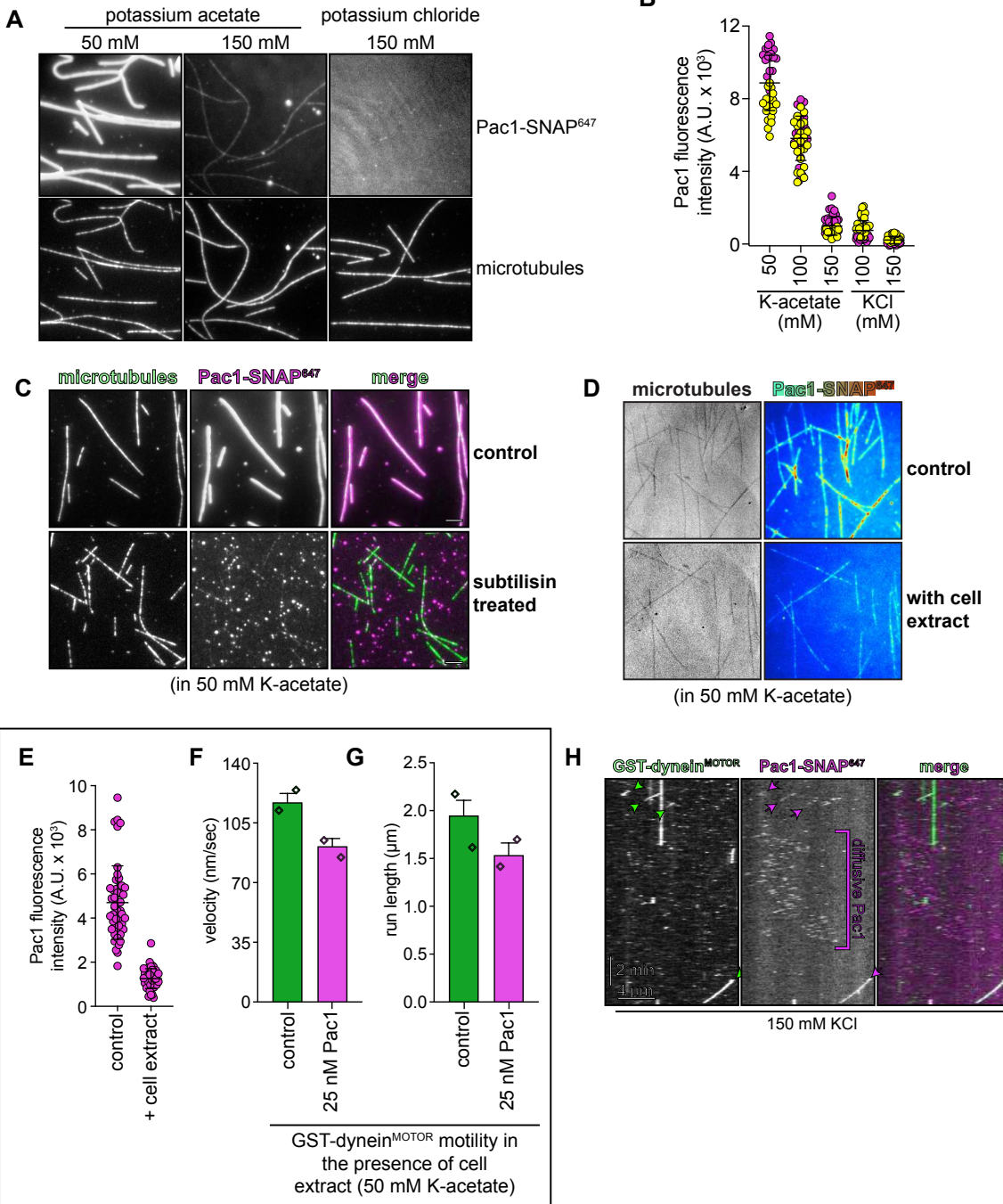


Figure 28. Pac1 binds to microtubule E-Hooks via electrostatic interactions. (A) Representative images and intensity scatter plots (B; bars depict mean \pm standard deviation) of microtubule-bound Pac1 in different buffers. Pac1-SNAP647 diluted in motility buffer (50 nM dimer concentration) with indicated salts was introduced into a chambers with coverglass-adhered microtubules, and images were acquired (yellow and magenta circles represent data acquired from each independent experiments; n = 38, 49, 41, 49, and 45 microtubules that span 911 μ m, 1074 μ m, 1077 μ m, 906 μ m, 1017 μ m in length for each condition, left to right). (C) Pac1-microtubule binding is reduced after proteolytic digestion of the unstructured tubulin carboxy-terminal tails (E-Hooks, see Methods; similar results were obtained from 2 independent experiments). (D - G) Addition of cell extracts reduces Pac1-microtubule binding, and attenuates Pac1-mediated dynein velocity reduction. Representative fluorescence images of Pac1-SNAP647 on microtubules (D; Pac1-SNAP647 shown as a heat map) and scatter plots depicting intensity values (E; bars depict mean \pm standard deviation; n= 48 and 47 microtubules that span 890 μ m and 841 μ m in length for each condition, left to right; similar results were obtained from 2 independent experiments). (F and G) Plots depicting the motility properties for GST-dynein in the absence and presence of 25 nM Pac1 (dimer concentration) in low ionic strength buffer (50 mM potassium acetate) in the presence of cell extracts (0.96 mg/ml final; 275 and 258 motors, left to right, from 2 independent experiments were quantitated). Note the small Pac1-mediated GST-dynein velocity reduction in the presence of cell extracts (22.1%, compared to 69.5% in the absence of extracts). (H) Representative kymograph of GST-dynein comigrating with Pac1 demonstrates the proteins stably interact even in buffers with 150 mM KCl (see Fig. 6D and S7E – G for quantitation and statistics). Note the diffusive behavior of Pac1 on microtubules. Scale bars in panels A, C and D, 4 μ m.

binding is prevented, likely due to the plethora of other microtubule associated proteins.

This is consistent with previous data which showed Pac1 does not bind microtubules *in vivo* in the absence of Bik1, even when it is overexpressed^{108,231}.

4. Discussion

4.4.1. Pac1/LIS1 prevents dynein autoinhibition by binding the open conformation which coordinates dynein cellular localization and activity

The results of our single molecule experiments indicate that Pac1 can directly promote dynein activity by stabilizing open complexes, through sterically preventing formation of the autoinhibited complex. These data, along with our cell biological experiments, demonstrate that the a major role for Pac1 in the cell is to relieve dynein autoinhibition. With this new information, we can improve on our previous model for dynein cortical targeting (Fig. 30). In our revised model, dynein molecules which are switching between open and closed states in the cytoplasm bind to Pac1, which maintains dynein in an open conformation. While switching of dynein to an open state

Figure 29

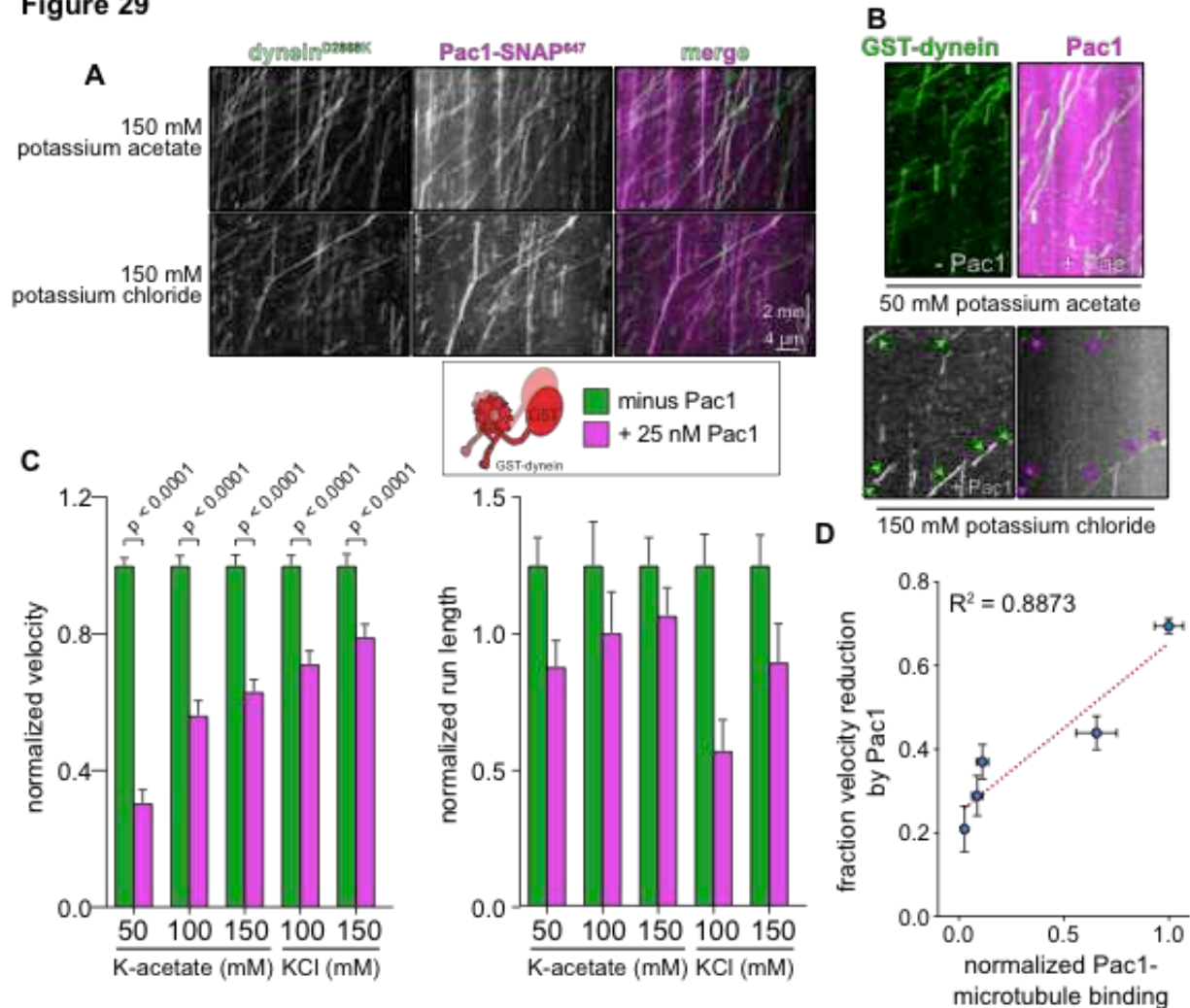


Figure 29. Pac1-microtubule binding leads to observed Pac1-mediated dynein velocity reduction. (A) Representative kymographs depicting comigrating dyneinD2868K-Pac1 complexes in motility buffers with increased ionic strength (from 3 and 2 independent replicates, top to bottom). Note that Pac1 and dynein still interact robustly in these conditions, as apparent from the high degree of persistent colocalization. (B) Representative kymographs depicting different motility characteristics of GST-dynein (used extensively in previous Pac1 studies in the presence of Pac1 when the latter is either extensively bound to the microtubule in 50mM salt, or to a much less extent in 150mM salt). (C) Mean normalized motility parameters of GST-dynein in the absence (green) or presence (magenta) of 25 nM Pac1 (dimer concentration; $n = 348, 268, 396, 226, 447, 359, 385, 315, 251, 320$ motors, from two independent experiments each; left to right). Error bars indicate standard error. (D) Relative degree of Pac1-microtubule binding (mean values normalized to 1; see Fig. S6B and E for scatter plot of intensity values, and n values for each) versus mean relative velocity of GST-dynein in the presence of Pac1 (mean GST-dynein velocity in the absence of Pac1 equals 1; see panel D, and Figs. 28 and 29 for relative and absolute velocity values, and n values). Blue and yellow points (error bars represent standard error) are from increasing ionic strength buffer experiment (see panel D) and the cell extract experiment (see Fig. 28), respectively. The blue points were fit to a linear regression with R^2 value shown.

does not appear to require other factors, the kinetics of this switching may be the target for mitotically regulated PTMs²⁰¹, or other proteins such as Ndl1^{202,205}. Next, Pac1-dynein bind to Bim1-Bik1 at microtubule plus ends, and dynein may then bind dynactin. Dynein-dynactin is then offloaded to the cell cortex for activation by Num1, and Pac1 is displaced from this complex, for reasons which are still areas of active research. However, Pac1 is not observed localized to the cortex during dynein-mediated spindle positioning or nuclear migration in budding yeast^{99,109}.

Previous data suggested that Pac1 was an inhibitor of dynein, whose function was to maintain dynein at microtubule plus ends through its inhibition¹⁰⁵⁻¹⁰⁷. While this result was borne out in several studies with Pac1, the results of this work indicates that Pac1 is not an inhibitor of dynein motility; rather, Pac1 binding to dynein allows it to be maintained in an open conformation which promotes interaction with other MAPS. Our results show that at least one function of the plus end targeting complex is to maintain dynein in the open conformation through Bim1-Bik1-Pac1-dynein complex interaction. While it is unclear why these active dynein complexes do not move to the minus-ends of microtubules, it is possible the geometry of this complex restricts dynein-microtubule interaction. Open dynein at the plus end of a microtubule is likely better positioned for interaction with the dynactin complex, and maintaining dynein on a platform of microtubules would facilitate their interaction. One important role of LIS1 in mammals which was discovered at the time of this work is that LIS1 promotes the assembly of two dyneins per dynactin by preventing autoinhibition, an identical mechanism¹⁶⁷⁻¹⁶⁸ to what we have proposed for yeast Pac1. This complex of dynein has never been identified in simpler eukaryotes; however, results from our mutant screen suggested that dynein-

Figure 30

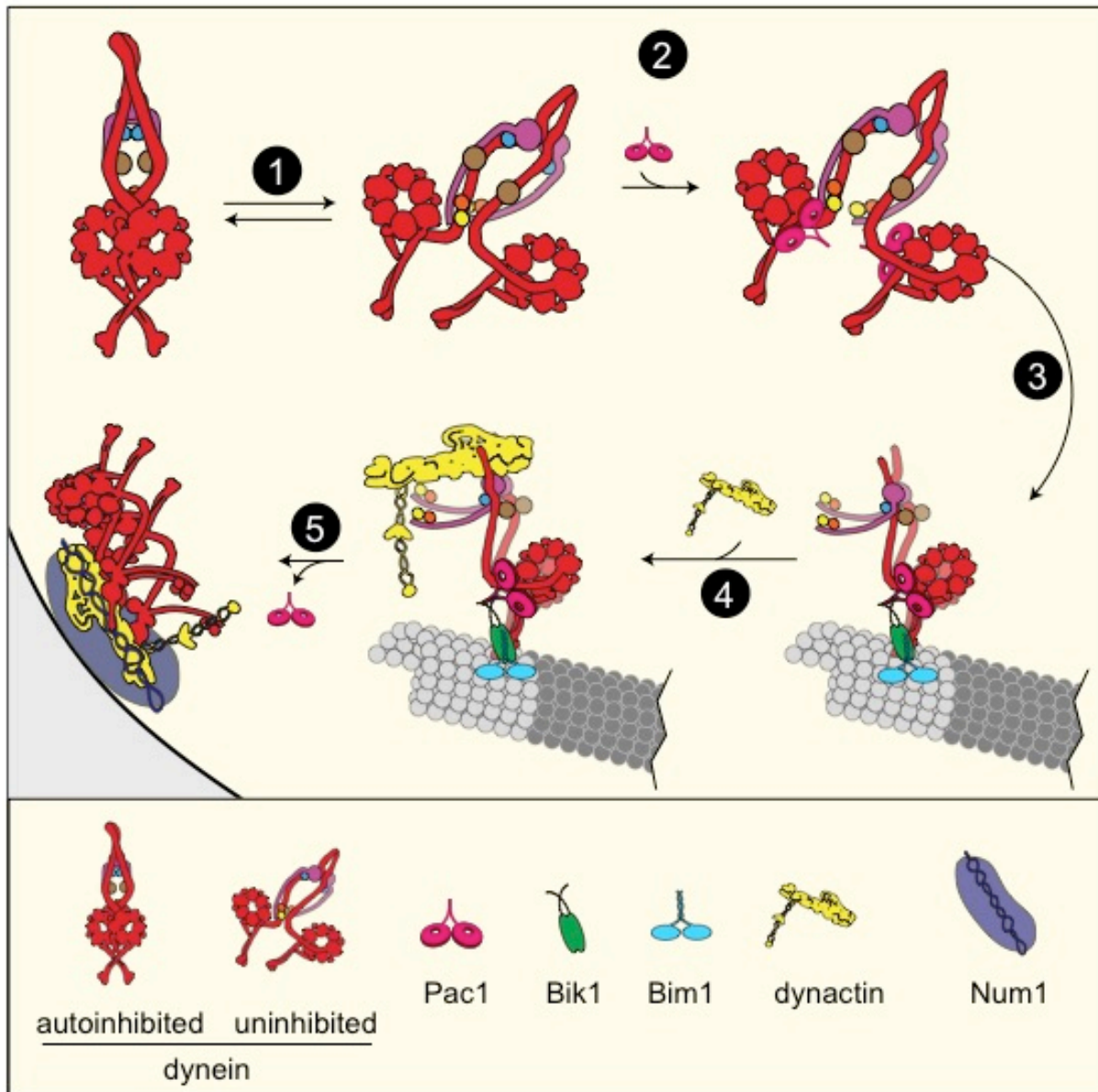


Figure 30. Model for dynein and Pac1 activity in cells. (1) Dynein stochastically switches between open and closed states in the cytoplasm, and the open conformation is stabilized by Pac1 binding (2); dynein-Pac1 associates with plus ends via direct interactions with Bik1 (3), which may rely partly on Bim1. (4) Plus end dynein-Pac1 associates with dynactin, which is then (5) offloaded to cortical Num1. Given the lack of apparent Pac1 cortical foci, Pac1 likely dissociates either concomitant with, or subsequent to dynein-dynactin offloading.

dynactin form similar higher order assemblies (such as the mammalian 2 dynein:1 dynactin complexes) in yeast. If Pac1 performs such a role in yeast, it is possible that

assembly of these complexes is most effectively done along microtubules, due to the concentration of these factors along astral microtubules during mitosis.

One role of accumulation of dynein at plus ends in yeast could be to accumulate a requisite number of dynein-dynactin molecules before offloading. Directed transport to Num1, rather than simple diffusive binding to cortical receptors, as has been demonstrated to occur in mammalian cells¹⁶⁴. This mechanism would be more efficient in the yeast cell, which has very few astral microtubules^{180,194}. Accumulating many motors may be necessary to generate optimally productive and processive motor ensembles at the cell cortex. Data from our mutant study¹⁹³ indicate that a few dyneins may be sufficient to position the mitotic spindle, but that larger ensembles of dynein are necessary for maximal nuclear translocation and activity. Limiting dynein-dynactin interaction to the plus-ends of microtubules ideally positions these proteins for interaction with each other before delivery to their cortical receptor. This delivery also optimally positions the DDN complex on its cargo, at the far plus end. While uninhibited mutant dyneins K1475E and D2868K may bind dynactin diffusively in the cytoplasm and may be offloaded to an even greater degree than wild-type dynein (Fig. 22A, 23D), these cortical populations are much less active than those offloaded through the canonical cortical targeting machinery. This mechanism of coupling of offloading and nuclear positioning is likely more efficient than a search-and-capture model for dynein-astral microtubule interaction. This is an important consideration for yeast spindle positioning, where only 2-4 astral microtubule bundles emanate from spindle pole bodies to interact with cortical dynein, instead of the larger population of asters present at mammalian spindle poles²⁰⁶. Future work may be focused on modeling mitotic timing

and how search-and-capture models compare to plus end loading followed by cortical targeting.

Despite these new insights several outstanding questions remain in understanding the transition from plus end dynein-dynactin to cortical dynein-dynactin-Num1 complexes. Firstly, why dynein is inactive at the plus end, despite it presumably being in an open conformation, is unclear. The most likely explanation is the nature of its plus end interaction does not position the MTBD for interaction with the lattice. Dynein-dynactin-EB3 and dynein-Lis1-CLIP-170 are noted for plus end tracking dynein in mammalian systems^{95,96}, and are only activated for motility upon coming in contact with an adaptor protein. Secondly, despite the persistent association of Pac1 with dynein and LIS1 with motile DDB complexes in single molecule experiments, Pac1 is not present at the cell cortex. However, it is currently unknown if this is because of competing interactions between dynein, dynactin-Num1 and Pac1, or because there is an allosteric change in cortical dynein which displaces Pac1 from the complex. Although Pac1 and LIS1 may not directly affect dynein mechanochemistry, they can affect dynein motility by promoting the assembly of dynein-dynactin-adaptor complexes and maintain open dynein along microtubules.

4.4.2. Microtubule binding activity of Pac1 is primarily responsible for inhibitor phenotypes

Our results directly challenge the model proposed by the results of previous experiments using Pac1 and yeast dynein, that Pac1 is an inhibitor of motility¹⁰⁵⁻¹⁰⁸ which acted like a “clutch,” maintaining dynein along a microtubule while having a fast ATPase rate. Based on our own work, we demonstrate these interpretations were

mostly a product of a non-specific interaction between dynein, Pac1, and microtubule lattice, likely the unstructured C-terminal domains. Similar experiments using human dynein and LIS1 have not observed that LIS1 reduced dynein velocity; rather, LIS1 has no effect on velocity, or indeed, increases dynein velocity^{95,111}. This disparity can be explained by LIS1 not binding microtubules in these assay conditions. As we were the first laboratory to publish data on Pac1-microtubule binding, we were the first to note the linear dependence of velocity reduction with microtubule binding. The degree of microtubule binding of Pac1 was the most important factor in modulating dynein velocity, both by titrating Pac1 binding with salt and by the addition of cellular extracts to prevent Pac1-microtubule binding. These results indicate that previous data describing Pac1 as an inhibitor were mainly, if not wholly, non-physiological artifacts of Pac1-microtubule binding.

The biologically relevant effect of Pac1 on dynein is instead the stabilization of the open complex by sterically preventing interaction between the dynein motor heads. It is also possible that Pac1/LIS1 has a role in modulating dynein activity through changing the conformation of the motor domain. If the only role of Pac1 were to block Phi particle formation, our data indicate this could be achieved by blocking binding of any of the stabilizing interfaces (stalk-stalk, for instance). Instead the main binding site of Pac1 and LIS1 are AAA3/AAA4 and the stalk domain, which have been shown to affect mechanochemistry of the yeast motor^{40,52}. However, our single molecule assays demonstrate unambiguously that Pac1-bound dynein may still be a very fast and highly processive *in vitro*, which is inconsistent with a model by which Pac1 slows dynein by sterically blocking the linker swing. If there is an effect of Pac1/LIS1 on dynein motor

activity, such as increasing association with microtubules or increasing force generation, and if these activities are maintained in yeast, Pac1 would be expected to localize to the cell cortex during nuclear transport. Further, it is possible that the conformational change induced by Pac1 is simply a further level of regulation of autoinhibition which promotes localization of the proteins through allosteric changes in the motor. The data presented here indicate that the primary activity of Pac1/LIS1 is to promote an open dynein conformation, by opportunistically binding the open state in solution. This regulation of dynein helps reconcile the previous discrepancies between yeast Pac1 acting as an inhibitor whereas human LIS1 was thought to be an activator.

4. CONCLUSIONS

This research has revealed that the effector Pac1/LIS1, promoted dynein activity by stabilizing the active motor and preventing dynein autoinhibition. This result has been corroborated by recent work in both mammalian dynein and *Aspergillus nidulans*¹⁶⁵⁻¹⁶⁸, indicating that indeed dynein autoinhibition, and its regulation by Pac1/LIS1/*nudF*, is an evolutionarily conserved mechanism. The function of Pac1 in all these systems is to promote dynein activity by acting as a “molecular wedge” and preventing autoinhibition. In support of this model, the effects of Pac1/LIS1 on dynein mutants which are not autoinhibited (dynein^{mt}) is minimal¹⁶⁷, and these two mechanisms of activating dynein are nearly entirely redundant with respect to each. Experiments presented here reveal that the inhibitory phenotypes previously identified were due partly to a contaminating artifact of Pac1-microtubule binding, and that Pac1 does indeed promote dynein motility *in vitro*. In summary, dynein regulation by Pac1 is highly similar to LIS1-dynein

interactions in mammals, and they represent a conserved mechanism to sequester, and subsequently offload, active dynein-dynactin complexes to sites of cargo adaptors.

Chapter 5. Pac1/LIS1: opening the door for dynein motility

5.1. Introduction

Dynein regulation across species shares many similar characteristics. The heavy chain is the core catalytic component, composed of a single polypeptide (in most species) which is a highly homologous protein between organisms, even between the humble yeast and humans. The multiple accessory chains facilitate folding, and may act as chaperones to correctly assemble the holoenzyme complex; additionally, they may be necessary for normal motility, and many have cellular functions outside of dynein in higher eukaryotes³⁶⁻³⁸. Dynactin is essential for tethering dynein to cargo and activating motility of the motor at vesicular cargos, and for dynein-mediated mitotic spindle positioning^{58,64,74,75}. While cargo adaptors may vary between species, all adaptor proteins so far identified mediate dynein-dynactin interaction through a coiled-coil domain^{88,98,131}. A fourth key regulator of dynein, Pac1/LIS1/nudF, is a WD40 domain protein^{141,159,218}, which along with other MAPs facilitated recruitment of dynein to microtubules and vesicular cargos^{99,110,113}. These regulators are conserved across cytoplasmic dyneins, from yeast to humans, to filamentous fungus, to slime molds.

However, the Pac1/LIS1/nudF proteins appeared to have conflicting roles in regulating dynein *in vitro*, having the capability to act as either an activator or an inhibitor of dynein motility. In bulk solution ATPase assays, LIS1 has been shown to increase dynein ATPase rate¹⁰⁸. In stark contrast, when used in ensemble gliding assays and optical trap experiments using only purified dynein, LIS1 induces dynein stalling along microtubules^{108,175}. Paradoxically, LIS1 increases the speed of dynein-

dynactin-adaptor complexes in single molecule assays⁹⁶. When added to cell extracts¹¹⁰, LIS1 increases dynein-dynactin association. The yeast LIS1 homologue, Pac1, has been demonstrated to inhibit single molecule motility of dynein^{84,101,105-107}.

Such experimental differences could abound for numerous reasons. In these diverse systems, there are different contexts of dynein activity, differences in need of force generation, as well as the differences between dynein-LIS1 alone and LIS1 with dynein-dynactin-adaptor complexes, and LIS1 *in vitro* compared to a cellular context. It could also be that the differences in Pac1 and LIS1 effects on dynein are due to the needs of different organisms for the dynein protein. Despite the evolutionary similarity, LIS1 is a divergent protein in different species. LIS1 and the *Aspergillus nidulans* homolog, nudF, share 43% sequence identity. However, Pac1 and LIS1 share only 27% sequence identity, which could account for the discrepancies between proteins (Figure 33). While the role of dynein in mitotic spindle positioning is highly conserved between yeast and mammals^{24,132} it is possible that the simplicity of the budding yeast pathway may not require the diverse LIS1 activities found in higher eukaryotes. A final possibility that the experimental differences are due to differences in the compositions of distinct LIS1 populations, either through differences in post-translational modifications, or due to differences in the stoichiometries of either LIS1 or regulators of LIS1 activity such as Ndel1^{110,205} in disparate organisms. While these various hypotheses may be possible, we propose in this chapter that the primary cellular function of LIS1 (including nudF in *Aspergillus nidulans* and Pac1 in *S. cerevisiae*) is conserved across species. The data presented in this thesis present a model for Pac1 regulation for dynein whereby Pac1 is an opportunistic binder of “open” cytoplasmic dynein. This promotes dynein activity by

sterically blocking the formation of the autoinhibited conformation, thereby preventing dynein autoinhibition while Pac1 is bound. These results have been supported by three similar findings, in both filamentous fungus and mammals, which identify the role of nudF and LIS1 in relieving dynein autoinhibition. These findings present a unifying mechanism of LIS1 regulation of dynein, which sheds new insight on previous studies, and further delineates the molecular basis for dynein cortical targeting and activation across diverse eukaryotes.

Many previous lines of experimentation on LIS1 will be presented here, detailing the role of LIS1 regulation of dynein during the development of the nervous system. Motor proteins are especially important for migration of neurons to form proper cortical layers in mammals, however; nuclear migration in other organisms, particularly filamentous fungus, is a phenomenon which also requires LIS1. The other roles of LIS1 in recruitment of dynein to microtubules and sites of activity, including the cell cortex and kinetochore, will be discussed. Finally, the *in vitro* biochemical evidence of LIS1 effects on dynein will be considered and contrasted with *in vivo* phenotypes observed. This chapter will attempt to synthesize these different lines of data, and present a comprehensive understanding of the Pac1/LIS1 protein, its molecular mechanisms of action, and its conserved role in effecting dynein-mediated transport in cells from yeast to humans.

5.2. LIS1 is a required cytoskeletal protein for neurological function

5.2.1. The dynein-LIS1 pathway is vital during early development in higher eukaryotes

LIS1 was first identified as platelet-activating factor acetylhydrolase IB subunit alpha (PafaH1B1) a non-catalytic subunit of an acetylhydrolase complex which

inactivates platelet-activating factor^{141,159,218}. This gene was associated with a variety of Miller-Dieker lissencephaly cases, and based on sequence comparison was initially proposed to be a subunit important for signal transduction in the neuronal migration pathway^{141,221}. The more common terminology of Lissencephaly-1 (LIS1) is usually used for this protein due to its prevalence in causing the devastating neurological disorder known as classical lissencephaly, or smooth brain^{141,221,222}. This disease is typically thought to be caused by a loss of neuronal migration during early brain development (<13 weeks) in humans, and produce a number of morphological and functional defects into the cerebral cortex. In humans, loss of LIS1 function can occur by exon deletions²²¹⁻²²² or even single point mutations of this protein²²³. The severity of morphological defects ranges from mild loss of cortical gyration to nearly completely smooth brain, and is accompanied by loss of cortical organization, neuronal heterotopia, and enlarged ventricles. Other symptoms commonly associated with lissencephaly are cranio-facial abnormalities, including incorrect development of the jaw, mouth, nose, and forehead. Morphological defects are typically accompanied by mild to severe cognitive impairment in affected individuals. The phenotypes associated with LIS1 are proposed to be due to haploinsufficiency, due to the dose-dependent effect of LIS1 expression on driving different severities of neurological phenotypes^{134,140,141}. This type of neurological disorder may also present in individuals who have gene deletions, or even *de novo* missense point mutations, leading to haploinsufficiency of the Lis1 gene. Similar phenotypes have been documented for loss of the doublecortin gene²²⁰. Recent sequencing studies from subjects with similar disorders leading to loss of cortical

development identified mutations in many different cytoskeletal proteins, such dynein, tubulin, or other essential microtubule-associated proteins (MAPs)¹¹⁹.

The contributions of MAPs in regulating intracellular transport in neurons are readily appreciated in developed organisms. The dynein complex and its effector LIS1 have been shown to be essential for many processes in neurological development, including many dynein functions important for cytoskeletal organization at the single cell level. These activities include the formation of growth cones and axon specification^{116,224} and dendritic specification, transport of preassembled microtubules^{126,241}, neuronal migration^{227,250}, and interkinetic nuclear migration¹³⁴⁻¹³⁷. Kinesin and dynein, as well as LIS1 and its effector Ndel1, are important for specification of axons and for pruning of the axon growth cone during development²²⁸. In axons, antibody blocking of either LIS1 or dynein is sufficient to prevent laminin-induced reorganization at the axon growth cone, and prevents microtubule penetration into the region¹²⁸, preventing cell-cell interactions and slowing rates of growth. In live cell imaging of mice, haploinsufficiency of LIS1 was shown to dampen the movement of the neuronal filopodia and the reorganization of dendritic spines^{229,250}. While it is unclear if this effect is due to microtubule organizing activities of dynein (or other known binding partners such as CLIP-170) or direct regulation of actin networks at dendritic spine, this haploinsufficiency leads to negative consequences in higher order functions in mice²²⁹. In these diverse processes, the presence of LIS1 is required to engage dynein activity with cargos and microtubules, and loss of LIS1 leads to loss of function of dynein-mediated cytoskeletal organization, which in turn causes loss of neuronal maturation

and directed cell movements. Together, these data indicate LIS1 activates dynein motor functions within cells.

One of the most well characterized roles of dynein-mediated transport during early neurological development, the process of interkinetic nuclear migration (INM), is especially important in the development of the brain. This process allows stem cells, which primarily reside at the ventricular basal lamina, to rapidly proliferate to generate the cells which will later form the developed cortex. These stem cells (radiogial precursor cells, RGPs) are maintained in their stem-like state at the basal ventricular zone, until the microtubule-based network of anterograde kinesin molecules move the nuclei to the upper ventricular zone where duplication of the genome occurs^{134,230}. These cells then migrate back to the ventricular surface, where cell division occurs^{134,135,230}. Following cell division, these cells begin to terminally differentiate into neurons, glia, or adult stem cells as they further migrate (and differentiate) along RGPs^{136,138}. During INM, ensembles of dyneins, coupled with the pulling forces of the cortically-anchored actin-myosin cytoskeleton, combine their efforts to generate enough force to move the nucleus from the apical to basal lamina. Live-cell imaging has shown^{135,235} that indeed, large numbers of dynein motors are located at the leading edge of the centrosome which precedes the nucleus. Perturbations to this process, especially minor changes to protein structure introduced by *de novo* point mutations, can be detrimental to proper formation of cortical layers and subsequent brain development, suggesting that maximal dynein activity is needed for proper and timely nuclear migration.

The importance of LIS1's role in the migration of nuclei and other large cargos is readily appreciated during INM in radiogial precursor cells, as dynein and LIS1 accumulate at the centrosome which precedes nuclear migration¹³³. In these cells, blocking LIS1 activity through antibody or siRNA treatment has been shown to reduce rates of cell migration¹³⁴ and ablate mitotic entry, which suggests loss of LIS1 leads to loss of all dynein transport of the nucleus. Similarly, introducing siRNA against LIS1 by *in utero* electroporation in mice leads to near total loss of nuclear movement, a result which is also observed upon siRNA inhibition of dynein heavy chain¹³⁷. Conversely, experiments overexpressing LIS1 in radiogial precursor cells have been shown to directly increase the rates of nuclear migration¹³⁴, demonstrating a direct correlation between LIS1 protein levels and rates of nuclear migration. This overexpression phenotype has severe consequences at the organism level²³⁴; however, all of the phenotypes observed are unlikely to be simply increase in dynein activity, and could be consequences of other roles of the protein.

However, LIS1 is not wholly required for all dynein-mediated nuclear interactions. In cells treated with an N-terminal fragment of LIS1 which blocks mitotic entry still permits overall movement of nuclei, though this movement is substantially slower¹³⁴. This indicates LIS1 is responsible for the initiation of cargo transport, rather than signaling pathways which recruit effectors of this movement. LIS1 or dynein knockdown also lead to different severity of phenotypes, suggesting there may be LIS1-independent roles for dynein in nuclear migration, such as a role in coordinating the actin cytoskeleton²⁰⁷. Alternatively, LIS1 may be needed²⁰⁷ for some, but not all, activation of dynein motility. Finally, LIS1 function in these examples as an initiation factor in dynein-

mediated nuclear transport, rather than assisting dynein in withstanding a pulling force directly. In support of recruitment, rather than mechanochemistry, being a major aspect of LIS1-dynein regulation, studies have demonstrated that directly tethering dynein to the nucleus via a BicD2-KASH domain fusion protein is sufficient to activate apical nuclear transport in the absence of other modes of dynein recruitment¹³³, suggesting dynein is a competent motor for transport once tethered to its nuclear cargo¹³⁸.

Dynein-mediated transport of nuclei is utilized by various other cell types such as in muscle cells, wherein nuclei migrate to form clusters beneath acetylcholine receptors in neuromuscular junctions, a process important in maintaining the position of the receptors²³². Furthermore, cerebellar granule cells and neural precursors from LIS1 heterozygous mice have also been reported to show decreased rates of migration *in vitro*²⁰⁸. Similar experiments assessing neurological development in *Drosophila melanogaster* have demonstrated that LIS1 is necessary for migration and maturation of neurons, and the proliferation of neuroblasts in developing animals²²⁴, all activities which appear common with the mammalian relatives. All these lines of data demonstrate that loss of dynein activity in initiating nuclear transport can be achieved either through directly inhibiting dynein, or through inhibition of its effector LIS1^{137,134}. Taken together these data indicate that a critical cellular concentration of LIS1 must be maintained for effective activation of cytoplasmic dynein force generation. This in turn suggests a critical number of dyneins are needed for normal nuclear migration, or that LIS1 increases dynein's ability to generate force, or perhaps both.

The LIS1 regulatory protein Ndel1 has been shown to increase the efficacy of LIS1 in mediating dynein-dynactin interaction, especially in high load transport^{116,214};

however, NDEL1 is proposed to be effecting this process via recruitment of Lis1 rather than having a complementary role to the Lis1-dynein pathway, as depletion of Ndel1 can be compensated for by overexpression of LIS1^{212,213}. Furthermore, this effect of Ndel1 on increasing formation of dynein-dynactin complexes required simultaneous dynein intermediate chain-binding and LIS-binding of NDEL1, suggesting NDEL1 is increasing the efficacy of LIS1 in this process^{213,214}. The activity of LIS1 during nuclear migration is then likely to increase the active dynein-dynactin pool in the cell by increasing these complexes' association, in order to maintain maximal forces. In addition to increasing complex formation, LIS1 and Ndel1 dependent recruitment of dynein-dynactin also likely plays a role in correctly shaping the temporal patterning of nuclear migration during development.

5.2.2. LIS1 promotes retrograde transport of diverse cargos by dynein

LIS1 has demonstrated many roles in activating dynein transport of a variety of cargos within mature neurons. The initiation of retrograde transport by dynein in neurons has been demonstrated at length to require LIS1^{224,225}. The local synthesis of this protein has been shown to be important for neurons to respond to chemogenic cues which initiate retrograde transport¹²¹. Overexpression of LIS1 induces retrograde transport and increases velocity of retrograde transport across many different organelle types²¹⁴, and likewise, the knockdown decreases retrograde flux and increases anterograde velocities, presumably due to decreased dynein-mediated drag on kinesin motor ensembles²³⁶. Many cellular cargos which are transported by dynein, including fibroblast growth factor receptors and cell adhesion molecules²²⁵ are important for structural development and maturation of cells. Studies have also implicated the LIS1

regulator NDEL1 in regulating entry of cargos into the axon compartment and have proposed that NDEL1 may pair dynein with dendritic cargos to prevent entry into the axonal space²³⁷ and to promote transport of these dendritic cargos back to the soma. Large cargos and the shaping of vesicular organelles have been shown to require LIS1²²⁹; however, loss of LIS1 has been demonstrated to lead to increased mitochondrial transport²³⁶. It is unclear what causes the discrepancy between LIS1 knockdown inhibiting organelle transport while increasing mitochondrial transport. One possibility is that mitochondrial transport uses distinct mechanism to recruit dynein-dynactin which is unique from other cargo trafficking processes. It has been suggested that high load cargos require LIS1 activity, due to increased recruitment of LIS1 to said cargos^{118,214}, and the observations that LIS1 increases dynein's resistance under load *in vitro*²¹¹ and *in vivo*¹⁵¹. Furthermore, it has been shown that decreasing dynein retrograde transport through disruption of either Lis1 or dynein-dynactin-adaptor complexes also has a negative effect on both retrograde and anterograde transport along the axon^{116,127,214}. This concomitant loss of anterograde and retrograde transport is due to either loss of vesicles from microtubule proximity due to fewer motors, or through loss of direct protein-protein interactions which stabilize active anterograde motor assemblies. Within neurons, it has been demonstrated that dynein complexes may interact with kinesin either through binding on the same cargos or through direct protein linkages^{116,176}. In the majority of these neuronal transport functions, Lis1 is directly promoting the motility of dynein-dynactin complexes for transport along microtubules, suggesting that LIS1's principal role in transport is that of an activator.

5.2.3. *LIS1 is an important dynein regulator in mitosis*

The contributions of dynein-LIS1 to dynein-mediated transport are vitally important for normal proliferation of cells, movement of nuclei, and the formation of tissues, and yet dynein has a several additional essential roles in mitosis. Nuclear envelope breakdown²³⁶, spindle positioning¹⁶⁴, and silencing of the spindle assembly checkpoint²³⁷ all require active dynein complexes recruited at the proper times to ensure mitotic progression and LIS1 has been demonstrated to be a key regulator of dynein in these processes. During prophase, dynein is recruited to the nuclear envelope through the BicD2 pathway, itself regulated by small GTPase cascades initiated at mitotic entry. Dynein at the nucleus promotes prophase NE invagination (PNEI) in a microtubule-dependent manner resulting in NE tearing²¹, although prophase recruitment of dynein occurs even in the absence of microtubules, indicating that dynein may reach the nucleus diffusively rather than requiring delivery by microtubules. During prophase LIS1 and Ndel1 are both highly enriched at the nuclear envelope, and loss of either these proteins greatly diminishes PNEI. Overexpression of either Ndel1 or LIS1 increases the amount of PNEI, and this phenotype requires phosphorylation of Ndel1 as phospho-null mutant overexpression does not reproduce similar phenotypes²¹⁵. Phosphorylation of Ndel1 is then an important regulatory step in recruiting LIS1, which in turn recruits dynein. This direct correlation between LIS1/Ndel1 recruitment of dynein, and dynein activity indicates that the primary role of LIS1 in NEBD is activation of dynein to initiate PNEI, and that, just as in the case of nuclear movement, this LIS1 activity at prophase is highly sensitive to gene dosage effects.

Outside of its role in nuclear movement and breakdown, LIS1 is important for other dynein activities during mitosis. In higher eukaryotes, dynein is required for spindle assembly and the focusing of spindle poles to form a stable bipolar spindle and to maintain tension from the kinetochores to the cell cortex^{206,241}. Recruitment of dynein to spindle poles and the cell cortex must be balanced, which is indicated through the loss of either spindle pole or cortical pool of dynein increasing dynein recruitment to the reciprocal compartment^{22,23}. During mitotic progression in animals, the dynamic localization of dynein to the cell cortex is mediated by direct offloading of dynein-dynactin by microtubule plus ends¹⁰³, and by direct binding to cortical receptor NuMA by dynein-dynactin complexes freely diffusing in the cytoplasm. Loss of the LIS1 pathway by perturbing upstream effector NDEL1 leads to loss of mitotic spindle integrity²⁰² via loss of dynein recruitment to spindle poles. LIS1 and dynein are both present at the kinetochore, although overexpression of dynamitin causes a loss of LIS1, indicating a dependence on the dynein motor for LIS1-kinetochore localization²¹⁷. One mechanism of kinetochore recruitment of dynein is thought to be delivery of CLIP-170-LIS1-dynein-EB1 by dynamic microtubule plus ends, as the recruitment of LIS1 has been demonstrated to be sensitive to CLIP-170 expression levels^{102,216}. In animals, the recruitment of LIS1-dynein to the kinetochore by the NDEL homolog NUD-2 is important for the timely eviction of SAC proteins such as Mad1/Mad2²⁴⁰. Finally, dynein at the cortex is responsible for spindle assembly and the dynamic oscillations of the mitotic spindle during metaphase. The timing of the deposition of dynein at the kinetochore may be regulated by various kinetochore proteins, or through post-translational modifications^{201,202}. Dynein-mediated spindle oscillations are dynamically regulated by

mitotic kinases and phosphatases²³, and targeting of dynein to the cortex by LIS1 through microtubule offloading¹⁰³. In these mitotic functions, LIS1 facilitates the organization and recruitment of dynein in the cell, and these functions may be patterned by specific mitotic factors.

In summary, LIS1 activates the dynein transport and maintenance of complex cytoskeletal networks, promotes the dynein-driven migration of nuclei, and recruits dynein to the cell cortex and kinetochore to fulfill its mitotic roles. Together, these diverse activities gives rise to the cellular proliferation and movements necessary for the formation of tissues²⁰⁸⁻²¹⁰. These observations demonstrate the necessity of LIS1 for complex roles of dynein in an organisms development, and how these roles are particularly important during neurological development. Further, these data provide a cellular basis for the roles of LIS1 in driving neurological diseases. These data strongly suggest that LIS1 is an activator of motility, and that its roles in effecting dynein-mediated nuclear transport are highly sensitive to gene dosage and expression, indicating that LIS1 is indeed promoting this process directly, by activating a maximal amount of dynein-dynactin complexes to engage with the nucleus. Similar observations of dynein nuclear transport, mediated by LIS1 recruitment and activation of motility, are apparent in nuclear migration in many cell types.

5.3. Conserved mechanisms of Pac1/LIS1 regulation of dynein

5.3.1. Pac1/LIS1 recruits dynein to sites of activity by promoting plus end localization

Across eukaryotes, microtubule plus ends serve as platforms for protein assembly and as molecular machines which deliver proteins and tether organelles^{82,84}. The dynein plus end targeting complex is evolutionarily conserved between yeast and

humans and is comprised of an end-binding protein (EB1 or EB3/Bim1), a CAP-GLY domain-containing protein (CLIP-170/Bik1 or p150), the LIS1/Pac1 protein, and in yeast, the kinesin Kip2. It has been demonstrated in yeast that the plus-end targeting of the dynein-LIS1 complex requires the microtubule binding protein CLIP-170/Bik1, which interacts directly with Pac1 through its C-terminal domain, a binding site shared by its human homologs^{100,102}. The localization of the dynein-PAC1-Bik1 to astral microtubules does not require tip-tracking proteins for plus-end localization in yeast⁹⁹, but CLIP-170 requires EB1 for proper microtubule localization. Loss of tip-tracking proteins may decrease the amount of Bik1-Pac1-dynein at microtubule plus-ends, however⁹⁹. This protein assembly allows dynein to track growing and shrinking microtubule ends, and is thought to be important for positioning dynein at the plus-ends where it may initiate minus-end directed microtubule movement in diverse eukaryotic cells which require dynein-mediated vesicle transport^{175,232}. This complex is also important for facilitating dynein-dynactin interaction, though many mechanistic details of this process are unclear^{84,233}.

Plus-end maintenance of cytoplasmic dynein may be important for either allosterically positioning dynein in a conformation amenable to dynactin interaction, or by providing a solid substrate (the microtubule lattice) to facilitate the interaction of these large complexes, or possibly a combination of both mechanisms. Since multiple dyneins may be assembled on a single ARP filament^{93,94}, it may be necessary to maintain dynein and dynactin along microtubules to facilitate higher ordered assemblies. Loss of Pac1 in *S. cerevisiae* is sufficient to decrease dynein offloading frequency below the threshold of detection for fluorescently-tagged dynein⁹⁹; however,

*pac1*Δ cells have a less pronounced spindle mispositioning phenotype than *dyn1*Δ cells⁸⁴, suggesting that loss of Pac1/LIS1 does not completely prevent dynein-mediated spindle positioning. Rather, loss of Pac1 limits the dynein pool which is offloaded by the cortical targeting machinery, and therefore Pac1 has an important role in ensuring dynein delivery to its cortical receptors. While the EB1-CLIP-170-LIS1 pathway appears conserved among eukaryotes, the mammalian dynein-dynactin complex has been demonstrated to be a tip-tracking complex in its own right⁹⁵, possibly facilitated by both dynein and the CAP-GLY domain of p150^{Glued}. However this tip-tracking complex is distinct from EB1/CLIP-170/LIS1/Dynein, and the tip-tracking properties of dynein-dynactin can be further enhanced with the addition of end binding proteins such as EB1 or EB3⁹⁵, or by the addition of Lis1⁹⁶.

Pac1/LIS1 binding to dynein is needed to target the proteins to microtubules *vis a vis* Bik1/CLIP-170, so at least one function of these proteins is to provide the binding site needed to form a tripartite complex. LIS1 has been shown to directly interact with CLIP-170 directly *in vitro* in mammalian cells^{101,102}, and loss of Pac1 completely removes dynein localization from microtubule plus-ends in yeast. Furthermore, the Pac1/LIS1 and Bik1/CLIP-170 interaction have not been observed in the absence of dynein. It is important to note that dynein-Pac1-Bik1 complexes maintained at the plus end are non-motile, which may be a consequence of the unique architecture of this complex prohibiting dynein from interacting with microtubules. It is still an outstanding question what, mechanistically, Bik1 is doing to maintain Pac1 and dynein at microtubule plus ends, but most data indicates maintaining this complex along microtubules is important for normal dynein driven vesicle transport¹¹⁵.

5.3.2. *Lis1* is required for initiation of dynein-mediated transport in diverse organisms

The functions of LIS1 in nuclear transport and the movement of other organelles appears to be remarkably conserved across eukaryotes. In many fungal species, LIS1 homologs nudF and Pac1 (from *A. nidulans* and *S. cerevisiae*, respectively) are similarly important for nuclear migration functions of dynein. In the simple budding yeast, which does not utilize microtubule transport of vesicular cargos, dynein-based nuclear transport is one of two redundant nuclear positioning pathways^{24,66}. In *A. nidulans*, the LIS1 homolog nudF has been studied for its roles in promoting retrograde transport within hyphae, highly specialized microtubule-based structures present in many types of filamentous fungus¹¹². Within hyphae, a unipolar microtubule array is assembled with minus ends clustering at the soma and plus ends oriented away from the cell. This array is evocative of the axon, which uses the same unipolar organization. In these cells, migration of nuclei is known to require nudF, and the regulator nudE, for which NudEL/Ndel1 in higher eukaryotes draws its name. In these cells, dynein and dynactin components²³³, as well as nudF¹¹³, are present along microtubules and cluster at microtubule plus ends¹¹⁵. The recruitment of nudF to microtubules has been demonstrated to be accomplished by direct recruitment through both nudE and the *A. nidulans* homologue for CLIP-170, CLIPA¹¹⁴, in a mechanism similar to those plus end recruitment mechanisms identified in yeast⁹⁹. In agreement with this hypothesis, it has been demonstrated that the initiation of directed retrograde transport for the nucleus¹¹² and a variety of vesicular cargos, including endosomes and lysosomes, requires nudF¹¹⁵. It is important to note that it is only the initiation of transport of vesicles, rather than sustained transport, that is thought to require nudF, as nudF has not been

observed to remain associated with moving vesicles. The reason for this dependence on nudF for transport initiation is likely that nudF recruits dynein to microtubule plus ends, which allows for its delivery to vesicular cargos, though it is probable transport occurs also along microtubules and not merely just at plus ends. Finally, many of these nuclear migration and microtubule functions of the LIS1-dynein pathway are conserved in other protists and filamentous fungus, including *Dictyostelium*, *Neurospora crassa* and *Ustilago maydis*. In *Ustilago*, the LIS1 homolog is required for nuclear migration and for the integrity of normal dimorphic transitions. Plus end localization of dynein by LIS1 is similarly important for initiation of retrograde transport functions as it is in *Aspergillus*. In *Dictyostelium*, impairing a LIS1 homolog by introducing mutations found in human lissencephaly disease causes Golgi dispersal and impairs cytoskeletal organization²⁴², illustrating the conserved nature of the LIS1-dynein interaction. In these cells, LIS1 is not targeted to microtubule plus ends, but instead binds across microtubules via other MAPs, and has been shown to directly regulate actin networks, likely through binding GTPases. While it is unclear if LIS1 similarly regulates actin in higher eukaryotes, there is some evidence LIS1 has roles in regulating the actin cytoskeleton^{246,247}.

5.4. Pac1 and LIS1 demonstrate disparate effects *in vitro*

5.4.1. Differences between Pac1 and LIS1 effects on dynein activity in vitro

Despite these similarities across eukaryotes *in vivo*, LIS1 and Pac1 have demonstrated divergent activities *in vitro*. In single-molecule experiments using recombinant dynein-dynactin-BicD2, and proteins of the plus-end targeting complex, LIS1 has been shown to have no effect on^{95,96} or increase the velocity¹⁰⁵ of dynein-dynactin-adaptor complexes. LIS1 increased dynein tip tracking, but was displaced

upon BicD2 binding, which initiated transport to the minus ends. Further, these experiments were able to visualize comigrating DDB-LIS1 complexes, and there was no apparent effect of LIS1 on dynein motility. Paradoxically, the addition of purified LIS1 to recombinant or natively purified dynein alone completely prevents microtubule translocation by dynein motors adsorbed to a coverslip^{108,175}, yet also increases ATPase activity of dynein alone in bulk solution ATPase assays. The effects observed in gliding assays can be abrogated by the addition of the LIS1 regulatory protein Ndel1, and dynein-LIS1-Ndel1 complexes are indistinguishable from dynein alone in microtubule gliding assays¹⁷⁵. These results are similar to what has been observed for dynein-LIS1-Ndel1 in optical trapping assays, whereby LIS1 is able to induce a force-persistent state of dynein, but these effects are promoted by the addition of Ndel1²⁰⁴.

The LIS1-NudE and dynein interaction may be antagonized by the assembly of dynein-dynactin complexes due to NudE and p150^{Glued} proteins sharing overlapping binding sites on the dynein intermediate chain²⁵³; however, studies using purified components have also shown that LIS1-dynactin-dynein interact to form intact complexes. The recruitment of dynein to microtubule plus-ends is an important step in the dynein cortical offloading pathway, and for subsequent mitotic spindle positioning, as well as important for the recruitment of dynein to the kinetochore. For these cellular functions, LIS1 appears to function as an activator or recruitment factor, strengthening dynein interactions with the dynamic microtubule lattice, leading to increased dynein-dynactin association. These cellular functions are highly conserved with respect to these proteins' yeast counterparts. While LIS1 inhibits dynein alone when used in

gliding assays^{96,108}, the exact mechanisms underlying this form of ensemble activity of thousands of motors are unclear.

To date, only Pac1 has been shown to inhibit yeast dynein alone when used in single molecule motility experiments. Pac1/LIS1 has been proposed to inhibit dynein activity at the plus-ends of microtubules by preventing processive minus-end direction motility of the motor^{101,104}. The first experiments examining dynein motility in the presence of Pac1 identified^{84,105} that dynein velocity is reduced in single-molecule TIRF experiments. Several studies since then have together proposed a mechanism^{101,105-107,249} whereby Pac1 binds to dynein's AAA+ ring between AAA3 and AAA4 and acts as a "clutch" on motor activity, which allows for dynein to actively catalyze ATP hydrolysis but sterically blocks the linker swing, thereby preventing dynein from moving processively. Indeed, studies using yeast dynein mutants have demonstrated that the linker swing vector (aided by the positioning of the microtubule binding domain) is the primary driving force of dynein motility in a minus-end directed fashion⁵⁵. In this model, Pac1 is an inhibitor which actively blocks dynein mechanochemistry and disrupts communication between the ATP hydrolysis at AAA1 and the mechanochemical changes that drive AAA+ ring remodeling and tuning of the affinity of the MTBD. This prevents dynein from attempting to walk to the minus-ends of microtubules and removes the force opposing the plus end targeting of dynein provided by kinesin.

Structural data from these studies demonstrated that Pac1 bound to dynein at the AAA3 domain and to the stalk region¹⁰⁶⁻¹⁰⁷, which would presumably prevent the full linker swing from occurring by sterically blocking this mechanical element. Additionally, the AAA3 domain has been shown to affect dynein mechanochemistry⁴⁸ and tune the

affinity of the microtubule binding domain. In electron microscopy images of Pac1-monomer bound dynein, the AAA ring of dynein adopts a closed conformation^{106,107}, which indicates a high-affinity microtubule state. However, these data used the GST-dynein minimal motor domain, which behaves distinctly different from the dynein full-length complex^{160,163,169}, and further, these studies were not able to resolve the conformational state of the MTBD. While it is likely that the MTBD would adopt the high affinity conformation given the AAA ring structure, these data are inconclusive. The induction of a high-affinity state by Pac1-dynein binding was further evidence that Pac1 inhibits dynein motility, as the dynein MTBD in the high-affinity microtubule state prevents detachment from the lattice and slows processive motility. These conflicting results indicate that either (1) Pac1 and LIS1 have distinct functions in plus-end targeting of dynein between budding yeast and mammals, respectively, or that (2) Pac1/LIS1 function may be context dependent and based on stoichiometries of dynein and other components; post-translational modifications; or some combination thereof.

5.4.2. An in vitro artifact of Pac1 binding microtubules is likely responsible for inhibitory effects on dynein

During the course of this thesis work, we identified that the previously characterized^{101,104-107} Pac1 constructs used to understand Pac1-dynein interaction bound to mammalian taxol-stabilized microtubules *in vitro* with nanomolar affinity in normal assay buffer conditions (Fig. 28). This effect was independent of labeling and had not been previously reported in studies using this construct. This finding was surprising to us, as MAPs which associate with microtubules, such as tau, are able to negatively regulate motor proteins^{111,152}. Importantly, work done by our lab¹⁶³ identified

that a budding yeast-specific protein She1 was a negative regulator of dynein activity, able to reduce dynein motor velocity by simultaneous binding to the dynein MTBD and the microtubule lattice. We then asked if Pac1 may be behaving in a similar way, by non-specifically interacting with the E-Hooks and the dynein motor domain simultaneously. Indeed, we found that upon removal of the E-Hooks, or by increasing the ionic strength of the motility buffer, or by adding in dilute cell extract (since previous work has not identified Pac1 as a microtubule-binding protein *in vivo*), we were successful in evicting Pac1 from the microtubule lattice. While Pac1 is well-known to associate with astral microtubules, this property requires a bona fide MAP (Bik1/CLIP-170) and dynein interaction, as previously delineated.

We then asked if by weakening the interaction between Pac1 and the microtubule lattice if we could decrease the Pac1 effect on reducing dynein's velocity. Indeed, removing Pac1 from the microtubule lattice by increasing the salt concentration or adding cell lysate mitigated the effects on dynein motility. When correlating the velocity reduction effect to the relative degree of Pac1-microtubule binding in each condition by comparing fluorescence intensity, we determined these effects were linearly correlated (Fig. 29D), indicating that the primary effects of reducing dynein velocity are almost entirely due to Pac1-microtubule binding. However, even in the highest strength ionic buffers, or by combining microtubule treatments, some minor effect of Pac1 on dynein velocity persisted (Figs. 27-29), indicating that Pac1 is likely affecting dynein's velocity in some negative way, or that the eviction from microtubules is incomplete. As Pac1 binds to dynein at AAA3/AAA4 as demonstrated by previous work¹⁰⁶⁻¹⁰⁷, it potentially has a role in regulating dynein-microtubule affinity. However,

what the cellular relevance of this modulation is or what role AAA3/AAA4 or stalk binding play in dynein localization or cellular activity remain ambiguous. Furthermore, this allosteric change to dynein may be necessary to effect binding to Bik1, and the decrease in velocity may not be relevant for LIS1 or Pac1 regulation *in vivo*.

5.5. Pac/LIS1/nudF relieves dynein autoinhibition to assemble dynein-dynactin .

The results from our experiments on dynein autoinhibition detail how dynein stochastically switches from open and closed conformations, and this property of the motor regulates its interaction with dynactin and Pac1¹⁶⁹. By removing autoinhibition, cells no longer require Pac1-mediated plus end targeting for cortical offloading, which leads to active dynein-dynactin-Num1 at the cortex. We demonstrate that Pac1 binds to uninhibited dynein, and by doing so sterically prevents the formation of the autoinhibited conformation. This increases *in vitro* processivity of the wild type motor to that of our open dynein mutants. However, this increase in run length are refractory to the activities of open mutants. Thereby, Pac1 activates dynein motility by localizing it to its cargo (the nucleus anchored to astral microtubules) and promotes its assembly with dynactin.

This property of yeast Pac1 is strikingly similar to recent reported effects of nudF/LIS1¹⁶⁶⁻¹⁶⁸, which have been demonstrated to activate dynein motility by pairing it with dynactin by overcoming autoinhibition. By preventing dynein autoinhibition, the addition of LIS1 to mixtures of dynein-dynactin-adaptor (DDA) proteins promotes the binding of dynein to dynactin, and in turn, promotes the assembly of 2 dynein: 1 dynactin complexes. This result satisfactorily identifies how LIS1 increases the velocity of DDA without remaining stably associated, as recruiting a second dynein should increase the velocity of these complexes⁹³. This *in vitro* result also demonstrates the

need for LIS1 in high load transport *in vivo*, and explains why loss of LIS1 inhibits the initiation of dynein motility, but not movement of already moving activated cargos¹¹⁵. By stabilizing an open dynein, LIS1 promotes the assembly of dynein-dynactin on cargos, and likely modulates the number of dyneins assembled on a dynactin. Targeting dynein to microtubule by the LIS1-CLIP-170 pathway may improve interaction with dynactin by other mechanisms, such as increasing the local concentrations of molecules to drive higher order assemblies. Why these factors dissociate before initiation of transport is still unclear, but it is clear from single molecule studies that LIS1 can associate with motile dynein-dynactin-adaptor complexes, and speed up these complexes through driving dynein-dynactin assembly^{167,168}.

This finding also has profound significance for the understanding LIS1 in the context of neurological disease. By recruiting open, active dyneins to microtubule ends, LIS1 positions dynein for transport and microtubule organization functions. The assembly of multiple dyneins onto cargos by LIS1 is important to oppose the anterograde directed transport of kinesins, and illustrates why loss of LIS1 increases anterograde transport velocities^{208,236}. In high load transport activities, including microtubule sliding^{131,192} and nuclear transport, and high load vesicular transport, LIS1 likely is needed to recruit teams of dynein to increase the force production of complexes bound to cargos. This also explains, in part, why cells are so sensitive to LIS1 expression levels, as the loss of even partial LIS1 function causes a depletion of active dynein, and disrupts regulation of motor autoinhibition across cell types. However, some processes, especially those which require high-load dynein activities, are particularly sensitive to depletion of the protein. These activities of LIS1 are assisted by Ndel, which

serves a further level of regulation of recruitment of LIS1 to dynein, and recruitment of dynein to sites of activity^{214,237}.

Because of the similarities between these pathways, and the striking evolutionary conservation of Pac1/nudF/LIS1 in all the (1) nuclear migration pathway^{89,1112,133,137}, the (2) plus end tracking apparatus^{95,96,110,117}, and the (3) cortical targeting machinery^{98,103,252}, we wondered if other eukaryotic organisms might use similar mechanisms to overcome dynein autoinhibition. Human cytoplasmic dynein-1 and yeast dynein, and human cytoplasmic dynein-2 both assume highly similar conformations when autoinhibited^{49,165,169,192}. Strikingly, both conformations rely on motor domain contacts which are palindromic, and both structures have stalks crossed over each other, in a dramatic demonstration of convergent evolution. However, studies have not identified LIS1 in the flagellum compartment, indicating that dynein-2 autoinhibition is not regulated by LIS1. Interestingly, dynein-2 has a 4 amino acid sequence deletion at the D3045 position, identified as being important to maintain autoinhibition in yeast and mammals¹⁶⁶⁻¹⁶⁹. We then asked if other organisms had the same conserved residues, and if so, did these same organisms also express LIS1/Pac1/nudF?

Performing sequence alignments of 21 dyneins from 20 organisms reveals that many organisms maintained Phi contacts at the AAA4-linker, AAA5-AAA5, and stalk-stalk, interface surfaces. These alignments focused on the residues we previously demonstrated to be conserved for maintaining the autoinhibited state between yeast and humans. Amazingly, all organisms which maintained the AAA4-linker contacts, and most of the other Phi particle contacts, expressed some isoform of LIS1 (Fig 34, 35). This included filamentous fungus such as *Ashbyaa gosypii* and *Ustilago maydis*, all

animals, and brown algae *E. siliculosus* (Table 3). The dynein homologues which lacked one, or several, important Phi particle contacts, including human cytoplasmic dynein-2, *S. pombe*, and *Giardaria intestinalis*, did not express a LIS1 isoform. This leads us to hypothesize that Pac1/LIS1/nudF isoforms primarily function to regulate dynein activity in cells by relieving autoinhibition. This functions to assemble multiple dyneins onto dynactin, and to position dynein along microtubules. In disparate organisms from both fungi and animals, this mechanism appears remarkably conserved to regulate the activities of cytoplasmic dynein. However, in species which do not require LIS1 activity, the Phi-particle contacts have been lost, and these species may then use other mechanisms to relieve dynein autoinhibition.

5.6 Conclusion

The regulator of dynein, LIS1, serves diverse roles in the cell. In all organism, we propose that the major function of LIS1 and its related proteins Pac1 and nudF, is to activate dynein motility by stabilizing the open dynein conformation, and to facilitate dynein interaction with dynactin. Furthermore, by dynein-LIS1 associating with microtubule plus end complexes, it becomes ideally positioned to interact with its microtubule cargo. In many of its cellular functions, LIS1 functions to increase dynein force production, by the recruitment of dynein motors to sites of transport, and potentially by directly affecting the mechanochemical force production abilities of dynein. By recruiting dynein and promoting assembly of dynein-dynactin, LIS1 improves dynein's transport abilities, and concentrates the protein to areas of cellular activity. Many aspects of LIS1 regulation of cytoskeletal proteins, including its roles in other MAPS and in actin-microtubule cross talk and its roles in dynein-dynactin assembly, are

not fully understood. However, one role of LIS1/Pac1/nudF, to stabilize the open dynein conformation, finally allows us to reconcile many disparate effects of these proteins in past biochemical studies.

Figure 31

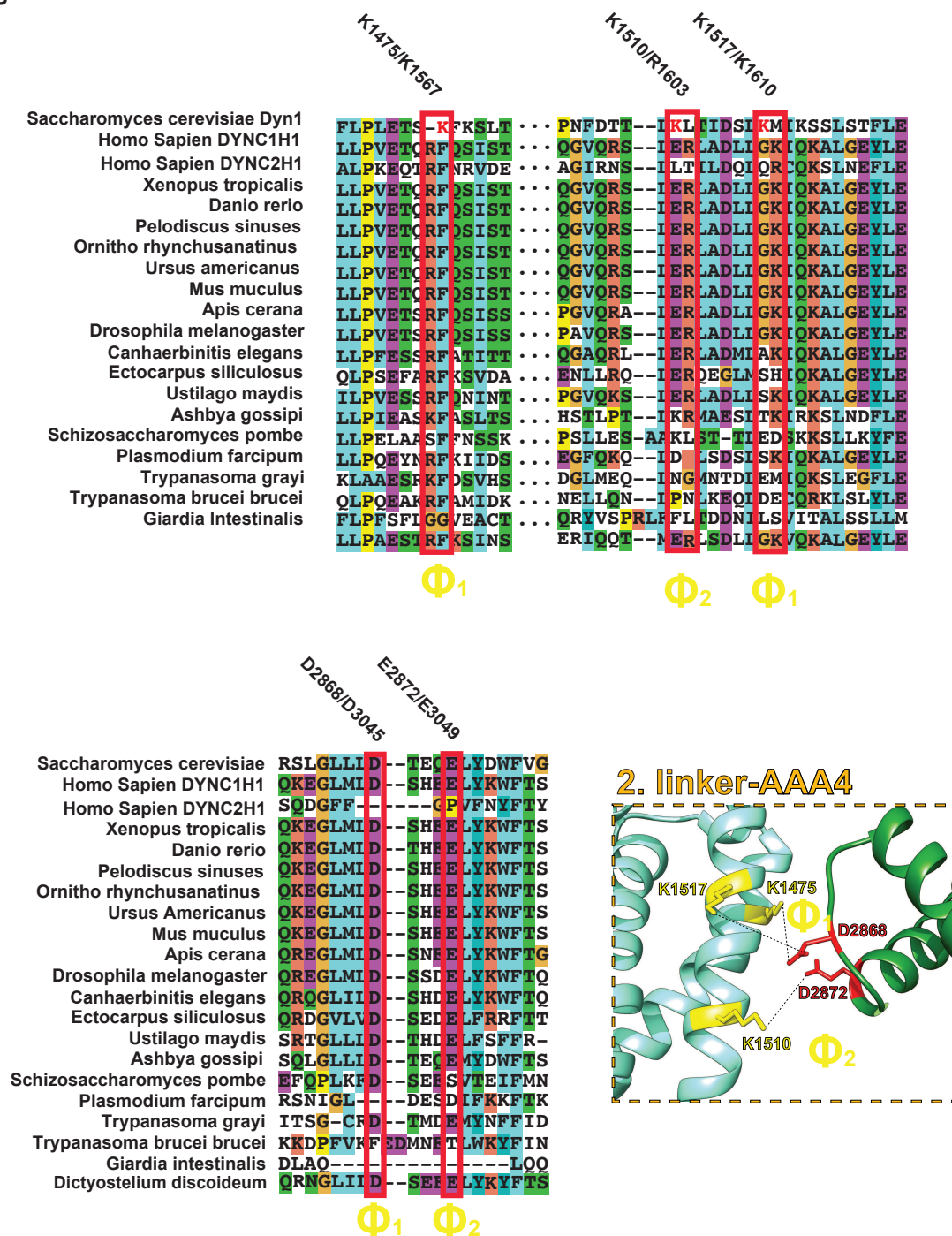


Figure 31. Sequence conservation of Phi particle contacts across eukaryotes. Sequence alignment of dyneins from twenty dynein isoforms, focused in on the Linker-AAA4 contact site. Phi symbols indicate paired residues identified in Zhang et al (Ref. 28). Site 1, indicated by a Φ_1 , was investigated in our study. Nearly all species surveyed retained the Phi contacts identified by this thesis work and others (Ref.27,30-33). Of particular note is human dynein-2, which has a deletion at D3045 (human numbering) and a proline at D3049. Dynein-2 is known to undergo a similar form of Phi inhibition, but this structure relies on different intermolecular contacts. Importantly, dynein-2 is not believed to be regulated by LIS1.

Figure 32

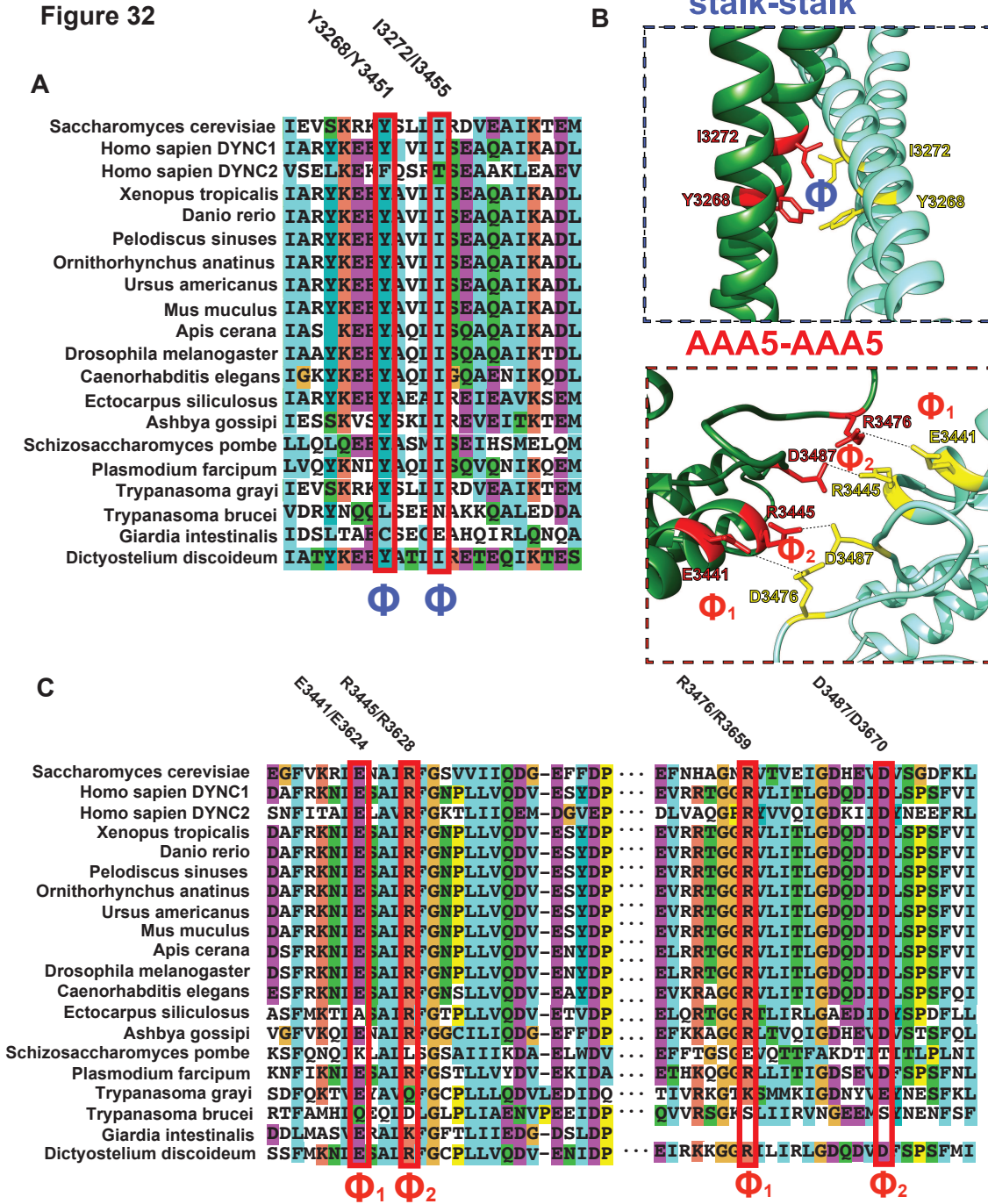


Figure 32. Sequence conservation of Phi particle contacts across eukaryotes. Sequence alignment of dyneins from twenty dynein isoforms, focused on the (A)stalk-stalk and AAA5-AAA5 (C) contact site. Phi symbols denote paired residues identified in Zhang et al (Ref 28). All species surveyed which expressed a LIS1 homologue retained the Phi contacts identified by this thesis work and others (Ref.28,30-33).

Figure 33



Figure 33. Sequence alignment of LIS1 homologs from species with predicted autoinhibited conformations. LIS1 sequences from species which have conserved autoinhibition contacts, focused on two areas important for dynein-LIS1 interaction. The highlighted arginine (R317 in humans, R378 in yeast) and tryptophan (W340 in humans, W419 in yeast) have been demonstrated to be necessary for stable dynein-LIS1 interactions. Despite large overall sequence differences and differences in size, areas important for dynein interaction were highly conserved.

Table 3. Sequence conservation of LIS1 and Phi-particle contacts across eukaryotes. Compilation of sequence alignments perform in Figs. 31-33, focused on residues demonstrated to be homologous between yeast and human dynein for maintaining the autoinhibited conformation^{165,169}. Residues that are conserved are marked with an X or a -1, in the case of residues which appear shifted.

	Pac1/ LIS1 Y/N	K1475/ R1567	R1517/ K1610	D2868/ D3045	Y3268/ I3451	I3272/ I3455	R3476/ R3659	D3487/ D3670
<i>Saccharomyces cerevisiae</i> Dyn1	Y	+1	-1	X	X	X	X	X
<i>Homo sapien</i> DYNC1H1	Y	X	X	X	X	X	X	X
<i>Homo sapien</i> DYNC2H1	N	X	X	-	-	-	X	X
<i>Xenopus tropicalis</i>	Y	X	X	X	X	X	X	X
<i>Danio rerio</i>	Y	X	X	X	X	X	X	X
<i>Pelodiscus sinuses</i>	Y	X	X	X	X	X	X	X
<i>Ornitho rhynchusanatinus</i>	Y	X	X	X	X	X	X	X
<i>Ursus americanus</i>	Y	X	X	X	X	X	X	X
<i>Mus mucus</i>	Y	X	X	X	X	X	X	X
<i>Apis cerana</i>	Y	X	X	X	X	X	X	X
<i>Drosophila melanogaster</i>	Y	X	X	X	X	X	X	X
<i>Canhaerbinitis elegans</i>	Y	X	X	X	X	X	X	X
<i>Ectocarpus siliculosus</i>	Y	X	X	X	X	X	X	X
<i>Ustilago maydis</i>	Y	X	X	X	-	X	-	-
<i>Ashbya gossipi</i>	Y	X	X	X	X	X	X	X
<i>Schizosaccharom yces pombe</i>	N	-	-1	X	X	X	-	-
<i>Plasmodium farcipum</i>	N	X	X	-	X	X	X	X
<i>Trypanasoma grayi</i>	N	X	-	X	X	-	X	X
<i>Trypanasoma brucei brucei</i>	N	X	-	-	-	-	-	-
<i>Giarardia intestinalis</i>	N	-	-	-	-	-	-	-
<i>Dictyostelium discoideum</i>	Y	X	X	X	X	X	X	X

CHAPTER 6: Conclusions

6.1. Introduction

The data presented in this thesis highlight the efficacy of using yeast dynein as a platform for rapid mutagenesis, and refines the current model of dynein cortical offloading. Even though there exists different functional specialization between dyneins across species, this protein bears remarkable similarities between disparate eukaryotes. This similarity is typified by the fundamental activities of dynein at the cell cortex, where it performs its conserved role of mitotic spindle positioning^{24,66}. The delivery of teams of motors to the cell cortex is accomplished through the plus-end clustering of the motor and its activator, dynactin, through a fundamental network of MAPs which associate with dynamic microtubule plus-ends¹⁰⁸⁻¹¹¹. In yeast and to a greater extent, animal cells, delivery of dynein-dynactin to their cortical receptor, NuMA/Num1, can also be achieved through diffusive binding. Ensembles of motor proteins anchored to the cortex together generate the forces necessary for the high-fidelity positioning of the mitotic nucleus by translocation of astral microtubules.

This thesis work demonstrates that the regulation, structural plasticity, and assembly of these motor protein complexes is fundamentally similar between *S. cerevisiae* and mammalian systems, perhaps even surprisingly so. In this summary, I will briefly review the outcomes of the study of disease-correlated mutations, and the suitability of our system to study such mutations. In addition, the proposed mechanism of dynein autoinhibition will be reviewed and its implication for LIS1 regulation of dynein, which we believe represents a striking example of protein conservation in Eukarya.

6.2. Yeast platform for assessing motor neuron diseases

While it seemed apparent at the start of this work that yeast dynein was a simple, fast, and robust system for studying the protein, the degree to which this system shares similarities with higher eukaryotes may have been underappreciated (at least by this student). In our mutant screen, nearly every disease-correlated mutation presented deficits in some aspect of motor activity, and of those mutants, nine demonstrated a severe degree of loss of function. These results demonstrated the suitability of yeast as a cell biological system and biochemical system for understanding of disease-correlated mutations. It is unsurprising that motor domain mutations produced the most severe phenotypes, given the homology of this region²⁴. What was surprising was that our results showed striking similarity between phenotypes described in a 2017 study of nine identical mutants of recombinant human dynein¹⁶⁵, which used microtubule gliding ensemble motility assays, as well as using recombinant dynein-dynactin-BicD2 (DDB) complexes. In both studies, R1852C (human R1962C) and H3639P (human H3822P) mutants led to almost no protein functionality, indicating that such severe loss of function mutations in the conserved motor domain is likely to have similar phenotypes across species. Additionally, the yeast system was able to identify that while both mutants affected the motor function, it additionally affected the ability of these mutants to localize properly *in vivo*. These results underscore the importance of having additional cellular readouts when address protein functionality. It is further important to note that the loss of motility was similar for both the human mutants using DDB and for yeast analyzing the dynein holoenzyme solely. This demonstrates the efficacy of the yeast system, and argues against (initially) performing the arduous task of assembling

recombinant DDB complexes, at least until mutations have been identified as driving severe phenotypes using a yeast system.

Possibly the greatest advantage of our experimental platform is the ability to perform rapid mutagenesis to compensate for the mutant deficits. By introducing additional compensatory mutations, we may more narrowly pinpoint the molecular defects introduced by single point mutations and evaluate molecular mechanisms underlying mutation phenotypes. This provides a basis for understanding future mutations which may be discovered. In the future, this system may allow for the high throughput testing of potential therapeutics to either single mutations, or perhaps more broadly defined classes of mutation-driven diseases.

Our spindle positioning assay using diploid yeast was the most suitable assay for determining phenotypic outcomes of mutations in a high-throughput manner. This assay may not be suitable for the screening of thousands of compounds for drug discovery approach, but it is very useful to determine rescue mutations to narrow down the motor deficit. It may also be necessary to develop additional assays to complement our initial approach, such as ATPase assays to understand mutations or microtubule-binding assays¹⁶³, or more expand the localization assays to include additional components of the plus-end dynein complex^{84,85}. These data also highlight the similarities of dynein between yeast and humans. The *in vivo* dynamics experiment could recapitulate the dominant nature of dynein alleles in disease in heterozygous organisms, and they also demonstrated what is known from previous mouse models¹⁵⁵ that hemizygous dynein expression drives much less severe cellular deficits than single point mutations. It would be interesting to repeat the spindle dynamics assay for haploid mutants which

presented mild *in vivo* phenotypes to determine if they exacerbate loss-of-function phenotypes similar to the E545V mutation. These data suggested a further similarity between yeast and human dynein, identifying that multiple dyneins may bind a single dynactin in yeast. While further experiments are required to characterize and understand the valence of dynein-dynactin-adaptor interactions, we now have preliminary data which indicates that higher order dynein-dynactin assemblies are similar between eukaryotes.

While autoinhibition was not believed to be necessary for yeast dynein owing to its single molecule processivity, we identified key interactions important for this regulatory mechanism are conserved between organisms. Indeed, yeast dynein is inhibited much the same way as human dynein, and many aspects of the functional relevance of the autoinhibited conformation are conserved amongst eukaryotes. This provides the most promising potential avenue for drug discovery, as inhibition of the protein will likely have a higher efficacy than trying to restore functionality to a compromised protein through pharmaceutical intervention. What's more, our results demonstrate that titrating down the effects of Pac1/LIS1 may be a potential avenue for rescuing phenotypes present in mutations with disrupted autoinhibition and over activation. This rescue could be achieved pharmacologically through antibody blocking of the LIS1 dynein binding surface¹³⁷ or through knockdown of the endogenous LIS1 protein¹³⁴.

6.3. Changing the paradigm of dynein regulation by autoinhibition and Pac1/LIS1

Yeast dynein has been used extensively to characterize dynein motor function for years; however, due to its *in vitro* activity¹⁶⁰, it was never examined for an autoinhibited

state. Our research has identified that yeast dynein is indeed autoinhibited, in a manner which appears nearly identical to its mammalian counterpart. The results from our negative stain-EM experiment and our ability to tune dynein's run-length demonstrates that the autoinhibited conformation is labile, and that this limits processivity in unloaded *in vitro* motility experiments. The transition between the open and closed states may be mitotically regulated, as dynein is most active during this time. While it is unclear if this is conserved in higher eukaryotes, our evidence suggests the mechanism of regulation persists across eukaryotes. However, what is evident is that at least one regulator, Pac1/LIS1, has a direct role in stabilizing the uninhibited conformation of dynein.

The previous paradigm in the field of yeast dynein was that Pac1 was an inhibitor of dynein motility which uncoupled ATPase activity of the motor from the mechanochemical changes in AAA3/4 and the stalk and MTBD which drive processive motility after ATP binding and hydrolysis. This model has been extensively characterized^{101,105-107}, despite stark differences between this model and findings using human proteins. Results from this thesis demonstrate that the major, biologically relevant function of Pac1, LIS1, and nudF (from *Aspergillus nidulans*) is to stabilize dynein in the open state and to prevent autoinhibition by acting as a “molecular wedge,” sterically blocking contacts which stabilize the autoinhibited conformation¹⁶⁶⁻¹⁶⁹. This finding represents an evolutionarily conserved mechanism throughout Eukarya, and presents an interesting understanding in the convergence of mechanisms of motor protein control. Together, our analysis of Pac1/LIS1 regulation of dynein challenges the current paradigm in the field and further refines the model for microtubule-dependent targeting and offloading of dynein to sites of required cellular activity.

6.4. The Vitruvian Yeast

Since the study of dynein began¹, this molecule has surprised, delighted, and confounded researchers. Yeast dynein, despite stiff competition from mammalian dynein systems, remains a rugged, reliable, and translational system to study mechanical processes. The simplicity, yet astounding conservation, of dynein, dynactin, and their regulators in the cytoskeleton, ensures yeast dynein will remain a vital system in precisely dissecting molecular information from complex cellular processes. The experimental results laid out in this work have delineated further similarities of yeast dynein with the dynein present in higher eukaryotes. This humble organism continues to be an invaluable tool in understanding the complexity of regulation of cellular activities, and for studying the implications these conserved mechanisms have for human disease.

WORKS CITED

1. Gibbons, Ian R.; Rowe, Arthur J. Dynein: a protein with adenosine triphosphatase activity from cilia *Science*. 1965;149(3582):424–426.
2. Wiggan O, Schroder B, Krapf D, Bamberg JR, DeLuca JG. Cofilin Regulates Nuclear Architecture through a Myosin-II Dependent Mechanotransduction Module. *Sci Rep*. 2017;7:40953.
3. DeLuca KF, Meppelink A, Broad AJ, et al. Aurora A kinase phosphorylates Hec1 to regulate metaphase kinetochore-microtubule dynamics. *J Cell Biol*. 2018;217(1):163–177. doi:10.1083/jcb.201707160
4. Goodson HV, Johansson EM. Microtubules and Microtubule-associated Proteins. *Cold Spring Harb Perspect Biol*. 2018;10(6). doi: 10.1101/cshperspect.a022608.
5. Weber A, Iturri J, Benitez R, Zemljic-Jokhadar S, Toca-Herrera JL. Microtubule disruption changes endothelial cell mechanics and adhesion. *Sci Rep*. 2019;9(1):14903. Published 2019 Oct 17. doi:10.1038/s41598-019-51024-z.
6. Moughamian, A. J., Osborn, G. E., Lazarus, J. E., Maday, S. & Holzbaur, E. L. Ordered recruitment of dynactin to the microtubule plus-end is required for efficient initiation of retrograde axonal transport. *J Neurosci*. 2013;33:13190-13203.
7. Maiato H, DeLuca J, Salmon ED, Earnshaw WC. The dynamic kinetochore-microtubule interface. *J Cell Sci*. 2004;117(Pt 23):5461-77.
8. Roostalu J, Thomas C, Cade NI, Kunzelmann S, Taylor IA, Surrey T. The speed of GTP hydrolysis determines GTP cap size and controls microtubule stability. *Elife*. 2020;9. pii: e51992. doi: 10.7554/eLife.51992.
9. Brouhard GJ, Rice LM. Microtubule dynamics: an interplay of biochemistry and mechanics. *Nat Rev Mol Cell Biol*. 2018;19(7):451–463. doi:10.1038/s41580-018-0009-y
10. Mitchison, T., and M. W. Kirschner. Dynamic instability of microtubule growth. *Nature*. 1984;312:237-242.
11. Roostalu J, Rickman J, Thomas C, Nédélec F, Surrey T. Determinants of Polar versus Nematic Organization in Networks of Dynamic Microtubules and Mitotic Motors. *Cell*. 2018;175(3):796–808.e14. doi:10.1016/j.cell.2018.09.029.
12. Ogawa K, Mohri T, Mohri H. Identification of dynein as the outer arms of sea urchin sperm axonemes. *Proc Natl Acad Sci U S A*. 1977;74(11):5006–5010. doi:10.1073/pnas.74.11.5006.

13. Paschal BM, Shpetner HS, Vallee RB. MAP 1C is a microtubule-activated ATPase which translocates microtubules in vitro and has dynein-like properties. *J Cell Biol.* 1987;105(3):1273–1282. doi:10.1083/jcb.105.3.1273.
14. Wickstead B, Gull K. Dyneins across eukaryotes: a comparative genomic analysis. *Traffic.* 2007;8(12):1708–1721. doi:10.1111/j.1600-0854.2007.00646.x.
15. Tovey CA, Conduit PT. Microtubule nucleation by γ -tubulin complexes and beyond. *Essays Biochem.* 2018;62(6):765–780. doi:10.1042/EBC20180028.
16. Reck-Peterson SL, Redwine WB, Vale RD, Carter AP. The cytoplasmic dynein transport machinery and its many cargoes [published correction appears in *Nat Rev Mol Cell Biol.* 2018 May 8;:]. *Nat Rev Mol Cell Biol.* 2018;19(6):382–398. doi:10.1038/s41580-018-0004-3.
17. Sladewski TE, Billington N, Ali MY, et al. Recruitment of two dyneins to an mRNA-dependent Bicaudal D transport complex. Musacchio A, Musacchio A, eds. *eLife.* 2018;7:e36306. doi:10.7554/eLife.36306.
18. Schroer TA, Sheetz MP. Two activators of microtubule-based vesicle transport. *J. Cell Biol.* 1991;115: 1309–1318.
19. Sure GR, Chatterjee A, Mishra N, et al. UNC-16/JIP3 and UNC-76/FEZ1 limit the density of mitochondria in *C. elegans* neurons by maintaining the balance of anterograde and retrograde mitochondrial transport. *Sci Rep.* 2018;8(1):8938. doi:10.1038/s41598-018-27211-9.
20. Ravichandran Y, Goud B, Manneville JB. The Golgi apparatus and cell polarity: Roles of the cytoskeleton, the Golgi matrix, and Golgi membranes. *Curr Opin Cell Biol.* 2020;62:104-113.
21. Salina D, Bodoor K, Eckley DM, Schroer TA, Rattner JB, Burke B. Cytoplasmic Dynein as a Facilitator of Nuclear Envelope Breakdown. *Cell.* 2002;108(1):97-107. doi:https://doi.org/10.1016/S0092-8674(01)00628-6.
22. Howell, B. J., McEwen, B. F., Canman, J. C., Hoffman, D. B., Farrar, E. M., Rieder, C. L. & Salmon, E. D. Cytoplasmic dynein/dynactin drives kinetochore protein transport to the spindle poles and has a role in mitotic spindle checkpoint inactivation. *J Cell Biol.* 2001;155:1159-1172. doi:10.1083/jcb.200105093.
23. Kiyomitsu T, Cheeseman IM. Cortical dynein and asymmetric membrane elongation coordinately position the spindle in anaphase [published correction appears in *Cell.* 2013 Sep 12;154(6):1401]. *Cell.* 2013;154(2):391–402. doi:10.1016/j.cell.2013.06.010.

24. Moore JK, Stuchell-Brereton MD, Cooper JA. Function of Dynein in Budding Yeast: Mitotic Spindle Positioning in a Polarized Cell. *Cell motility and the cytoskeleton*. 2009;66(8):546-555. doi:10.1002/cm.20364.
25. Schmidt H, Carter AP (2016) Review: Structure and mechanism of the dynein motor ATPase. *Biopolymers*. 2016;105(8):557–567.
26. Bell TA, Baker TA, Sauer RT. Hinge-Linker Elements in the AAA+ Protein Unfoldase ClpX Mediate Intersubunit Communication, Assembly, and Mechanical Activity. *Biochemistry*. 2018;57(49):6787-6796. doi: 10.1021/acs.biochem.8b00907.
27. Roberts AJ, Numata N, Walker ML, et al. AAA+ Ring and linker swing mechanism in the dynein motor. *Cell*. 2009;136(3):485–495. doi:10.1016/j.cell.2008.11.049
28. Burgess SA, et al. Dynein structure and power stroke. *Nature*. 2003;421(6924):715-8.
29. Nishikawa Y, Oyama T, Kamiya N, Kon T, Toyoshima YY, Nakamura H, Kurisu G. Structure of the Entire Stalk Region of the Dynein Motor Domain. *Jour Mol Biol*. 2014;426(19):3232-3245.
30. Uchimura S, Fujii T, Takazaki H, et al. A flipped ion pair at the dynein-microtubule interface is critical for dynein motility and ATPase activation. *J Cell Biol*. 2015;208(2):211–222. doi:10.1083/jcb.201407039.
31. Carter, A.P., Cho, C., Jin, L., Vale, R.D. Crystal structure of the dynein motor domain. *Science*. 2011;331(6021):1159-65.
32. Kon T, Imamula K, Roberts AJ, et al. Helix sliding in the stalk coiled coil of dynein couples ATPase and microtubule binding. *Nat Struct Mol Biol*. 2009;16(3):325–333. doi:10.1038/nsmb.1555.
33. Gibbons IR, Garbarino JE, Tan CE, Reck-Peterson SL, Vale RD, Carter AP. The affinity of the dynein microtubule-binding domain is modulated by the conformation of its coiled-coil stalk. *J Biol Chem*. 2005;280(25):23960–23965. doi:10.1074/jbc.M501636200
34. McKenney, R.J. The tail wags the motor. *Nat Chem Biol*. 2019;15:1033–1034. <https://doi.org/10.1038/s41589-019-0367-6>.
35. Harms, M. B., Ori-McKenney, K. M., Scoto, M., Tuck, E. P., Bell, S., Ma, D., Masi, S., Allred, P., Al-Lozi, M., Reilly, M. M., Miller, L. J., Jani-Acsadi, A., Pestronk, A., Shy, M. E., Muntoni, F., Vallee, R. B. & Baloh, R. H. Mutations in the tail domain of DYNC1H1 cause dominant spinal muscular atrophy. *Neurology*. 2012;78:1714-1720, doi:10.1212/WNL.0b013e3182556c05.

36. Ori-McKenney KM, Xu J, Gross SP, Vallee RB. A cytoplasmic dynein tail mutation impairs motor processivity. *Nat Cell Biol.* 2010;12(12):1228–1234. doi:10.1038/ncb2127
37. Jie J, Löhr F, Barbar E. Interactions of Yeast Dynein with Dynein Light Chain and Dynactin: General implications for intrinsically disordered duplex scaffolds in Multi Protein Assemblies. *J Biol Chem.* 2015;290(39):23863–23874. doi:10.1074/jbc.M115.649715.
38. Lee IG, Olenick MA, Boczkowska M, Franzini-Armstrong C, Holzbaur ELF, Dominguez R. A conserved interaction of the dynein light intermediate chain with dynein-dynactin effectors necessary for processivity. *Nat Commun.* 2018;9(1):986. Published 2018 Mar 7. doi:10.1038/s41467-018-03412-8.
39. Rao L, Romes EM, Nicholas MP, et al. The yeast dynein Dyn2-Pac11 complex is a dynein dimerization/processivity factor: structural and single-molecule characterization. *Mol Biol Cell.* 2013;24(15):2362–2377. doi:10.1091/mbc.E13-03-0166.
40. Nurminsky DI, Nurminskaya MV, Benevolenskaya EV, Shevelyov YY, Hartl DL, Gvozdev VA. Cytoplasmic dynein intermediate-chain isoforms with different targeting properties created by tissue-specific alternative splicing. *Mol Cell Biol.* 1998;18(11):6816–6825. doi:10.1128/mcb.18.11.6816.
41. Zhang J., Twelvetrees A.E., Lazarus J.E., Blasier K.R., Yao X., Inamdar N.A., Holzbaur E.L.F., Pfister K.K., Xiang X. Establishing a novel knock-in mouse line for studying neuronal cytoplasmic dynein under normal and pathologic conditions. *Cytoskeleton.* 2013;70:215–227.
42. Schmidt, H., Gleave, E.S., Carter, A.P. (2012). Insights into dynein motor domain function from a 3.3-Å crystal structure. *Nat. Struct. Mol. Biol.* 19(5): 492-7.
43. Carter, A. P. Crystal clear insights into how the dynein motor moves. *J Cell Sci.* 2013;126:705-713, doi:10.1242/jcs.120725.
44. Carter, A.P., Vale, R.D. Communication between the AAA+ ring and microtubule-binding domain of dynein. *Biochem Cell Biol.* 2010;88(1): 15-21.
45. Roberts AJ, Kon T, Knight PJ, Sutoh K, Burgess SA. Functions and mechanics of dynein motor proteins. *Nat Rev Mol Cell Biol.* 2013;14(11):713–726. doi:10.1038/nrm3667.
46. Imamula K, Kon T, Ohkura R, Sutoh K. The coordination of cyclic microtubule association/dissociation and tail swing of cytoplasmic dynein. *Proc Natl Acad Sci USA.* 2007;104(41):16134–16139. doi:10.1073/pnas.0702370104.

47. Vale RD, Reese TS, Sheetz MP. Identification of a novel force-generating protein, kinesin, involved in microtubule-based motility. *Cell*. 1985;42(1):39–50. doi:10.1016/s0092-8674(85)80099-4.
48. DeWitt MA, Cypranowska CA, Cleary FB, Belyy V, Yildiz A. The AAA3 domain of cytoplasmic dynein acts as a switch to facilitate microtubule release. *Nat Struct Mol Biol*. 2015;22(1):73–80. doi:10.1038/nsmb.2930.
49. Toropova, K., Mladenov, M. & Roberts, A. J. Intraflagellar transport dynein is autoinhibited by trapping of its mechanical and track-binding elements. *Nat Struct Mol Biol*. 2017;24:461-468.
50. Roberts AJ, Malkova B, Walker ML, et al. ATP-driven remodeling of the linker domain in the dynein motor. *Structure*. 2012;20(10):1670–1680. doi:10.1016/j.str.2012.07.003
51. Mizuno N, Toba S, Edamatsu M, et al. Dynein and kinesin share an overlapping microtubule-binding site. *EMBO J*. 2004;23(13):2459–2467. doi:10.1038/sj.emboj.7600240.
52. Imamula K.; Kon T.; Ohkura R, Sutoh K. *Proc Natl Acad Sci USA*. 2007;104:16134–16139.
53. Can, S., Lacey, S., Gur, M., Carter, A.P., Yildiz, A. Directionality of dynein is controlled by the angle and length of its stalk. *Nature*. 2019;566(7744): 407-410.
53. Cleary FB, Dewitt MA, Bilyard T, et al. Tension on the linker gates the ATP-dependent release of dynein from microtubules. *Nat Commun*. 2014;5:4587. doi:10.1038/ncomms5587.
54. Qiu W, Derr ND, Goodman BS, et al. Dynein achieves processive motion using both stochastic and coordinated stepping. *Nat Struct Mol Biol*. 2012;19(2):193–200. doi:10.1038/nsmb.2205.
55. Can S, Dewitt MA, Yildiz A. Bidirectional helical motility of cytoplasmic dynein around microtubules. *Elife*. 2014;3:e03205. doi:10.7554/eLife.03205.
56. DeWitt MA, Chang AY, Combs PA, Yildiz A. Cytoplasmic dynein moves through uncoordinated stepping of the AAA+ ring domains. *Science*. 2012;335(6065):221–225. doi:10.1126/science.1215804.
57. Ferro LS, Can S, Turner MA, ElShenawy MM, Yildiz A. Kinesin and dynein use distinct mechanisms to bypass obstacles. *Elife*. 2019;8:e48629. doi:10.7554/eLife.48629.

58. Gill SR, Schroer TA, Szilak I, Steuer ER, Sheetz MP, Cleveland DW. Dynactin, a conserved, ubiquitously expressed component of an activator of vesicle motility mediated by cytoplasmic dynein. *J Cell Biol.* 1991;115(6):1639–1650. doi:10.1083/jcb.115.6.1639.
59. Kardon, J. R., Reck-Peterson, S. L. & Vale, R. D. Regulation of the processivity and intracellular localization of *Saccharomyces cerevisiae* dynein by dynactin. *Proc Natl Acad Sci USA.* 2009;106;5669-5674.
60. Zhang J, Qiu R, Xiang X. The actin capping protein in *Aspergillus nidulans* enhances dynein function without significantly affecting Arp1 filament assembly. *Sci Rep.* 2018;8(1):11419. Published 2018 Jul 30. doi:10.1038/s41598-018-29818-4.
61. Urnavicius, L., Zhang, K., Diamant, A.G., Motz, C., Schlager, M.A., Yu, M., Patel, N.A., Robinson, C.V., Carter, A.P. The structure of the dynactin complex and its interaction with dynein. *Science.* 2015;347(6229): 1441-1446.
62. Qiu R, Zhang J, Xiang X. p25 of the dynactin complex plays a dual role in cargo binding and dynactin regulation. *J Biol Chem.* 2018;293(40):15606–15619. doi:10.1074/jbc.RA118.004000.
63. Carter, A.P., Diamant, A.G., Urnavicius, L. How dynein and dynactin transport cargos: a structural perspective. *Curr Opin Struct Biol.* 2016;37:62-70.
64. Burkhardt JK, Echeverri CJ, Nilsson T, Vallee RB. Overexpression of the dynamitin (p50) subunit of the dynactin complex disrupts dynein-dependent maintenance of membrane organelle distribution. *J Cell Biol.* 1997;139(2):469–484. doi:10.1083/jcb.139.2.469.
65. Yu, J., Lai, C., Shim, H. et al. Genetic ablation of dynactin p150Glued in postnatal neurons causes preferential degeneration of spinal motor neurons in aged mice. *Mol Neurodegeneration.* 2018;13(10). <https://doi.org/10.1186/s13024-018-0242-z>.
66. Eshel D, Urrestarazu LA, Vissers S, Jauniaux JC, van Vliet-Reedijk JC, Planta RJ, Gibbons IR. Cytoplasmic dynein is required for normal nuclear segregation in yeast. *Proc Natl Acad Sci USA.* 1993; 90(23):11172-6.
67. Tokito MK, Howland DS, Lee VM, Holzbaur EL. Functionally distinct isoforms of dynactin are expressed in human neurons. *Mol Biol Cell.* 1996;7(8):1167–1180. doi:10.1091/mbc.7.8.1167
68. Kim H, Ling SC, Rogers GC, et al. Microtubule binding by dynactin is required for microtubule organization but not cargo transport. *J Cell Biol.* 2007;176(5):641–651. doi:10.1083/jcb.200608128

69. McKenney, R. J., Huynh, W., Vale, R. D. & Sirajuddin, M. Tyrosination of alpha-tubulin controls the initiation of processive dynein-dynactin motility. *EMBO Jour.* 2016;35:1175-1185.
70. Tripathy SK, Weil SJ, Chen C, Anand P, Vallee RB, Gross SP. Autoregulatory mechanism for dynactin control of processive and diffusive dynein transport. *Nat Cell Biol.* 2014;16(12):1192–1201. doi:10.1038/ncb3063.
71. Gicking AM, Qiu W, Hancock WO. Mitotic kinesins in action: diffusive searching, directional switching, and ensemble coordination. *Mol Biol Cell.* 2018;29(10):1153–1156. doi:10.1091/mbc.E17-10-0612.
72. Moore, J. K., Sept, D. & Cooper, J. A. Neurodegeneration mutations in dynactin impair dynein-dependent nuclear migration. *Proc Natl Acad Sci USA.* 2009;106:5147-5152.
73. Collins ES, Balchand SK, Faraci JL, Wadsworth P, Lee W-L. Cell cycle-regulated cortical dynein/dynactin promotes symmetric cell division by differential pole motion in anaphase. *Molecular Biology of the Cell.* 2012;23(17):3380-3390. doi:10.1091/mbc.E12-02-0109.
74. Moore, J. K., Li, J. & Cooper, J. A. Dynactin function in mitotic spindle positioning. *Traffic.* 2008;9: 510-527.
75. Hammesfahr B, Kollmar M. Evolution of the eukaryotic dynactin complex, the activator of cytoplasmic dynein. *BMC Evol Biol.* 2012;12:95. doi:10.1186/1471-2148-12-95.
76. Kahana JA, Schlenstedt G, Evanchuk DM, Geiser JR, Hoyt MA, Silver PA. The yeast dynactin complex is involved in partitioning the mitotic spindle between mother and daughter cells during anaphase B. *Mol Biol Cell.* 1998;9(7):1741–1756. doi:10.1091/mbc.9.7.1741.
77. Clark SW, Rose MD. Arp10p is a pointed-end-associated component of yeast dynactin. *Mol Biol Cell.* 2006;17(2):738–748. doi:10.1091/mbc.e05-05-0449.
78. Eckley DM, Gill SR, Melkonian KA, Bingham JB, Goodson HV, Heuser JE, Schroer TA. Analysis of dynactin subcomplexes reveals a novel actin-related protein associated with the Arp1 minifilament pointed end. *J Cell Biol.* 1999;147:307–320.
79. Clark SW, Rose MD. Alanine scanning of Arp1 delineates a putative binding site for Jnm1/dynamitin and Nip100/p150glued. *Mol Biol Cell.* 2005;9:3999–4012.
80. Kahana JA, Schlenstedt G, Evanchuk DM, Geiser JR, Hoyt MA, Silver PA. The yeast dynactin complex is involved in partitioning the mitotic spindle between mother and daughter cells during anaphase B. *Mol Biol Cell.* 1998;9:1741–1756.

81. Estrem C, Moore JK. Astral microtubule forces alter nuclear organization and inhibit DNA repair in budding yeast. *Mol Biol Cell*. 2019;30(16):2000–2013. doi:10.1091/mbc.E18-12-0808.
82. Yao X, Zhang J, Zhou H, Wang E, Xiang X. In vivo roles of the basic domain of dynactin p150 in microtubule plus-end tracking and dynein function. *Traffic*. 2012;13(3):375–387.
83. Markus SM, Kalutkiewicz KA, Lee WL. She1-mediated inhibition of dynein motility along astral microtubules promotes polarized spindle movements. *Curr Biol*. 2012;22(23):2221–2230. doi:10.1016/j.cub.2012.10.017.
84. Markus, S. M. & Lee, W. L. Regulated offloading of cytoplasmic dynein from microtubule plus ends to the cortex. *Dev Cell*. 2011;20:639-651.
85. Lammers, L. G. & Markus, S. M. The dynein cortical anchor Num1 activates dynein motility by relieving Pac1/LIS1-mediated inhibition. *J Cell Biol*. 2015;211:309-322.
86. McKenney, R. J., Huynh, W., Tanenbaum, M. E., Bhabha, G. & Vale, R. D. Activation of cytoplasmic dynein motility by dynactin-cargo adapter complexes. *Science*. 2014;345:337-341.
87. Schlager MA, Hoang HT, Urnavicius L, Bullock SL, Carter AP. In vitro reconstitution of a highly processive recombinant human dynein complex. *The EMBO Journal*. 2014;33(17):1855-1868. doi:10.15252/embj.201488792.
88. Redwine WB, DeSantis ME, Hollyer I, et al. The human cytoplasmic dynein interactome reveals novel activators of motility. *Elife*. 2017;6:e28257. doi:10.7554/eLife.28257.
89. Bloom K. Nuclear migration: cortical anchors for cytoplasmic dynein. *Curr Biol*. 2001;11:R326–9.
90. Kotak, S., Busso, C. & Gonczy, P. Cortical dynein is critical for proper spindle positioning in human cells. *J. Cell Biol*. 2012;199:97–110.
91. Tang X, Punch JJ, Lee WL. A CAAX motif can compensate for the PH domain of Num1 for cortical dynein attachment. *Cell Cycle*. 2009;8(19):3182–3190. doi:10.4161/cc.8.19.9731.
92. Pirovano L, Culurgioni S, Carminati M, et al. Hexameric NuMA:LGN structures promote multivalent interactions required for planar epithelial divisions. *Nat Commun*. 2019;10(1):2208. doi:10.1038/s41467-019-09999-w.

93. Grotjahn DA, Chowdhury S, Xu Y, McKenney RJ, Schroer TA, Lander GC. Cryo-electron tomography reveals that dynactin recruits a team of dyneins for processive motility [published correction appears in *Nat Struct Mol Biol*. 2018 Feb 23]. *Nat Struct Mol Biol*. 2018;25(3):203–207. doi:10.1038/s41594-018-0027-7
94. Urnavicius, L., Lau, C.K., Elshenawy, M.M., Morales-Rios, E., Motz, C., Yildiz, A., Carter, A.P. Cryo-EM shows how dynactin recruits two dyneins for faster movement. *Nature*. 2018;554(7691):202-206.
95. Jha, R., Roostalu, J., Cade, N. I., Trokter, M. & Surrey, T. Combinatorial regulation of the balance between dynein microtubule end accumulation and initiation of directed motility. *EMBO J*. 2017;36:3387-3404.
96. Baumbach J, Murthy A, McClintock MA, et al. Lissencephaly-1 is a context-dependent regulator of the human dynein complex. *Elife*. 2017;6:e21768. doi:10.7554/eLife.21768.
97. Elshenawy MM, Canty JT, Oster L, Ferro LS, Zhou Z, Blanchard SC, Yildiz A. Cargo adaptors regulate stepping and force generation of mammalian dynein-dynactin. *Nat Chem Biol*. 2019;15(11):1093-1101. doi: 10.1038/s41589-019-0352-0.
98. Markus SM, Lee WL. Microtubule-dependent path to the cell cortex for cytoplasmic dynein in mitotic spindle orientation. *Bioarchitecture*. 2011;1(5):209–215. doi:10.4161/bioa.18103.
99. Markus SM, Plevock KM, St Germain BJ, Punch JJ, Meaden CW, Lee WL. Quantitative analysis of Pac1/LIS1-mediated dynein targeting: Implications for regulation of dynein activity in budding yeast. *Cytoskeleton (Hoboken)*. 2011;68(3):157–174. doi:10.1002/cm.20502.
100. Caudron F, Andrieux A, Job D, Boscheron C. A new role for kinesin-directed transport of Bik1p (CLIP-170) in *Saccharomyces cerevisiae*. *J Cell Sci*. 2008 May 1; 121(Pt 9):1506-13.
101. Roberts AJ, Goodman BS, Reck-Peterson SL. Reconstitution of dynein transport to the microtubule plus end by kinesin. *eLife*. 2014;3:e02641 .
102. Coquelle, F. M. et al. LIS1, CLIP-170's key to the dynein/dynactin pathway. *Mol Cell Biol*. 2002;22:3089-3102.
103. Schmidt R, Fielmich LE, Grigoriev I, Katrukha EA, Akhmanova A, van den Heuvel S. Two populations of cytoplasmic dynein contribute to spindle positioning in *C. elegans* embryos. *J Cell Biol*. 2017;216(9):2777–2793. doi:10.1083/jcb.201607038.

104. Carvalho P, Gupta ML, Jr., Hoyt MA, Pellman D. Cell cycle control of kinesin-mediated transport of Bik1 (CLIP-170) regulates microtubule stability and dynein activation. *Dev Cell*. 2004;6:815–829.
105. Huang, J., Roberts, A. J., Leschziner, A. E. & Reck-Peterson, S. L. Lis1 acts as a "clutch" between the ATPase and microtubule-binding domains of the dynein motor. *Cell* 150, 975-986, (2012).
106. Toropova K, Zou S, Roberts AJ, et al. Lis1 regulates dynein by sterically blocking its mechanochemical cycle. *Elife*. 2014;3:e03372. doi:10.7554/eLife.03372
107. DeSantis, M. E. et al. Lis1 Has Two Opposing Modes of Regulating Cytoplasmic Dynein. *Cell*. 2017;170:1197-1208 e1112.
108. Mesngon MT, Tarricone C, Hebbar S, Guillotte AM, Schmitt EW, Lanier L, Musacchio A, King SJ, Smith DS. Regulation of cytoplasmic dynein ATPase by Lis1. *J Neurosci*. 2006;26(7):2132-9. doi: 10.1523/JNEUROSCI.5095-05.2006.
109. Lee WL, Oberle JR, Cooper JA. The role of the lissencephaly protein Pac1 during nuclear migration in budding yeast. *J Cell Biol*. 2003;160(3):355–364. doi:10.1083/jcb.200209022.
110. Wang S, Ketcham SA, Schön A, Goodman B, Wang Y, Yates J, Freire E, Schroer TA, Zheng Y. Nudel/NudE and Lis1 promote dynein and dynactin interaction in the context of spindle morphogenesis. *Mol Biol Cell*. 2013;24(22):3522-33. doi: 10.1091/mbc.E13-05-0283.
111. Gutierrez, P. A., Ackermann, B. E., Vershinin, M. & McKenney, R. J. Differential effects of the dynein-regulatory factor Lissencephaly-1 on processive dynein-dynactin motility. *J Biol Chem*. 2017;292:12245-12255.
112. Xiang X, Osmani AH, Osmani SA, Xin M, Morris NR. NudF, a nuclear migration gene in *Aspergillus nidulans*, is similar to the human LIS-1 gene required for neuronal migration. *Mol Biol Cell*. 1995;6(3):297–310. doi:10.1091/mbc.6.3.297
113. Han G, Liu B, Zhang J, Zuo W, Morris NR, Xiang X. The *Aspergillus* cytoplasmic dynein heavy chain and NUDF localize to microtubule ends and affect microtubule dynamics. *Curr Biol*. 2001;11(9):719-24.
114. Efimov VP, Zhang J, Xiang X. CLIP-170 homologue and NUDE play overlapping roles in NUDF localization in *Aspergillus nidulans*. *Mol Biol Cell*. 2006;17(4):2021–2034. doi:10.1091/mbc.e05-11-1084.
115. Egan MJ, Tan K, Reck-Peterson SL. Lis1 is an initiation factor for dynein-driven organelle transport. *J Cell Biol*. 2012;197(7):971–982. doi:10.1083/jcb.201112101.

116. Twelvetrees AE, Pernigo S, Sanger A, et al. The Dynamic Localization of Cytoplasmic Dynein in Neurons Is Driven by Kinesin-1. *Neuron*. 2016;90(5):1000–1015. doi:10.1016/j.neuron.2016.04.046.
117. Roy S. Seeing the unseen: the hidden world of slow axonal transport. *Neuroscientist*. 2014;20:71-81.
118. Yi JY, Ori-McKenney KM, McKenney RJ, Vershinin M, Gross SP, Vallee RB. High-resolution imaging reveals indirect coordination of opposite motors and a role for LIS1 in high-load axonal transport. *The Journal of Cell Biology*. 2011;195(2):193-201. doi:10.1083/jcb.201104076.
119. Poirier, K., Lebrun, N., Broix, L., Tian, G., Saillour, Y., Boscheron, C., Parrini, E., Valence, S., Pierre, B. S., Oger, M., Lacombe, D., Genevieve, D., Fontana, E., Darra, F., Cances, C., Barth, M., Bonneau, D., Bernadina, B. D., N'Guyen, S., Gitiaux, C., Parent, P., des Portes, V., Pedespan, J. M., Legrez, V., Castelnau-Ptakine, L., Nitschke, P., Hieu, T., Masson, C., Zelenika, D., Andrieux, A., Francis, F., Guerrini, R., Cowan, N. J., Bahi-Buisson, N. & Chelly, J. Mutations in TUBG1, DYNC1H1, KIF5C and KIF2A cause malformations of cortical development and microcephaly. *Nat Genetics*. 2013;45:639-647. doi:10.1038/ng.2613.
120. Harms, M. B., Ori-McKenney, K. M., Scoto, M., Tuck, E. P., Bell, S., Ma, D., Masi, S., Allred, P., Al-Lozi, M., Reilly, M. M., Miller, L. J., Jani-Acsadi, A., Pestronk, A., Shy, M. E., Muntoni, F., Vallee, R. B. & Baloh, R. H. Mutations in the tail domain of DYNC1H1 cause dominant spinal muscular atrophy. *Neurology*. 2012;78:1714-1720, doi:10.1212/WNL.0b013e3182556c05.
121. Villarin JM, Hengst U, et al. Local synthesis of dynein cofactors matches retrograde transport to acutely changing demands. *Nature Comm*. 2016;7:13865. doi: 10.1038/ncomms13865.
122. Hendricks, A. G., Perlson, E., Ross, J. L., Schroeder, H. W., 3rd, Tokito, M. & Holzbaaur, E. L. Motor coordination via a tug-of-war mechanism drives bidirectional vesicle transport. *Curr Biol*. 2010;20:697-702. doi:10.1016/j.cub.2010.02.058.
123. Horak, M., Petralia, R. S., Kaniakova, M. & Sans, N. ER to synapse trafficking of NMDA receptors. *Front Cell Neurosci*. 2014;8:394, doi:10.3389/fncel.2014.00394.
124. Vilmont, V., Cadot, B., Vezin, E. et al. Dynein disruption perturbs post-synaptic components and contributes to impaired MuSK clustering at the NMJ: implication in ALS. *Sci Rep*. 2016;6:27804. <https://doi.org/10.1038/srep27804>
125. Schapitz IU, Behrend B, Pechmann Y, Lappe-Siefke C, Kneussel SJ, Wallace KE, Stempel AV, Buck F, Grant SG, Schweizer M, et al. Neuroligin 1 is dynamically exchanged at postsynaptic sites. *J Neurosci*. 2010;30:12733–12744.

126. Rao, A. N., Patil, A., Black, M. M., Craig, E. M., Myers, K. A., Yeung, H. T. & Baas, P. W. Cytoplasmic Dynein Transports Axonal Microtubules in a Polarity-Sorting Manner. *Cell Rep.* 2017;19:2210-2219, doi:10.1016/j.celrep.2017.05.064.
127. Del Castillo U, Winding M, Lu W, Gelfand VI. Interplay between kinesin-1 and cortical dynein during axonal outgrowth and microtubule organization in *Drosophila* neurons. Allan V, ed. *eLife.* 2015;4:e10140. doi:10.7554/eLife.10140.
128. Grabham, P. W., Seale, G. E., Bennechib, M., Goldberg, D. J. & Vallee, R. B. Cytoplasmic dynein and LIS1 are required for microtubule advance during growth cone remodeling and fast axonal outgrowth. *J Neurosci.* 2007;27:5823-5834, doi:10.1523/JNEUROSCI.1135-07.2007.
129. Nirschl JJ, Ghiretti AE, Holzbaaur ELF. The impact of cytoskeletal organization on the local regulation of neuronal transport. *Nat Rev Neurosci.* 2017;18(10):585–597. doi:10.1038/nrn.2017.100.
130. Fu, M. M. & Holzbaaur, E. L. JIP1 regulates the directionality of APP axonal transport by coordinating kinesin and dynein motors. *J Cell Biol.* 2013;202:495-508. doi:10.1083/jcb.201302078.
131. Tanenbaum, M. E., Vale, R. D., & McKenney, R. J. (2013). Cytoplasmic dynein crosslinks and slides anti-parallel microtubules using its two motor domains. *ELife*, 2013(2). <https://doi.org/10.7554/eLife.00943>.
132. Grill SW, Hyman AA. Spindle positioning by cortical pulling forces. *Dev Cell.* 2005; 8(4):461-5.
133. Hu DJ-K, Baffet AD, Nayak T, Akhmanova A, Doye V, Vallee RB. Dynein recruitment to nuclear pores activates apical nuclear migration and mitotic entry in brain progenitor cells. *Cell.* 2013;154(6):10.1016/j.cell.2013.08.024. doi:10.1016/j.cell.2013.08.024.
134. Tsai, J. W., Bremner, K. H. & Vallee, R. B. Dual subcellular roles for LIS1 and dynein in radial neuronal migration in live brain tissue. *Nat Neurosci.* 2007;10:970-979.
135. Tsai J-W, Lian W-N, Kemal S, Kriegstein A, Vallee RB. An Unconventional Kinesin and Cytoplasmic Dynein Are Responsible for Interkinetic Nuclear Migration in Neural Stem Cells. *Nature neuroscience.* 2010;13(12):1463-1471. doi:10.1038/nn.2665.
136. Del Bene F. Interkinetic nuclear migration: cell cycle on the move [published correction appears in *EMBO J.* 2011;30(12):2510]. *EMBO J.* 2011;30(9):1676–1677. doi:10.1038/emboj.2011.114

137. Tsai, J. W., Chen, Y., Kriegstein, A. R. & Vallee, R. B. LIS1 RNA interference blocks neural stem cell division, morphogenesis, and motility at multiple stages. *J Cell Biol.* 2005;170:935-945.
138. Will L, Portegies S, van Schelt J, van Luyk M, Jaarsma D, Hoogenraad CC. Dynein activating adaptor BICD2 controls radial migration of upper-layer cortical neurons in vivo. *Acta Neuropathol Commun.* 2019;7(1):162. Published 2019 Oct 26. doi:10.1186/s40478-019-0827-y.
139. Hakanen J, Ruiz-Reig N, Tissir F. Linking Cell Polarity to Cortical Development and Malformations. *Front Cell Neurosci.* 2019;13:244. doi:10.3389/fncel.2019.00244.
140. Youn YH, Pramparo T, Hirotsune S, Wynshaw-Boris A. Distinct dose-dependent cortical neuronal migration and neurite extension defects in Lis1 and Ndel1 mutant mice. *J Neurosci.* 2009;29(49):15520–15530. doi:10.1523/JNEUROSCI.4630-09.2009.
141. Reiner O, et al. Isolation of a Miller–Dicker lissencephaly gene containing G protein β -subunit-like repeats. *Nature.* 1993;364:717–721.
142. Marchionni E, Méneret A, Keren B, et al. KIF1C Variants Are Associated with Hypomyelination, Ataxia, Tremor, and Dystonia in Fraternal Twins. *Tremor Other Hyperkinet Mov (N Y).* 2019;9:10.7916/tohm.v0.641. doi:10.7916/tohm.v0.641.
143. Scoto M, Rossor AM, Harms MB, et al. Novel mutations expand the clinical spectrum of DYNC1H1-associated spinal muscular atrophy. *Neurology.* 2015;84(7):668–679. doi:10.1212/WNL.0000000000001269.
144. Willemsen, M. H. et al. Mutations in DYNC1H1 cause severe intellectual disability with neuronal migration defects. *Jour of Med Genet.* 2012;49:179-183, (2012).
145. Peeters, K., Bervoets, S., Chamova, T., Litvinenko, I., De Vriendt, E., Bichev, S., Kancheva, D., Mitev, V., Kennerson, M., Timmerman, V., De Jonghe, P., Tournev, I., MacMillan, J. & Jordanova, A. Novel mutations in the DYNC1H1 tail domain refine the genetic and clinical spectrum of dyneinopathies. *Human mutation.* 2015;36(3):287-91. doi: 10.1002/humu.22744.
146. Laquerriere A, Maillard C, Cavallin M, Chapon F, Marguet F, Molin A, Sigaudy S, Blouet M, Benoist G, Fernandez C, Poirier K, Chelly J, Thomas S, Bahi-Buisson N. Neuropathological Hallmarks of Brain Malformations in Extreme Phenotypes Related to DYNC1H1 Mutations. *J Neuropathol Exp Neurol.* 2017;76(3):195-205. doi:10.1093/jnen/nlw124.
147. Tsurusaki, Y., Saitoh, S., Tomizawa, K., Sudo, A., Asahina, N., Shiraishi, H., Ito, J., Tanaka, H., Doi, H., Saito, H., Miyake, N. & Matsumoto, N. A DYNC1H1 mutation causes a dominant spinal muscular atrophy with lower extremity predominance. *Neurogenetics.* 2012;13:327-332. doi:10.1007/s10048-012-0337-6 (2012).

148. Weedon, M. N., Hastings, R., Caswell, R., Xie, W., Paszkiewicz, K., Antoniadis, T., Williams, M., King, C., Greenhalgh, L., Newbury-Ecob, R. & Ellard, S. Exome sequencing identifies a DYNC1H1 mutation in a large pedigree with dominant axonal Charcot-Marie-Tooth disease. *American journal of human genetics*. 2011;89:308-312. doi:10.1016/j.ajhg.2011.07.002.
149. Vissers, L. E., de Ligt, J., Gilissen, C., Janssen, I., Steehouwer, M., de Vries, P., van Lier, B., Arts, P., Wieskamp, N., del Rosario, M., van Bon, B. W., Hoischen, A., de Vries, B. B., Brunner, H. G. & Veltman, J. A. A de novo paradigm for mental retardation. *Nature genetics*. 2010;42:1109-1112. doi:10.1038/ng.712.
150. Fiorillo, C., Moro, F., Yi, J., Weil, S., Brisca, G., Astrea, G., Severino, M., Romano, A., Battini, R., Rossi, A., Minetti, C., Bruno, C., Santorelli, F. M. & Vallee, R. Novel dynein DYNC1H1 neck and motor domain mutations link distal spinal muscular atrophy and abnormal cortical development. *Human mutation*. 2014;35:298-302. doi:10.1002/humu.22491.
151. Strickland, A. V., Schabhuhtl, M., Offenbacher, H., Synofzik, M., Hauser, N. S., Brunner-Krainz, M., Gruber-Sedlmayr, U., Moore, S. A., Windhager, R., Bender, B., Harms, M., Klebe, S., Young, P., Kennerson, M., Garcia, A. S., Gonzalez, M. A., Zuchner, S., Schule, R., Shy, M. E. & Auer-Grumbach, M. Mutation screen reveals novel variants and expands the phenotypes associated with DYNC1H1. *J Neurol*. 2015;262:2124-2134. doi:10.1007/s00415-015-7727-2.
152. Monroy BY, Sawyer DL, Ackermann BE, Borden MM, Tan TC, Ori-McKenney KM. Competition between microtubule-associated proteins directs motor transport. *Nat Commun*. 2018;9(1):1487. doi:10.1038/s41467-018-03909-2.
153. Ramkumar A, Jong BY, Ori-McKenney KM. ReMAPping the microtubule landscape: How phosphorylation dictates the activities of microtubule-associated proteins. *Dev Dyn*. 2018;247(1):138–155. doi:10.1002/dvdy.24599
154. Schiavo G, Greensmith L, Hafezparast M, Fisher EM. Cytoplasmic dynein heavy chain: the servant of many masters. *Trends Neurosci*. 2013;36(11):641–651. doi:10.1016/j.tins.2013.08.001
155. S. Ilieva, HS et al. Mutant dynein (Loa) triggers proprioceptive axon loss that extends survival only in the SOD1 ALS model with highest motor neuron death. *PNAS*. 2008;105(34):12599-12604. DOI:10.1073/pnas.0805422105
156. Harada A, Takei Y, Kanai Y, Tanaka Y, Nonaka S, Hirokawa N. Golgi vesiculation and lysosome dispersion in cells lacking cytoplasmic dynein. *J Cell Biol*. 1998;141(1):51–59. doi:10.1083/jcb.141.1.51

157. Kamal, A., Stokin, G. B., Yang, Z., Xia, C. H. & Goldstein, L. S. Axonal transport of amyloid precursor protein is mediated by direct binding to the kinesin light chain subunit of kinesin-I. *Neuron*. 2000;28:449-459.
158. Bamburg JR, Bernstein BW. Actin dynamics and cofilin-actin rods in alzheimer disease. *Cytoskeleton (Hoboken)*. 2016;73(9):477–497. doi:10.1002/cm.21282.
159. Hattori M, et al. Miller-Dieker lissencephaly gene encodes a subunit of brain platelet-activating factor acetylhydrolase [corrected]. *Nature*. 1994;21;370(6486):216-8.
160. Reck-Peterson, S. L., Yildiz, A., Carter, A. P., Gennerich, A., Zhang, N. & Vale, R. D. Single-molecule analysis of dynein processivity and stepping behavior. *Cell*. 2006;126:335-348.
161. Reck-Peterson SL, Vale RD. Molecular dissection of the roles of nucleotide binding and hydrolysis in dynein's AAA domains in *Saccharomyces cerevisiae*. *Proceedings of the National Academy of Sciences of the United States of America*. 2004;101(6):1491-1495. doi:10.1073/pnas.2637011100.
162. Cho C, Reck-Peterson SL, Vale RD. Regulatory ATPase Sites of Cytoplasmic Dynein Affect Processivity and Force Generation. *The Journal of Biological Chemistry*. 2008;283(38):25839-25845. doi:10.1074/jbc.M802951200.
163. Ecklund KH, Morisaki T, Lammers LG, Marzo MG, Stasevich TJ, and Markus SM. She1 affects dynein through direct interactions with the microtubule and the dynein microtubule-binding domain. *Nature Communications*. 2017;8:2151.
164. Hoang HT, Schlager MA, Carter AP, Bullock SL. DYNC1H1 mutations associated with neurological diseases compromise processivity of dynein–dynactin–cargo adaptor complexes. *PNAS USA*. 2017;114(9):E1597-E1606. doi:10.1073/pnas.1620141114.
165. Zhang K, Foster HE, Rondelet A, et al. Cryo-EM Reveals How Human Cytoplasmic Dynein Is Auto-inhibited and Activated. *Cell*. 2017;169(7):1303–1314.e18. doi:10.1016/j.cell.2017.05.025
166. Qiu, R., Zhang, J. & Xiang, X. LIS1 regulates cargo-adaptor-mediated activation of dynein by overcoming its autoinhibition in vivo. *J Cell Biol*. 2019;218(11):3630-3646. doi: 10.1083/jcb.201905178.
167. Mohamed M. Elshenawy, E. K., Sara Volz, Janina Baumbach, Simon L. Bullock, Ahmet Yildiz. Lis1 activates dynein motility by pairing it with dynactin. *bioRxiv*. 2019.
168. Zaw Min Htet, J. P. G., Richard W. Baker, Andres E. Leschziner, Morgan E. DeSantis, Samara L. Reck-Peterson. Lis1 promotes the formation of maximally activated cytoplasmic dynein-1 complexes. *bioRxiv*. 2019.

169. Marzo MG, Griswold JR, Markus SM. Pac1/Lis1 stabilizes an open conformation of dynein which coordinates its localization and activity. *Nat Cell Biol.* 2020 (in press).
170. Sako Y, Ninomiya K, Okuno Y, et al. Development of an orally available inhibitor of CLK1 for skipping a mutated dystrophin exon in Duchenne muscular dystrophy. *Sci Rep.* 2017;7:46126. doi:10.1038/srep46126
171. Schroeder, C. M. & Vale, R. D. Assembly and activation of dynein-dynactin by the cargo adaptor protein Hook3. *J. Cell Biol.* 2016;214:309–318.
172. Hutchins JR, et al. Systematic analysis of human protein complexes identifies chromosome segregation proteins. *Science.* 2010;328:593–599.
173. Schaedel L, Triclin S, Chrétien D, et al. Lattice defects induce microtubule self-renewal. *Nat Phys.* 2019;15(8):830–838. doi:10.1038/s41567-019-0542-4.
174. Miller RK, Rose MD. Kar9p is a novel cortical protein required for cytoplasmic microtubule orientation in yeast. *J Cell Biol.* 1998;140(26):377-90.
175. Yamada M, Toba S, Yoshida Y, et al. LIS1 and NDEL1 coordinate the plus-end-directed transport of cytoplasmic dynein. *EMBO J.* 2008;27(19):2471–2483. doi:10.1038/emboj.2008.182.
176. Fu MM, Nirschl JJ, Holzbaur ELF. LC3 binding to the scaffolding protein JIP1 regulates processive dynein-driven transport of autophagosomes. *Dev Cell.* 2014;29(5):577-590.
177. Bi E, Pringle JR. ZDS1 and ZDS2, genes whose products may regulate Cdc42p in *Saccharomyces cerevisiae*. *Mol Cell Biol.* 1996;16(10):5264–5275. doi:10.1128/mcb.16.10.5264.
178. Knop, Michael, et al. “Epitope Tagging of Yeast Genes Using a PCR-Based Strategy: More Tags and Improved Practical Routines.” *Yeast.* 1999;15(10B):963–972. doi:10.1002/(sici)1097-0061(199907)15:10b<963::aid-yea399>3.0.co;2-w.
179. Longtine MS, et al. Additional modules for versatile and economical PCR-based gene deletion and modification in *Saccharomyces cerevisiae*. *Yeast.* 1998;14(10):953-61.
180. Markus, Steven M., et al. Improved Plasmids for Fluorescent Protein Tagging of Microtubules In *Saccharomyces Cerevisiae*. *Traffic.* 2015;16(7);773–786. doi:10.1111/tra.12276.
181. Song S, Lee KS. A novel function of *Saccharomyces cerevisiae* CDC5 in cytokinesis. *J Cell Biol.* 2001;152(3):451–469. doi:10.1083/jcb.152.3.451

182. Kushnirov, Vitaly. (2000). Kushnirov, V.V. Rapid and reliable protein extraction from yeast. *Yeast*. 2000;16;857-60.
183. CD Nicholls, KG McLure, MA Shields, PW Lee. Biogenesis of p53 involves cotranslational dimerization of monomers and posttranslational dimerization of dimers. implications on the dominant negative effect. *Jour Biol Chem*. 2002;277:12937–12945. <https://doi.org/10.1074/jbc.M108815200>.
184. Chen X, Widmer LA, Stangier MM, Steinmetz MO, Stelling J, Barral Y. Remote control of microtubule plus-end dynamics and function from the minus-end. *Elife*. 2019;8:e48627. doi:10.7554/eLife.48627.
185. Seiler S, et al. Cargo binding and regulatory sites in the tail of fungal conventional kinesin. *Nat Cell Biol*. 2000; 2:333-338.
186. Kaan HY, Hackney DD, Kozielski F. The structure of the kinesin-1 motor-tail complex reveals the mechanism of autoinhibition. *Science*. 2011;333(6044):883–885. doi:10.1126/science.1204824.
187. Shimo T, Maruyama R, Yokota T. Designing Effective Antisense Oligonucleotides for Exon Skipping. *Methods Mol Biol*. 2018;1687:143-155.
188. Milton DL, Schneck AN, Ziech DA, et al. Direct evidence for functional smooth muscle myosin II in the 10S self-inhibited monomeric conformation in airway smooth muscle cells. *Proc Natl Acad Sci U S A*. 2011;108(4):1421–1426. doi:10.1073/pnas.1011784108.
189. Siddiqui N, Zwetsloot AJ, Bachmann A, Roth D, Hussain H, Brandt J, Kaverina I, Straube A. PTPN1 and Hook3 relieve KIF1C autoinhibition and activate intracellular transport. *Nat Comm*. 2019;10(2693).
190. Trokter M, Mücke N, Surrey T. Reconstituted dynein. *PNAS*. 2012;109(51):20895-20900; DOI:10.1073/pnas.1210573110.
191. Torisawa T, Ichikawa M, Furuta A, Saito K, Oiwa K, Kojima H, Toyoshima YY, Furuta K. Autoinhibition and cooperative activation mechanisms of cytoplasmic dynein. *Nat Cell Biol*. 2014;16(11):1118-24. doi: 10.1038/ncb3048.
192. Amos L.A. Brain dynein crossbridges microtubules into bundles. *J. Cell Sci*. 1989;93:19–28.
193. Marzo MG, Griswold JM, Ruff KM, Buchmeier RE, Fees CP, Markus SM. Molecular basis for dyneinopathies reveals insight into dynein regulation and dysfunction. *Elife*. 2019;8:e47246. doi:10.7554/eLife.47246.

194. Markus SM, Punch JJ, Lee WL. Motor- and tail-dependent targeting of dynein to microtubule plus ends and the cell cortex. *Curr Biol.* 2009;19(3):196–205. doi:10.1016/j.cub.2008.12.047.
195. Weissmann, F. et al. biGBac enables rapid gene assembly for the expression of large multisubunit protein complexes. *Proc Natl Acad Sci USA.* 2016;113:E2564-2569, (2016).
196. Curran, K. A. et al. Short Synthetic Terminators for Improved Heterologous Gene Expression in Yeast. *ACS Synth Biol.* 2015;4:824-832.
197. Gibson, D. G. et al. Enzymatic assembly of DNA molecules up to several hundred kilobases. *Nat Methods.* 2018; 6:343-345.
198. Mahamdeh, M., Simmert, S., Luchniak, A., Schaffer, E. & Howard, J. Label-free high-speed wide-field imaging of single microtubules using interference reflection microscopy. *J Microsc.* 2018;272:60-66.
200. Stellwagen, E., Prantner, J. D. & Stellwagen, N. C. Do zwitterions contribute to the ionic strength of a solution? *Anal Biochem.* 2008;373:407-409.
201. Monda JK, Cheeseman IM. Dynamic regulation of dynein localization revealed by small molecule inhibitors of ubiquitination enzymes. *Open Biol.* 2018;8(9):180095. doi:10.1098/rsob.180095.
202. Monda JK, Cheeseman IM. Nde1 promotes diverse dynein functions through differential interactions and exhibits an isoform-specific proteasome association. *Mol Biol Cell.* 2018;29(19):2336–2345. doi:10.1091/mbc.E18-07-0418.
203. Gennerich A, Carter AP, Reck-Peterson SL, Vale RD. Force-induced bidirectional stepping of cytoplasmic dynein. *Cell.* 2007;131(5):952–965. doi:10.1016/j.cell.2007.10.016.
204. McKenney RJ, Vershinin M, Kunwar A, Vallee RB, Gross SP. LIS1 and NudE induce a persistent dynein force-producing state. *Cell.* 2010;141(2):304–314. doi:10.1016/j.cell.2010.02.035.
205. Li J, Lee WL, Cooper JA. NudEL targets dynein to microtubule ends through LIS1. *Nat Cell Biol.* 2005;7(7):686–690. doi:10.1038/ncb1273.
206. Hueschen CL, Kenny SJ, Xu K, Dumont S. NuMA recruits dynein activity to microtubule minus-ends at mitosis. *Elife.* 2017;6:e29328. Published 2017 Nov 29. doi:10.7554/eLife.29328

207. Moon HM, Hippenmeyer S, Luo L, Wynshaw-Boris A. LIS1 determines cleavage plane positioning by regulating actomyosin-mediated cell membrane contractility. *bioRxiv* 751958; doi: <https://doi.org/10.1101/751958>.
208. McManus, M.F., Nasrallah, I.M., Pancoast, M.M., Wynshaw-Boris, A. & Golden, J.A. Lis1 is necessary for normal non-radial migration of inhibitory interneurons. *Am. J. Pathol.* 165, 775–784 (2004).
209. Hirotsune, S. et al. Graded reduction of Pafah1b1 (Lis1) activity results in neuronal migration defects and early embryonic lethality. *Nature Genet.* 19, 333–339 (1998).
210. Fleck, M. W. et al. Hippocampal abnormalities and enhanced excitability in a murine model of human lissencephaly. *J. Neurosci.* 2000;20:2439–2450.
211. McKenney RJ, Vershinin M, Kunwar A, Vallee RB, Gross SP. LIS1 and NudE induce a persistent dynein force-producing state. *Cell.* 2010;141(2):304–314. doi:10.1016/j.cell.2010.02.035.
212. Shu T1, Ayala R, Nguyen MD, Xie Z, Gleeson JG, Tsai LH. Ndel1 operates in a common pathway with LIS1 and cytoplasmic dynein to regulate cortical neuronal positioning. *Neuron.* 2004;44(2):263-77.
213. Zylkiewicz E., Kijańska M., Choi W.C., Derewenda U., Derewenda Z.S., Stukenberg P.T. 2011. The N-terminal coiled-coil of Ndel1 is a regulated scaffold that recruits LIS1 to dynein. *J. Cell Biol.* 192:433–445 doi:10.1083/jcb.201011142.
214. Pandey JP, Smith DS. A Cdk5-dependent switch regulates Lis1/Ndel1/dynein-driven organelle transport in adult axons. *J Neurosci.* 2011;31(47):17207–17219. doi:10.1523/JNEUROSCI.4108-11.2011.
215. Sasaki S, Shionoya A, Ishida M, Gambello MJ, Yingling J, Wynshaw-Boris A, Hirotsune S. A LIS1/NUDEL/cytoplasmic dynein heavy chain complex in the developing and adult nervous system. *Neuron.* 2000; 28(3):681-96.
216. Tai CY, Dujardin DL, Faulkner NE, Vallee RB. Role of dynein, dynactin, and CLIP-170 interactions in LIS1 kinetochore function. *J Cell Biol.* 2002;156(6):959-68.
217. Faulkner NE, Dujardin DL, Tai CY, Vaughan KT, O'Connell CB, Wang Y, Vallee RB. A role for the lissencephaly gene LIS1 in mitosis and cytoplasmic dynein function. *Nat Cell Biol.* 2000 Nov;2(11):784-91.
218. Tarricone C, Perrina F, Monzani S, Massimiliano L, Kim M-H, Derewenda ZS, Knapp S, Tsai L-H, Musacchio A. Coupling PAF Signaling to dynein regulation: Structure of LIS1 I complex with PAF-Acetylhydrolase. *Neuron.* 2004;44(5):809-821.

219. Whyte J, Bader JR, Tauhata SB, Raycroft M, Hornick J, Pfister KK, Lane WS, Chan GK, Hinchcliffe EH, Vaughan PS, Vaughan KT. Phosphorylation regulates targeting of cytoplasmic dynein to kinetochores during mitosis. *J Cell Biol.* 2008;183(5):819-34.
220. JG, Allen KM, Fox JW, Lamperti ED, Berkovic S, Scheffer I, Cooper EC, Dobyns WB, Minnerath SR, Ross ME, Walsh CA. Doublecortin, a brain-specific gene mutated in human X-linked lissencephaly and double cortex syndrome, encodes a putative signaling protein. *Cell.* 1998; 92(1):63-72.
221. Di Donato N, Chiari S, Mirzaa GM, et al. Lissencephaly: Expanded imaging and clinical classification. *Am J Med Genet A.* 2017;173(6):1473–1488. doi:10.1002/ajmg.a.38245.
222. Dobyns W. B., Reiner O., Carrozzo R. and Ledbetter D. H. Lissencephaly. A human brain malformation associated with deletion of the LIS1 gene located at chromosome 17p13. *JAMA.* 1993;270:2838-2842. 10.1001/jama.1993.03510230076039.
223. Lo Nigro C1, Chong CS, Smith AC, Dobyns WB, Carrozzo R, Ledbetter DH. Point mutations and an intragenic deletion in LIS1, the lissencephaly causative gene in isolated lissencephaly sequence and Miller-Dieker syndrome. *Hum Mol Genet.* 1997;6(2):157-64.
224. Liu Z., Steward R., Luo L. 2000. *Drosophila* Lis1 is required for neuroblast proliferation, dendritic elaboration and axonal transport. *Nat. Cell Biol.* 2:776–783 10.1038/35041011.
225. Kudumala SR, Penserga T, Börner J, et al. Lissencephaly-1 dependent axonal retrograde transport of L1-type CAM Neuroglian in the adult *drosophila* central nervous system. *PLoS One.* 2017;12(8):e0183605. Published 2017 Aug 24. doi:10.1371/journal.pone.0183605.
226. Yin, H., Pruyne, D., Huffaker, T. C. & Bretscher, A. Myosin V orientates the mitotic spindle in yeast. *Nature* 406, 1013-1015, (2000).
227. Dujardin DL, Barnhart LE, Stehman SA, Gomes ER, Gundersen GG, Vallee RB. A role for cytoplasmic dynein and LIS1 in directed cell movement. *Jour Cell Biol.* 2003; 163(6):1205-1212.
228. Kumamoto K, Iguchi T, Ishida R, Uemura T, Sato M, Hirotsune S. Developmental downregulation of LIS1 expression limits axonal extension and allows axon pruning. *Biol Open.* 2017;6(7):1041–1055. doi:10.1242/bio.025999.

229. Lam C, Vergnolle MA, Thorpe L, Woodman PG, Allan VJ. Functional interplay between LIS1, NDE1 and NDEL1 in dynein-dependent organelle positioning. *J Cell Sci.* 2010;123:202-12.
230. Will L, Portegies S, van Schelt J, van Luyk M, Jaarsma D, Hoogenraad CC. Dynein activating adaptor BICD2 controls radial migration of upper-layer cortical neurons in vivo. *Acta Neuropathol Commun.* 2019;7(1):162. doi:10.1186/s40478-019-0827-y.
231. Sudarov A, Zhang XJ, Braunstein L, et al. Mature Hippocampal Neurons Require LIS1 for Synaptic Integrity: Implications for Cognition. *Biol Psychiatry.* 2018;83(6):518–529. doi:10.1016/j.biopsych.2017.09.011.
232. B. Cadot, et al. Nuclear movement during myotube formation is microtubule and dynein dependent and is regulated by Cdc42, Par6 and Par3. *EMBO Rep.* 2012;(13):741-749.
233. Xiang X, Han G, Winkelmann DA, Zuo W, Morris NR. Dynamics of cytoplasmic dynein in living cells and the effect of a mutation in the dynactin complex actin-related protein Arp1. *Curr Biol.* 2000;10(10):603-6.
234. Bi, W., Sapir, T., Shchelochkov, O. et al. Increased LIS1 expression affects human and mouse brain development. *Nat Genet* 2009;41, 168–177 (2009). <https://doi.org/10.1038/ng.302>.
235. Dantas TJ, Carabalona A, Hu DJ, Vallee RB. Cytoskeleton (Hoboken). Emerging roles for motor proteins in progenitor cell behavior and neuronal migration during brain development. 2016;73(10):566-576. doi: 10.1002/cm.21293.
236. Vagnoni A, Hoffmann PC, Bullock SL. Reducing Lissencephaly-1 levels augments mitochondrial transport and has a protective effect in adult *Drosophila* neurons. *J Cell Sci.* 2016;129(1):178–190. doi:10.1242/jcs.179184.
237. Kuijpers et al. Dynein Regulator NDEL1 Controls Polarized Cargo Transport at the Axon Initial Segment. *Neuron.* 2016;89(3):461-471.
238. Rai A, et al. Dynein clusters into lipid microdomains on phagosomes to drive rapid transport of lysosomes. *Cell.* 2016;16:722-734.
239. Wang S, Zheng Y. Identification of a novel dynein binding domain in nudel essential for spindle pole organization in *Xenopus* egg extract. *J Biol Chem.* 2011;286(1):587–593. doi:10.1074/jbc.M110.181578.
240. Simões PA, Celestino R, Carvalho AX, Gassmann R. NudE regulates dynein at kinetochores but is dispensable for other dynein functions in the *C. elegans* early embryo. *J Cell Sci.* 2018;131(1):jcs212159. Published 2018 Jan 8. doi:10.1242/jcs.212159.

241. Tan R, Foster PJ, Needleman DJ, McKenney RJ. Cooperative Accumulation of Dynein-Dynactin at Microtubule Minus-Ends Drives Microtubule Network Reorganization. *Dev Cell*. 2018 Jan 22; 44(2):233-247.e4.
242. Rehberg M, Kleylein-Sohn J, Faix J, Ho TH, Schulz I, Gräf R. Dictyostelium LIS1 is a centrosomal protein required for microtubule/cell cortex interactions, nucleus/centrosome linkage, and actin dynamics. *Mol Biol Cell*. 2005;16(6):2759–2771. doi:10.1091/mbc.e05-01-0069.
243. Lenz JH, Schuchardt I, Straube A, Steinberg G. A dynein loading zone for retrograde endosome motility at microtubule plus-ends. *EMBO J*. 2006;25(11):2275–2286. doi:10.1038/sj.emboj.7601119
244. Valinluck M, Ahlgren S, Sawada M, Locken K, Banuett F. Role of the nuclear migration protein Lis1 in cell morphogenesis in *Ustilago maydis*. *Mycologia*. 2010;102(3):493–512. doi:10.3852/09-193
245. Hartwell LH, Mortimer RK, Culotti J, Culotti M. Genetic Control of the Cell Division Cycle in Yeast: V. Genetic Analysis of *cdc* Mutants. *Genetics*. 1973;74(2):267-86
246. Kholmanskikh SS, Dobrin JS, Wynshaw-Boris A, Letourneau PC, Ross ME. Disregulated RhoGTPases and actin cytoskeleton contribute to the migration defect in Lis1-deficient neurons. *J Neurosci*. 2003;23(25):8673–8681. doi:10.1523/JNEUROSCI.23-25-08673.2003.
247. Chhatre A, Sanghavi P, Mallik R. LIS1 regulates phagocytosis by co-localising with actin at the Phagocytic cup. *BioRxiv*. <https://doi.org/10.1101/835769>.
248. Chaudhary AR, Berger F, Berger CL, Hendricks AG. Tau directs intracellular trafficking by regulating the forces exerted by kinesin and dynein teams. *Traffic*. 2018;19(2):111–121. doi:10.1111/tra.12537.
249. Cianfrocco MA, DeSantis ME, Leschziner AE, Reck-Peterson SL. Mechanism and regulation of cytoplasmic dynein. *Annu Rev Cell Dev Biol*. 2015;31:83–108. doi:10.1146/annurev-cellbio-100814-125438.
250. Sudarov A, Gooden F, Tseng D, Gan WB, Ross ME. Lis1 controls dynamics of neuronal filopodia and spines to impact synaptogenesis and social behaviour. *EMBO Mol Med*. 2013;5(4):591–607. doi:10.1002/emmm.201202106.
251. Reddy BJ, Mattson M, Wynne CL, et al. Load-induced enhancement of Dynein force production by LIS1-NudE in vivo and in vitro. *Nat Commun*. 2016;7:12259. doi:10.1038/ncomms12259.

252. Zhang J, Zhuang L, Lee Y, Abenza JF, Peñalva MA, Xiang X. The microtubule plus-end localization of *Aspergillus* dynein is important for dynein-early-endosome interaction but not for dynein ATPase activation. *Jour Cell Sci.* 2010;123(20):3596-604.

253. McKenney RJ, Weil SJ, Scherer J, Vallee RB. Mutually exclusive cytoplasmic dynein regulation by NudE-Lis1 and dynactin. *J Biol Chem.* 2011;286(45):39615–39622. doi:10.1074/jbc.M111.289017.

APPENDIX

Table 4. List of strains used in this thesis.

Strain number	Genotype	Source
287	Mata GAL1p:8xHis-ZZ-TEV-Pac1-g-1XFLAG-gaSNAP::KANR dyn1Δ::cgLEU2 ndl1Δ::HPH prb1Δ his3-11,15 ura3-1 leu2-3,112 ade2-1 trp1-1 pep4Δ::HIS5	W303 Ref. 105
576	Mata GFP-TUB1::LEU2 kar9Δ::KAN ura3-52 lys2-801 leu2-Δ1 his3-Δ200 trp1-Δ63	YEF473 This study
SMY1010	Mata DYN1-3GFP::TRP1 TUB1+3'UTR::HPH::HIS3p:mRuby2-TUB1 ura3-52 lys2-801 leu2-Δ1 his3-Δ200 trp1-Δ63	YEF473 This study
SMY1066	Mata dyn1 ^{E109I} -3GFP::TRP1 TUB1+3'UTR::HPH::HIS3p:mRuby2-TUB1 ura3-52 lys2-801 leu2-Δ1 his3-Δ200 trp1-Δ63	YEF473 This study
SMY1068	Mata dyn1 ^{L213I} -3GFP::TRP1 TUB1+3'UTR::HPH::HIS3p:mRuby2-TUB1 ura3-52 lys2-801 leu2-Δ1 his3-Δ200 trp1-Δ63	YEF473 This study
SMY1073	Mata dyn1 ^{W612C} -3GFP::TRP1 TUB1+3'UTR::HPH::HIS3p:mRuby2-TUB1 ura3-52 lys2-801 leu2-Δ1 his3-Δ200 trp1-Δ63	YEF473 This study
SMY1074	Mata dyn1 ^{W612C} -3GFP::TRP1 TUB1+3'UTR::HPH::HIS3p:mRuby2-TUB1 ura3-52 lys2-801 leu2-Δ1 his3-Δ200 trp1-Δ63	YEF473 This study
SMY1089	Mata dyn1 ^{K540C} -3GFP::TRP1 TUB1+3'UTR::HPH::HIS3p:mRuby2-TUB1 ura3-52 lys2-801 leu2-Δ1 his3-Δ200 trp1-Δ63	YEF473 This study
SMY1090	Mata dyn1 ^{K3160Q} -3GFP::TRP1 TUB1+3'UTR::HPH::HIS3p:mRuby2-TUB1 ura3-52 lys2-801 leu2-Δ1 his3-Δ200 trp1-Δ63	YEF473 This study
SMY1105	Mata dyn1 ^{D2439K} -3GFP::TRP1 TUB1+3'UTR::HPH::HIS3p:mRuby2-TUB1 ura3-52 lys2-801 leu2-Δ1 his3-Δ200 trp1-Δ63	YEF473 This study
SMY1107	Mata dyn1 ^{H3639P} -3GFP::TRP1 TUB1+3'UTR::HPH::HIS3p:mRuby2-TUB1 ura3-52 lys2-801 leu2-Δ1 his3-Δ200 trp1-Δ63	YEF473 This study
SMY1111	Mata dyn1 ^{E545V} -3GFP::TRP1 TUB1+3'UTR::HPH::HIS3p:mRuby2-TUB1 ura3-52 lys2-801 leu2-Δ1 his3-Δ200 trp1-Δ63	YEF473 This study
SMY1112	Mata dyn1 ^{E545V} -3GFP::TRP1 TUB1+3'UTR::HPH::HIS3p:mRuby2-TUB1 ura3-52 lys2-801 leu2-Δ1 his3-Δ200 trp1-Δ63	YEF473 This study
SMY1113	Mata dyn1 ^{I554M} -3GFP::TRP1 TUB1+3'UTR::HPH::HIS3p:mRuby2-TUB1 ura3-52 lys2-801 leu2-Δ1 his3-Δ200 trp1-Δ63	YEF473 This study
SMY1116	Mata dyn1 ^{K1475Q} -3GFP::TRP1 TUB1+3'UTR::HPH::HIS3p:mRuby2-TUB1 ura3-52 lys2-801 leu2-Δ1 his3-Δ200 trp1-Δ63	YEF473 This study

SMY1117	Mata <i>dyn1</i> ^{L2557M} -3GFP::TRP1 <i>TUB1+3'UTR::HPH::HIS3p:mRuby2-TUB1 ura3-52</i> <i>lys2-801 leu2-Δ1 his3-Δ200 trp1-Δ63</i>	YEF473	This study
SMY1119	Mata <i>dyn1</i> ^{R3152N} -3GFP::TRP1 <i>TUB1+3'UTR::HPH::HIS3p:mRuby2-TUB1 ura3-52</i> <i>lys2-801 leu2-Δ1 his3-Δ200 trp1-Δ63</i>	YEF473	This study
SMY1160	Mata <i>DYN1-3GFP::TRP1 kar9Δ::KAN^R GFP-</i> <i>TUB1::LEU2 ura3-52 lys2- 801 leu2-Δ1 his3-Δ200</i> <i>trp1-Δ63</i>	YEF473	This study
SMY1161	Mata <i>Dyn1-3GFP::TRP1 kar9Δ::KAN^R GFP-</i> <i>TUB1::LEU2 ura3-52 lys2- 801 leu2-Δ1 his3-Δ200</i> <i>trp1-Δ63</i>	YEF473	This study
SMY1178	Mata <i>dyn1</i> ^{R3201N} -3GFP::TRP1 <i>TUB1+3'UTR::HPH::HIS3p:mRuby2-TUB1 ura3-52</i> <i>lys2-801 leu2-Δ1 his3-Δ200 trp1-Δ63</i>	YEF473	This study
SMY1179	Mata <i>dyn1</i> ^{R3201N} -3GFP::TRP1 <i>TUB1+3'UTR::HPH::HIS3p:mRuby2-TUB1 ura3-52</i> <i>lys2-801 leu2-Δ1 his3-Δ200 trp1-Δ63</i>	YEF473	This study
SMY1185	Mata <i>Dyn1-3GFP::TRP1 NUP133-3mCherry::URA3</i> <i>kar9Δ::KAN^R GFP-TUB1::LEU2 ura3-52 lys2- 801</i> <i>leu2-Δ1 his3-Δ200 trp1-Δ63</i>	YEF473	This study
SMY1186	Mata <i>Dyn1-3GFP::TRP1 NUP133-3mCherry::URA3</i> <i>kar9Δ::KAN^R GFP-TUB1::LEU2 ura3-52 lys2- 801</i> <i>leu2-Δ1 his3-Δ200 trp1-Δ63</i>	YEF473	This study
SMY1196	Mata <i>dyn1</i> ^{E545V} -3GFP::TRP1 <i>NUP133-</i> <i>3mCherry::URA3 kar9Δ::KAN^R GFP-TUB1::LEU2</i> <i>ura3-52 lys2- 801 leu2-Δ1 his3-Δ200 trp1-Δ63</i>	YEF473	This study
SMY1198	Mata <i>dyn1</i> ^{E109I} -3GFP::TRP1 <i>NUP133-</i> <i>3mCherry::URA3 kar9Δ::KAN^R GFP-TUB1::LEU2</i> <i>ura3-52 lys2- 801 leu2-Δ1 his3-Δ200 trp1-Δ63</i>	YEF473	This study
SMY1200	Mata <i>dyn1</i> ^{L2557M} -3GFP::TRP1 <i>NUP133-</i> <i>3mCherry::URA3 kar9Δ::KAN^R GFP-TUB1::LEU2</i> <i>ura3-52 lys2- 801 leu2-Δ1 his3-Δ200 trp1-Δ63</i>	YEF473	This study
SMY1201	Mata <i>dyn1</i> ^{L2557M} -3GFP::TRP1 <i>NUP133-</i> <i>3mCherry::URA3 kar9Δ::KAN^R GFP-TUB1::LEU2</i> <i>ura3-52 lys2- 801 leu2-Δ1 his3-Δ200 trp1-Δ63</i>	YEF473	This study
SMY1220	Mata <i>dyn1</i> ^{R2439K} -3GFP::TRP1 <i>NUP133-</i> <i>3mCherry::URA3 kar9Δ::KAN^R GFP-TUB1::LEU2</i> <i>ura3-52 lys2- 801 leu2-Δ1 his3-Δ200 trp1-Δ63</i>	YEF473	This study
SMY1222	Mata <i>dyn1</i> ^{K540C} -3GFP::TRP1 <i>NUP133-</i> <i>3mCherry::URA3 kar9Δ::KAN^R GFP-TUB1::LEU2</i> <i>ura3-52 lys2- 801 leu2-Δ1 his3-Δ200 trp1-Δ63</i>	YEF473	This study
SMY1243	Mata <i>dyn1</i> ^{H3639P} -3GFP::TRP1 <i>TUB1+3'UTR::HPH::HIS3p:mRuby2-TUB1 ura3-52</i> <i>lys2-801 leu2-Δ1 his3-Δ200 trp1-Δ63</i>	YEF473	This study
SMY1254	Mata <i>dyn1</i> ^{R3152N} -3GFP::TRP1 <i>NUP133-</i> <i>3mCherry::URA3 kar9Δ::KAN^R GFP-TUB1::LEU2</i> <i>ura3-52 lys2- 801 leu2-Δ1 his3-Δ200 trp1-Δ63</i>	YEF473	This study
SMY1266	Mata <i>DYN3-13MYC::HPH PAC11-13MYC::TRP ZZ-</i> <i>TEV-3HA-DYN1-HaloTag::KAN^R nip100Δ pep4Δ::HIS5</i> <i>prb1Δ his3-11,15 ura3-52 leu2-3,112 ade2-1 trp-1</i>	W303	This study

SMY1317	Mata <i>dyn1</i> ^{R1852C} -3GFP::TRP1 <i>TUB1+3'UTR::HPH::HIS3p:mRuby2-TUB1 ura3-52</i> <i>lys2-801 leu2-Δ1 his3-Δ200 trp1-Δ63</i>	YEF473	This study
SMY1318	Mata <i>dyn1</i> ^{R3201N} -3GFP::TRP1 <i>TUB1+3'UTR::HPH::HIS3p:mRuby2-TUB1 ura3-52</i> <i>lys2-801 leu2-Δ1 his3-Δ200 trp1-Δ63</i>	YEF473	This study
SMY1327	Mata <i>dyn1</i> ^{R241L} -3GFP::TRP1 <i>TUB1+3'UTR::HPH::HIS3p:mRuby2-TUB1 ura3-52</i> <i>lys2-801 leu2-Δ1 his3-Δ200 trp1-Δ63</i>	YEF473	This study
SMY1351	Mata <i>dyn1</i> ^{R1852C} -3GFP::TRP1 NUP133- <i>3mCherry::URA3 kar9Δ::KAN^R GFP-TUB1::LEU2</i> <i>ura3-52 lys2- 801 leu2-Δ1 his3-Δ200 trp1-Δ63</i>	YEF473	This study
SMY1369	Mata <i>dyn1</i> ^{W3640P} -3GFP::TRP1 <i>TUB1+3'UTR::HPH::HIS3p:mRuby2-TUB1 ura3-52</i> <i>lys2-801 leu2-Δ1 his3-Δ200 trp1-Δ63</i>	YEF473	This study
SMY1370	Mata <i>dyn1</i> ^{W3640P} -3GFP::TRP1 <i>TUB1+3'UTR::HPH::HIS3p:mRuby2-TUB1 ura3-52</i> <i>lys2-801 leu2-Δ1 his3-Δ200 trp1-Δ63</i>	YEF473	This study
SMY1371	Mata <i>dyn1</i> ^{F3641P} -3GFP::TRP1 <i>TUB1+3'UTR::HPH::HIS3p:mRuby2-TUB1 ura3-52</i> <i>lys2-801 leu2-Δ1 his3-Δ200 trp1-Δ63</i>	YEF473	This study
SMY1372	Mata <i>dyn1</i> ^{F3641P} -3GFP::TRP1 <i>TUB1+3'UTR::HPH::HIS3p:mRuby2-TUB1 ura3-52</i> <i>lys2-801 leu2-Δ1 his3-Δ200 trp1-Δ63</i>	YEF473	This study
SMY1373	Mata <i>dyn1</i> ^{Y3642P} -3GFP::TRP1 <i>TUB1+3'UTR::HPH::HIS3p:mRuby2-TUB1 ura3-52</i> <i>lys2-801 leu2-Δ1 his3-Δ200 trp1-Δ63</i>	YEF473	This study
SMY1374	Mata <i>dyn1</i> ^{I3644P} -3GFP::TRP1 <i>TUB1+3'UTR::HPH::HIS3p:mRuby2-TUB1 ura3-52</i> <i>lys2-801 leu2-Δ1 his3-Δ200 trp1-Δ63</i>	YEF473	This study
SMY1381	Mata <i>dyn1</i> ^{N283R} -3GFP::TRP1 <i>TUB1+3'UTR::HPH::HIS3p:mRuby2-TUB1 ura3-52</i> <i>lys2-801 leu2-Δ1 his3-Δ200 trp1-Δ63</i>	YEF473	This study
SMY1386	Mata <i>dyn1</i> ^{R3201N} -3GFP::TRP1 NUP133- <i>3mCherry::URA3 kar9Δ::KAN^R GFP-TUB1::LEU2</i> <i>ura3-52 lys2- 801 leu2-Δ1 his3-Δ200 trp1-Δ63</i>	YEF473	This study
SMY1420	Mata <i>dyn1</i> ^{G3643P} -3GFP::TRP1 <i>TUB1+3'UTR::HPH::HIS3p:mRuby2-TUB1 ura3-52</i> <i>lys2-801 leu2-Δ1 his3-Δ200 trp1-Δ63</i>	YEF473	This study
SMY1443	Mata DYN3-13MYC::HPH PAC11-13MYC::TRP ZZ- <i>TEV-3HA-dyn1</i> ^{R3201N} -HaloTag::KAN ^R <i>nip100Δ</i> <i>pep4Δ::HIS5 prb1Δ his3-11,15 ura3-52 leu2-3,112</i> <i>ade2-1 trp-1</i>	W303	This study
SMY1444	Mata DYN3-13MYC::HPH PAC11-13MYC::TRP ZZ- <i>TEV-3HA-dyn1</i> ^{R3201N} -HaloTag::KAN ^R <i>nip100Δ</i> <i>pep4Δ::HIS5 prb1Δ his3-11,15 ura3-52 leu2-3,112</i> <i>ade2-1 trp-1</i>	W303	This study
SMY1445	Mata DYN3-13MYC::HPH PAC11-13MYC::TRP ZZ- <i>TEV-3HA-dyn1</i> ^{D2439K} -HaloTag::KAN ^R <i>nip100Δ</i> <i>pep4Δ::HIS5 prb1Δ his3-11,15 ura3-52 leu2-3,112</i> <i>ade2-1 trp-1</i>	W303	This study

SMY1447	Mata DYN3-13MYC::HPH PAC11-13MYC::TRP ZZ-TEV-3HA-dyn1 ^{L2557M} -HaloTag::KAN ^R nip100Δ pep4Δ::HIS5 prb1Δ his3-11,15 ura3-52 leu2-3,112 ade2-1 trp-1	W303	This study
SMY1448	Mata DYN3-13MYC::HPH PAC11-13MYC::TRP ZZ-TEV-3HA-dyn1 ^{K1475Q} -HaloTag::KAN ^R nip100Δ pep4Δ::HIS5 prb1Δ his3-11,15 ura3-52 leu2-3,112 ade2-1 trp-1	W303	This study
SMY1449	Mata DYN3-13MYC::HPH PAC11-13MYC::TRP ZZ-TEV-3HA-dyn1 ^{W612C} -HaloTag::KAN ^R nip100Δ pep4Δ::HIS5 prb1Δ his3-11,15 ura3-52 leu2-3,112 ade2-1 trp-1	W303	This study
SMY1455	Mata DYN3-13MYC::HPH PAC11-13MYC::TRP ZZ-TEV-3HA-dyn1 ^{H3639P} -HaloTag::KAN ^R nip100Δ pep4Δ::HIS5 prb1Δ his3-11,15 ura3-52 leu2-3,112 ade2-1 trp-1	W303	This study
SMY1456	Mata DYN3-13MYC::HPH PAC11-13MYC::TRP ZZ-TEV-3HA-dyn1 ^{E545V} -HaloTag::KAN ^R nip100Δ pep4Δ::HIS5 prb1Δ his3-11,15 ura3-52 leu2-3,112 ade2-1 trp-1	W303	This study
SMY1458	Mata/Mata DYN1-3GFP::TRP1/ DYN1-3GFP::TRP1 NUP133-3mCherry::URA3/NUP133-3mCherry::URA3 kar9Δ::KAN ^R /kar9Δ::KAN ^R GFP-TUB1::LEU2/GFP-TUB1::LEU2 ura3-52/ura3-52 lys2- 801/lys2- 801 leu2-Δ1/leu2-Δ1 his3-Δ200/his3-Δ200 trp1-Δ63/trp1-Δ63	YEF473	This study
SMY1481	Mata DYN3-13MYC::HPH PAC11-13MYC::TRP ZZ-TEV-3HA-dyn1 ^{R241L} -HaloTag::KAN ^R nip100Δ pep4Δ::HIS5 prb1Δ his3-11,15 ura3-52 leu2-3,112 ade2-1 trp-1	W303	This study
SMY1507	Mata dyn1 ^{C1822S} -3GFP::TRP1 TUB1+3'UTR::HPH::HIS3p:mRuby2-TUB1 ura3-52 lys2-801 leu2-Δ1 his3-Δ200 trp1-Δ63	YEF473	This study
SMY1508	Mata dyn1 ^{R1822S,R1852C} -3GFP::TRP1 TUB1+3'UTR::HPH::HIS3p:mRuby2-TUB1 ura3-52 lys2-801 leu2-Δ1 his3-Δ200 trp1-Δ63	YEF473	This study
SMY1509	Mata dyn1 ^{R1822S,R1852C} -3GFP::TRP1 TUB1+3'UTR::HPH::HIS3p:mRuby2-TUB1 ura3-52 lys2-801 leu2-Δ1 his3-Δ200 trp1-Δ63	YEF473	This study
SMY1520	Mata DYN3-13MYC::HPH PAC11-13MYC::TRP ZZ-TEV-3HA-dyn1 ^{K3160Q} -HaloTag::KAN ^R nip100Δ pep4Δ::HIS5 prb1Δ his3-11,15 ura3-52 leu2-3,112 ade2-1 trp-1	W303	This study
SMY1532	Mata dyn1 ^{C1822S,R1852C} -3GFP::TRP1 NUP133-3mCherry::URA3 kar9Δ::KAN ^R GFP-TUB1::LEU2 ura3-52 lys2- 801 leu2-Δ1 his3-Δ200 trp1-Δ63	YEF473	This study
SMY1533	Mata dyn1 ^{N283R} -3GFP::TRP1 NUP133-3mCherry::URA3 kar9Δ::KAN ^R GFP-TUB1::LEU2 ura3-52 lys2- 801 leu2-Δ1 his3-Δ200 trp1-Δ63	YEF473	This study

SMY1545	Mata DYN3-13MYC::HPH PAC11-13MYC::TRP ZZ-TEV-3HA-dyn1 ^{K540C} -HaloTag::KAN ^R nip100Δ pep4Δ::HIS5 prb1Δ his3-11,15 ura3-52 leu2-3,112 ade2-1 trp-1	W303	This study
SMY1546	Mata DYN3-13MYC::HPH PAC11-13MYC::TRP ZZ-TEV-3HA-dyn1 ^{K540C} -HaloTag::KAN ^R nip100Δ pep4Δ::HIS5 prb1Δ his3-11,15 ura3-52 leu2-3,112 ade2-1 trp-1	W303	This study
SMY1547	Mata DYN3-13MYC::HPH PAC11-13MYC::TRP ZZ-TEV-3HA-dyn1 ^{E545V} -HaloTag::KAN ^R nip100Δ pep4Δ::HIS5 prb1Δ his3-11,15 ura3-52 leu2-3,112 ade2-1 trp-1	W303	This study
SMY1565	Mata dyn1 ^{C1822S,R1852C} -3GFP::TRP1 NUP133-3mCherry::URA3 kar9Δ::KAN ^R GFP-TUB1::LEU2 ura3-52 lys2- 801 leu2-Δ1 his3-Δ200 trp1-Δ63	YEF473	This study
SMY1585	Mata GAL1p::ZZ-TEV-6HIS-GFP-3HA-GST-dyn1 ₃₃₁ ^{C1822S} -HaloTag::KAN ^R prb1Δ pep4Δ::HIS5 his3-11,15 ura3-52 leu2-3,112 ade2-1 trp-1	W303	This study
SMY1588	Mata GAL1p::ZZ-TEV-6HIS-GFP-3HA-GST-dyn1 ₃₃₁ ^{R1852C} -HaloTag::KAN ^R prb1Δ pep4Δ::HIS5 his3-11,15 ura3-52 leu2-3,112 ade2-1 trp-1	W303	This study
SMY1589	Mata GAL1p::ZZ-TEV-6HIS-GFP-3HA-GST-dyn1 ₃₃₁ ^{R1852C} -HaloTag::KAN ^R prb1Δ pep4Δ::HIS5 his3-11,15 ura3-52 leu2-3,112 ade2-1 trp-1	W303	This study
SMY1591	Mata dyn1 ^{H3639P} -3GFP::TRP1 NUP133-3mCherry::URA3 kar9Δ::KAN ^R GFP-TUB1::LEU2 ura3-52 lys2- 801 leu2-Δ1 his3-Δ200 trp1-Δ63	YEF473	This study
SMY1592	Mata/Mata DYN1-3GFP::TRP1/ dyn1Δ::HIS3 NUP133-3mCherry::URA3/NUP133-3mCherry::URA3 kar9Δ::KAN ^R /kar9Δ::KAN ^R GFP-TUB1::LEU2/GFP-TUB1::LEU2 ura3-52/ura3-52 lys2- 801/lys2- 801 leu2-Δ1/leu2-Δ1 his3-Δ200/his3-Δ200 trp1-Δ63/trp1-Δ63	YEF473	This study
SMY1627	Mata dyn1 ^{R2543K} -3GFP::TRP1 TUB1+3'UTR::HPH::HIS3p:mRuby2-TUB1 ura3-52 lys2-801 leu2-Δ1 his3-Δ200 trp1-Δ63	YEF473	This study
SMY1628	Mata dyn1 ^{R2543K} -3GFP::TRP1 TUB1+3'UTR::HPH::HIS3p:mRuby2-TUB1 ura3-52 lys2-801 leu2-Δ1 his3-Δ200 trp1-Δ63	YEF473	This study
SMY1651	Mata GAL1p::ZZ-TEV-6HIS-GFP-3HA-GST-dyn1 ₃₃₁ ^{H3639P} -HaloTag::KAN ^R prb1Δ pep4Δ::HIS5 his3-11,15 ura3-52 leu2-3,112 ade2-1 trp-1	W303	This study

SMY1678	Mata/Mata <i>DYN1/ dyn1^{E545V}</i> :: <i>TRP1 NUP133-3mCherry::URA3/NUP133-3mCherry::URA3 kar9Δ::KAN^R/kar9Δ::KAN^R GFP-TUB1::LEU2/GFP-TUB1::LEU2 ura3-52/ura3-52 lys2- 801/lys2- 801 leu2-Δ1/leu2-Δ1 his3-Δ200/his3-Δ200 trp1-Δ63/trp1-Δ63</i>	YEF473	This study
SMY1679	Mata/Mata <i>DYN1/ dyn1^{H3639P}</i> :: <i>TRP1 NUP133-3mCherry::URA3/NUP133-3mCherry::URA3 kar9Δ::KAN^R/kar9Δ::KAN^R GFP-TUB1::LEU2/GFP-TUB1::LEU2 ura3-52/ura3-52 lys2- 801/lys2- 801 leu2-Δ1/leu2-Δ1 his3-Δ200/his3-Δ200 trp1-Δ63/trp1-Δ63</i>	YEF473	This study
SMY1697	Mata <i>dyn1^{C1822S}-3GFP::TRP1 NUP133-3mCherry::URA3 kar9Δ::KAN^R GFP-TUB1::LEU2 ura3-52 lys2- 801 leu2-Δ1 his3-Δ200 trp1-Δ63</i>	YEF473	This study
SMY1698	Mata <i>GAL1p::ZZ-TEV-6HIS-GFP-3HA-GST-dyn1₃₃₁^{C1822S,R1852C}-HaloTag::KAN^R prb1Δ pep4Δ::HIS5 his3-11,15 ura3-52 leu2-3,112 ade2-1 trp-1</i>	W303	This study
SMY1699	Mata <i>GAL1p::ZZ-TEV-6HIS-GFP-3HA-GST-dyn1₃₃₁^{C1822S,R1852C}-HaloTag::KAN^R prb1Δ pep4Δ::HIS5 his3-11,15 ura3-52 leu2-3,112 ade2-1 trp-1</i>	W303	This study
SMY1727	Mata <i>dyn1^{I554M}-3GFP::TRP1 NUP133-3mCherry::URA3 kar9Δ::KAN^R GFP-TUB1::LEU2 ura3-52 lys2- 801 leu2-Δ1 his3-Δ200 trp1-Δ63</i>	YEF473	This study
SMY1732	Mata <i>dyn1^{R2543K}-3GFP::TRP1 NUP133-3mCherry::URA3 kar9Δ::KAN^R GFP-TUB1::LEU2 ura3-52 lys2- 801 leu2-Δ1 his3-Δ200 trp1-Δ63</i>	YEF473	This study
SMY1733	Mata <i>dyn1^{R2543K}-3GFP::TRP1 NUP133-3mCherry::URA3 kar9Δ::KAN^R GFP-TUB1::LEU2 ura3-52 lys2- 801 leu2-Δ1 his3-Δ200 trp1-Δ63</i>	YEF473	This study
SMY1740	Mata <i>DYN3-13MYC::HPH PAC11-13MYC::TRP ZZ-TEV-3HA-dyn1^{I554M}-HaloTag::KAN^R nip100Δ pep4Δ::HIS5 prb1Δ his3-11,15 ura3-52 leu2-3,112 ade2-1 trp-1</i>	W303	This study
SMY1744	Mata <i>dyn1^{R241L}-3GFP::TRP1 NUP133-3mCherry::URA3 kar9Δ::KAN^R GFP-TUB1::LEU2 ura3-52 lys2- 801 leu2-Δ1 his3-Δ200 trp1-Δ63</i>	YEF473	This study
SMY1754	Mata <i>DYN3-13MYC::HPH PAC11-13MYC::TRP ZZ-TEV-3HA-dyn1^{R2543K}-HaloTag::KAN^R nip100Δ pep4Δ::HIS5 prb1Δ his3-11,15 ura3-52 leu2-3,112 ade2-1 trp-1</i>	W303	This study
SMY1755	Mata <i>DYN3-13MYC::HPH PAC11-13MYC::TRP ZZ-TEV-3HA-dyn1^{R2543K}-HaloTag::KAN^R nip100Δ pep4Δ::HIS5 prb1Δ his3-11,15 ura3-52 leu2-3,112 ade2-1 trp-1</i>	W303	This study
SMY1756	Mata <i>DYN3-13MYC::HPH PAC11-13MYC::TRP ZZ-TEV-3HA-dyn1^{R3152N}-HaloTag::KAN^R nip100Δ pep4Δ::HIS5 prb1Δ his3-11,15 ura3-52 leu2-3,112 ade2-1 trp-1</i>	W303	This study

SMY1766	Mata <i>dyn1</i> ^{K3160Q} -3GFP::TRP1 NUP133-3mCherry::URA3 <i>kar9Δ</i> ::KAN ^R GFP-TUB1::LEU2 <i>ura3-52 lys2- 801 leu2-Δ1 his3-Δ200 trp1-Δ63</i>	YEF473	This study
SMY1774	Mata <i>dyn1</i> ^{W612C} -3GFP::TRP1 NUP133-3mCherry::URA3 <i>kar9Δ</i> ::KAN ^R GFP-TUB1::LEU2 <i>ura3-52 lys2- 801 leu2-Δ1 his3-Δ200 trp1-Δ63</i>	YEF473	This study
SMY1816	Mata <i>dyn1</i> ^{H3639P,W3640G} -3GFP::TRP1 TUB1+3'UTR::HPH::HIS3p:mRuby2-TUB1 <i>ura3-52 lys2-801 leu2-Δ1 his3-Δ200 trp1-Δ63</i>	YEF473	This study
SMY1832	Mata DYN3-13MYC::HPH PAC11-13MYC::TRP ZZ-TEV-3HA- <i>dyn1</i> ^{L213I} -HaloTag::KAN ^R <i>nip100Δ pep4Δ</i> ::HIS5 <i>prb1Δ his3-11,15 ura3-52 leu2-3,112 ade2-1 trp-1</i>	W303	This study
SMY1833	Mata <i>dyn1</i> ^{L213I} -3GFP::TRP1 NUP133-3mCherry::URA3 <i>kar9Δ</i> ::KAN ^R GFP-TUB1::LEU2 <i>ura3-52 lys2- 801 leu2-Δ1 his3-Δ200 trp1-Δ63</i>	YEF473	This study
SMY1834	Mata <i>dyn1</i> ^{K1475Q} -3GFP::TRP1 NUP133-3mCherry::URA3 <i>kar9Δ</i> ::KAN ^R GFP-TUB1::LEU2 <i>ura3-52 lys2- 801 leu2-Δ1 his3-Δ200 trp1-Δ63</i>	YEF473	This study
SMY1841	Mata <i>dyn1</i> ^{F3638G,H3639P} -3GFP::TRP1 TUB1+3'UTR::HPH::HIS3p:mRuby2-TUB1 <i>ura3-52 lys2-801 leu2-Δ1 his3-Δ200 trp1-Δ63</i>	YEF473	This study
SMY1842	Mata <i>dyn1</i> ^{F3638G,H3639P} -3GFP::TRP1 TUB1+3'UTR::HPH::HIS3p:mRuby2-TUB1 <i>ura3-52 lys2-801 leu2-Δ1 his3-Δ200 trp1-Δ63</i>	YEF473	This study
SMY1857	Mata <i>dyn1</i> ^{R1822S,R1852V} -3GFP::TRP1 TUB1+3'UTR::HPH::HIS3p:mRuby2-TUB1 <i>ura3-52 lys2-801 leu2-Δ1 his3-Δ200 trp1-Δ63</i>	YEF473	This study
SMY1858	Mata <i>dyn1</i> ^{R1852V} -3GFP::TRP1 TUB1+3'UTR::HPH::HIS3p:mRuby2-TUB1 <i>ura3-52 lys2-801 leu2-Δ1 his3-Δ200 trp1-Δ63</i>	YEF473	This study
SMY1866	Mata <i>dyn1</i> ^{R1852V} -3GFP::TRP1 NUP133-3mCherry::URA3 <i>kar9Δ</i> ::KAN ^R GFP-TUB1::LEU2 <i>ura3-52 lys2- 801 leu2-Δ1 his3-Δ200 trp1-Δ63</i>	YEF473	This study
SMY1867	Mata <i>dyn1</i> ^{C1822S,R1852V} -3GFP::TRP1 NUP133-3mCherry::URA3 <i>kar9Δ</i> ::KAN ^R GFP-TUB1::LEU2 <i>ura3-52 lys2- 801 leu2-Δ1 his3-Δ200 trp1-Δ63</i>	YEF473	This study
SMY1868	Mata DYN3-13MYC::HPH PAC11-13MYC::TRP ZZ-TEV-3HA- <i>dyn1</i> ^{E109I} -HaloTag::KAN ^R <i>nip100Δ pep4Δ</i> ::HIS5 <i>prb1Δ his3-11,15 ura3-52 leu2-3,112 ade2-1 trp-1</i>	W303	This study
SMY1883	Mata DYN3-13MYC::HPH PAC11-13MYC::TRP ZZ-TEV-3HA- <i>dyn1</i> ^{N283R} -HaloTag::KAN ^R <i>nip100Δ pep4Δ</i> ::HIS5 <i>prb1Δ his3-11,15 ura3-52 leu2-3,112 ade2-1 trp-1</i>	W303	This study
SMY1922	Mata <i>dyn1</i> ^{F3638G,H3639P,W3640G} -3GFP::TRP1 TUB1+3'UTR::HPH::HIS3p:mRuby2-TUB1 <i>ura3-52 lys2-801 leu2-Δ1 his3-Δ200 trp1-Δ63</i>	YEF473	This study

SMY1923	Mata <i>dyn1</i> ^{F3638G,H3639P,W3640G} -3GFP::TRP1 TUB1+3'UTR::HPH::HIS3p:mRuby2-TUB1 <i>ura3-52</i> <i>lys2-801 leu2-Δ1 his3-Δ200 trp1-Δ63</i>	YEF473	This study
SMY1933	Mata <i>dyn1</i> ^{F3638G,H3639P,F3640G} -3GFP::TRP1 NUP133- 3mCherry::URA3 <i>kar9Δ</i> ::KAN ^R GFP-TUB1::LEU2 <i>ura3-52 lys2- 801 leu2-Δ1 his3-Δ200 trp1-Δ63</i>	YEF473	This study
SMY1934	Mata <i>dyn1</i> ^{F3638G,H3639P,F3640G} -3GFP::TRP1 NUP133- 3mCherry::URA3 <i>kar9Δ</i> ::KAN ^R GFP-TUB1::LEU2 <i>ura3-52 lys2- 801 leu2-Δ1 his3-Δ200 trp1-Δ63</i>	YEF473	This study
SMY1955	Mata <i>pep4</i> ::HIS3 <i>prb1Δ</i> DYN3-13MYC::HPH PAC11-13MYC::TRP ZZ-TEV-3XHA- <i>dyn1</i> ^{K1475E} -GS- HALOTAG::KAN <i>nip100Δ</i>	W303	This study
SMY1957	Mata <i>dyn1</i> ^{K1475E} - 3XGFP::TRP1TUB1+3'UTR::HPH::HIS3p:mRuby2- TUB1 <i>ura3-52 lys2- 801 leu2-Δ1 his3-Δ200 trp1-Δ63</i>	YEF473	This study
SMY1959	Mata DYN3-13MYC::HPH PAC11-13MYC::TRP ZZ- TEV-3HA- <i>dyn1</i> ^{F3638G,H3639P,W3640G} -HaloTag::KAN ^R <i>nip100Δ pep4Δ</i> ::HIS5 <i>prb1Δ his3-11,15 ura3-52 leu2-3,112 ade2-1 trp-1</i>	W303	This study
SMY1960	Mata DYN3-13MYC::HPH PAC11-13MYC::TRP ZZ- TEV-3HA- <i>dyn1</i> ^{F3638G,H3639P,W3640G} -HaloTag::KAN ^R <i>nip100Δ pep4Δ</i> ::HIS5 <i>prb1Δ his3-11,15 ura3-52 leu2-3,112 ade2-1 trp-1</i>	W303	This study
SMY1965	Mata <i>pep4</i> ::HIS3 <i>prb1Δ</i> DYN3-13MYC::HPH PAC11-13MYC::TRP ZZ-TEV-3XHA- <i>dyn1</i> ^{D2868K} -GS- HALOTAG::KAN <i>nip100Δ</i>	W303	This study
SMY1973	Mata <i>pep4</i> ::HIS3 <i>prb1Δ</i> DYN3-13MYC::HPH PAC11-13MYC::TRP ZZ-TEV-3XHA- <i>dyn1</i> ^{K1517E} -GS- HALOTAG::KAN <i>nip100Δ</i>	W303	This study
SMY1977	Mata <i>dyn1</i> ^{K1475E} - 3XGFP::TRP1TUB1+3'UTR::HPH::HIS3p:mRuby2- TUB1 <i>ura3-52 lys2- 801 leu2-Δ1 his3-Δ200 trp1-Δ63</i>	YEF473	This study
SMY1992	Mata <i>dyn1</i> ^{D2868K} - 3XGFP::TRP1TUB1+3'UTR::HPH::HIS3p:mRuby2- TUB1 <i>ura3-52 lys2- 801 leu2-Δ1 his3-Δ200 trp1-Δ63</i>	YEF473	This study
SMY2013	Mata <i>dyn1</i> ^{D2868K} - 3XGFP::TRP1TUB1+3'UTR::HPH::HIS3p:mRuby2- TUB1 <i>ura3-52 lys2- 801 leu2-Δ1 his3-Δ200 trp1-Δ63</i>	YEF473	This study

SMY2039	Mata pep4::HIS3 prb1Δ DYN3-13MYC::HPH PAC11-13MYC::TRP ZZ-TEV-3XHA-dyn1 ^{K1475E/K1517E} -GS-HALOTAG::KAN nip100Δ	W303	This study
SMY2083	Mata kar9Δ::KAN pac1Δ::HIS3 GFP-Tub1::LEU2 ura3-52 lys2-801 leu2-Δ1 his3-Δ200 trp1-Δ63	YEF473	This study
SMY2084	Mata dyn1 ^{D2868K} -3GFP::TRP1 kar9Δ::KAN pac1Δ::HIS3 GFP-Tub1::LEU2 ura3-52 lys2-801 leu2-Δ1 his3-Δ200 trp1-Δ63	YEF473	This study
SMY2104	Mata DYN3-13MYC::HPH PAC11-13MYC::TRP ZZ-TEV-3HA-dyn1 ^{R1852C} -HaloTag::KAN ^R nip100Δ pep4Δ::HIS5 prb1Δ his3-11,15 ura3-52 leu2-3,112 ade2-1 trp-1	W303	This study
SMY2129	Mata dyn1 ^{C1822A,R1852C} -3GFP::TRP1 NUP133-3mCherry::URA3 kar9Δ::KAN ^R GFP-TUB1::LEU2 ura3-52 lys2-801 leu2-Δ1 his3-Δ200 trp1-Δ63	YEF473	This study
SMY2183	Mata pep4::HIS3 prb1Δ DYN3-13MYC::HPH PAC11-13MYC::TRP ZZ-TEV-3XHA-dyn1 ^{K1475D/D2868K} -GS-HALOTAG::KAN nip100Δ	W303	This study
SMY2195	Mata num1Δ::HPH nip100Δ::LEU3 ura3-1::GAL1p-DYN2:GAL1p-DYN3:GAL1p-PAC11:GAL1p-8xHis-ZZ-2XTEV-SNAPf-DYN1::URA3 his3-11,15 leu2-3,112 ade2-1 trp-1 pep4Δ::HIS5 prb1Δ	W303	This study
SMY2220	Mata num1Δ::HPH nip100Δ::LEU3 ura3-1::GAL1p-DYN2:GAL1p-DYN3:GAL1p-PAC11:GAL1p-8xHis-ZZ-2XTEV-SNAPf-dyn1 ^{D2868K} ::URA3 his3-11,15 leu2-3,112 ade2-1 trp-1 pep4Δ::HIS5 prb1Δ	W303	This study
SMY2237	Mata pep4::HIS3 prb1Δ DYN3-13MYC::HPH PAC11-13MYC::TRP ZZ-TEV-3XHA-dyn1 ^{R3476D} -GS-HALOTAG::KAN nip100Δ	W303	This study
SMY2273	Mata pep4::HIS3 prb1Δ DYN3-13MYC::HPH PAC11-13MYC::TRP ZZ-TEV-3XHA-dyn1 ^{Y3268A} -GS-HALOTAG::KAN nip100Δ	W303	This study
SMY2275	Mata pep4::HIS3 prb1Δ DYN3-13MYC::HPH PAC11-13MYC::TRP ZZ-TEV-3XHA-dyn1 ^{I3272A} -GS-HALOTAG::KAN nip100Δ	W303	This study
SMY2289	Mata pep4::HIS3 prb1Δ DYN3-13MYC::HPH PAC11-13MYC::TRP ZZ-TEV-3XHA-dyn1 ^{K1475D/K1517A/D2868K} -GS-HALOTAG::KAN nip100Δ	W303	This study

SMY2290	Mata pep4::HIS3 prb1Δ DYN3-13XMYC::HPH PAC11-13XMYC::TRP ZZ-TEV-3XHA-dyn1 ^{K1475D/K1517D/D2868K} -GS-HALOTAG::KAN nip100Δ	W303	This study
SMY2343	Mata Δnip100::LEU2 ura3-1::GAL1p-DYN2:GAL1p-DYN3:GAL1p-PAC11:GAL1p-8xHis-ZZ-2XTEV-HALO-DYN1::URA3 his3-11,15 ura3-1 leu2-3,112 ade2-1 trp-1 pep4Δ::HIS5 prb1Δ	W303	This study
SMY2344	Mata Δnip100::LEU2 ura3-1::GAL1p-DYN2:GAL1p-DYN3:GAL1p-PAC11:GAL1p-8xHis-ZZ-2XTEV-HALO-DYN1::URA3 his3-11,15 ura3-1 leu2-3,112 ade2-1 trp-1 pep4Δ::HIS5 prb1Δ	W303	This study
SMY2373	Mata Δnip100::LEU2 ura3-1::GAL1p-DYN2:GAL1p-DYN3:GAL1p-PAC11:GAL1p-8xHis-ZZ-2XTEV-HALO-dyn1 ^{D2868K} ::URA3 his3-11,15 ura3-1 leu2-3,112 ade2-1 trp-1 pep4Δ::HIS5 prb1Δ	W303	This study
SMY2383	Mata dyn1-3XGFP::TRP1TUB1+3'UTR::HPH::HIS3p:mRuby2-TUB1 ura3-52 lys2- 801 leu2-Δ1 his3-Δ200 trp1-Δ63	YEF473	This study
SMY2397	Mata dyn1 ^{2XHL4} -3YFP::TRP pac1Δ::HIS3 kar9Δ::KAN GFP-Tub1::LEU2 ura3-52 lys2-801 leu2-Δ1 his3-Δ200 trp1-Δ63	YEF473	This study
SMY2414	Mata Δnip100::LEU2 ura3-1::GAL1p-DYN2:GAL1p-DYN3:GAL1p-PAC11:GAL1p-8xHis-ZZ-2XTEV-HALO-dyn1 ^{2XHL4} ::URA3 his3-11,15 ura3-1 leu2-3,112 ade2-1 trp-1 pep4Δ::HIS5 prb1Δ	W303	This study
SMY2443	Mata pep4::HIS3 prb1Δ DYN3-13XMYC::HPH PAC11-13XMYC::TRP ZZ-TEV-3XHA-dyn1 ^{D3487K} -GS-HALOTAG::KAN nip100Δ	W303	This study
SMY2475	Mata his3-11,15 leu2-3,112 ade2-1 trp-1 pep4Δ::HIS5 prb1Δ ura3-1::GAL1p:ZZ-2TEV-6His-GFP-GST-dyn1-331-HALO::URA3	W303	This study
SMY2497	Mata his3-11,15 leu2-3,112 ade2-1 trp-1 pep4Δ::HIS5 prb1Δ ura3-1::GAL1p:ZZ-2TEV-6His-GFP-GST-dyn1 ^{D2868K} -331-HALO::URA3	W303	This study
SMY2501	Mata dyn1 ^{K1475E} -3GFP::TRP1 kar9Δ::KAN pac1Δ::HIS3 GFP-Tub1::LEU2 ura3-52 lys2-801 leu2-Δ1 his3-Δ200 trp1-Δ63	YEF473	This study